A *PEX13* KNOCKOUT IN GERM CELLS INDUCES A SPERMATOGENIC ARREST

INAUGURAL DISSERTATION

to obtain the academic degree
D o c t o r r e r u m n a t u r a l i u m
(Dr. rer. nat.)

by

ANN-KRISTIN BRAUNS

Submitted to the
Faculty of Mathematics, Informatics and Natural Sciences of the University of Hamburg
Realised at the
Department of Anatomy and Experimental Morphology of the University Medical Centre Hamburg-Eppendorf

July 2017 in Hamburg

First Supervisor and Committee Member: Prof. Dr. med Georg Lüers

Second Supervisor and Committee Member: Prof. Dr. Thorsten Burmester

Committee Members: Prof. Dr. med. Udo Schumacher

Prof. Dr. Jörg Ganzhorn

Dr. Sabine Lüthje

Dr. Daniel Wicklein

Date of the oral examination: 15th December 2017

DECLARATION ON OATH

"I hereby declare, on oath, that I have written the present dissertation by my own and have not used other than the acknowledged resources and aids. I have appropriately acknowledged and referenced all text passages that are derived literally from or are based on the content of published or unpublished work of others, and all information that relates to verbal communications."

Hamburg, 17th July 2017 Ann-Kristin Brauns

CONTENT

LIST OF ABBREVIATIONS

ABC	ATP-binding cassette family of transporters
ABP	Androgen-binding protein
ACOX	Acyl-CoA oxidase
Acr	Acrosome
ALD	Adrenoleukodystrophy
Am	Acrosomal matrix
AMACR	2-methylacyl-CoA racemase
AMH	Anti-Müllerian hormone
AMN	Adrenomyeloneuropathy
Ana	Anaphase
B	Bladder
Bc	Basal cell
BSA	Bovine serum albumin
Bspg	B-type spermatogonia
BTB	Blood-testis barrier
CAT	Catalase
Cc	Columnar cells
cDNA	Complementary deoxyribonucleic acid
Cuc	Cuboidal cells
℃	Degree celsius
DAB	Alkaline 3, 3′-diaminobenzidine
Dd	Ductus deferens
DHEA	Dehydroepiandrosterone
DHT	Dihydrotestosterone
DMSO	Dimethyl sulfoxide
DNA	Deoxyribonucleic acid
DNL	*De novo* lipogenesis
E	Epididymis
EDTA	Ethylene-diamine tetraacetate
Elovl	Elongation of very long-chain fatty acids
Ep	Early pachytene sparmatocyte
eMet	Early metaphase
lMet	Late metaphase
ER	Endoplasmic reticulum
Es	Elongated spermatids
FADS	Fatty acid desaturase
FSH	Follicle-stimulating hormone
GFP	Green fluorescent protein
GnRH	Gonadotropin-releasing hormone
Golgi	Golgi apparatus
H_2O	Water
H_2O_2	Hydrogen peroxide
hr(s)	Hour(s)
HRP	Horseradish peroxidase
HTZ	Heterozygous

IF	Immunofluorescence
IHC	Immunohistochemistry
IL	Interleukin
In	Intermediate spermatogonia
IP	Intraperitoneal
IRD	Infantile Refsum disease
IV	Intravenous
K	Kidney
KH_2PO_4	Potassium dihydrogen phosphate
KO	Knockout
L	Leptotene spermatocyte
LCFA	Long-chain fatty acid
LD	Lipid droplet
LH	Luteinizing hormone
M	Molar
MASP	Marker assisted selection protocol
Mei	Meiosis
mg	Milligram
Mic	Microvilli
min	Minute(s)
Mit	Mitochondria
ml	Millilitre
mm	Micrometer
MNC	Multinucleated giant cell
MUFA	Monounsaturated fatty acids
N-ALD	Neonatal Adrenoleukodystrophy
Nu	Nucleus
O_2	Oxygen
OH	Hydroxyl radical
ORO	Oil Red O
%	Percentage
PBD	Peroxisome biogenesis disorder
PBS	Phosphate-buffered saline
PBST	Phosphate-buffered saline with Tween
PCR	Polymerase chain reaction
Pex	Gene encoding a peroxin (peroxisome biogenesis protein)
PFA	Paraformaldehyde
Pha	Phagosome
PL	Plasmalogens
PMP	Peroxisomal membrane protein
PPAR	Peroxisome proliferator activated receptor
Pro	Prophase
PTC	peritubular myoid cell
PTS	Peroxisomal targeting signal
PUFA	Polyunsaturated fatty acid
qPCR	Qualitative PCR
RCDP	Rhizomelic chondrodysplasia punctata

RNA	Ribonucleic acid
ROS	Reactive oxygen species
Rs	Round spermatid
RT	Room temperature
RXR	Retinoid x receptors
s	second(s)
S	Spermatocytes
Sci	Stereocilia
SCP	Sterol carrier protein X
sER	Smooth endoplasmic reticulum
SF-1	Steroidogenic factor 1
SFA	Saturated fatty acids
Sm	Smooth muscle
SOD	Superoxide dismutase
Spz	Spermatozoon
Sv	Seminal vesicle
SRY	Sex-determining region of the Y chromosome
Psc	Pseudostratified columnar epithelium
T	Testosterone
TAE	Tris acetate EDTA buffer
TdT	Terminal deoxynucleotidyl transferase
Tel	Telophase
TG	Triglycerides
TGF	Transforming growth factor-beta
THIO	Peroxisome 3-ketoacyl-CoA thiolase
TJ	Tight junction
TPR	Tetratricopeptide repeat
Tris	Tris (hydroxymethyl) aminomethane
Tt	Testicles
U	Ureter
UMI	Unexplained male infertility
V	Vacuole
VLCFA	Very long-chain fatty acid
v/v	Volume/volume
WB	Western blot
WHO	World Health Organization
WT	Wild-type
w/v	Weight/volume
X-ALD	X-linked Adrenoleukodystrophy
Z	Zygotene spermatocyte
ZS	Zellweger syndrome

ABSTRACT

Peroxisomes are cell organelles with important functions in metabolic processes, including *β*-oxidation of very long-chain fatty acids and branched-chain fatty acids, ether lipid synthesis, catabolism of D-amino acids and polyamines, as well as the degradation of reactive oxygen species (ROS), particularly hydrogen peroxide.

As lipids have a specific functional significance in the nervous system, peroxisomal disorders lead to disturbed myelination of axons, resulting in severe neurological diseases. In addition, patients show testicular abnormalities, including the reduction of seminiferous tubules or a spermatogenic arrest that leads to azoospermia. Underlying alterations in the testes due to a peroxisomal defect are not well characterized. Peroxisomes do not synthesise proteins on their own, therefore they require an import machinery to translocate proteins from the cytosol into the organelle. The peroxisomal membrane protein PEX13 is part of this translocation machinery. Its inactivation leads to a biogenesis defect of peroxisomes with loss of all metabolic functions.

Based on the Cre-*lox* technique, two mouse models with a conditional knockout for *Pex13* were established in either pre- or post-meiotic germ cells mediated by the transgenic *Stra8*-Cre or *Prm*-Cre promoter, respectively. The effects of a peroxisomal knockout were analysed with focus on germ cell differentiation and maturation. The *Stra8*-Cre mediated peroxisomal knockout induced a severe impairment of spermatogenesis. Germ cell differentiation was interrupted at the round spermatid stage, leading to the generation of multinucleated giant cells and thus infertility of male mice. More lipid droplets were accumulated in the cytoplasm of Sertoli cells, compared to control mice. In addition, gas chromatography revealed an alteration in the composition of polyunsaturated fatty acids in the testis. Whereas precursors of the peroxisomal *β*-oxidation were up-regulated, docosapentaenoic acid (C22:5(ω-6)) and docosahexaenoic acid (C22:6(ω-3)) were significantly down-regulated. Fatty acid elongases and desaturases that are involved in peroxisomal *β*-oxidation were significantly increased. Peroxisomal genes involved in the metabolite transport, *β*-oxidation, ether lipid synthesis as well as retinoid and ROS metabolism were strongly down-regulated in the *Stra8*-Cre mediated *Pex13* KO mice.

In contrast to that, spermatogenesis was not affected in the *Prm*-Cre mediated *Pex13* knockout mice. Mice were still fertile and showed no obvious impairments of the peroxisomal compartment.

This study provides evidence that peroxisomes are inevitable to ensure proper germ cell differentiation. Moreover, peroxisomes seem to be more important for germ cells prior to meiosis than for cells that further differentiate into spermatozoa.

1 INTRODUCTION

Peroxisomes are ubiquitous eukaryotic cell organelles with various important functions to maintain cellular homeostasis. They are mainly involved in *β*-oxidation of very long-chain fatty acids (VLCFAs), synthesis and generation of ether lipids, steroids, cholesterol and bile acid (Wanders and Waterham 2006a). As by-product of the *β*-oxidation pathway, reactive oxygen species (ROS) are generated, whose accumulation leads to oxidative stress in the cell. Through their degradation within the peroxisomal compartment, they will be disposed of to prevent cellular intoxication (Islinger *et al.* 2012).

Peroxisomes are either synthesized *de novo* or derive from pre-existing ones through division. Their biogenesis is maintained by essential proteins, called peroxins or PEX proteins, of which PEX5, PEX 7, PEX10, PEX12, PEX13, PEX14 are involved in the import of enzymes into the cellular compartment (Hasan *et al.* 2013). Peroxisomal matrix proteins will be synthesized on free ribosomes in the cytoplasm. They contain a recognition sequence, defined as the peroxisomal targeting signal (PTS1) that will be post-translationally recognised by receptors. The PEX proteins will subsequently be translocated via an import machinery complex into the lumen of the peroxisome (Stanley and Wilmanns 2006). Impaired peroxisomal function, characterized by defects in the biogenesis, protein import or impaired metabolic pathways, may lead to severe neurological diseases that can be lethal, as shown for the Zellweger syndrome (Gould and Valle 2000). Peroxisomal dysfunction can also lead to less severe diseases displayed by patients affected with X-linked adrenoleukodystrophy (X-ALD) or adrenomyeloneuropathy (AMN), whose symptoms result from an accumulation of VLCFAs. Interestingly, patients also show alterations in their reproductive tract, including degenerating Leydig cells, reduction of the seminiferous tubules or even a spermatogenic arrest. Spermatogenesis comprises restructuring of the Blood-testis barrier (BTB), endocrine and paracrine regulation (Weinbauer and Nieschlag 1997), mitotic and meiotic events. It therefore relies on the availability of steroids, plasmalogens and scavenging of ROS that implies peroxisomal function.

Based on the evidence that peroxisomes are present in all germ cells except for spermatozoa, the study focused on the importance of peroxisomes during germ cell differentiation. The experimental design aimed at the characterization of the effects of abolished peroxisome biogenesis in murine testicular cells to analyse which peroxisome specific metabolic pathways are required and indispensable for germ cells to differentiate into fully functioning sperm.

Based on the Cre-*lox* system, the deletion of *exon 2* of the peroxisomal protein PEX13 was mediated by a transgenic *Stra8*-Cre promoter or a *Prm*-Cre promoter to interfere with the protein import and thus abolishing peroxisomal function in either pre- or post-meiotic germ cells, respectively.

1.1 Peroxisomes

Peroxisomes were first discovered at the ultrastructural level by Rhodin (Rhodin 1954). Together with glyoxysomes (in plants and filamentous fungi), glycosomes (e.g. in human pathogens *Leishmania* and *Trypanosoma spp.*) and hydrogenosomes, they were grouped into the organelle family of microbodies. Peroxisomes were defined as a distinct organelle, when De Duve and colleagues identified urate oxidase and D-amino acid oxidase activity, as well as peroxisome specific catalase (De Duve and Baudhuin 1966). In the oxidative reaction, hydrogen peroxide (H_2O_2) is produced, which in turn will be catalysed to oxygen (O_2) and water (H_2O) to maintain cellular function and homeostasis. Morphologically, they are characterized by a fine granular proteinaceous matrix surrounded by a single membrane at the ultrastructural level. The membrane is permeable to small molecules such as urate or amino acids (De Duve and Baudhuin 1966). For larger substrates (e.g. acetyl-CoA) and cofactors (e.g. NAD), shuttle systems are used that connect the peroxisomal lumen to the cytosol (Tabak *et al.* 1995; van Roermund *et al.* 2008). Small solutes (MW < 300 D) can easily pass through pore-like structures (Antonenkov *et al.* 2004). The size and number of peroxisomes is adaptable to the requirements and composition of their environment and has an impact on their function and reactions (Lizana *et al.* 2008). Peroxisomes are usually spherical shaped organelles that are present in almost all eukaryotic cells, except for erythrocytes. In sebaceous and preputial glands and regenerating liver they are interconnected and organized into a peroxisomal reticulum (Gorgas 1984; Yamamoto and Fahimi 1987). The size of peroxisomes varies depending on the organ. In kidney and liver, they are relatively large (0.3-1.0 µm in diameter), whereas in the brain and muscle their size ranges from 0.1-0.25 µm (Holtzman *et al.* 1973; Usuda *et al.* 1988). Peroxisomes are involved in a multitude of catabolic and anabolic processes including the degradation of VLCFs and their derivatives via *β*-oxidation, synthesis of ether lipids, steroids and cholesterol, catabolism of purines and biosynthesis of glycerolipids and bile acids (Figure 1).

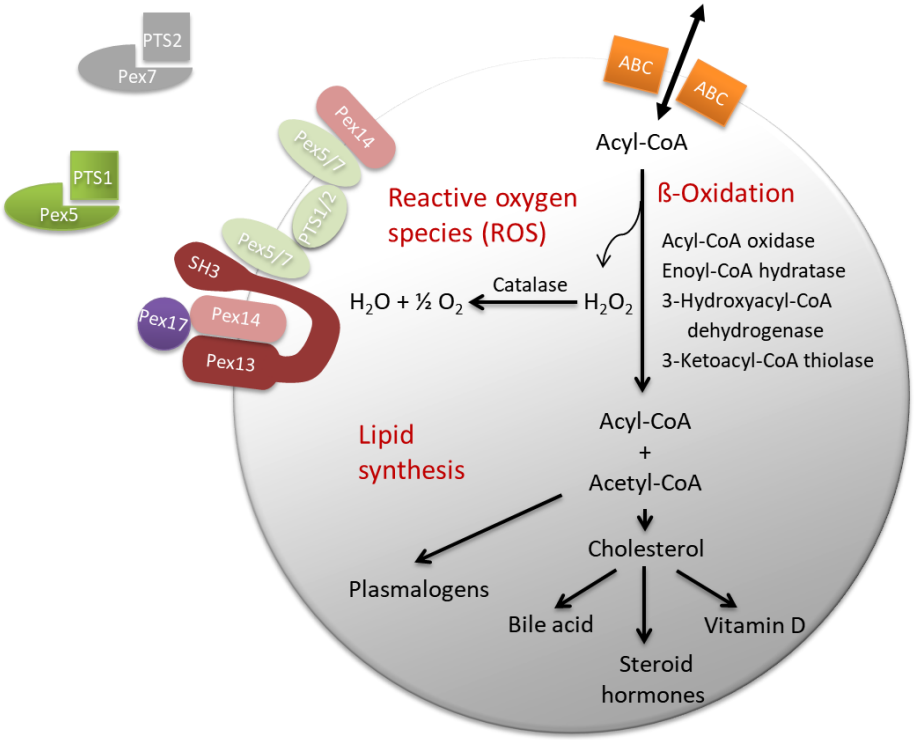

Figure 1| Simplified scheme of the peroxisomal compartment. The peroxisome is mainly involved in the degradation of VLCFs and their derivatives via *β*-oxidation, synthesis of ether lipids, steroids and cholesterol, catabolism of purines and biosynthesis of glycerolipids and bile acids (modified according to (Nenicu *et al.* 2007).

1.1.1 Peroxisome biogenesis

As most other organelles, peroxisomes lack their own DNA. They do not have an endosymbiotic origin and proteins were derived from primitive eukaryotes (Gabaldon *et al.* 2006). Peroxisomes are generated *de novo* from the endoplasmic reticulum (ER) through budding and heterotypic fusion of two vesicles under the control of PEX1 and PEX6. The mechanism was initially described in *Saccharomyces cerevisiae* (Titorenko *et al.* 2000). As also shown in mammalian cells, mature peroxisomes multiply by growth and fission, mediated by PEX11 (Opalinski *et al.* 2011; Schrader *et al.* 2016). Peroxisomal assembly and division are maintained by the function of essential peroxisomal proteins, called peroxins (Purdue and Lazarow 2001; Ma *et al.* 2011). Peroxisomes elongate by means of PEX11 (PEX11*β* in mammalian cells) and membrane anchored dynamin-related protein (DRP)-interacting proteins (Lazarow and Fujiki 1985). Tubulation and elongation is regulated by external stimuli and the exposure to growth factors or polyunsaturated fatty acids (PUFAs) (Schrader *et al.* 1999).

1.1.2 Peroxisomal protein synthesis and their import

Peroxin proteins are encoded by PEX genes. Their nomenclature refers to the date of their discovery (Distel *et al.* 1996). Nearly 30 peroxins have been identified so far.

PEX proteins are synthesized on free ribosomes in the cytosol and are post-translationally imported into peroxisomes (Lazarow and Fujiki 1985). Newly synthesized peroxisomal matrix proteins are recognized by cytosolic receptors and are directed to a docking and translocation complex at the peroxisomal membrane. Peroxisomes are able to transport cargoes in a fully folded, co-factor bound and even oligomeric state (Schrader and Fahimi 2008). The import of matrix cargo is enabled by two peroxisomal targeting signals, PTS1 and PTS2 (Erdmann and Schliebs 2005). PTS1 is located at the C-terminal end of the protein and shares a conserved, non-cleavable tripeptide SKL (S/A/C)(K/H/R)(L/M) (Gould *et al.* 1988). PTS1 containing cargoes are post-translationally recognised by PEX5 that contains a conserved C-terminal domain with a tetratricopeptide repeat (TPR) motif and a divergent N-terminal domain (Stanley and Wilmanns 2006). PEX5 has binding capacity not only for PTS1 but also for membrane-bound proteins such as PEX14, PEX3, PEX8 and RING-finger peroxins among its N-terminal region (PEX2, PEX10 and PEX12) (Erdmann and Schliebs 2005; Ma *et al.* 2011). The consensus sequence of PTS2 (R/K)(L/I/V)(X5)(H/Q)(L/A) is recognized by the specific cytoplasmic shuttling receptor PEX7, that directs the proteins to the peroxisomes. Loaded with their cargo, the shuttling receptors bind to the peroxisomal protein import machinery, also described as docking complex or importomer, before the receptor-cargo complex will be translocated into the peroxisome (Nair *et al.* 2004; Rayapuram and Subramani 2006).

The docking complex is assembled by PEX13, PEX14 and PEX17 (Schell-Steven *et al.* 2005). It is linked to a RING-finger motif by PEX8 (Agne *et al.* 2003). The RING subcomplex is composed of PEX2, PEX10 and PEX12 which is a characteristic element of E3 ubiquitin ligases and therefore facilitates PTS receptor recycling and degradation. The last complex is a receptor/ co-receptor recycling machinery composed of PEX4 and two ATPases. PEX4 is a member of the E2 family of ubiquitin-conjugating enzymes; it is anchored to the peroxisomal membrane through the cytosolic domain of PEX22. The two ATPases (PEX1 and PEX6) are associated with a variety of different cellular activities (AAA+ proteins); the AAA+ complex is attached to the membrane through membrane protein PEX26 (Erdmann and Schliebs 2005).

1.1.3 Peroxisomal function

Peroxisomes are involved in catabolic and anabolic processes which are important for proper cell function and proliferation. Metabolic processes include degradation of VLCFs via β-oxidation,

synthesis of ether lipids and cholesterol, catabolism of purines and biosynthesis of glycerolipids and bile acids (Wanders and Waterham 2006a).

1.1.3.1 Metabolite transport

The transport of molecule substrates and products across the membrane is facilitated through specific proteins that either function as carrier of matrix proteins to maintain all metabolic functions or are part of a transport system (Subramani 1996; Girzalsky *et al.* 2009; Girzalsky *et al.* 2010). One of the major constituents of the peroxisomal membrane is the ATP-binding cassette (ABC) transporter of subfamily D (ABCD) that functions in the translocation of substrates for peroxisomal β-oxidation.
In mammalian peroxisomes, three ATB-binding cassette transporters of type D have been identified. ABC transporters require homo- or hetero-dimerization to constitute a fully active unit (Baker *et al.* 2015). The most prominent one is ABCD1 that is also known as ALDP (adrenoleukodystrophy protein). As a result of mutated *ABCD1* gene, unbranched, saturated and VLCFAs are accumulated in the cell which is the main characteristic of ALD (Mosser *et al.* 1993; Kemp and Wanders 2007). The two other members are ABCD2 (adrenoleukodystrophy-related protein (ALDR) (Feigenbaum *et al.* 1996) and ABCD3 (70 kDa peroxisomal membrane protein (PMP70) (Imanaka *et al.* 1996; Tanaka *et al.* 2002).
The specificity of ABCD transporters for acyl-CoA esters is different in yeast. ABCD1 prefers the transport of hydrophobic C24:0-CoA and C26:0-CoA, whereas ABCD2 preferentially transports C22:0-CoA, C22:6-CoA and C24:6-CoA. ABCD3 is required for the metabolic transport of long-chain unsaturated acyl-CoAs, 2-methyl branched-chain acyl-CoAs and long-chain dicarboxylic CoA esters across the peroxisomal membrane (Baker *et al.* 2015).

1.1.3.2 Fatty acids (FA)

Fatty acids are either synthesized and elongated by *de novo* lipogenesis (DNL) in the liver (Hellerstein 1999), by peripheral lipolysis (breakdown of lipids) or derived from the diet (fruits, vegetable oils, seeds, nuts, animal fats, and fish oils). They consist of long hydrocarbon chains with a carboxyl group and a various number of double bonds. Fatty acids are distinguished into saturated (SFA), monounsaturated (MUFA; ω-7 and ω-9) and PUFAs (ω-3 and ω-6), depending on the position of an incorporated double bond, counted from the first methyl group. Usually, they consist of even numbers of carbon atoms, ranging from 14 to 24 (Gibson 1965).
De novo fatty acid synthesis up to palmitic acid (C16:0) takes place in the cytosol by means of fatty acid synthase (FAS). For DNL, acetyl-CoA is required, that mainly derives from carbohydrates via the glycolytic pathway, and will be carboxylated to malonyl-CoA to produce a keto acid. A polymer is produced through condensation, dehydration and reduction of the keto acid, to synthesize a methylene

group from the carbonyl group. This process will be repeated until a C16-fatty acid will be fully synthesized (Gibson 1965). VLCFAs (≥ C20) are synthesized in the ER, peroxisomes (Horie *et al.* 1989) and in mitochondria by elongation of corresponding enzymes (ELOVLs) (Das *et al.* 2000).
Seven ELOVL proteins are known of which ELOVL1, ELOVL3, ELOVL6 and ELOVL7 are involved in the elongation of MUFAs, whilst ELOVL2, ELOVL4 and ELOVL5 utilize PUFAs as substrate (Pereira *et al.* 2004; Jakobsson *et al.* 2006). Elongation of α-linolenic (18:3(ω-3)) and stearidonic acid (18:4(ω-3)) as well as linoleic (C18:2(ω-6)) and γ-linolenic acid (C18:3(ω-6)) is regulated by ELOVL5 (Sprecher *et al.* 1995). The desaturation step from linoleic into γ-linolenic acid and α-linolenic into stearidonic acid is performed by Δ6-fatty acid desaturase (FADS2) (Cho *et al.* 1999).
Fatty acid *β*-oxidation is a central metabolic process. During mitochondrial *β*-oxidation, fatty acids up to a length of 22 carbon atoms will be catabolized, providing electrons to the respiratory chain and thus energy in form of ATP (Bartlett and Eaton 2004). VLCFAs are shortened in peroxisomes (van de Beek *et al.* 2017) for further mitochondrial fatty acid *β*-oxidation and as a pre-requisite for plasmalogens and cholesterol biosynthesis (Ghisla 2004). Saturated fatty acids with an even number of C-atoms will be degraded by usual *β*-oxidation, producing a trans-Δ-enoyl-CoA double bond, followed by hydration and oxidation to produce acetyl-CoA and acyl-CoA. Oxidation of unsaturated fatty acids requires two additional enzymes: isomerase and reductase. The enzyme isomerase recruits existing *cis*-Δ-double bonds into *trans*-Δ-double bonds followed by oxidation steps. The enzyme reductase is involved in the *β*-oxidation and metabolism of polyunsaturated fatty enoyl-CoA esters during the conversion of the intermediate 2,4-dienoyl-CoA thioesters to *trans*-Δ^3-enoyl-CoA. To end up in a hydrocarbon chain, the carbonyl group must be reduced (Reddy and Hashimoto 2001).

1.1.3.3 Peroxisomal *β*-oxidation

During peroxisomal *β*-oxidation, free energy is released in form of heat (Schrader and Fahimi 2006). The chain shortening of acyl-CoA esters is catalysed yielding chain-shortened acyl-CoA and acetyl-CoA (Poirier *et al.* 2006), as well as octanoyl-CoA and propionyl-CoA that are conjugated to carnitine and shuttled to mitochondria. The shortened products will further be oxidized under the generation of ATP via the mitochondrial electron transfer chain (Ferdinandusse *et al.* 1999; Reddy and Hashimoto 2001). In the initial step of peroxisomal *β*-oxidation, H_2O_2 is produced through electron transfer onto an oxygen molecule performed by a flavoprotein dehydrogenase. The enzyme catalase is needed to catalyse the decomposition of hydrogen peroxide to water and oxygen (Braverman *et al.* 2013).
The basic processes of fatty acid *β*-oxidation are similar to mitochondrial *β*-oxidation, but performed with different enzymatic isoforms. Substrates used for peroxisomal metabolism are pristanic acid which is derived from dietary sources, hexacosanoic acid (C26:0), and di-and trihydroxycholestanoic acid (DHCA and THCA) from cholesterol in the liver, long-chain dicarboxylic acids as product of omega-oxidation of long-chain monocarboxylic acids, specific prostaglandins and leukotriens, some

xenobiotics as well as vitamins E and K (Wanders and Waterham 2005). One cycle of peroxisomal *β*-oxidation is also required for the synthesis of docosahexaenoic acid (C22:6ω3; DHA), a ω-3 PUFA. DHA is synthesized from linolenic acid and requires several desaturation and elongation steps and is regulated by ELOVL5 and ELOVL2 (Gregory *et al.* 2013). DHA together with arachidonic acid (20:4(ω-6); AA) and eicosapentaenoic (20:5(ω-3); EPA) contributes to phospholipids and therefore regulate cell membrane fluidity (Stoffel *et al.* 2008). DHA is highly abundant in membrane phospholipids of round spermatids (Grogan *et al.* 1981) and mature spermatozoa (Rejraji *et al.* 2006).

1.1.3.4 Reactive oxygen species (ROS)

ROS are formed as by-products from electron-transfer reactions that are produced by mitochondria, peroxisomes and the ER. ROS is a collective term for oxygen-derived radical species, including superoxide anion (primary form), hydrogen peroxide, hydroxyl radical and peroxyl radical (secondary form) as well as nitrogenous compounds (peroxynitrous acid, nitroxyl anion, peroxynitrile, and nitrous oxide) (tertiary form) (Iommiello *et al.* 2015). They are considered to have toxic effects on lipids, proteins and nucleic acids (Freeman and Crapo 1982; Pizzimenti *et al.* 2010) and they are linked to cytoskeletal modifications and inhibition of cellular mechanisms (Hinshaw *et al.* 1986; Davies 1987). To protect the cell from damaging effects caused by ROS, they must be degraded by antioxidant enzymes such as superoxide dismutase (which reduces O_2^- to H_2O_2), catalase, and glutathione peroxidase (which reduces H_2O_2 to H_2O). Peroxisomal detoxification includes several H_2O_2 generating enzymes: glycolateoxidase, D-amino acidoxidase, urateoxidase, L-a-hydroxyacidoxidase, and fatty acyl-CoA oxidase (Boveris *et al.* 1972). The oxidative reactions are important to detoxify a variety of toxic molecules (e.g. ethanol), particularly in liver and kidney. The main contributors of H_2O_2 generation in mammals are the peroxisomal *β*-oxidation of fatty acids (1.1.3.3), the enzymatic reactions of the flavin oxidases, the disproportionation of superoxide radicals (Schrader and Fahimi 2006). The expression of *β*-oxidation enzymes is elevated when activators of the peroxisome proliferator activator receptors (PPARs), like fibrates or free fatty acids, are applied (Fahimi *et al.* 1982; Schrader and Fahimi 2006). These conditions generate oxidative stress that describes an imbalance of oxidant production and antioxidant capacity (Thannickal and Fanburg 2000). It may lead to age-related and chronic diseases including aging, cancer, cardiovascular disease, diabetes, chronic inflammation, and neurodegenerative disorders (Cooke *et al.* 2003; Chakravarti and Chakravarti 2007). In terms of male fertility, ROS can negatively influence the sperm concentration, motility and morphology leading to leukocytospermia, varicocele and idiopathic infertility (Pasqualotto *et al.* 2000). Besides their harmful roles, ROS have also important function as mediators in cell signalling and regulation (Finkel 1998). Low concentration of H_2O_2 is required for proliferation, apoptosis and carbohydrate metabolism (Bonekamp *et al.* 2009).

1.1.4 Peroxisomal disorders

Peroxisomal disorders are subdivided into two groups. One group comprises peroxisomal biogenesis disorders (PBD), the other one includes single peroxisomal enzyme and substrate transport deficiencies (Wanders and Waterham 2006b).

1.1.4.1 Peroxisomal biogenesis deficiencies (PBD)

Peroxisomal biogenesis deficiencies (PBDs) are characterized by defective PTS1- and PTS2- mediated import of peroxisomal matrix proteins (Slawecki *et al.* 1995), leading to peroxisomal metabolic dysfunction and a decline in peroxisome formation (Maxwell *et al.* 2003).

Mutations in one of the 13 *PEX* genes cause Zellweger spectrum disorders that are a heterogenous group of autosomal recessive disorders (Waterham and Ebberink 2012; Fujiki *et al.* 2014). ZSDs include Zellweger syndrome (ZS), neonatal adrenoleukodystrohpy (N-ALD) and infantile Refsum disease (IRD), whose symptoms result from the accumulation of VLCFAs, phytanic- and pristanic acid, C27-bile acid intermediates and pipecolic acid in plasma (Wanders and Waterham 2006a). The ZS, also known as cerebrohepatorenal syndrome, is the most severe form of PBDs (Steinberg *et al.* 2006). It affects the physical development with defects in brain morphogenesis (e.g. characteristic craniofacial dysmorphism with high forehead) as well as the sensory system with impact on the muscle tone, resulting in hypotonia, seizures, loss of vision and hearing. Infants do not survive their first year (Braverman *et al.* 2013).

Patients with neonatal ALD (N-ALD) show less severe symptoms. N-ALD results from mutations in *PEX1* (encodes a protein that is a member of AAA-type ATPases), *PEX5*, encoding for PTS1, *PEX10* and *PEX13* that interacts with the PTS1 receptor. Leukodystrophy occurs in early childhood with active demyelination in the cerebrum, midbrain and cerebellum, resulting in progressive psychomotor regression (Aubourg *et al.* 1986). Patients can at least survive a decade.

Brain development is also affected in patients with IRD (Scotto *et al.* 1982; Steinberg *et al.* 1993). Due to mutated *PEX1*, *PEX3*, *PEX6*, *PEX12* and *PEX26* (Waterham and Ebberink 2012), patients have increased phytanic acid levels and display minor dysmorphism, mental retardation, hepatomegaly, sensorineural hearing loss, retinal pigmentary degeneration and hypocholesterolaemia (Dubois *et al.* 1991; Naidu and Moser 1991). In contrast to the more severe types of ZSD, no neuronal migration disorder and progressive white matter disease can be observed in these patients (Wanders and Waterham 2006b).

Another candidate of the group of PBDs is rhizomelic chondrodysplasia punctata (RCDP) type 1. Unlike ZSDs, mutations in *PEX7* are associated with RCDP type 1 (Braverman *et al.* 2010). Patients usually suffer from dwarfism, with shortened proximal parts of the extremities, typical facial appearance, severe mental retardation with spasticity and ocular abnormalities (de Kretser *et al.* 1981).

1.1.4.2 Peroxisomal single-enzyme/ transporter deficiencies

Peroxisomal single enzyme or transport deficiencies are classified with respect to the affected peroxisomal pathway. A defect in ether phospholipid biosynthesis results in RCDP of type 2. Due to a mutation in *GNPAT*, the enzyme DHAPAT is deficient (Wanders *et al.* 1992) resulting in the inability to synthesize ether phospholipids, including plasmalogens (Wanders and Waterham 2006b; Wanders and Waterham 2006a). The symptoms overlap with those of RCDP of type 1. These refer to abnormalities, hypotonia, dwarfism and shortening of extremities (Braverman *et al.* 2013).
A disturbance in peroxisomal β-oxidation results in an increase of peroxisomal metabolites. Five disorders that belong to this group are characterized so far: X-ALD, acyl-CoA oxidase deficiency, D-bifunctional protein deficiency, sterol carrier protein X (SCPx) deficiency, and 2-methylacyl-CoA racemase (AMACR) deficiency (Wanders and Waterham 2006b). The most frequent single peroxisomal disorder with a minimum incidence of 1:21.000 males in the USA to 1:15.000 males in France is X-ALD (Kemp *et al.* 2001) that is characterized by a mutation in the *ABCD1* gene that causes the accumulation of VLCFAs in the cell (Mosser *et al.* 1993). One phenotype is referred to as AMN, a combination of a myelopathy and a peripheral neuropathy (Moser *et al.* 2007). The other phenotype is termed as childhood cerebral ALD (CCALD). Symptoms include behavioural, cognitive and neurologic deterioration (Wanders and Waterham 2006b). It can also occur during adolescence (adolescence cerebral ALD; ACALD) or adulthood (adult-cerebral ALD) (Wanders and Waterham 2006b; Wanders and Waterham 2006a). Patients with X-ALD are predominantly affected by adrenocortical dysfunction, most of them before having entered adulthood. Consequently, they do not produce adequate amounts of steroid hormones and display myelopathies (Dubey *et al.* 2005). In a publication from 1981, X-ALD could be associated with abnormalities in testicular function and development (Powers and Schaumburg 1981).

1.1.5 Peroxisomal dysfunction and male fertility

Powers and Schaumburg analysed testes biopsies of young X-ALD patients (from 8 to 9-year-old boys) at the ultrastructural level. Although the number of interstitial cells was equal to healthy control biopsies, they detected perinuclear linear clefts with electron-dense lamellar fragments intermixed with vesicles of the ER and pale lipid droplets (LD; (Powers and Schaumburg 1981). The group of Assies (1997) also examined the effects of X-ALD on testicular function. In more than 50 % of tested cases, erectile dysfunction and diminished body sexual hair was described. Beyond these findings, patients showed a diminished libido, cryptorchidism (absence of at least one testis in the scrotum), gynaecomastia (enlargement of male breast tissue) and small testes. Interestingly, plasma testosterone (T) concentrations were at the lowest level of normal range. In a more recent study published by

Stradomska et al. (2012) X-ALD and AMN patients (aged 24-48) displayed Leydig cell and/or Sertoli cell dysfunction with very high levels of ABCD1 in Sertoli cells. Luteinizing hormone (LH) and follicle-stimulating hormone (FSH) levels were slightly increased in both groups. A semen analysis was performed in a case study, published in 1998. The 22-year-old patient showed severe asthenoteratozoospermia with abnormal sperm motility and morphology as double heads and disrupted membranes. The sperm number was reduced, accompanied with a decline of fertility (Aversa *et al.* 1998).

1.2 Infertility

The proper definition for infertility is the failure to conceive after one year of unprotected intercourse. It approximately concerns 72.4 million people worldwide (Coutton *et al.* 2015a; Coutton *et al.* 2015b). The parameter for testing male fertility are sperm concentration, sperm motility and morphology (Kumar and Singh 2015). Parameters below the World Health Organization (WHO) values count for male factor infertility (Plachot *et al.* 2002). According to statistics from 2014, imposed by the European Society of Human Reproduction and Embryology (ESHRE), 20-30 % of infertility cases are explained by physiological causes in men, 20-35 % cases are attributed to the female, and 25-40 % cases to both partners (https://www.eshre.eu/guidelines-and-legal/art-fact-sheet.aspx). Unexplained male infertility (UMI) still affects approximately 15 %, although studies range from 6 % to 37 % UMI. The studies also include infertile patients with normal semen analysis, normal history and physical examination and when the female factor infertility can be excluded (Moghissi and Wallach 1983; Collins and Rowe 1989; Collins and Crosignani 1992; Hamada *et al.* 2011). Environmental, behavioural and genetic factors are the source of infertility (Cooke and Saunders 2002). These include the presence of antisperm antibodies, sperm DNA damage, elevated levels of ROS and sperm dysfunction. Dysfunction along the hypothalamic-pituitary gonadal axis affects hypogonadotrophic hypogonadism and Kallmann syndrome, direct trauma, inflammation or infection of the testis, varicocele, cryptorchidism, Y-chromosome microdeletions, testicular cancer, erectile dysfunction, infrequent or retrograde ejaculation, epididymitis, congenital bilateral absence of the vas deferens, Klinefelter's syndrome (47,XXY), and Sertoli cell-only syndrome (Agarwal *et al.* 2014). Sperm abnormalities are categorized into azoospermia (no spermatozoa in the ejaculate), oligospermia (sperm concentration is less than 20 mio ml^{-1}), asthenospermia (less than 50 % of spermatozoa have normal motility or less than 25 % have any motility) and teratozoospermia (less than 30 % of spermatozoa have a normal morphology).

1.3 The male reproductive system

The genital ridge is established through migration of primordial germ cells and somatic progenitor cells that express a variety of transcription factors. In mammalian species, the *SRY* gene (sex-determining region of the Y chromosome) determines the sex of the gonads. Androgens maintain the male phenotype, that is characterized by external and internal male reproductive organs (Lejeune *et al.* 1998). The internal sex organs refer to the accessory glands including the vas deferens (*Ductus deferens*), the seminal vesicles (*Glandulae vesiculosae*), the prostate and the bulbourethral glands (Cowper´s gland). The external organs comprise the penis, the testes that are embedded in the scrotum, and the epididymis. The testes are oval shaped organs; they are involved in androgen synthesis, designated as steroidogenesis, and the production of spermatozoa, as consequence of differentiating germ cells, a process called spermatogenesis.

The testicles are covered by a multi-layered tunica: the *Tunica vasculosa*, the *Tunica albuginea* and the *Tunica vaginalis*. The *Tunica vasculosa* is the inner layer and facilitates blood supply to the testes. It is covered by the *Tunica albuginea* that encapsulate the testis. It connects to fibres surrounding the epididymis. The *Tunica albuginea* is involved in blood flow regulation, inter-testicular pressure and contraction to induce sperm movement (Setchell 1994). It is overlaid by a third layer, the *Tunica vaginalis*. The *Mediastinum testis*, which is a network of thick fibrous connective tissue, extends from the top to the bottom of the testis. It contains the rete testis, blood and lymphatic vessels.

Testicular septa radiate from the *Mediastinum testis* to the *Tunica albuginea* (de Kretser 1979). They partition the testis into lobules (*Lobuli testis*) that contain the seminiferous tubules (*Tubuli seminiferi*), arranged as tubes. They contribute to approximately 90 % of adult mass; the remaining 10 % are interstitium consisting of blood and lymph vessels as well as the steroid producing Leydig cells (Schlatt and Ehmcke 2014). Spermatogenesis takes place in the germinal epithelium of the seminiferous tubules, containing germ cells and Sertoli cells. The outer layer of seminiferous tubules are composed of contractile peritubular cells that support the release of immature spermatozoa from the seminiferous epithelium into the tubule lumen (Dym and Fawcett 1970). The spermatozoa still lack the capacity to swim and to fertilize an egg. They acquire their function during the transit in the tubules to the epididymis. Spermatozoa initially enter the head (*caput*) of the epididymis via the efferent ducts of the *Mediastinum testis*. They proceed through the body (*corpus*) to the tail (*Cauda*) that serves as a storage reservoir (Cooper *et al.* 1986; Thong *et al.* 2014). During ejaculation, the prostate glands produce and secrete alkaline seminal fluids (about 30-35 % of the semen ejaculate) that help the sperm to survive in the acidic vaginal environment. The fluids from the prostate are mixed with those from the seminal vesicles and other accessory glands. Smooth muscle cells are inside the prostate stroma that contract to press the fluid into the urethra. Semen is formed, which will then be released as ejaculate (Verze *et al.* 2016).

1.3.1 Spermatogenesis

Spermatogenesis is the process of germ cell division and differentiation to produce spermatozoa. It occurs in the germinal epithelium of coiled seminiferous tubules (Lie *et al.* 2013). It is regulated by growth factors and hormones via the hypothalamic-pituitary-gonadal axis to facilitate a gene-controlled cyclic process, with successive mitotic, meiotic and post-meiotic phases.
In mammals, spermatogenesis can be divided into three phases: in the first phase, diploid spermatogonia proliferate and undergo a series of mitotic divisions to progressively develop into primary and secondary spermatocytes. During the second phase, spermatocytes meiotically divide into spermatids. In the last phase, a process that is characterized as spermiogenesis, spermatozoa will be released from the epithelium (O'Donnell *et al.* 2011). Immotile spermatozoa will finally mature in the epididymis (Hess and Renato de Franca 2008).

1.3.1.1 Germ cell differentiation and spermiogenesis

Germ cells are arranged in a highly-structured, sequential order from the basement membrane towards the lumen. The stem cells of the germinal epithelium, known as spermatogonia, reside at the peripheral basement of the seminiferous tubule. In men, undifferentiated spermatogonia are classified into type A dark spermatogonia (A_d), type A pale spermatogonia (A_p), and type B spermatogonia (B). Type A_d spermatogonia maintain the supply of stem cells, type A_p mitotically divide to produce identically clones that are linked via cytoplasmic bridges and type B mitotically divide into primary spermatocytes (Clermont 1972). In rodents, self-renewing, undifferentiated spermatogonia correspond to A single (A_s), A paired (A_{pr}), and A aligned (A_{al}) spermatogonia (Nishimune *et al.* 1978; de Rooij 2001). A_s spermatogonia either undergo self-renewal to generate new spermatogonial stem cells or differentiate into two A_{pr} spermatogonia (de Rooij 1998). The latter will divide into 4, 8, 16 and sometimes 32 Aal spermatogonia (Jan *et al.* 2012). After a series of mitotic cell divisions, spermatogonia of type B are formed (de Rooij and Russell 2000; Aponte *et al.* 2005). B spermatogonia mitotically divide into primary spermatocytes. Preleptotene/leptotene spermatocytes undergo the first round of meiosis to give rise to secondary spermatocytes. After a second round of meiotic division, chromatids will finally be separated generating haploid round spermatids (Handel and Schimenti 2010). Meiosis into haploid spermatids lasts ~11 days in mouse (Eddy 1998). During spermiogenesis, round spermatids transform into spermatozoa with fully compacted chromatin. Spermiogenesis includes several events like acrosome formation, condensation of the nucleus and sperm tail development, reorganization of cellular organelles and reduction of cytoplasm. The acrosome is formed by the Golgi complex and contains hydrolytic enzymes as a prerequisite to penetrate the egg during fertilization. It eventually forms a cap structure over the nucleus in mature spermatozoa (Cooke and Saunders 2002). Mature spermatozoa free themselves from Sertoli cells. With entering the lumen

of the seminiferous tubule, they will finally be released as spermatozoon, in a process called spermiation (O'Donnell *et al.* 2011) (Figure 2) .

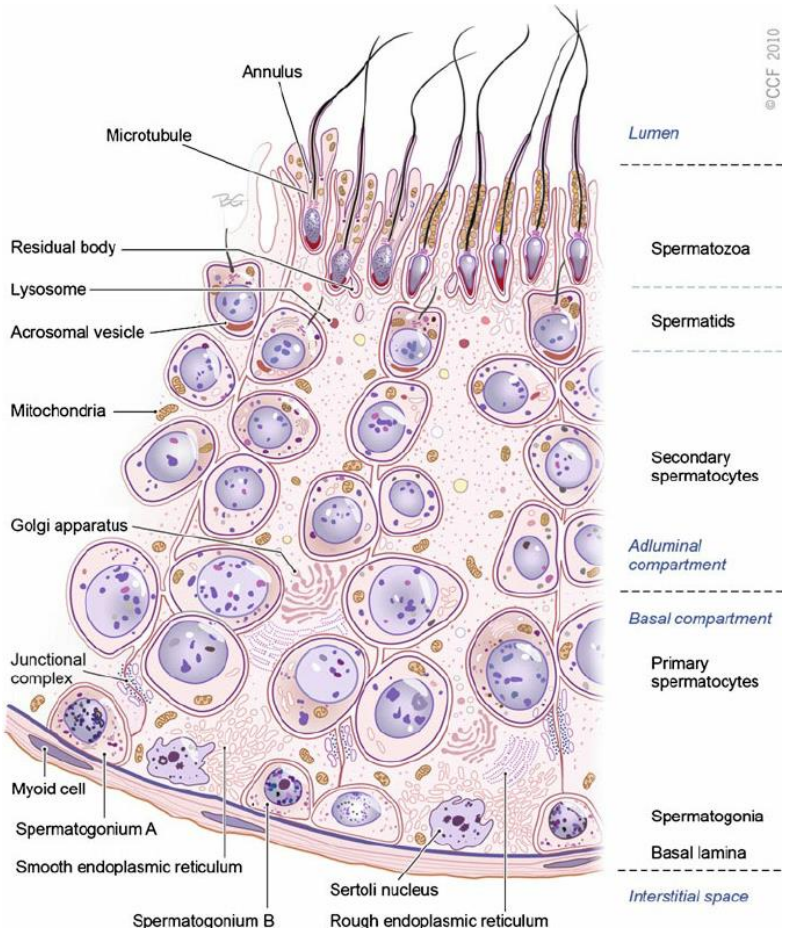

Figure 2| Schematic representation of the germinal epithelium. The germinal epithelium is divided into a basal lamina and an adluminal compartment, maintained by Sertoli cells. The basal lamina contains self-renewing spermatogonia of type A and mitotically dividing spermatogonia of type B that form primary spermatocytes, diploid (2n) cells. Primary spermatocytes will traverse the BTB whilst undergoing first meiotic divisions generating secondary spermatocytes, haploid cells (1n) cells. These undergo a second series of meiotic divisions to generate round or early spermatids. This type of spermatids is characterized by nuclear condensation, acrosome and flagellum formation and several intracellular transformations to develop into late or elongating spermatids. After the withdrawal of their cytoplasmic content (residual bodies), spermatozoa will be released into the lumen (Sharma and Agarwal 2011).

Depending on the developmental stage, defined physiological characteristics and cell associations are found (Hermo *et al.* 2010). In the mouse, sperm is continuously produced in a well-defined cycle and in an asynchronous manner, characterized as spermatogenic wave. Germ cells enter the cycle of the seminiferous epithelium progressively along the longitudinal axis of the tubules (Davis *et al.* 2013). All stages are involved in spermatogenesis, but spermatozoa are released only in stage VIII. In

humans, sperm is also produced constantly and continuously, but their spermatogenesis is synchronized (Johnson 1994). It is a spiral cellular arrangement that progresses down the tubule (Schulze and Rehder 1984). In humans, spermatogenesis is reported to persist 74 days, with 12 defined stages. One cycle of the seminiferous epithelium lasts 16 days (Amann 2008; Muciaccia *et al.* 2013).

In mouse, 12 different stages of the germinal epithelium were described (Leblond and Clermont 1952; Oakberg 1957; Ahmed and de Rooij 2009) that are defined as followed (Hess and Renato de Franca 2008):

Stage I: Early pachytene spermatocytes are present. The Golgi apparatus, lacking PAS^+ granular material, is small.

Stage I-VIII: In these stages, round and elongated spermatids are found. Round spermatids are recognized by a small nucleus and a large central nucleolus.

Stage II: PAS^+ proacrosomal granules appear in the centre of the Golgi apparatus.

Stage III: Within the larger round Golgi vesicle, an acrosomic granule is formed.

Stage IV: The acrosomic granule begins to flatten.

Stage V: Acrosome forms a cap-like structure over the anterior half of the sperm´s head. B-type spermatogonia are prominent.

Stage VI: The granules of the acrosome are distinct. B-type spermatogonia undergo mitotic divisions to form preleptotene spermatocytes. Elongated spermatids start migrating adluminal.

Stage VII: Thinning of the acrosome that spreads across the nucleus. The elongated spermatids, whose cytoplasm still covers the sperm head and about ½ of the tail, are found at the lumen.

> **Early VII**: The cytoplasm is prominent at the mid-piece of elongated spermatids.
>
> **Middle VII**: A cytoplasmic lobe begins to form as the cytoplasm at the mid-piece continuously vanishes. Distinct, dark granules are still present in the cytoplasm.
>
> **Late VII**: A cytoplasmic lobe is present between sperm head and the basement membrane. The granules are located near the sperm head and below. Preleptotene spermatocytes develop into leptotene spermatocytes as identified by small and fine clumps of chromatin.

Stage VIII: The spermatid´s nucleus is covered by a flattened acrosomal cap. Spermiation starts as elongated spermatids are released into a lumen.

Stage IX: At this stage, round spermatids begin their transition into elongated spermatids. Cytoplasmic lobes that have been released during the former stage fuse into residual bodies that will be phagocytosed by Sertoli cells.

Stage X: The spermatid head forms a protrusion that is covered with a granular acrosome on its ventral side.

Stage XI: Chromatin condensation starts in elongated spermatids as it is identified by a thinner and more elongated nucleus. Diplotene spermatocytes enter diakinesis of meiosis I.

Stage XII: Meiotic and secondary spermatocytes can be found at this stage.

1.3.1.2 Endocrine regulation via the hypothalamic-pituitary-gonadal axis

Testicular cell interactions are mediated by endocrine, autocrine and paracrine signaling via the hypothalamic-pituitary-testicular axis (Steinberger 1971; Parvinen 1982). The release of the gonadotropin-releasing hormone (GnRH) in the hypothalamus is regulated by secreted melatonin, derived from the pineal glands (Blanchard *et al.* 1998). GnRH induces the stimulation of the anterior pituitary to release the main gonadotropic hormones FSH and LH ((Clarke and Cummins 1982). LH stimulates androgen production in Leydig cells upon binding to its LH receptor. It is regulated by feed-back inhibition through testosterone and its aromatized product estradiol (Blok *et al.* 1989). Consequently, testosterone will be reduced and thus stimulate GnRH and LH production again (Matsumoto and Bremner 1989; Roser 2008). FSH directly stimulates the FSH receptor expressing Sertoli cells and induces the synthesis of androgen binding protein (ABP) that is a glycoprotein that acts as carrier for testosterone (Santiemma *et al.* 1992). Inhibin acts over an endocrine feedback signalling between germline stem cells and the pituitary by inhibiting FSH production (Rivier *et al.* 1987; Risbridger *et al.* 1990a; Risbridger *et al.* 1990b; Schlatt and Ehmcke 2014). It antagonizes activins that are members of the transforming growth factor-beta (TGF-β) family and are formed by dimerization of the two subunits β_A and β_B. Activin and FSH influence Sertoli cell and germ cell proliferation in an age-dependent manner (Boitani *et al.* 1995) (Figure 3). The increase of steroidogenesis relies on organelle components, including peroxisomes interacting with lipid droplets (Binns *et al.* 2006) that provide precursors for androgen biosynthesis.

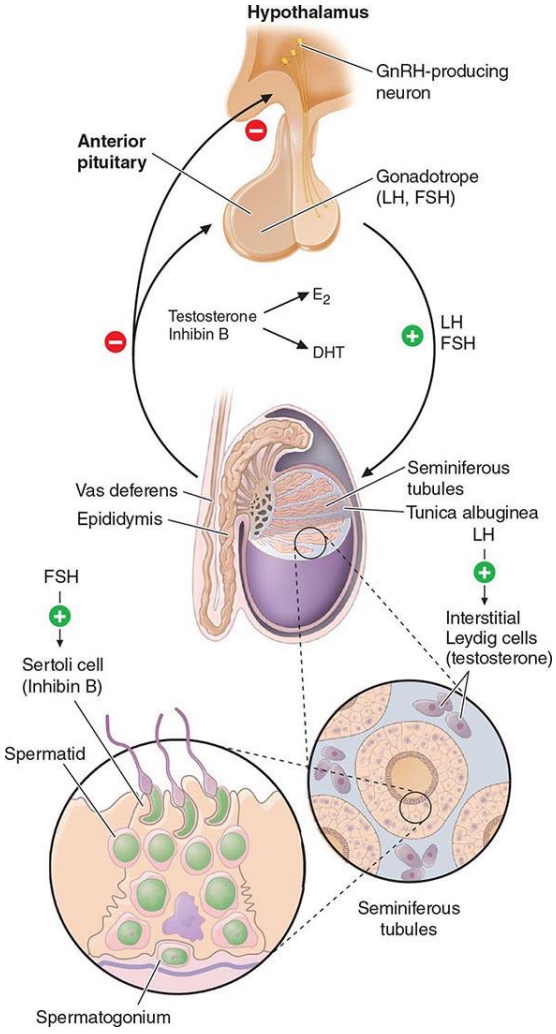

Figure 3| Hormonal control of spermatogenesis via the hypothalamic-pituitary-testicular axis. The pituitary gland secretes LH and FSH that bind to their receptors, located on either Leydig cells or Sertoli cells, respectively. Their secretion is regulated by GnRH. Upon LH secretion, testosterone will be produced. FSH stimulates Sertoli cells to produce ABP, inhibin, DHT and estradiol. ABP bound to testosterone is required for spermatogenesis. LH is negatively regulated by sex steroids, whereas FSH is regulated by feed-back inhibition of sex steroids and inhibin. ABP- Androgen-binding protein; DHT- Dihydrotestosterone; LH- Luteinizing hormone; FSH- Follicle-stimulating hormone (http://clinicalgate.com/wp-content/uploads/2015/04/image1237926.jpeg).

1.3.2 The Sertoli cell

The Sertoli cell is easily recognized by its irregular shaped nucleus and its large centrally located nucleolus (Jean *et al.* 1983; Ye *et al.* 1993). Sertoli cells have a thick basal lamina and are thus classified as epithelial cells. However, they differ from all other epithelial cells as they lack intermediate sized filaments of the keratin type but have in return vimentin intermediate filaments (Franke *et al.* 1979; Domke *et al.* 2014). In addition to sER, mitochondria, peroxisomes and

lysosomes, they also contain lipid inclusions and protein crystals. The amount of LDs varies according to the stage of the spermatogenic cycle (Niemi and Kormano 1965; Jutte *et al.* 1985). Compared to germinal cells, Sertoli cells have a higher ratio of esterified to un-esterified cholesterol. Sertoli cell functions comprise phagocytosis (Chemes 1986) and paracrine regulation of testicular size, structural organization and regulation of the number of spermatozoa through secretion of regulatory proteins as peptide growth factors and hormones (Orth *et al.* 1988).

1.3.2.1 Blood-testis barrier (BTB)

The BTB is formed by the junctional complex between Sertoli cells that divides the epithelium into a basal and an apical compartment (Griswold 1995). The apical and lateral processes of Sertoli cells surround adjacent germ cells to mechanically support and provide germ cells with important nutritional and physical factors (Mruk and Cheng 2004). It has been claimed for a long time that Sertoli cell to germ cell contact is maintained by desmosomes and desmosome like-junctions (Gilula *et al.* 1976), gap junctions, ectoplasmic specialization (Russell *et al.* 1988) and tubulobular complexes (Russell and Malone 1980). However, the group of Werner Franke clarified that Sertoli cells lack desmosomes and "desmosome-like" junctions (Domke *et al.* 2014). The dynamics of the BTB is regulated by specific adherens junctions based on N-cadherin (Domke *et al.* 2014), gap junctions, polarity proteins and tight junction (TJ) proteins, such as claudins, occludin and zonula occludens (ZO) (Chihara *et al.* 2010; Cheng *et al.* 2011a). Another barrier is formed by TJs in microvessels within the interstitium. However, the endothelial barrier does not remarkably support the BTB in rodents and primates (Dym and Fawcett 1970). Most of the BTB proteins are anchored to tightly packed actin filament bundles between cisternae of ER and the opposing plasma membranes of two adjacent Sertoli cells (Cheng *et al.* 2011a; Cheng *et al.* 2011b). The TJ proteins, namely claudins and occludins, consist of four transmembrane domains whose N-and C-terminal ends are directed to the cytoplasm (Tsukita *et al.* 2001). Their major function is to protect germ cells from the circulatory and lymphatic system and therefore providing them an immune privileged microenvironment for meiosis (Griswold 1995; Fijak and Meinhardt 2006), by preventing trespassing of molecules larger than 1.000 Da. In total, 24 members of the claudin family are known with organ-specific expression patterns (Tsukita *et al.* 2001). In mice, claudin-11 is specifically expressed in the Sertoli cells (Morita *et al.* 1999) and peaks between postnatal day 6-16 as BTB formation initiates (Jiang *et al.* 2014). From late stage VIII to early stage IX of the seminiferous epithelial cycle (Russell, 1977), preleptotene/leptotene spermatocytes traverse the barrier from the basal to the adluminal part whereby the BTB undergoes structural rearrangements to facilitate the transit of the spermatocytes that are connected by intercellular bridges as "clones" (Fawcett 1961). During the migration of spermatocytes through the BTB, the TJ protein claudin-3 is mainly involved by establishing new TJ fibrils below the preleptotene/leptotene spermatocytes (Chihara *et al.* 2010; Smith and Braun 2012).

1.3.2.2 Phagocytosis of residual bodies

As late spermatids enter spermiogenesis, their caudal cytoplasmic mass consists of a Golgi complex, mitochondria, peroxisomes, annulate lamellae, a chromatoid body, ribosomes, a few large vacuoles, myelin-like membrane profiles and sporadic LDs (Breucker *et al.* 1985). At the step of detachment, late spermatids shed the excess cytoplasm as residual bodies that remain at the surface of the seminiferous tubule (Kerr and de Kretser 1974). The cytoplasmic content is avoid of the chromatoid body, but still contains organelles, as condensed mitochondria and peroxisome-like structures (Nenicu *et al.* 2007), ribosomes as a single complex, and lipids. The Golgi complex is present as aggregations of vesicles (Breucker *et al.* 1985). Upon cytokine stimulation, residual bodies and apoptotic germ cells will be endocytosed and degraded by Sertoli cells (Kerr and de Kretser 1974; Chemes 1986; Lui and Cheng 2007). These vesicles merge to give rise to endosomes which then transform into acid phosphatase-positive multivesicular bodies and into secondary lysosomes (Morales *et al.* 1986). Lysosomes fuse with internalized residual bodies to form a phagolysosome that migrates to the base of the Sertoli cells during stage IX of spermatogenesis (Morales *et al.* 1985; Morales *et al.* 1986). At this step, residual bodies will lose their defined margins and release lipid components that coalesce to form large lipid inclusions within the Sertoli cells at around stage X. These lipid droplets will be incorporated into primary spermatocytes to enable meiosis (Kerr and De Kretser 1975).

1.3.3 Lipid composition in all cells of the seminiferous tubule

As described in the previous section (1.3.2.2), a variety of LDs and vacuoles are found in the cytoplasm of Sertoli cells and will be transmitted to primary spermatocytes (Schulze 1984). Two types of lipid inclusions are found in the cytoplasm of most Sertoli cells: small electron-dense lipid droplets and large electron-lucent lipid vacuoles. Stearic and oleic acids, as well as arachidonic, and docosa-7,10,13,16-tetraenoic acid are most abundant in Sertoli cells. Compared to Sertoli cells, germ cells mainly contain palmitic acid (C16:0) as well as PUFAs, like docosa-4,7,10,13,16-pentaenoic acid (C22:5) and docosa-4,7,10,13,16,19-hexaenoic acid (C22:6) that are products of peroxisomal β-oxidation (Beckman and Coniglio 1979). However, the changes in lipid droplets correlate with the cycle of the seminiferous epithelium (Niemi and Kormano 1965; Paniagua *et al.* 1987). During sexual maturation, 22-carbon polyenes, like docosa-4,7,10,13,16-pentanoic acid in the rat and docosa-4,7,10,13,16-hexanoic acid in the human, accumulate in the testes (Beckman and Coniglio 1979).

1.4 Mouse models of male infertility

Mice are the most favoured animal model to study spermatogenesis due to similarities of germ cells differentiation in mouse and human, conserved gene regulation (Kennedy, 2014), their short reproductive cycle with a large litter size and relatively cheap housing conditions (Cooke and Saunders 2002; Jamsai and O'Bryan 2011). Several studies about testicular dysfunction associated with a single-enzyme deficiency in peroxisomes have been published during the last two decades.

In a study of Rodemer et al (2003), KO mice with a disruption in GNPAT (formerly abbreviated DAPAT or DHAPAT; dihydroxyacetone-phosphate acyltransferase (GNPAT), being associated with a deficiency in plasmalogen synthesis, were sterile. KO mouse testes were atrophic with a spermatogenic arrest and elongated spermatids and spermatozoa were absent. The disruption of the peroxisomal fatty acyl-CoA oxidase (ACOX1) gene in a mouse model created by Fan (1996) (Fan *et al.* 1996b) (Fan *et al.* 1996b) caused a pseudo-neonatal ALD phenotype. The number of Leydig cells and spermatids were significantly reduced, resulting in hypo-spermatogenesis (Fan *et al.* 1996b). Peroxisomal *β*-oxidation has also been interrupted in MFP-2 (multifunctional protein 2, also known as d-bifunctional enzyme) KO mice. The phenotypic profile showed accumulations of neutral lipids in Sertoli cells and a reduction of the PUFA docosapentaenoic acid. Prepubertal mice displayed a loss of post-meiotic germ cells which resulted in a complete testicular atrophy (Huyghe *et al.* 2006).

1.5 Objectives

The most severe forms of peroxisomal disorders are lethal, as lipids and cholesterol are a pre-requisite for cell structure. Moreover, ROS metabolism is essential to provide a toxic-free environment. In less severe forms of peroxisomal dysfunction, as described for patients with AMN and X-ALD, testicular alterations including degenerating Leydig cells, reduction of the seminiferous tubules or even spermatogenic arrest were diagnosed.

So far, only peroxisomal single-enzyme deficiencies have been studied in mouse models. The aim of the present study was to analyse the consequences of a complete peroxisomal dysfunction due to a biogenesis defect in germ cells. The hypothesis is that more severe disturbances will result on cellular level due to abolished peroxisomal function.

Based on the Cre-*loxP* system, a conditional KO of the importomer constituent *Pex13* was induced in either pre- or post-meiotic germ cells, mediated by a transgenic *Stra8*-Cre or *Prm*-Cre promoter, respectively. As an integral membrane protein, PEX13 is involved in the translocation of PEX proteins from the cytosol into the organelle via its cytosolic SH3 domain that interacts with the receptors for PTS1 and PTS2 (Elgersma *et al.* 1996; Erdmann and Blobel 1996). With interfering with the *Pex13*

gene, peroxisomal matrix protein import will be impaired and thus abolish peroxisomal biogenesis. The major aims of the study were:

- To investigate the effects of a peroxisomal dysfunction in the testis and to analyse phenotypic and cellular differences between the pre- and post-meiotic induced peroxisomal KO
- To study spermatogenesis and male fertility in this context
- To characterize the morphology of the testis, pathological alterations of the germinal epithelium and structural integrity
- To identify affected metabolic pathways with focus on peroxisomal β-oxidation, including metabolites and enzyme composition.

2 MATERIALS AND METHODS

All details for primary and secondary antibodies are listed in Table 5 (2.10). Buffer solutions are mentioned in Table 6 (2.11). Reagents and chemicals are summarized in Table 7 (2.12). Kits (Table 8), equipment (Table 9) and specific materials (Table 10) which were used in this study are listed in the last paragraph of the material and method section (2.13).

2.1 Mouse strains used for the study

All mice listed below were housed under standard conditions with free access to standard laboratory food and water and a 12 hrs dark-/light-cycle. The use of mice was in accordance with the Guide for the Care and Use of Laboratory Animals from the Institute for Laboratory Animal Research. The local Ethics Committee approved the study and the procedures were in compliance with the current national laws ("Tierschutzgesetz" TierSchG from 25.05.1998; BGBI IS.1105).

2.1.1 C57Bl/6J mice

Male C57Bl/6J mice (Charles River Laboratories; Sulzfeld, Germany) at the minimum age of 2 months were used for all experiments in order to characterize peroxisomes in germ cells. They were mainly used to backcross either FVB/N or 129S background into C57Bl/6 WT strain to generate a congenic mouse strain based upon marker assisted selection protocol (MASP). After the fourth backcross to B6, the offspring were less than 1 % original background strain and > 99 % B6 (2.2).

2.1.2 GFP-PTS1 transgenic mice

A fusion protein of the green fluorescent protein (GFP) and PTS1 is frequently used for visualization of peroxisomes in living cells (Monosov *et al.* 1996). The transgenic mouse line used in this study has been generated in the laboratory of Professor Zimmer (Department of Neurobiology; University of Bonn, Germany) by injecting a GFP-PTS1 cDNA fragment under the control of the murine *Rosa26* promoter into the pronucleus of CD1 mouse zygotes. The animals used were obtained from the animal facility in Marburg and housed at the animal facility at the University Medical Center Hamburg-Eppendorf (UKE).

2.1.3 *Pex13loxP* transgenic mice

The *Pex13loxP* transgenic mouse line in C57Bl/6J background was provided by Eveline Baumgart-Vogt (Institute for Anatomy and Cell Biology II; Justus-Liebig University, Gießen). The animals went through the embryo transfer at the transgenic animal facilities at the UKE Hamburg. In the transgenic animals, the e*xon 2* of the murine *Pex13* gene is flanked by *loxP* sites (*loxP*: locus of crossing over of the P1 phage). The encoded cDNA sequence of 35 bp is recognized by the enzyme Cre-recombinase (Cre: "catalyses recombination" in the P1 phage). Heterozygous animals of this line were crossed with C57Bl/6J wild-type (WT) animals. Mice heterozygous for *Pex13loxP* were crossed inbred to obtain homozygous mice.

2.1.4 *Stra8*-Cre transgenic mice

The *Stra8*-Cre transgenic animals in FVB/N background were obtained from Jackson laboratory (Bar Harbor, Maine, USA). Heterozygous *Stra8*-Cre animals were crossed with C57Bl/6J WT animals in the central animal facility. The animals specifically express the Cre recombinase in spermatogonia and pachytene spermatocytes before entering meiosis (Oulad-Abdelghani *et al.* 1996), under the control of a transgenic *Stra8* promoter.

2.1.5 *Prm*-Cre transgenic mice

The *Prm*-Cre transgenic animals in 129S background were obtained from Jackson laboratory (Bar Harbor, Maine, USA). Heterozygous *Prm*-Cre animals were crossed with C57Bl/6J WT animals in the central animal facility. The expression of the Cre recombinase is directed by a transgenic *Prm* promoter fragment that is exclusively expressed in spermatids.

2.2 Backcrossing of mouse strains

Mice in either FVB/N or 129S background were backcrossed into C57Bl/6 WT strain to generate a congenic mouse strain, based upon MASP. Mice heterozygous for Cre recombinase (*Stra8*; stimulated by retinoic acid gene 8 or *Prm*; protamine) were selected as parents and crossed to C57Bl/6 mice (F0). Offspring were first screened for their Cre transgene and then screened for the genetic background by single nucleotide polymorphism (SNP) to detect strain differences. SNP enables the identification of mice with highest percentage recipient strain background in each backcross round. Only Cre-transgene positive male mice were selected for SNP analysis by using speed congenics. SNP genotyping was carried out by LGC genomics (Herts, UK). A panel of 100 SNPs in total was tested. Male mice with

the highest percentage of recipient strain were selected to continue with the next cross with the recipient strain. After the fourth backcross to B6 the offspring are less than 1 % original background strain and > 99 % B6.

2.2.1 Breeding strategy to generate *Stra8*-Cre or *Prm*-Cre mediated *Pex13* KO mice

To analyse the physiological function of peroxisomes in testes, a germ cell specific peroxisomal KO was generated before spermatogonia enter meiosis and after meiotic division. The germ cell specific deletion of *exon 2* of *Pex13* was achieved by crossing homozygous male (or female) $Pex13^{loxP/loxP}$ mice in C57Bl/6J background to corresponding female (or male) animals expressing Cre recombinase exclusively in pre- (mediated by *Stra8*) or post-meiotic (mediated by *Prm*) germ cells, respectively, designated as P0 (parental line). Heterozygous male mice (gc*Pex13*HTZ) with one WT allele and either one floxed *Pex13* allele or excised *exon 2* of *Pex13* and positive for Cre recombinase (gc$Pex13^{WT/loxP}$/$Cre^{cr+/cr-}$ or gc$Pex13^{WT/\Delta ex2}$/$Cre^{cr+/cr-}$ from the F1 generation) were obtained and inbred with female siblings of the same genotype to generate KOs (gc$Pex13^{\Delta ex2/\Delta ex2}$/$Cre^{cr+/cr+}$). Mice in the F2 generation carried following genotypes: gc*Pex13*KO (gc$Pex13^{\Delta ex2/\Delta ex2}$/*Stra8*$Cre^{cr+/cr+}$; gc$Pex13^{\Delta ex2/\Delta ex2}$/*Prm*-$Cre^{cr+/cr+}$), gc*Pex13*HTZ ($Pex13^{WT/\Delta ex2}$/*Stra8*-$Cre^{cr+/cr+}$; $Pex13^{WT/\Delta ex2}$/*Prm*$Cre^{cr+/cr+}$) and control (gc*Pex13*WT; $Pex13^{WT/WT}$/*Stra8*-$Cre^{cr+/cr+}$; $Pex13^{WT/WT}$/*Prm*-$Cre^{cr+/cr+}$) mice. Mice of this F2 generation were born with the expected Mendelian frequency and were phenotypically indistinguishable from their littermates after birth. For all experiments, F2 male mice were used (Figure 4).

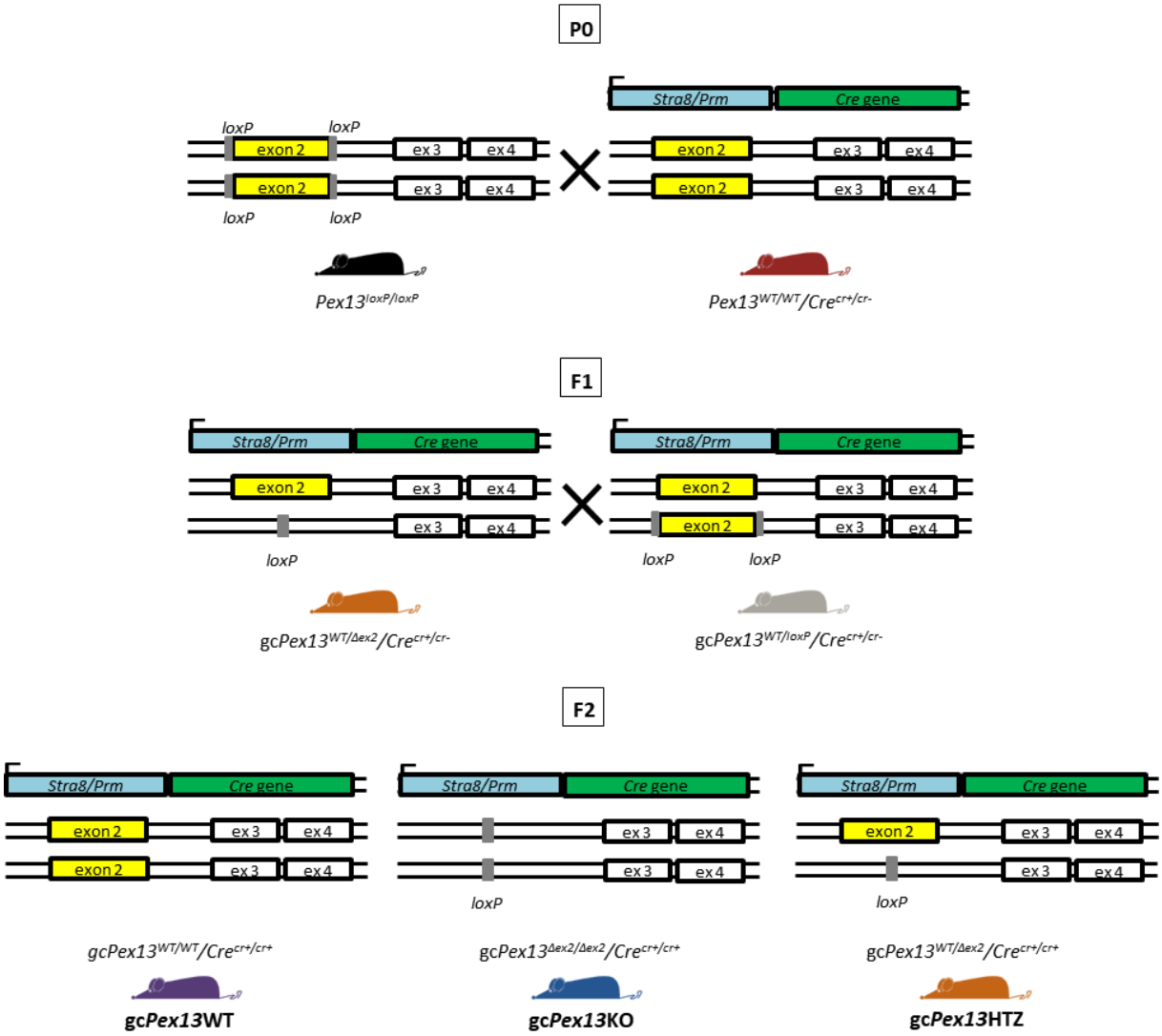

Figure 4| Mating strategy to create tissue-specific gc*Pex13*KO mice. Parental generation **P0**: *Pex13*$^{loxP/loxP}$ (black; homozygous *Pex13-loxP* mouse line) and *Pex13*$^{WT/WT}$/Cre $^{cr+/cr+}$, mediated by either the transgenic *Stra8* or *Prm* promoter (red; heterozygous *Stra8- / Prm*-Cre mouse line); obtained first generation (**F1** offspring), containing heterozygous male (female) (grey; gc*Pex13*$^{WT/loxP}$/Cre$^{cr+/cr-}$ or (orange) gc*Pex13* $^{WT/\Delta ex2}$/Cre$^{cr+/cr-}$), were inbred with female (male) siblings of the same genotype to generate KOs (gc*Pex13* $^{\Delta ex2/\Delta ex2}$/Cre$^{cr+/cr+}$). Mice in the **F2** generation were born with the expected Mendelian frequency carrying following genotypes: control (purple; gc*Pex13*WT; *Pex13*$^{WT/WT}$/*Stra8*-Cre$^{cr+/cr+}$; *Pex13*$^{WT/WT}$/*Prm*-Cre$^{cr+/cr+}$), gc*Pex13*KO (blue; gc*Pex13*$^{\Delta ex2/\Delta ex2}$/*Stra8*-Cre$^{cr+/cr+}$; gc*Pex13*$^{\Delta ex2/\Delta ex2}$/*Prm*-Cre$^{cr+/cr+}$) and gc*Pex13*HTZ (orange; *Pex13*$^{WT/\Delta ex2}$/*Stra8*-Cre$^{cr+/cr+}$; *Pex13*$^{WT/\Delta ex2}$/*Prm*-Cre$^{cr+/cr+}$) mice.

2.3 Genotyping with polymerase chain reaction (PCR)

Mouse tail biopsies were collected for DNA extraction, using the REDExtract-N-Amp Tissue polymerase chain reaction (PCR) Kit. Biopsies were incubated with 50 µl of extraction solution and 12.5 µl tissue preparation for 30 min at room temperature (RT), to extract DNA. The reaction was stopped by heat inactivation at 95 °C and by adding 50 µl neutralization buffer. Mice were tested by

qualitative PCR (qPCR) for their genotype, using the REDExtract-N-Amp PCR Ready Mix. The correct genotype was confirmed by appropriate primer pairs detecting the transgenic *Stra8* or *Prm* promoter mediated Cre recombinase and the flanked *Pex13* gene. For the detection of *Pex13*, the 5´-3´ primer PEX13*loxP*_for and 3´-5´primer PEX13*loxP*_rev were used, to yield a band at 490 bp, representing the WT allele and a band at 540 bp, which represents the floxed *Pex13* allele with two *loxP* sites flanking *exon 2*. Excised *Pex13* was further confirmed by forward and reverse primer pair PEX13Δ, to detect a band at 410 bp. Cre recombinase, mediated by the transgenic *Stra8* promoter, was initially identified with primer pair 5´-3´ *Stra8*_oIMR8773_for and 3´-5´ *Stra8*_oIMR8774_rev to detect a band at 179 bp. Primer sequences were provided by Jackson Laboratory. During the time of the experimental procedures, primer sequences were changed by Jackson Laboratory (for unknown reasons). The oligo-nucleotides were renamed into *Stra8*_oIMR9266_for and 3´-5´ *Stra8*_oIMR9267_rev primer, resulting in a product length of 236 bp. Product size differences are indicated in the appropriate figures. For the detection of the Cre recombinase mediated by the transgenic *Prm* promoter, 5´-3´ primer *Prm*-Cre_Yu_for and 3´-5´ primer *Prm*-Cre_Yu_rev were used, yielding a product of 95 bp. Appropriate primers are listed in Table 1.

Cre-PCR conditions were as follows: first denaturation step at 94 °C for 3 min, followed by 34 cycles (denaturation at 94 °C for 30 sec, annealing at 55 °C for 45 sec, elongation at 72 °C for 1 min), and final elongation at 72 °C for 5 min. For simultaneous detection of the *Pex13loxP* allele and the *Pex13* WT allele, appropriate primers (Table 1) were applied, generating a 540 bp *Pex13*floxed amplicon and a 490 bp *Pex13*WT amplicon. PCR conditions were as follows: first denaturation at 94 °C for 3 min, followed by 29 cycles (denaturation at 94 °C for 3 min, annealing at 57 °C for 45 sec, elongation at 72 °C for 1 min), and final elongation at 72 °C for 5 min. PCR products were separated on a 2.0 % agarose gel containing 0.05 µl/ ml ethidium bromide (10 mg/ml).

Table 1| Primers used for genotyping

Primer	Sequence	Annealing temperature	Product length
PEX13*loxP*_for	ATGGCTCCCAAGTTAGTTCTG	57.9 °C	490 bp WT allele
PEX13*loxP*_rev	TCTGTTTCCCTCCCACCTC	58.8 °C	540 bp *loxP* allele
PEX13Δ_for	TGGCTCCCAAGTTAGTTCTGTC	60.3 °C	410 bp
PEX13 Δ_rev	CCTCTCTATTTGTTGCTTACCCC	60.6 °C	
*Stra8*_oIMR8773_for	GTGCAAGCTGAACAACAGGA	57.3 °C	179 bp
*Stra8*_oIMR8774_rev	AGGGACACAGCATTGGAGTC	59.4 °C	
*Stra8*_oIMR9266_for	AGATGCCAGGACATCAGGAACCTG	64.4 °C	236 bp
*Stra8*_oIMR9267_rev	ATCAGCCACACCAGACACAGAGATC	64.6 °C	
Prm-Cre_Yu_for	GCATTTCTGGGGATTGCTTA	55.3 °C	95 bp
Prm-Cre_Yu_rev	ATTCTCCCACCGTCAGTACG	59.4 °C	

2.4 Laser-capture microdissection (LCM)

In order to confirm the peroxisomal KO, paraformaldehyde (PFA) fixed paraffin-embedded testes from adult gc*Pex13*KO, gc*Pex13*HTZ and control mice were used for laser-capture microdissection (LCM; Institute for Anatomy and Cell Biology; Justus-Liebig-University, Gießen). Slides of 6 µm thickness were cut using a microtome and placed on nuclease-free specimen slides. Sections were stained with Mayer´s haematoxylin as follows:
70 % ethanol fixative for 3 sec, DEPC water for 5 sec, Mayer´s haematoxylin for 15 sec, DEPC water for 5 sec, 70 % ethanol for 5 sec, 2 times 95 % ethanol for 10 sec. After air drying, specimens were inspected using an Axio Observator microscope and microdissected with a P.A.L.M laser-capture micro-dissection control unit. Specimens were visualized by a P.A.L.M RoboSoftware 4.0. Cross-sections from MNCs and spermatocytes of *Stra8*-Cre mediated gc*Pex13*KO mouse testes as well as spermatocytes and round spermatids of gc*Pex13*HTZ and control mice were catapulted into a lid of a 500 µl LPC-Microfuge tube and resuspended in RLT buffer. For each genotype, a total number of 50 tubules was needed to gain a minimum of one thousand cells that were catapulted as starting material for DNA isolation. DNA was isolated with Arcturus® PicoPure DNA Extraction Kit. Prior to use, lyophilised proteinase K was reconstituted with reconstitution buffer. A total volume of 30 µl was transferred onto collected cells, placed in the lid. Cells were incubated at 65 °C for 3 hrs. Proteinase K was inactivated at 95 °C for 10 min. DNA concentration was measured with a NanoDrop instrument. 200 ng of DNA were used for qPCRs.

2.5 Morphological analyses

2.5.1 Preparation of testis biopsies

Mice were anaesthetized by intraperitoneal (IP) injection using a mixture of 100 mg/kg ketamine and 10 mg/kg xylazine and euthanized by cervical dislocation. Testes were removed by a single transverse incision at the caudal abdomen. Skin was separated from the muscle layer, followed by a similar transverse incision through the muscle. The fat pads were pulled through the incision using blunt forceps and testes were carefully detached. Epididymis of adult control, gc*Pex13*HTZ and gc*Pex13*KO mice was also removed. For macroscopic analyses, testes were weighed by means of an analytical balance and their length was measured. They were further immersed in 4 % PFA (pH 7.4) at 4 °C overnight. For paraffin embedding, testes were transferred into phosphate buffer (PBS; Table 6) until embedded into paraffin, using a paraffin dispensing system. The paraffin blocks were stored at RT. Paraffin blocks of testes were cut on a microtome into sections of 2-4 µm thickness. For cryopreservation, testes were transferred to a 30 % sucrose solution.

2.5.2 Fixation and processing of testes for cryopreservation

Mice of each animal genotype (control, gc*Pex13*HTZ and gc*Pex13*KO mice) were anesthetized as described (2.5.1). The testes were excised, the capsule punctured at both poles with a needle and immersed with 4 % (w/v) PFA overnight at 4 °C. Thereafter, they were incubated in 30 % sucrose for a minimum of 24 hrs. For snap freezing, a stainless-steel bucket was filled with 2-methyl butane and placed into a cryobucket, filled with liquid nitrogen. 2-methyl butane rapidly cooled down, indicated by vapour formation. With freezing of the 2-methyl butane to its freezing point of -150 °C, solid white ice was visible at the bottom of the steel bucket. One specimen at a time was carefully transferred into 2-methyl butane. Complete freeze was achieved after 60 sec. The tissue was immediately transferred into a cryotube and stored at -80 °C. Prior to use, tissue was directly embedded into a cryo-preservative solution (O.C.T). Cryosections of 6 and 10 µm thickness, obtained on a cryostat, were subjected to immunofluorescent (2.5.4) and Oil Red O (ORO) staining (2.5.7).

2.5.3 Fixation and processing of tissue for electron microscopy

gc*Pex13*KO, gc*Pex13*HTZ and control mice were anaesthetized as described (2.5.1). Testes were surgically removed and fixed by perfusion with 4 % depolymerized PFA (w/v), pH 7.4. Dissected testes fragments were post-fixed with 5.5 % glutaraldehyde in 0.05 M phosphate-buffered saline (v/v) over-night (Table 6). For routine electron microscopy, testes fragments were incubated in 1 % aqueous osmium tetroxide for 90 min and subjected to dehydration in a series of graded alcohol (35 % to absolute) before they were embedded in a mixture of 1,2,3-propanetriol glycidyl ether (Epon) and propylene oxide (Table 6). One µm semithin sections were cut to determine the region of interest. For electron microscopy, 80 nm-ultrathin sections were cut. The sections were examined on an electron microscope (Philips).

2.5.4 Haematoxylin and eosin staining (HE)

Paraffin sections (2 µm) of prepubertal and adult mouse testes from all genotypes were stained with haematoxylin and eosin in an automated system. Sections were deparaffinized and rehydrated as follows: Xylene 3 x 10 min, absolute ethanol 2 x 5 min, 96 % ethanol, 80 % ethanol, 70 % ethanol, and distilled water, each step for 1 x 5 min. The sections were stained for 3 min in 10 % Mayer's Haematoxylin. After a washing step in distilled water for 2 min, the cytoplasm was stained for 3 min in 1 % eosin containing 0.2 % glacial acetic acid. The slides were shortly washed in distilled water (30 sec), followed by dehydration steps in 70 % (15 sec), 2 x 96 % (30 sec) and 2 x 5 min 100 % ethanol, followed by 3 x 5 min in Xylene. The sections were examined on a light microscope (Zeiss).

2.5.5 Immunohistochemistry (IHC)

For immunohistochemistry, tissue sections were deparaffinised and rehydrated. Antigen retrieval and accessibility of epitopes was achieved by subjecting the sections to the target retrieval solution S1699 (pH 6), followed by microwaving (2 x 4 min at full power) in a conventional household microwave oven. Cuvettes were filled up to the same volume with water between each microwaving step. Specimens were three times washed in TBS-T. Subsequently, sections were incubated with the primary antibody anti-CD45 (1:25 diluted in antibody diluent; Table 5) for 1 hr at RT. After washing 3 x 5 min with TBS-T, specimens were incubated with secondary antibody for 30 min at RT. Specimens were further incubated with alkaline phosphatase (Vectastain ABC-AP) for 30 min at RT. For visualization, permanent red was added (15 min at RT) followed by rinsing under water. The nuclei were counterstained with diluted haemalum for 10 sec at RT and mounted with eukitt mounting medium. The sections were examined on a light microscope (Zeiss).

2.5.6 Immunofluorescence (IF)

For indirect immunofluorescence stainings, paraffin and cryosections of all genotypes were used. Paraffin sections were deparaffinised and rehydrated and subsequently subjected to digestion with trypsin for 7 min at 37 °C, followed by microwave treatment for 3 x 5 min at 900 W in 10 mM citrate buffer at pH 6.0 (modified according to Grabenbauer *et al.* 2001) for improved retrieval of peroxisomal antigens and accessibility of epitopes. Nonspecific binding sites were blocked with 4 % BSA in PBS for 2 hrs at RT, and sections were incubated with primary antibodies (Table 5) in 1 % BSA in TBS-T overnight at RT. On the following day, the sections were incubated with fluorochrome-conjugated secondary antibodies in 1 % BSA in TBS-T. For DNA labelling, the secondary antibody was supplemented with 1 µg/ml 4′,6-Diamidino-2-phenylindole (DAPI). Specimens were washed in PBS and mounted with Mowiol 4–88. For fluorescence staining of cryosections, specimens were initially rehydrated and permeabilized in TBS-TT for 30 min and then incubated with 10 % (v/v) Roti-Block (diluted in PBS) for 1 hr to reduce non-specific binding of antibodies. Sections were further incubated with primary antibodies (Table 5) in 10 % (v/v) Roti-Block for 1 hr at RT. After extensive washing with TBS, tissue sections were incubated with a secondary antibody, suspended in 10 % (v/v) Roti-Block, for 1 hr, to visualize immune complexes. The secondary antibody was supplemented with 1 µg/ml DAPI. Specimens were washed in TBS and mounted with Mowiol 4-88. Negative controls were processed in parallel by addition of TBS-T buffer instead of the first antibodies.
Specimens were analysed using a Confocal Laser Microscope (Nikon) with standard filters for detection of Cy3, Alexa488 and DAPI. Digital images were obtained with a Nikon A1plus camera using the Nikon NIS Elements Advanced Research software.

2.5.7 Oil Red O staining (ORO)

Frozen sections of prepubertal and adult gc*Pex13*KO, gc*Pex13*HTZ and control mice were stained with ORO for the detection of lipid droplets. ORO staining was performed according to the protocol of Lillie *et al.* (1943) using a 0.5% ORO stock solution in isopropanol. Cryosections (6 µm) were cut with a cryostat and air dried for 30 min, followed by fixation with ice cold 10 % formalin for 5 min. Thereafter, the sections were rinsed in running tap water followed by 60 % isopropanol to avoid carrying of water into the ORO solution. The sections were stained with freshly prepared 0.3 % ORO working solution for 15 min at RT and rinsed ones with 60 % isopropanol. Nuclei were counter-stained with Mayer's haematoxylin (5 dips for 5 sec) and rinsed thereafter with distilled water. The stained sections were mounted in aqueous mountant.

2.5.8 TUNEL assay

The TUNEL assay, using DeadEnd™ Colorimetric TUNEL System, was performed to detect DNA fragments resulting from apoptotic signalling cascades. Discontinuities in the DNA will be identified by terminal deoxynucleotidyl transferase (TdT) that catalyses the addition of dUTPs that are secondarily labelled with a marker (Ellis *et al.* 1991). Paraffin-embedded testis sections of adult gc*Pex13*KO, gc*Pex13*HTZ and control mice were deparaffinized in xylene. Slides were washed two times in 100 % ethanol (5 min, RT), followed by rehydration through grading ethanol (95 %, 85 %, 70 % and 50 %). The tissue sections were fixed in 4 % PFA and immersed in PBS (5 min, RT). The sections were covered in a 20 µl/ml proteinase K solution for 15 min at RT to permeabilize the tissues, followed by a washing step in PBS. Tissue sections were refixed in 4 % PFA and immersed in PBS (5 min, RT). Areas were equilibrated and incubated (60 min at 37 °C) with biotinylated nucleotide that is incorporated at the 3´-hydroxyl radical (OH) DNA ends using the recombinant Tdt enzyme. The reaction was terminated by immersing the slides in 2 x SSC (15 min, RT), followed by a washing step in PBS. Endogenous peroxidase was blocked by 0.3 % hydrogen peroxide (3-5 min, RT). Horseradish peroxidase-labelled streptavidin (Streptavidin HRP) was added that binds to biotinylated nucleotides. For visualization, the peroxidase substrate, hydrogen peroxide, and the stable chromogen, diaminobenzidine (DAB) were added until apoptotic nuclei turned dark brown whilst a light brown background was still visible. The slides were rinsed in deionized water to stop the reaction and mounted in aqueous mounting medium (Table 6).

2.5.9 Evans Blue

The visualization of the BTB integrity was achieved by using the azo dye Evans Blue. Evans Blue was applied by an intravenous (IV) injection at a dose of 100 µl (50 mg/ml PBS). Adult mice of all

genotypes were used. The azo dye was circulating in the blood system for 1 hr until mice were anaesthetized and intracardially perfused with 1 % BSA in NaCl to remove free dye within the circulation. Mice were immediately perfused with 3.7 % formalin. Testes were surgically removed and fixed overnight in an additional step of 3.7 % formalin. As control for endothelial permeability, liver, kidney and brain were also removed. For cryopreservation, the samples were first transferred to 15 % sucrose, followed by 30 % sucrose and stored at -80 °C. Prior to use, tissue samples were directly embedded into a cryo-preservative solution (O.C.T). Cryosections of 6 µm thickness were obtained on a cryostat. The level of incorporated Evans Blue was assessed at 620 nm using a Confocal Laser Microscope.

2.6 Preparation of a testicular single cell suspension

Cells were isolated from 8 to 53 weeks old control, gc*Pex13*HTZ and gc*Pex13*KO mice. Adult mice were anaesthetized by IP injection using a cocktail of 100 mg/kg ketamine and 10 mg/kg xylazine and euthanized by cervical dislocation. The testes were surgically removed aseptically by opening the abdomen and incising the peritoneum. The epididymis was disconnected. The *Tunica albuginea* was carefully removed and seminiferous tubules were dissociated by treating the decapsulated testes with collagenase type IV (0.4 mg/ml), dispase (1.2 U/ml) and DNAse (20 µg/ml) in PBS. The cells were incubated at 33 °C for 30 min, under rotating motion. The cells were strained through a 70 µm cell strainer to exclude interstitial cells and tissue from the tubules. The resulting whole cell suspension was further dissociated by using a second enzymatic digestion. The cells were incubated at 33 °C for 10 min, under shaking conditions. For the removal of cell clumps in cell suspensions of control, gc*Pex13*HTZ and *Prm*-Cre mediated gc*Pex13*KO testes, cells were strained through a Falcon® 40 µm cell strainer and triturated with a Pasteur pipette until they were dissociated to a single cell suspension. In terms of *Stra8*-Cre mediated gc*Pex13*KO testicles, cells were again strained through a Falcon® 70 µm cell strainer to reduce shear stress and damage of MNCs. For FACS analysis, separated germ cells were sedimented by centrifugation for 5 min at 1500 rpm at 18 °C. The cell pellet was resuspended in 5 ml PBS and stained with Hoechst 33342 (5 µg/ml) followed by centrifugation (1500 rpm, 5 min at RT). Testicular cells were fixed with 2 % formaldehyde for 5 min at RT. Cells were again centrifuged and washed in 5 ml PBS. For qRT-PCR, a cell sample from the appropriate cell suspension of all genotypes was taken.

2.6.1 Separation of cells by velocity sedimentation

The separation of germ cells was performed by velocity sedimentation, as already described by Bellvé (1993). (Bellve 1993)(Bellve 1993)The principle of this method is to allow cells to sediment in a

continuous gradient of BSA (Platz *et al.* 1975), under the influence of gravity by the following equation:

$$S = \frac{2(\rho - \rho')}{9 * \eta} g r^2$$

ρ = density of the cell

ρ' = density of the medium

η = coefficient of viscosity

g = acceleration due to gravity

r = radius of the cells

Following this relationship, the density of the medium linearly increases from top to the bottom in a specific glassware. Separation is carried out according to the radius of a cell in a defined time frame. Testes biopsies were prepared as described in the previous sections (2.5.1). Cells were spinning (1500 rpm, 10 min) and finally resuspended in 0.5 % BSA to avoid any enzymatic influence. The method was initially established in control mice, using a 1-5 % BSA gradient. For *Stra8*-Cre mediated KO mice, a 2-4% BSA gradient was adjusted. Solutions were prepared as described in Table 6.

Cell separation was carried out at 4 °C in a ECET Celsep-Systems 5440 (Figure 5) that included two measuring cylinder filled with either 1 % (2 %) or 5 % (4 %) BSA, whilst the cylinder containing 1 % BSA had a magnetic stirrer. The gradient was established by mixing 1 % (2 %) BSA with 5 % (4 %) BSA that was gradually pumped into the sedimentation chamber via a pipe. To avoid cell adhesion on the bottom of the chamber, the chamber was finally cushioned with 10 % BSA. The single cell suspension was loaded onto the gradient. Prior to sedimentation, the chamber was tilted from the upright into the horizontal position, by means of a motor. After 8 hrs of sedimentation, the chamber was set into the upright position. Cells were pumped back via the pumping system and finally collected in 50 ml Falcon tubes. Cells were centrifuged, stained with DAPI and further used for morphological analyses (2.6.4).

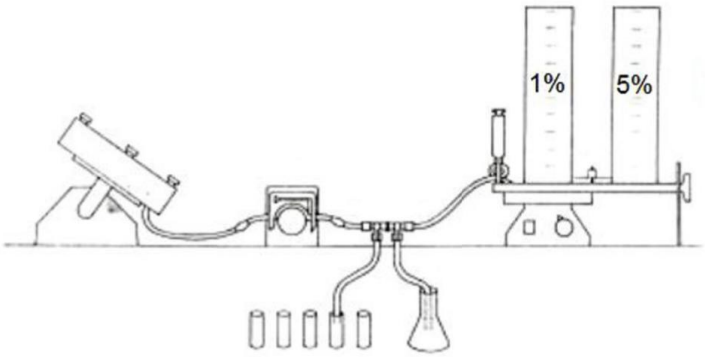

Figure 5| Schematic represenation of the ECET Celsep-Systems 5440. The chamber was filled with BSA that was pumped via a pumping system from measuring cylinders, containing either 1 % or 5 % BSA. The single cell suspension was loaded onto the gradient in the sedimentation chamber. Cell fractions were taken in a volume of 50 ml and used for further analyses. The scheme was taken from a former doctoral thesis (Dastig *et al*. 2011).

2.6.2 Flow cytometric analysis and cell sorting

Analysis and cell sorting were performed on a BD FACSAriaIII Fusion cell sorter. For cell sorting, 20 million cells were diluted in 5 ml PBS and strained through a 35 µm nylon mesh of a falcon round-bottom tube to ensure a single cell suspension. Hoechst blue fluorescence emissions were collected using a combination of 400 nm long pass and 505 short pass filters, and a 630/30 band pass filter. Analysis and sorting was done with a 100 µm nozzle. Cells were sorted according to DNA content, granularity and size.

2.6.2.1 Preparation of FACS purified cells for electron microscopy

For electron microscopy, a cell suspension was prepared as described above (2.6). The cell suspension was fixed with 4 % depolymerized formaldehyde (w/v), 0.05 % glutaraldehyde (v/v), 2 % sucrose (w/v) and 0.1 M HEPES, pH 7.4. For routine electron microscopy, the sorted cells were placed in 1.5 % agarose. Fixed cells, embedded in agarose, were packed into a dense pellet by centrifugation. The cell pellets were incubated in 1 % aqueous osmium tetroxide for 90 min and subjected to dehydration in a series of graded alcohol (35 % to absolute) before they were embedded in a mixture of 1,2,3-propanetriol glycidyl ether (Epon) and propylene oxide. One µm semithin sections were cut to determine the region of interest. For electron microscopy, 80 nm-ultrathin sections were cut. The sections were examined on an electron microscope (Philips).

2.6.2.2 RNA isolation and cDNA synthesis of purified fixed germ cells

For RNA purification, from 30.000 to 6.700.000 cells were sorted in Falcon round-bottom FACS tubes containing PBS. Total RNA from formaldehyde-fixed isolated cells was isolated with the RNeasy FFPE Kit to reverse formaldehyde modification of RNA. RNA was eluted in 20 µl RNase-free water. The concentration of extracted RNA was determined with a nanodrop ND-1000 Spectrophotometer. For cDNA synthesis, purified RNA was reverse transcribed using the RT^2 First Strand Kit according to manufacturer´s instructions. Due to small amounts of extracted RNA, the maximum of the yield was reverse transcribed into cDNA (100-500 ng).

2.6.2.3 QRT-PCR and primers used to characterize purified germ cells of WT mice

The expression level of distinct mRNA was measured by qRT-PCR using the LightCycler 480 SYBR Green I Master. Primer design was performed with Primer Blast (http://www.ncbi.nlm.nih.gov/tools/primer-blast/). The quality of the oligonucleotides was checked by oligocalc (http://www.basic.northwestern.edu/biotools/oligocalc.html). Oligonucleotides used for gene

expression analysis are listed in Table 2. 5 ng of cDNA were used per reaction. Reactions were run in duplicate wells.

An initial denaturation at 95 °C for 15 min was followed by 45 cycles of denaturation (94 °C, 15 s), annealing (56 °C, 30s for *Crem*, *Tacstd*, *Sycp3* and *Tnp*; 64 °C, 30 sec for *Prm1*, *Stmn1*, *AR* and *Acrv1*) and polymerization (72 °C, 30 sec). Thereafter, a melting curve was generated over temperatures of 55–95 °C with 30 sec/1 °C. The analysis of gene expression in all distinct cell types was performed on 96-well plates with the qRT-PCR system LightCycler 480. As reference genes, *Gapdh* and *β-actin* were formerly identified as optimal for the testis (Dastig *et al.* 2011). All expression levels were calculated as relative values using the mean of both reference genes. The samples were run following the MIQE guidelines (Bustin *et al.* 2009). The quantification of the expression of a target gene was calculated using the difference of the C_T-values (ΔC_T) from the target gene and the mean of the C_T-values from both housekeeping genes (C_T reference gene). As control sample for qRT-PCR reactions, no-template control and cDNA obtained from a single cell suspension of whole testis were run.

Table 2| Primers used for germ cell specific marker expression

Primer	Sequence	Accession number	Annealing temperature	Product length
*Tacstd*_for (5´-3´)	TTGCTCCAAACTGGCGTCT	NM_008532.2	59.85 °C	100 bp
*Tacstd*_rev (3´-5´)	GTTGTTCTGGATCGCCCCTT		60.32 °C	
*AR*_for (5´-3´)	TGAGTACCGCATGCACAAGT	NM_013476.4	57.3 °C	149 bp
*AR*_rev (3´-5´)	GCCCATCCACTGGAATAATGC		59.8 °C	
*Sycp3*_for (5´-3´)	CAGAAGAAGATGTTGCTGATGAA	NM_011517.2	57.1 °C	141 bp
*Sycp3*_rev (3´-5´)	CCAGCATATTCTGTACTTCACCTC		61.0 °C	
*Stmn1*_for (5´-3´)	TCCTTGCCAGTGGATTGTGTA	NM_019641.4	57.9 °C	143 bp
*Stmn1*_rev (3´-5´)	CTTTTGACCGAGGGCTGAGAA		59.8 °C	
Crem _for (5´-3´)	ACTCTAGCTCAGGTAGCAACA	XM_0065255	57.9 °C	192 bp
Crem _rev (3´-5´)	AGGTGGTGTCCCTTCTTCCT	75.2	59.4 °C	
*Acrv1*_for (5´-3´)	GGTGAAGTTTCGGGTGACGA	NM_007391.2	59.4 °C	202 bp
*Acrv1*_rev (3´-5´)	ACATGCACTGCTGGGAGTTT		57.3 °C	
*Tnp*_for (5´-3´)	AGCCGCAAGCTAAAGACTCA	NM_009407.2	57.3 °C	146 bp
*Tnp*_rev (3´-5´)	CGGTAATTGCGACTTGCAT		54.5 °C	
*Prm1*_for (5´-3´)	GAAGATGTCGCAGACGGAGG	NM_013637.4	61.4 °C	192 bp
*Prm1*_rev (3´-5´)	CGGACGGTGGCATTTTTCAA		59.8 °C	
*Gapdh*_for (5´-3´)	TGTCCGTCGTGGATCTGAC	NM_008084.2	58.8 °C	75 bp
*Gapdh*_rev (3´-5´)	CCTGCTTCACCACCTTCTTG		59.4 °C	
β-actin _for (5´-3´)	ATGTGGATCAGCAAGCAGGA	NM_007393.1	57.3 °C	100 bp
β-actin _rev (3´-5´)	AAAGGGTGTAAAACGCAGCTC		57.9 °C	

2.6.3 Counterflow centrifugal elutriation (CCE)

The principal of CCE is to separate cells according to cell size and density based on centrifugal force and counterflow (Lindahl 1948). An elutriator from Beckman Coulter was used with a 4-ml standard chamber. A single cell suspension was prepared as described above (2.6). Testicular cells of pre-meiotic induced gc*Pex13*KO mice were used. Cells were centrifuged and resuspended in 2 ml PBS. The total volume of cells was injected under sterile conditions upstream of the pump using a syringe (minus piston) as a reservoir connected to a 3-way valve in-line as described by Kauffman *et al* (1990). The cells were pumped into a triangular-shaped separation chamber situated in a centrifuge rotor while spinning and opposing the cells to centrifugal force. A flow pump is needed as counterflow to push the cells out of the chamber into a collecting flask. Rotor speed and pump rate were calculated according to *Stoke´s law*. *Stoke´s law* describes normal cellular run conditions (assuming that $\rho_p - \rho_m = 0.05$ g/ml, $\eta = 1.002$ mPa/s), a relationship between flow rate *F*, cell diameter *d* and centrifugal speed (*RPM*) that follows the equation:

$$F = xd^2 * \left(\frac{RPM}{1000}\right)^2$$

2.6.4 Cytospin and morphological analyses of sorted cells by fluorescent microscopy

For first morphological analysis and purity calculations, cytospin adaptors for low-speed centrifugation of cells onto slides were used. The chambers were loaded with 100 µl of each sample of sorted cells and spun at 1500 rpm for 10 min (Hettich). After centrifugation, the excess was carefully withdrawn. The slides were covered with coverslips. The cells were analysed in a confocal microscope (Nikon) using a blue excitation filter at 405 nm and a 450-nm emission filter. The slides were photographed at 400 x magnifications. The cells were scored according to criteria of size, shape, stain intensity, and nuclear size and shape.

2.7 Total RNA isolation from testis biopsies

Total RNA from testis was isolated by phenol-chloroform extraction. Testis biopsies were taken from all genotypes (control, gc*Pex13*HTZ, gc*Pex13*KO mice; 2.5.1). The *Tunica albuginea* was removed and decapsulated testicles were immediately transferred to liquid nitrogen. Cooled mortar and pistil were used to mince the tissue. 1 ml TRIzol was added to the pulverized tissue and kept at RT. Homogenate was transferred to an Eppendorf tube and chloroform was added at one fifth of the total volume. After centrifugation (14.000 x g, 20 min at 4 °C), the upper liquid phase was carefully removed and transferred to another Eppendorf tube. RNA was precipitated with isopropyl alcohol,

followed by cooling at -20 °C for 30' and centrifugation (14.000 x g, 20 min at 4 °C). The pellet was washed two times with 70 % ethanol and solubilised in 100 µl RNase-free water. RNA concentrations were quantified using a nanodrop ND-1000 spectrophotometer.

2.7.1 QRT-PCR to characterize the peroxisomal compartment in testes biopsies

For cDNA synthesis, purified RNA of whole testes as well as single cell populations was reverse transcribed using theRT^2 First Strand Kit (Qiagen, Hilden, Germany) according to manufacturer´s instructions. For the evaluation of the mRNA level of peroxisomal genes being involved in biogenesis (*Pex13*, *Pex14*, *Pex19*), *β*-oxidation (*Acox1*, *Hsd17b4*), ROS metabolism (*Sod1*, *Cat*), metabolite transport (*Abcd1*), ether lipid synthesis (*Gnpat*), retinoid metabolism (*Dhrs4*) and polyamine metabolism (*Paox*), a customized RealTime ready custom Panel in a 384 multiwell plate format was used (Table 3). A reaction volume of 10 µl per well was prepared, resulting in a primer concentration of 0.4 µmol for each primer and a cDNA concentration of 5 ng equivalent of total RNA/PCR reaction. The fold change of gene expression in gc*Pex13*HTZ and gc*Pex13*KO was calculated by normalizing the mRNA level in control testis.

Table 3| Primers used for peroxisomal gene expression

Gene	Symbol	Forward primer	Reverse primer
synaptonemal complex protein 3	*Sycp3*	GGGACAGCGACAGCTCAC	CCAGATTTCCCAGAATGCTT
polyamine oxidase (exo-N4-amino)	*Paox*	CCTCCCTGAAGATGGAACTG	GCCCCATGTGTGGTAGAATAA
dehydrogenase/reductase (SDR family) member 4	*Dhrs4*	GCTGCTGTCAACCCTTTCTT	TCATGGCTGTAGCTGTCACAT
glyceronephosphate O-acyltransferase	*Gnpat*	GCAGCTTTCGTGAGACTGG	GCAGGCCCGTTCACATAATA
ATP-binding cassette, sub-family D (ALD), member 1	*Abcd1*	GCCAGCCTCAACATCAGG	ACTCTTGCCACAGCCATTG
Catalase	*Cat*	CCTTCAAGTTGGTTAATGCAGA	CAAGTTTTTGATGCCCTGGT
Superoxide dismutase 1	*Sod1*	CAGGACCTCATTTTAATCCTCAC	TGCCCAGGTCTCCAACAT
Hydroxysteroid (17-beta) dehydrogenase 4	*Hsd17b4*	AGCATGGGACCATATGAAGAA	TATAATTCGCCTGGCCAAAG
Acyl-Coenzyme A oxidase 1, palmitoyl	*Acox1*	TGGAGATCACGGGCACTTAT	TTCCAAGCCTCGAAGATGAG
Peroxisomal biogenesis factor 19	*Pex19*	TGCTGTACCCATCCCTGAA	GGAGGAGTGGAGTCCTGGT
Peroxisomal biogenesis factor 14	*Pex14*	ACTCCGCAGCCATACAGC	CTGCCATGATGATAGCCAAG

Peroxisomal biogenesis factor 13	*Pex13*	TAGACCAGACTGGCTTCGAACT	CATGCCTTTAATCCCAGCAC
Acrosomal vesicle protein 1	*Acrv1*	TGGAGAAGGAGTATGCACCA	ACCCTTGAACCATGAACTGG
Protamine 1	*Prm1*	CACAGCCCACAAAATTCCA	CAGAGCAGGGGACACCAC
Actin beta	*Actb*	GGATGCAGAAGGAGATTACTGC	CCACCGATCCACACAGAGTA
Glyceraldehyde-3-phosphate dehydrogenase	*Gapdh*	AGCTTGTCATCAACGGGAAG	TTTGATGTTAGTGGGGTCTCG

2.7.2 QRT-PCR and primers used to characterize the BTB and fatty acid synthesis in testes biopsies

For cDNA synthesis, purified RNA was reverse transcribed using theRT^2 First Strand Kit according to manufacturer´s instructions. Real-time PCR amplification was performed on 96-well plates on a Light Cycler 480 using SYBR Green I Master kit. For relative quantification, *β-actin* and *Gapdh* were used as housekeeping genes. Primer design was performed with Primer Blast (http://www.ncbi.nlm.nih.gov/tools/primer-blast/). The quality of the oligonucleotides was checked by oligocalc (http://www.basic.northwestern.edu/biotools/oligocalc.html). All oligonucleotides were initially tested by a gradient PCR to evaluate the appropriate temperature. Oligonucleotides used for gene expression analyses are listed in Table 4. 5 ng of cDNA were used per reaction. Reactions were run in duplicate wells. The thermocycler protocol was set as follows: an initial denaturation step of 95 °C for 5 min, followed by 45 cycles of 95 °C for 15 sec, annealing temperature at 58 °C (for *Elovl2*, *Elovl5* and *Fads2*) or 61 °C (for *Tjp1*, *Cldn3* and *Ocln*) for 30 sec and 72 °C for 30 sec. As control sample for qRT-PCR reactions, a no-template control including RNase-free water instead of cDNA was run. Melting curves were generated over temperatures from 55–95 °C with 30s/1 °C and evaluated for each gene using the Light Cycler 480 software. All expression levels were calculated as relative values using the mean of both reference genes. The samples were run following the MIQE guidelines (Bustin *et al.* 2009). The quantification of the expression of a target gene was calculated using the difference of the C_T-values (ΔC_T) from the target gene and the mean of the C_T-values from both housekeeping genes *Gapdh* and *β-actin* (C_T reference gene). The fold change of gene expression in gc*Pex13*HTZ and gc*Pex13*KO was calculated by normalizing the mRNA level in control testis.

Table 4| Primers used for BTB marker expression

Primer	Sequence	Accession number	Annealing temperature	Product length
Marker of fatty acid synthesis				
*Elovl2*_for (5´-3´)	GAGAAGGTGATGTCCGGGTAG	NM_019423.2	61.8 °C	144 bp

*Elovl2*_rev (3´-5´)	ACATGGACGCGTGGTGATAG		59.4 °C	
*Elovl5*_for (5´-3´)	TTCCTCTTGCATCGCGGCT	NM_134255.3	58.8 °C	200 bp
*Elovl5*_rev (3´-5´)	CCATCCTTTGACTCTTGTATCTCGG		63.0 °C	
*Fads2*_for (5´-3´)	ACCTTCCGTTGGGAGGAGAT	NM_019699.1	59.4 °C	160 bp
*Fads2*_rev (3´-5´)	GGAAGGCATCCGTAGCATCTT		59.8 °C	
Marker of the BTB				
*Tjp1*_for (5´-3´)	GGAGATGTTTATGCGGACGG	NM_009386.2	59.4 °C	136 bp
*Tjp1*_rev (3´-5´)	CCATTGCTGTGCTCTTAGCG		59.4 °C	
*Cldn3*_for (5´-3´)	GTACAAGACGAGACGGCCAA	NM_009902.4	59.4 °C	175 bp
*Cldn3*_rev (3´-5´)	CGTACAACCCAGCTCCCATC		61.4 °C	
*Ocln*_for (5´-3´)	GTGAGCACCTTGGGATTCCG	NM_008756.2	61.4 °C	153 bp
*Ocln*_rev (3´-5´)	GGGTTTGAATTCATCAGGTCTGT		58.9 °C	
Housekeeping genes				
*Gapdh*_for (5´-3´)	TGTCCGTCGTGGATCTGAC	NM_008084.2	58.8 °C	75 bp
*Gapdh*_rev (3´-5´)	CCTGCTTCACCACCTTCTTG		59.4 °C	
*β-actin*_for (5´-3´)	ATGTGGATCAGCAAGCAGGA	NM_007393.1	57.3 °C	100 bp
*β-actin*_rev (3´-5´)	AAAGGGTGTAAAACGCAGCTC		57.9 °C	

2.8 Testes biopsies for lipid analysis

Adult mice of all genotypes (control, gc*Pex13*HTZ, gc*Pex13*KO mice) were anaesthetized by IP injection using a cocktail of 100 mg/kg ketamine and 10 mg/kg xylazine and euthanized by cervical dislocation. Testes were removed aseptically. The *Tunica albuginea* was carefully removed. Decapsulated testes were freezed in nitrogen. Total testicular triglyceride (TG) and phospholipid (PL) levels were quantified by gas chromatography-mass spectrometry (GC-MS) (in collaboration with Dr. Klaus Tödter, Department of Biochemistry and Molecular Cell Biology, UKE, Hamburg-Eppendorf).

2.8.1 Gas chromatography-mass spectrometry (GC-MS)

Tissue lipid extracts were prepared according to Folch *et al.* (1957) and total tissue fatty acid profiling was performed as already described (Bartelt *et al.* 2013), using 20 µl of solvent per mg of tissue. TG and phospholipids were separated on silica gel 60 plates: 100 µl of extract were evaporated to drying and re-dissolved in 25 µl chloroform/methanol in a 2:1 ratio. The solutions were spotted onto the plate and developed with an eluent containing hexane, diethylether and acetic acid (80:20:1.5). Visualization of lipid bands was performed with primuline (5 mg in 100 ml acetone:water 80:20). Fatty acid methyl esters were prepared from 25 µl extract (total FA) or of the scratched bands without further extraction, based on the method of Lepage and Roy (Lepage *et al.* 1989) by adding 1 ml methanol/toluene (4:1), 100 µl heptadecanoic acid (200 µg/ml in methanol/toluene, 4:1), 100 µl acetyl chloride and heating in a capped tube for 1 h at 100 °C. After cooling to RT, 3 ml of 6 % sodium carbonate was added. The mixture was centrifuged (1800 x g, 5 min.). 5 µl of the upper layer was

diluted 1:5 with toluene and transferred to auto sampler vials. Gas chromatography analyses were performed using an HP 5890 gas chromatograph (Hewlett Packard) equipped with flame ionization detector (Stationary phase: DB-225 30 m x 0.25 mm id., film thickness 0.25 µm; Agilent, Böblingen, Germany). Peak identification and quantification were performed by comparing retention times, respectively, peak areas to standard chromatograms. All calculations are based on fatty acid methyl esters values. Concentration of individual fatty acids was calculated as % of total fatty acids.

2.9 Serum collection for steroid measurements

Five individuals per genotype (including control, gc*Pex13*HTZ and gc*Pex13*KO mice) were anesthetized by IP injection using a cocktail of 100 mg/kg ketamine and 10 mg/kg xylazine. Blood samples were taken by direct cardiac puncture.

For this purpose, a 22-gauge needle, fitted onto a 1 ml-syringe, was inserted from the centre of the thorax towards the animal's mandible, 5-10 mm deep, and held at 25-30 ° away from the chest. When blood appeared in the syringe, the plunger was gently pulled back to obtain the maximum amount of blood (1 ml). Blood samples were immediately transferred to 1.5 ml Eppendorf tubes and clotted at RT for 1 hr. The samples were centrifuged for 10 min at 13.000 x g at RT to separate the serum from the rest of the cells. Serum was removed and stored at -80 °C until the hormonal measurements were performed. The samples were analysed by ELISA kits for testosterone, follicle-stimulating hormone and luteinizing hormone.

2.9.1 ELISA assay

Serum hormone concentrations were measured using a competitive inhibition enzyme immunoassay. The ELISA was performed on FSH, LH and Testosterone (Table 8) according to manufacturer´s instruction. Serum was collected (2.9) and used from all genotypes of both mouse strains. Prior to use, serum was five times diluted with PBS. 50 µl of standard, blank and sample were used per well. The same volume of reconstituted detection reagent A was added and incubated for 1 hr at 37 °C. After several washing steps (350 µl one- fold wash solution; 5 times à 2 min), 100 µl of detection reagent B was added and incubated for 30 min at 37 °C. After another washing step (350 µl one- fold wash solution; 5 times à 2 min), 90 µl of substrate solution was added and incubated for 20 min at 37 °C. The total reaction was stopped by adding 50 µl of stop solution.

2.10 Primary and secondary antibodies

Table 5| Primary and secondary antibodies

Host	Primary Antibodies	Conc.	Supplier	Function of Antigen
Rabbit	Rat ABC-transporter D3 70kDa Peroxisomal membrane protein (ABCD3 / PMP70), polyclonal antibody	IF 1:500	Gift from Alfred Völkl, Dept. Anat. Cell Biol. II, Univ. Heidelberg	ABC-transporter for lipid derivatives; generally used as marker protein for the peroxisomal membrane
Rabbit	Bax (D3R2M), #14796, monoclonal	IF 1:100	Cell Signaling Technology, Cambridge, UK	Key component for cellular induced apoptosis
Rabbit	Cleaved Caspase-3, #9661 (Asp175), polyclonal	IF 1:300	Cell Signaling Technology, Cambridge, UK	Used as marker for apoptosis
Rabbit	Mouse Catalase (CAT), polyclonal	IF 1:2000	Gift from Denis I. Crane, Biomol. Biomed. Sci., Griffith Univ., Nathan, Brisbane, Qld 4111, Australia	generally used as marker protein for the peroxisomal matrix; degradation of H_2O_2
Rat	CD45	IHC 1:25	BD Biosciences	Pan-leukocyte marker
Rabbit	Mouse OSP/Claudin 11, polyclonal	IF 1:500	Invitrogen, Carlsbad, CA, USA	Structural component of tight junctions; located in epithelial and endothelial cells
Mouse	Mouse Oxidation Phosphorylation Complex III (OxPhosIII), monoclonal	IF 1:2000	Molecular Probes/Invitrogen, Carlsbad, CA 92008, USA Cat. no: A11143	complex 3 of the mitochondrial respiratory chain
Rabbit	Mouse Peroxin 13 (Pex13p), polyclonal	IF 1:1000	Gift from Denis I. Crane (address see above)	peroxisomal biogenesis protein 13 - integral peroxisomal membrane protein; involved in docking complex for matrix protein import
Rabbit	Mouse Peroxin 14 (Pex14p), polyclonal	IF 1:2000	Gift from Denis I. Crane (address see above)	peroxisomal biogenesis protein 14 - function is similar to the one of Pex13p (see

				above)
Rabbit	Mouse Thiolase A/B, polyclonal	IF 1:500	Gift from P. Van Veldhoven (Leuven, Belgium)	third enzyme of peroxisomal β-oxdation pathway
Rabbit	Tom70	IF 1:1000		Mitochondrial import receptor protein
Mouse	Monoclonal anti-Vimentin, clone VIM 13.2	IF 1:2000	Sigma-Aldrich, St Louis, MO 63103, USA Cat. no: A2547	Intermediate filament; generally used as marker for Sertoli cells
Rabbit	Vimentin (D21H3) XP mAB (AlexaFluor 488 conjugate)	IF 1:1000	Cell Signaling, Cambridge, UK	Intermediate filament; generally used as marker for Sertoli cells

Host	**Secondary Antibodies**	**Conc.**	**Supplier**
Goat	Cy3-conjugated AffiniPure goat anti-mouse IgG (H+L)	IF 1:1000	Jackson Immuno Research
Donkey	Cy3-conjugated AffiniPure donkey anti-rabbit IgG (H+L)	IF 1:1000	Jackson Immuno Research
Donkey	anti-mouse IgG TexasRed	IF 1:300	VECTOR, Burlingame, CA 94010 USA Cat. no: Ti-2000
Donkey	anti-rabbit IgG AlexaFluor488	IF 1:300	Molecular Probes/ Invitrogen, Carlsbad, CA 92008, USA Cat. no: A21206
Rabbit	mouse IgG AlexaFluor488	IF 1:500	Jackson Immuno Research

Isotypes	**Conc.**	**Supplier**
Rat IgG2b	1:200 In AK diluent (Dako)	Antigenix America

Counterstain of the nucleus

	Conc.	**Supplier**
Hoechst 33342	1:1000	Sigma-Aldrich; St. Louis; Missouri, USA
DAPI	1:1000	Thermo Fisher Scientific; Massachusetts, USA

2.11 Buffer solutions

Table 6| Buffer solutions

Solutions for Molecular Biology	
2 % agarose gel, 50ml	1 g of agarose, 50 ml of 1x TAE, 1 µl of ethidium bromide (10 mg/ml)
TE buffer	10 mM Tris-HCL, 0.2 mM EDTA, pH 7.5
Phosphate buffer (0.2 M)	28,42 g Na_2HPO_4 x 2 H_2O, 2,76 g Na_2HPO_4 x H_2O ad 1000 ml ddH_2O, pH 7,2-7,4
Solutions for light microscopy	
BSA (4 %)	4 g BSA, 400 ml PBS
Citrate buffer	Buffer A: 1 mM $C_6H_8O_7$ H_2O; Buffer B: 50 mM $C_6H_5Na_3O_7$ $2H_2O$ Citrate buffer: 0.15 mM buffer A, 8.5 mM buffer B, pH 6.0
Fixation solution	4% depolymerized paraformaldehyde
H_2O_2 (3%)	30% H_2O_2 10 ml, ddH_2O 90 ml
Haematoxylin and eosin staining	Xylene, absolute ethanol, 96% ethanol, 80% ethanol, 70% ethanol, ddH_2O, 10% Mayer's Haematoxylin, 1% acetic acid Eosin
PBS 10 x	1.5 M NaCl, 131 mM K_2HPO_4, 50 mM KH_2PO_4, pH 7.4
Sucrose buffer (30 %)	30 g sucrose, 100 ml
Sudan black (0.3 %)	0.03 g Sudan black, 10 ml ethanol
TBS 10 x	0.5 M Trizma-Base, 1.5 M NaCl, ad 1000 ml ddH_2O, pH 7.4
TBS-TT	TBS with 0.2 % Triton-X and 0.2 % Tween 20
Oil Red O staining	
Formalin (10 %)	270 ml formalin, 500 ml phosphate buffer (0.2 M), ad 1000 ml ddH_2O
Oil Red O working solution	0.3 % Oil Red O stock solution (30 ml stock and 20 ml ddH_20)
TUNEL Assay	
1 x PBS (pH 7.4)	137 mM NaCl, 2.68 mM KCl, 1.47 mM KH_2PO_4, 8.1 mM Na_2HPO_4
DNase I buffer	40 mM Tris-HCl (pH 7.9) 10 mM NaCl 6 mM $MgCl_2$ 10 mM $CaCl_2$
20 x SSC (pH 7.2)	87.7g NaCl, 44.1g sodium citrate
Proteinase K buffer	100 mM Tris-HCl (pH 8.0), 50 mM EDTA
Equilibration buffer	200 mM potassium cacodylate (pH 6.6 at 25 °C), 25 mM Tris-HCl (pH

	6.6 at 25 °C), 0.2 mM DTT, 0.25mg/ml BSA, 2.5 mM cobalt chloride
Solutions for fluorescent microscopy	
IF blocking solution	4% bovine serum albumin (BSA) in Tris-buffered saline containing 0.05% Tween 20 (TBS-T)
IHC blocking solution	4% BSA, 0.05% TBS-T (pH 7.4)
Mowiol 4-88	16.7% Mowiol 4-88, 80 ml 1 x PBS, stir overnight; add 40 ml glycerol stir again overnight; centrifuge at 15.000 g for 1h, store at -20ºC
Solutions for electron microscopy	
Na-Cacodylate buffer	0.1 M sodium cacodylate, pH 7.4
Epon	24 g epoxy resin, 16g DDSA, 10 g MNA, stir 30 min, add drop by drop 1.5 g BBMA, stir 30 min
Fixation solution	4% depolymerized paraformaldehyde, 0.05% glutaraldehyde in 0.01 M cacodylate buffer (pH 7.4) and 2% sucrose
Osmium post fixation	1-2 % aqueous osmium tetroxide
BSA gradient	
Medium for cell suspension (0.5 % BSA)	2 ml 5% BSA, 18 ml PBS
Lowest concentration (1 % BSA)	4.5 g BSA, 450 ml PBS
Highest concentration (5 % BSA)	22.5 g BSA, 450 ml PBS
Cushion (10 % BSA)	20 g BSA, 200 ml PBS

2.12 Reagents, chemicals and kits

Table 7| Reagents and chemicals

Reagent	Supplier
ABC-AP	Vector Labs (Burlingame, USA)
Antibody-Diluent	Medac (Wedel, Germany)
Agarose Seakem® LE	Axon (Kaiserslautern, Germany)
Aquatex	Merck Millipore (Darmstadt, Germany)
Bovine serum albumin (BSA)	Sigma-Aldrich (St. Louis, Missouri, USA)
Chloroform	Sigma-Aldrich (St. Louis, Missouri, USA)

Collagenase type IV	Sigma-Aldrich (St. Louis, Missouri, USA)
Collagenase	Sigma-Aldrich (St. Louis, Missouri, USA)
Diamidino-2-phenylindole (DAPI)	Thermo Fisher Scientific (Waltham, Massachusetts, USA)
Dispase	Gibco
DNase I	Roche (Basel, Switzerland)
Dodecenylsuccinic anhydride	Serva (Heidelberg, Germany)
Dulbecco's PBS ([-]$CaCl_2$, [-]$MgCl_2$)	Gibco (Detroit, USA)
Ethidium bromide	Promega, Molecular Grade (Madison, WI, USA)
Eosin	Merck (Darmstadt, Germany)
Eukitt	Kindler (Freiburg, Germany)
Ethanol for analysis	Merck (Darmstadt, Germany)
Evans Blue azo-dye	Sigma-Aldrich (St. Louis, Missouri, USA)
Formaldehyde 37 %	Merck (Darmstadt, Germany)
Glutaraldehyde 25 %	Merck (Darmstadt, Germany)
Glycidether Hardener DBA	Roth (Karlsruhe, Germany)
Haemalum	Sigma-Aldrich (St. Louis, Missouri, USA)
Hoechst 33342	Sigma-Aldrich (St. Louis, Missouri, USA
Hydrogen peroxide 30 %	Merck (Darmstadt, Germany)
Hydrochloric acid	Chemsolute Th. Geyer (Hamburg, Germany)
Isopropanol	Merck Millipore (Darmstadt, Germany)
Ketamine	WDT (Garbsen, Germany)
LightCycler 480 SYBR Green I Master	Roche (Basel, Switzerland)
Mayer's hematoxylin	Merck Millipore (Darmstadt, Germany)
Methanol	Roth (Karlsruhe, Germany)
Mowiol 4–88	Roth (Karlsruhe, Germany)
O.C.T, Tissue-tek®;	Sakura Finetek Germany GmbH (Staufen, Germany)
Oil O Red	Sigma-Aldrich (St. Louis, Missouri, USA)
Osmium tetroxide	Roth (Karlsruhe, Germany)
Roti-Block	Roth (Karlsruhe, Germany)
Paraformaldehyde (PFA)	Sigma-Aldrich (St. Louis, Missouri, USA)
Permanent Red Substrate Chromogen	Agilent
Protease K	Sigma-Aldrich (St. Louis, Missouri, USA)
Propylene oxide	Serva (Heidelberg, Germany)
RLT buffer	Qiagen (Hilden, Germany)
RNeasy kit 74104	Qiagen (Hilden, Germany)
Rompun	WDT (Garbsen, Germany)
Sodium Cacodylate	Fluka
Sudan III	Merck Millipore (Darmstadt, Germany)
Sucrose	Merck Millipore (Darmstadt, Germany)
Sodium chloride	Merck Millipore (Darmstadt, Germany)
Toluidine blue	Merck Millipore (Darmstadt, Germany)
TRIzol	Qiagen (Hilden, Germany)
Trizma®Base	Sigma-Aldrich (St. Louis; Missouri, USA)

Table 8| Kits

Kit	Cat. no.	Supplier
Arcturus® PicoPure® DNA Extraction Kit	KIT0103	Thermo Fisher Scientific (Waltham, Massachusetts, USA)
DeadEnd™ Colorimetric TUNEL System	G7360	Promega, Molecular Grade (Madison, WI, USA)
REDExtract-N-Amp Tissue polymerase chain reaction (PCR) Kit	XNAT-1000RXN	Sigma-Aldrich (St. Louis, Missouri, USA)
REDExtract-N-Amp PCR Ready Mix	R4775	Sigma-Aldrich (St. Louis, Missouri, USA)
RNeasy FFPE Kit	73504	Qiagen (Hilden, Germany)
RT^2 First Strand Kit		Qiagen (Hilden, Germany)
QIAamp DNA Micro Kit 50	56304	Qiagen (Hilden, Germany
FSH ELISA Kit	CEA830Mu	Cloud- Clone Corp (Houston, USA)
LH ELISA Kit	CEA441Mu	Cloud- Clone Corp (Houston, USA)
Testosterone ELISA Kit	CEA441Mu	Cloud- Clone Corp (Houston, USA)

2.13 Equipment and materials

Table 9| Equipment

Device name	Supplier
Analytical balance AUW220	SHIMADZU (Scientific Instruments, Kyōto, Japan)
Axio Observator microscope	Carl Zeiss (Oberkochen, Germany)
Block Thermostate	HLC (Bovenden, Germany)
Cryostat CM 3050	Leica (Wetzlar, Germany)
Confocal Laser Microscope	Nikon Eclipse Ti NIS-Elements
Centrifugal counterflow elutriator	Beckman Coulter Inc. (Indianapolis, USA)
Electron microscope	Philips
ECET Celsep-Systems 5440	Eppendorf (Hamburg, Germany)
FACS AriaIII Fusion cell sorter	BD Biosciences (Franklin Lakes, New Jersey, USA)
Flame ionization detector	Agilent (Böblingen, Germany)
Gel Imaging Work station Azure c150	Azure Biosystems (CA, USA)
HP 5890 gas chromatograph	Hewlett Packard
LightCycler 480	Roche (Basel, Switzerland)
Universal 32 R centrifuge	Hettich (Tuttlingen; Germany)
Microtome RM 2135	Leica (Wetzlar, Germany)
Microcentrifuge; Heraeus Pico 17	Thermo Fisher Scientific (Massachusetts, USA)
NanoDrop instrument ND-1000	Thermo Fisher Scientific (Massachusetts, USA)
Nuclease-free specimen slides	Carl ZEISS (Microimaging GmbH)

P.A.L.M laser-capture micro-dissection	P.A.L.M Microlaser Technologies GmBH (Bernried, Germany)
Paraffin dispensing system EG 1160	Leica (Wetzlar, Germany)
Thermal cylcer Gene Touch	Biozym (Hessisch Oldendorf, Germany)
Tissue Lyser II	Qiagen (Hilden, Germany)
Ultramicrotome EM UC7	Leica (Wetzlar, Germany)
Ultra-Microtome MT2-B	Sorvall Dupont Instruments (Connecticut, USA)

Table 10| Materials

Material	**Supplier**
Falcon® 40 µm Cell Strainer	BD Biosciences (Franklin Lakes, New Jersey, USA)
Falcon® 70 µm Cell Strainer	BD Biosciences (Franklin Lakes, New Jersey, USA)
FACS tubes	BD Biosciences (Franklin Lakes, New Jersey, USA)
Falcon round-bottom tube (35 µm)	BD Biosciences (Franklin Lakes, New Jersey, USA)
LPC-Microfuge tube	P.A.L.M. Microlaser Technologies GmbH (Bernried Germany)

3 RESULTS

3.1 Generation of germ cell specific peroxisome deficient KO mice

For the analysis of peroxisomal function in germ cells, the Cre/*loxP* technology was applied to generate a conditional germ cell specific KO mouse in the peroxisomal translocation machinery that would interfere with peroxisomal matrix protein biogenesis and protein import. Cre transgenic mice were initially backcrossed to the recipient C57Bl/6 strain to establish a congenic mouse strain. SNP genotyping enabled the identification of mice with highest percentage recipient strain background in each backcross round. It took five backcrosses to obtain male mice with 99.99 % C57Bl/6 background (Figure 6).

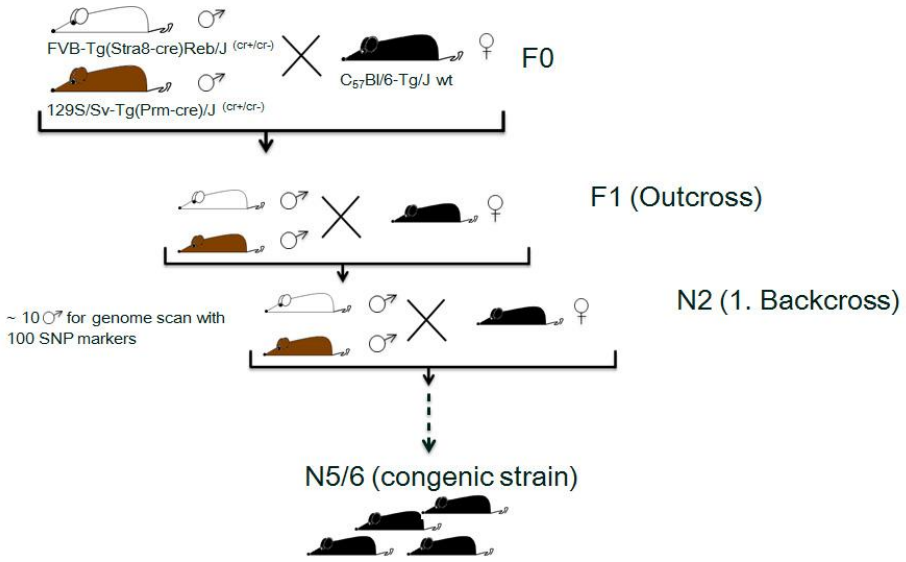

Figure 6| Backcrossing of Cre transgenic mice into C57B6/J mouse strain. Mice in either FVB/N or 129S background were backcrossed into C57Bl/6 WT strain to generate a congenic mouse strain, based upon marker assisted selection protocol (MASP). Parental mice, heterozygous for Cre recombinase (*Stra8*; stimulated by retinoic acid gene 8 or *Prm*; protamine), were crossed to C57Bl/6 mice (**F0**). Offspring (**F1**) were screened for their Cre transgene and for their genetic background by single nucleotide polymorphism (SNP). Only Cre-transgene positive male mice were selected for SNP analysis. Male mice with the highest percentage of recipient C57Bl/6 strain were further crossed with the recipient strain (**N2**). After the fourth backcross to B6, the offspring were less than 1 % original background strain and > 99 % B6.

Offspring with a floxed *Pex13* allele, carrying the Cre transgene, was selected for subsequent mating. With respect to the Mendelian breeding pattern, heterozygous mice with one WT allele and one allele with floxed *Pex13* (gc*Pex13*$^{WT/loxP}$/Cre$^{cr+/cr-}$) or one WT allele and one deletion of the *exon 2* of *Pex13* (gc*Pex13*$^{WT/\Delta ex2}$/Cre$^{cr+/cr-}$) were obtained. Heterozygous male mice (gc*Pex13*HTZ) with either one

floxed *Pex13* allele or excised *exon 2* of *Pex13* and positive for Cre recombinase (gc*Pex13*$^{WT/loxP}$/Cre$^{cr+/cr-}$ or gc*Pex13* $^{WT/\Delta ex2}$/Cre$^{cr+/cr-}$ from the F1 generation), were inbred with female siblings of the same genotype to generate KOs (gc*Pex13*$^{\Delta ex2/\Delta ex2}$/Cre$^{cr+/cr+}$).

New born pups with different genotypes showed no obvious differences in their phenotype, apart from different testes sizes, which will be discussed in 3.2. Animals with two WT alleles for *Pex13*, showing only one band at 490 bp and no floxed *Pex13* allele, were considered as control (gc*Pex13*WT; gc*Pex13*$^{WT/WT}$/Cre$^{cr+/cr+}$; Figure 7B). These animals also expressed Cre recombinase, that was confirmed by PCR showing a band at either 236 bp in case for the *Stra8*-Cre transgene (Figure 7C), or a product of 95 bp representing the transgenic Cre recombinase mediated by the *Prm* promoter (Figure 7D). Animals that were positive for Cre recombinase with one WT *Pex13* allele and a deletion in *Pex13*, were considered as HTZ (gc*Pex13*HTZ; gc*Pex13*$^{WT/\Delta ex2}$/Cre$^{cr+/cr+}$; Figure 7C, D). The gc*Pex13*KO mice had a deletion in *exon 2* of floxed *Pex13* gene, exhibiting a single band at 540 bp, and homozygous Cre recombinase expression (gc*Pex13*$^{\Delta ex2/\Delta ex2}$/Cre$^{cr+/cr+}$). An additional PCR on gc*Pex13*KO genotyped mice was performed with different primer pairs to demonstrate the disruption of *Pex13* gene by Cre-mediated excision at *loxP* sites. The reaction produced a 410 bp product of the disrupted gene (Figure 7C, D).

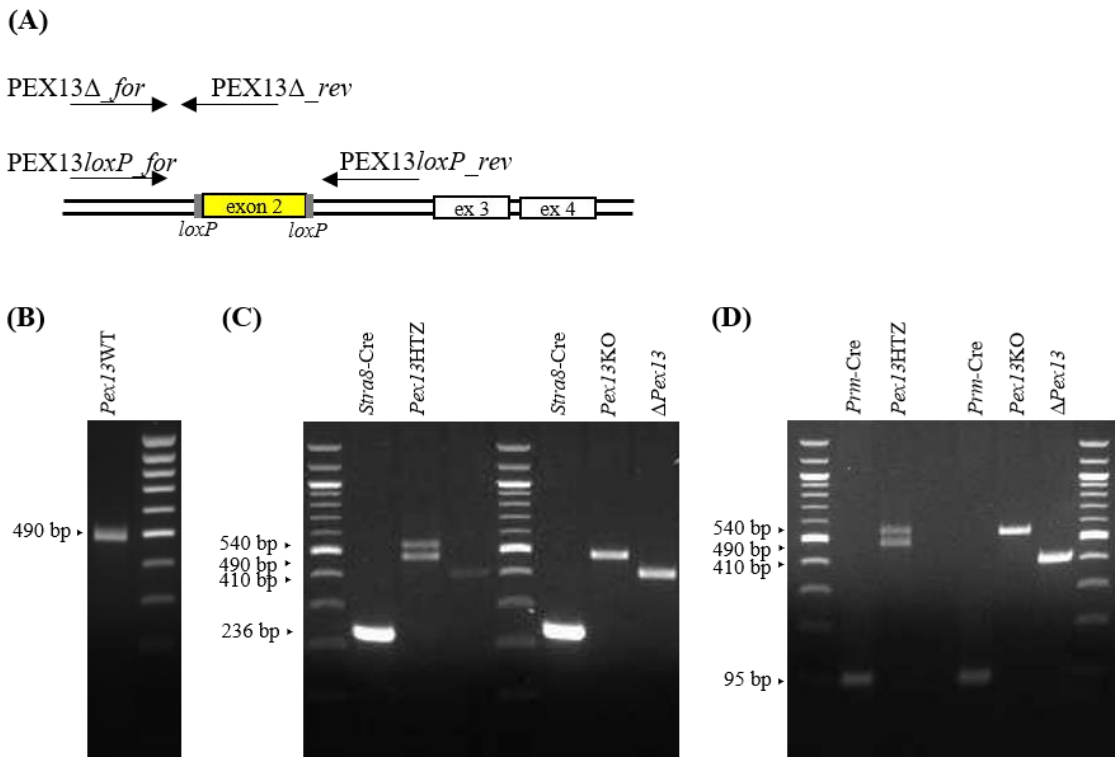

Figure 7| Confirmation of the correct genotypes for floxed *Pex13* alleles and either *Stra8*-Cre or *Prm*-Cre recombinase transgene, using DNA extracted from mouse tail biopsies. (A) Schematic drawing of designed primers to detect either floxed or excised *exon 2* of *Pex13*. The upstream primer PEX13*loxP_for* and downstream primer PEX13*loxP_rev* were generated to detect the flanking *loxP* sites of *exon 2*, resulting in an

amplicon of 490 bp for the WT allele and 540 bp for the floxed *Pex13* allele. Excised *exon 2* was confirmed by PEX13Δ*_for* and PEX13Δ*_rev*. PEX13Δ*_for/* PEX13Δ*_rev* generated an amplicon of 410 bp, following Cre mediated excision of floxed *exon 2*. **(B- D)** The amplification products were visualized on an agarose gel. **(B)** Cre transgenic mice with a single band at 490 bp were considered as control (*Pex13*WT; +/+) animals. **(C)** The amplified *Stra8*-Cre transgene displayed a product at 236 bp. *Stra8*-Cre recombinase positive animals, showing a double band for the floxed *Pex13* allele at 540 bp and a product at 490 bp for the WT allele, were considered as heterozygous (*Pex13*HTZ (-/+). Cre-mediated excision of *exon 2* was confirmed by a single band at 540 bp for floxed *Pex13* (*Pex13*KO; -/-) and a band at 410 bp for excised *exon 2* (Δ*Pex13*). **(D)** The Cre transgene under the *Prm* promoter control showed a band at 95 bp. *Prm*-Cre recombinase positive animals that were heterozygous for floxed *Pex13,* displaying a double band at 540 bp and at 490 bp, were named *Pex13*HTZ. *Pex13*KO mice exhibited a single band at 540 bp for floxed *Pex13* and a band at 410 bp for excised exon 2 (Δ*Pex13*). A 1 kb DNA ladder was used.

3.2 Testes of *Stra8*-Cre mediated gc*Pex13*KO mice vary in weight and size

The gross morphology of juvenile (5-7.5 weeks, corresponding digit “1” in the box plot; Figure 8) and adult mouse testes (8-53 weeks, corresponding digit “2” in the box plot; Figure 8) was studied. The litter size of the breeding pair, producing a pre-meiotic induced gc*Pex13*KO, decreased to 50 % with sequential mating. Their testicles were clearly atrophic. Compared to the testicle length of 0.780 ± 0.076 cm in adult control (Figure 9A) and 0.764 ± 0.075 cm in gc*Pex13*HTZ (Figure 9B) mice, *Stra8*-Cre mediated gc*Pex13*KO testes (Figure 9C) were much smaller with an average length of 0.442 ± 0.311 cm. Statistical analysis revealed that the total testis weight (0.046 ± 0.008 g) of adult *Stra8*-Cre mediated gc*Pex13*KO mice was significantly reduced ($p < 0.01$) compared to control (0.101 ± 0.012 g) and gc*Pex13*HTZ mice (0.093 ± 0.010 g; Figure 8).

Testes weight of juvenile control testes was 0.069 ± 0.014 g. The average weight of juvenile *Stra8*-Cre mediated peroxisomal gc*Pex13*KO testes was slightly decreased (0.049 ± 0.005 g; Figure 8). Neither gross abnormalities of external genitalia nor differences in epididymes, deferent ducts, seminal vesicles or prostate glands were detected. Male gc*Pex13*KO mice were tested for fertility (90 and 130 day-old), through mating with fertile WT females. WT females produced no offspring, indicating that *Stra8*-Cre mediated gc*Pex13*KO males were sterile.

Mouse testicles with a *Pex13* KO in post-meiotic germ cells did not differ in their length (0.840 ± 0.042 cm; Figure 9D) nor in their average weight (juvenile testicles: 0.069 ± 0.019; adult testes: 0.102 ± 0.013 g) compared to control testes (Figure 8). Male mice were also fertile.

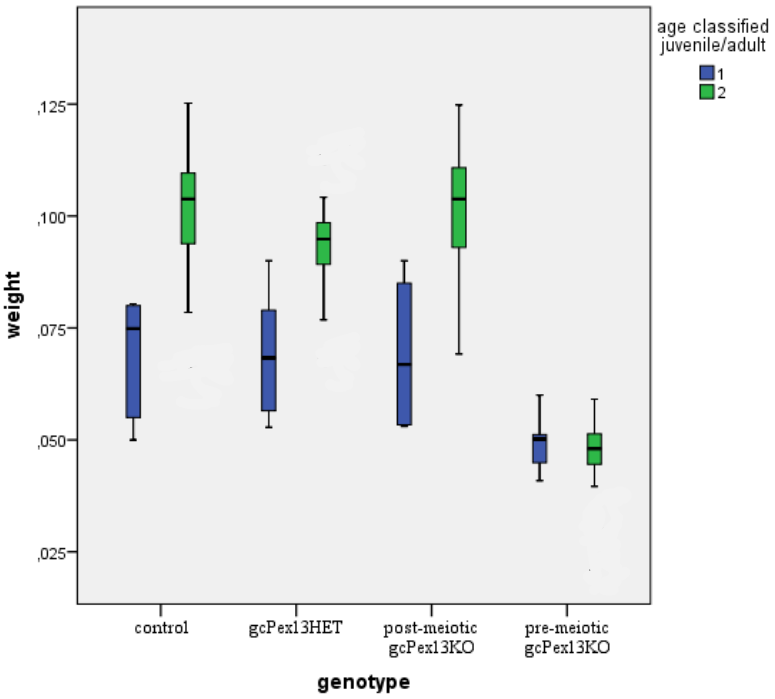

Figure 8| Analyses of testicular weight of all genotypes of juvenile (blue bars; 1) and adult (green bars; 2) animals. *Stra8*-Cre (pre-meiotic) mediated gc*Pex13*KO testes of juvenile and adult mice showed a significant reduction in their weight compared to gc*Pex13*HTZ and control testes. In post-meiotic (*Prm*-Cre) induced gc*Pex13*KO testes, no differences were observed. For data collection, a minimum of 30 individual testicles from adult mice and a minimum of 4 testicles from juvenile animals was considered.

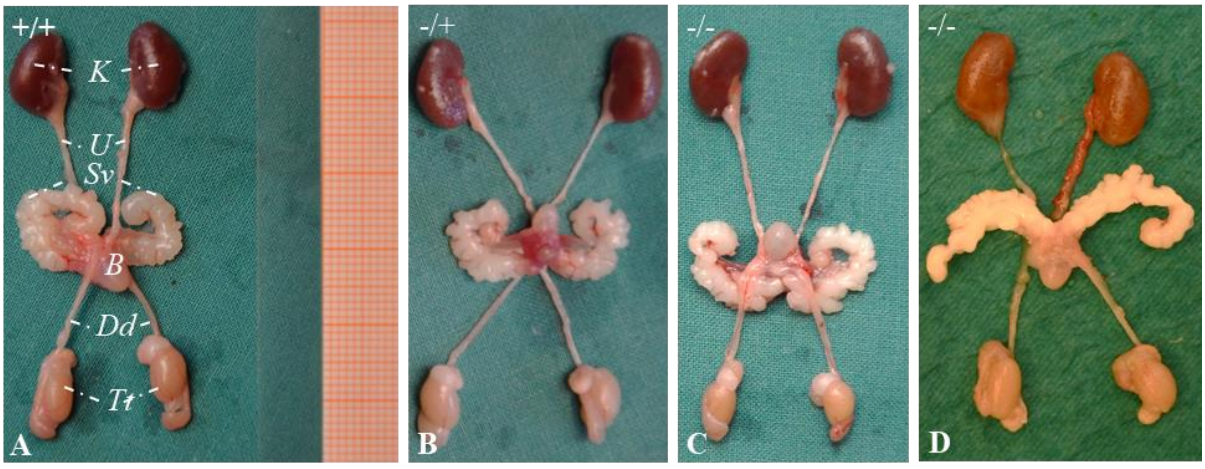

Figure 9| Macroscopic analyses of the urogenital tract of (A; +/+) control, (B; -/+) gc*Pex13*HTZ and both (C; -/-) *Stra8*-Cre and (D; -/-) *Prm*-Cre mediated gc*Pex13*KO mice. (C) Pre-meiotic induced gc*Pex13*KO testes were significantly reduced (of 0.442 ± 0.311 cm) compared to **(B)** gc*Pex13*HTZ (0.764 ± 0.075 cm) and **(A)** control testes (0.780 ± 0.076 cm). **(D)** In *Prm*-Cre mediated gc*Pex13*KO mice, no significant differences were found (0.840 ± 0.042 cm) compared to **(A)** control animals. *K*- Kidney; *U*- Ureter; *Sv*- Seminal vesicle, *B*- Bladder, *Dd*- Ductus deferens, *E*- Epididymis, *Tt*- Testicles.

3.3 Testicular histology of *Prm*-Cre and *Stra8*-Cre mediated mouse testes

Testes of all genotypes were histologically analysed using paraffin-embedded, HE stained specimens. Stage VII seminiferous tubules of pre- and post-meiotic induced gc*Pex13*KO testes of early mature (P30), mature (P70) and senior mice (P360) were compared to control.

Compared to control testes (253.1 ± 33.0 µm), the diameter of the seminiferous tubules of pre-meiotic induced gc*Pex13*KO mice was significantly smaller (177 ± 18.82 µm; $p < 0{,}0001$; Figure 10). Regular spermatogenesis was found in early mature (Figure 11A, D), mature (Figure 11B, E) and senior (Figure 11C, F) control and gc*Pex13*HTZ testes, as well as *Prm*-Cre mediated gc*Pex13*KO (Figure 11J- L) mice. Tubules were mainly round or oval shaped. The tubules´ size increased in aging control (Figure 11A-C), heterozygous (Figure 11D-F), and post- meiotic induced gc*Pex13*KO mice (Figure 11J- L). Whereas normal littermates revealed spermatogenic cells at all stages, including spermatozoa, a severe defect in germ cell differentiation in *Stra8*-Cre mediated gc*Pex13*KO testes was observed in HE stained paraffin sections (Figure 11G- I). Seminiferous tubules with a pre-meiotic induced peroxisomal KO showed a spermatogenic arrest. Instead of single round spermatids, spermatid-stage nuclei were arranged as multinucleated giant cells (MNCs) with an average size of 39.83 ± 8.78 µm (Figure 11G- I). With aging, most of the MNCs were lacking nuclei and seemed to lyse, leading to vacuolization of the tubules. The tubules showed a more irregular shape (Figure 11I) and displayed an increased number of interstitial cells (hyperplastic; Figure 11I). Since MNCs were frequently present in the seminiferous tubules of *Stra8*-Cre mediated gc*Pex13*KO animals, even in early mature mice, subsequent analyses were conducted on mature testes.

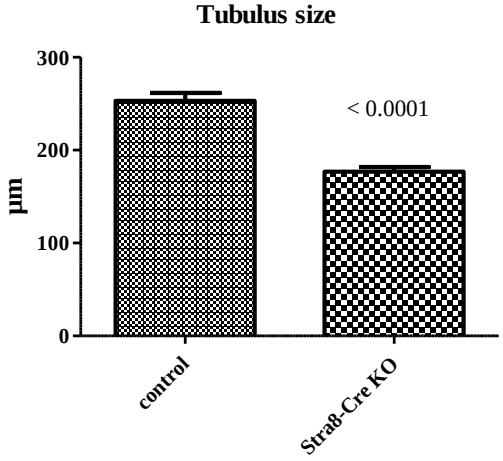

Figure 10| Comparison of the average size of the seminiferous tubules of control and *Stra8*-Cre mediated KO testes. The size of the seminiferous tubules of the pre-meiotic induced gc*Pex13*KO was significantly reduced ($p < 0{,}0001$) compared to control testes. Statistical significance was determined using t-test (non-parametric Mann-Whitney *U* test). *$p \leq .05$; **$p\ 0.001 < p \leq 0.01$; *** $p \leq 0.001$

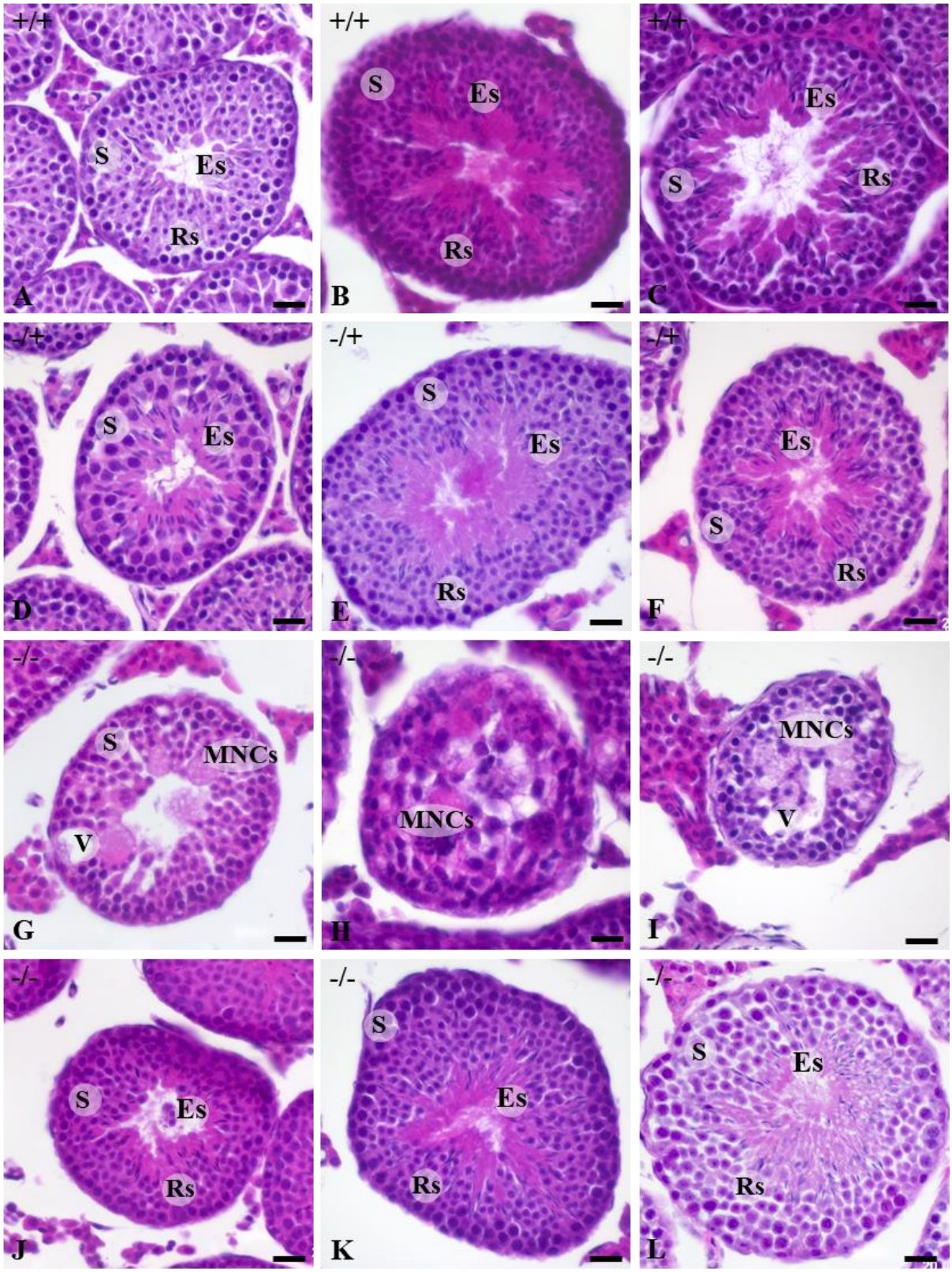

Figure 11| Histological analyses of control, gc*Pex13*HTZ, and post- or pre-meiotic induced gc*Pex13*KO testes of early mature (P30), mature (P70) and senior (P360) mice. Cross-sections of all genotypes of different ages represent germ cell development at stage VII. The germinal epithelium of **(A)** control, **(D)** HTZ

and **(J)** *Prm*-Cre mediated gc*Pex13*KO testes of early mature mice (P30) showed regular spermatogenesis with meiotically dividing spermatocytes (S) round (Rs) and elongated spermatids (Es), whose cytoplasm is distributed along head and tail of spermatids. **(G)** In testis with a pre-meiotic induced peroxisomal KO, spermatid nuclei were arranged as MNCs. At stage VII, most of the MNCs were lacking nuclei. Instead, tubules were mainly vacuolized. **(B, E, K)** The seminiferous tubules of control, gc*Pex13*HTZ, and post- meiotic induced gc*Pex13*KO mature and **(C, F, L)** senior mice were slightly increased. **(H, I)** Germ cell development was comparable to that of early mature mice. *Stra8*-Cre mediated gc*Pex13*KO seminiferous tubules decreased in size in aging mice, compared to control and *Prm*-Cre mediated gc*Pex13*KO. The germinal epithelium contained many vacuoles (V). Bars represent 20 µm.

3.4 Confirmation of gc*Pex13*KO by PCR analysis of laser capture micro dissected cells

Cre-mediated excision of floxed *Pex13* was confirmed by PCR of laser micro-dissected cells from paraffin-embedded specimens (Figure 12A- C).

In pre-meiotic induced gc*Pex13*KO, all luminal cells representing MNCs and cells from the basal compartment were defined. In post-meiotic mediated gc*Pex13*KO, heterozygous and control testes, elongated spermatids, round spermatids and Sertoli cells, as well as the basal compartment, containing spermatocytes and spermatogonia, were collected. Control mice exhibited a band at 490 bp, representing the WT allele (Figure 13A). Cells collected from gc*Pex13*HTZ testes, represented one floxed *Pex13* allele (including the *loxP* sites) at 540 bp, and a WT allele at 490 bp. An amplicon of excised floxed *Pex13* was present at lower abundance, because animals also carried the Cre transgene that recombined with the floxed *Pex13* allele (Figure 13B). *Prm*-Cre mediated gc*Pex13*KO cells had a floxed *Pex13* allele and a deletion in *exon 2*, assuming a contamination with Sertoli cells that were still carrying the floxed *Pex13* allele (Figure C). Genotyping of *Stra8*-Cre mediated gc*Pex13*KO confirmed the complete KO in both alleles, since no floxed *Pex13* allele was detectable (Figure 13D). The amplicon of deleted *exon 2* of *Pex13* was increased in germ cells of *Prm*-Cre mediated gc*Pex13*KO (Figure 13C) and in MNCs of *Stra8*-Cre mediated gc*Pex13*KO (Figure 13D).

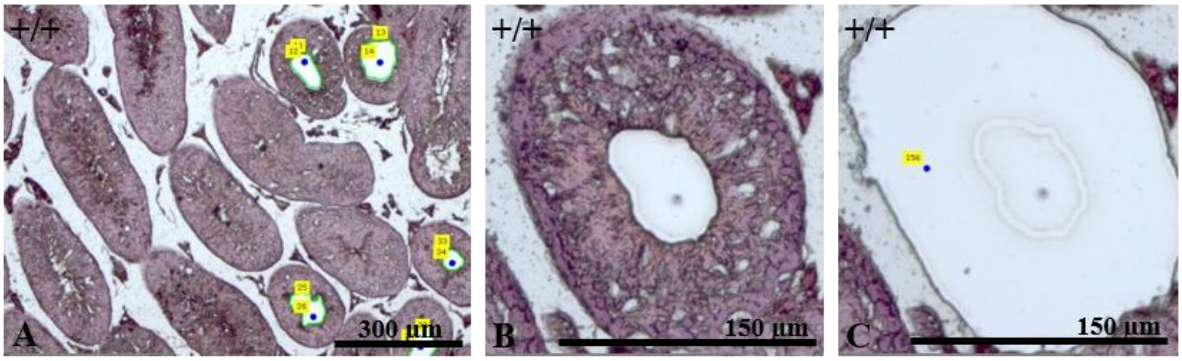

Figure 12| Laser capture microdissection of testicular cells to confirm the genotypes. (A- C) Paraffin-embedded sections (6 µm) of control and gc*Pex13*KO testes were stained with HE. Prior to microdissection with a P.A.L.M. laser, tubuli of interest were marked (indicated in yellow). **(B, C)** In case of control and post-meiotic induced gc*Pex13*KO tubuli, round spermatids, spermatocytes, as well as apically residing sperm heads were cut

out. In tubuli of pre-meiotic induced peroxisomal KO, MNCs were separately cut out from spermatocytes (data not shown).

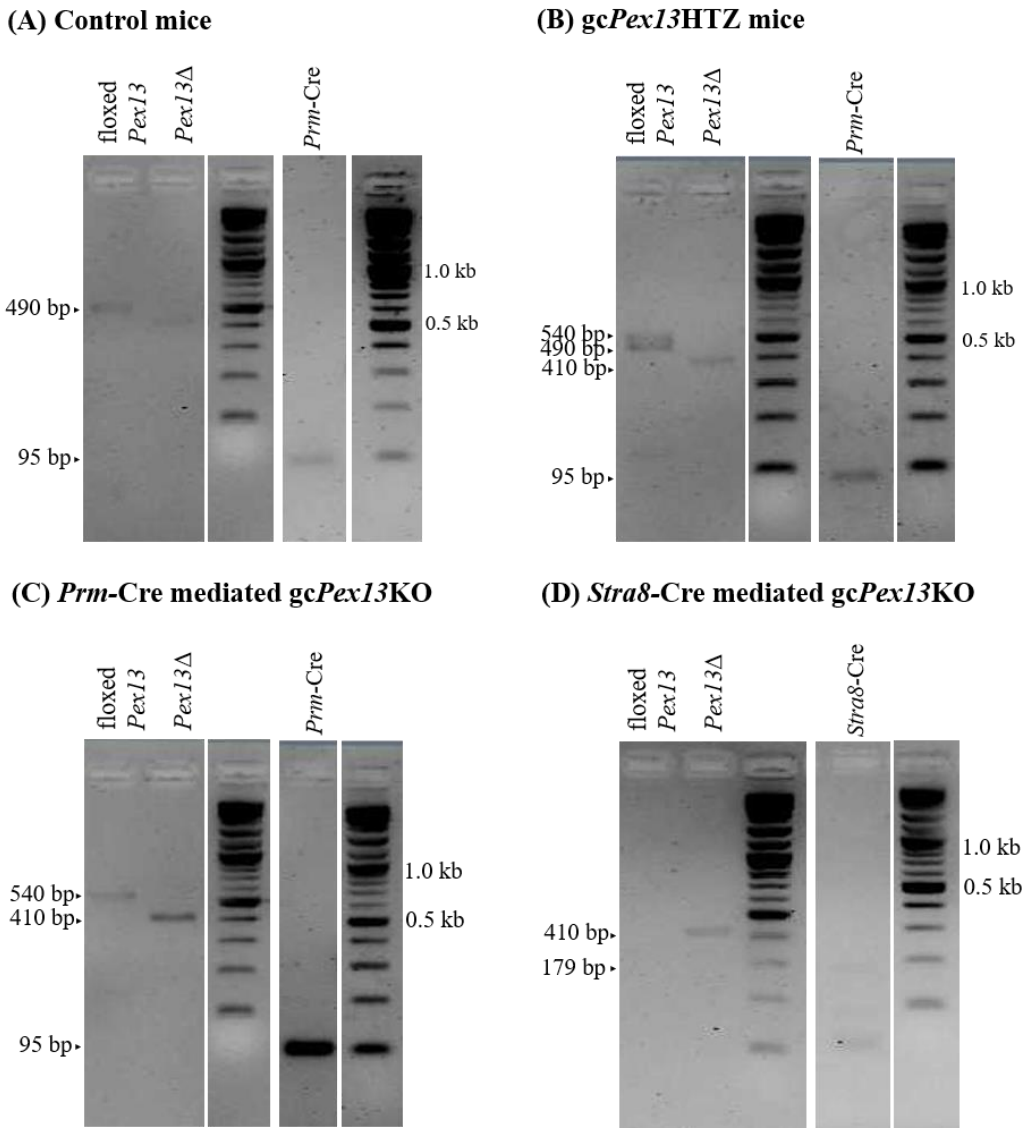

Figure 13| Targeted disruption of *Pex13* was confirmed by PCR of microdissected cells. (A- D) A total number of 1000 cells per genotype was used for DNA extraction and subsequent genotyping by PCR. **(A)** Cre-transgenic mice with a WT allele at 490 bp, were considered as control mice. In case of the *Prm*-Cre transgene, a band at 95 bp was visible (as shown in **C**). WT mice, positive for the *Stra8*-Cre recombinase, had an additional band at 179 bp (as shown in **D**). **(B)** gc*Pex13*HTZ mice were genotyped according to the floxed *Pex13* allele (including the *loxP* sites), represented by a 540 bp amplicon, and a WT allele at 490 bp. A faint band was visible at 410 bp, representing the excised *exon 2* of *Pex13* **(C)** Haploid germ cells of the *Prm*-Cre mediated peroxisomal KO carried a floxed *Pex13* allele at 540 bp and a deletion in *exon 2* at 410 bp (Δ*Pex13*). Genotyping represented an incomplete KO, because of a contamination by Sertoli cells. **(D)** In the *Stra8*-Cre mediated gc*Pex13*KO, the floxed *Pex13* allele was not detectable in MNCs, confirming a complete KO in both alleles. Excised *exon 2* of floxed *Pex13* was further confirmed by an amplicon at 410 bp. A 1 kb DNA ladder was used.

3.5 Peroxisomal protein localization is altered in pre-meiotic induced gc*Pex13*KO

To confirm the peroxisomal KO in *Pex13*, male GFP-PTS1 transgenic mice were crossed into homozygous *Stra8*-Cre mediated peroxisomal gc*Pex13*KO female mice. In the control group, peroxisomes were present in Leydig cells and in all germ cells, except for spermatozoa. Although the presence of peroxisomes was already confirmed in Sertoli cells, GFP-PTS1 was not visible in these cells (Figure 14A, B). In pre-meiotic induced gc*Pex13*KO testes, GFP was only detected in peritubular myoid cells, in the basal epithelium and in Leydig cells (Figure 14C, D). Whereas residual bodies were present in the lumen of control mice (indicated as green dots), no residual bodies were found in seminiferous tubules of *Stra8*-Cre mediated gc*Pex13*KO mice (Figure 14D).

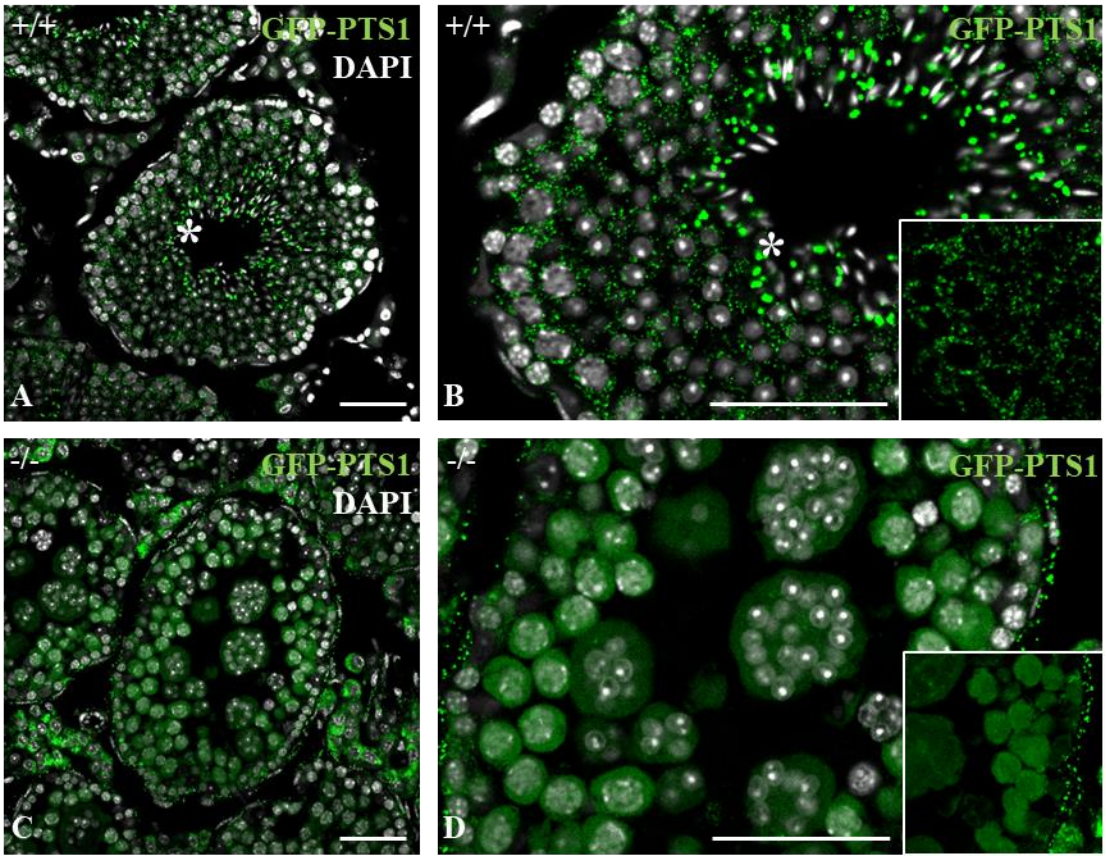

Figure 14| Cross-sections of control and *Stra8*-Cre mediated gc*Pex13*KO testes with a GFP-PTS1 signal. (A, B) In control mice, peroxisomes were abundant in interstitial Leydig cells and all germ cells, except for spermatozoa. Luminal fluorescent signals represent residual bodies (∗), containing cytoplasmic debris. **(C, D)** In pre-meiotic induced gc*Pex13*KO testes that were GFP positive and homozygous for the Cre translocon and floxed *Pex13*, peroxisomes were only present in Leydig cells, peritubular myoid cells and spermatogonia. **(A-D)** Nuclei were counterstained with DAPI (grey). Bars represent 50 µm.

Staining with the PEX13 antibody revealed a punctate localization in all cell types including testis-specific somatic cells (Sertoli cells and peritubular cells) and germ cells (spermatogonia, primary and secondary spermatocytes, round and elongated spermatids), in the seminiferous tubules of control (Figure 15A, B) and *Prm*-Cre mediated gc*Pex13*KO mice (Figure 15E, F), with the exception for mature spermatozoa. PEX13 was abundantly expressed in spermatocytes and spermatids but it was weaker expressed in Sertoli-, peritubular myoid and Leydig cells. In testes with a *Pex13* KO in pre-meiotic germ cells, the distribution was clearly cytoplasmic in all germ cells, including MNCs (Figure 15C, D). In contrast to control testes, no punctate structures were found in a pattern that is typical for peroxisomes, indicating a loss of PEX13 already in early germ cells. In *Prm*-Cre mediated gc*Pex13*KO testes (Figure 15E, F), PEX13 localization resembled that of control mice (Figure 15A, B).

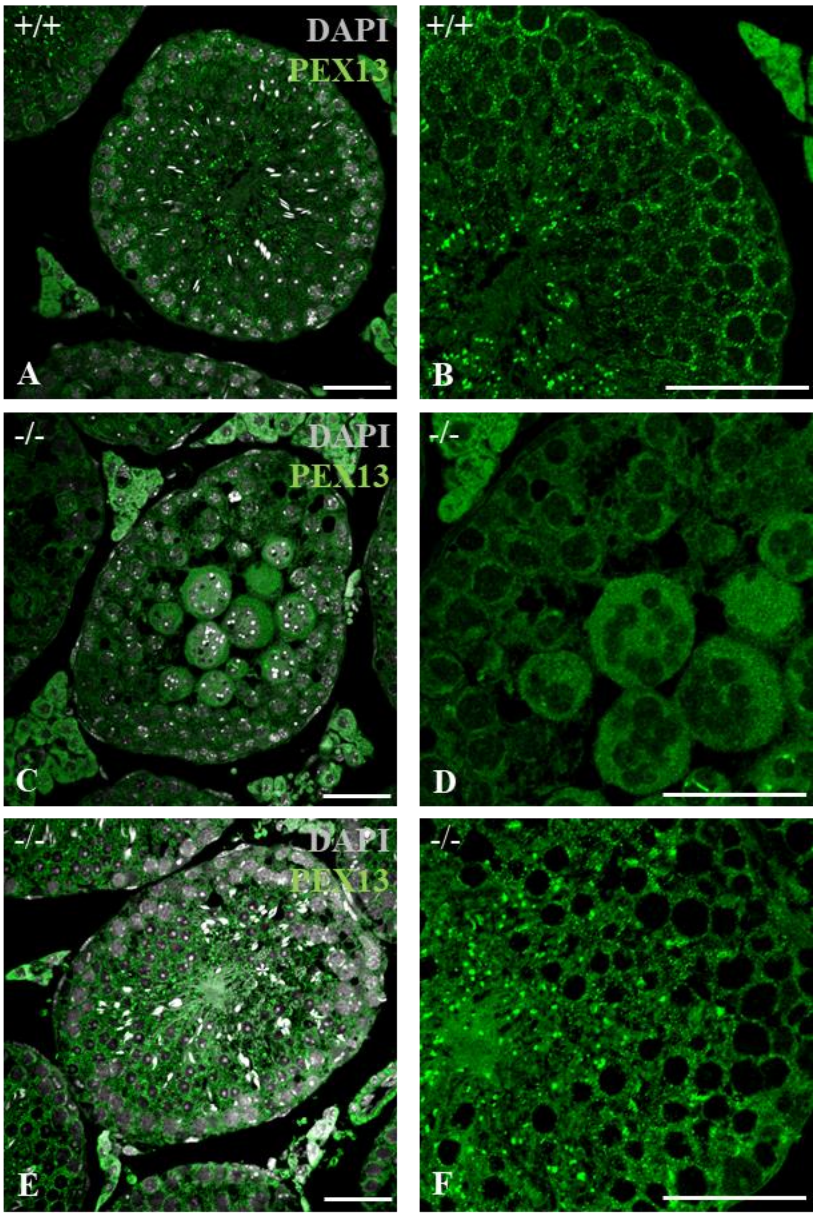

Figure 15| Immunofluorescent detection of PEX13 in the seminiferous tubules of all genotypes. (A, B) Paraffin-embedded specimens of control (P60), **(C, D)** pre- and **(E, F)** post-meiotic induced peroxisomal KO (P80) testes were labelled with PEX13. **(A, B)** In the testis of control and **(E, F)** post-meiotic induced peroxisomal KO, PEX13 was mainly localized in punctate structures in spermatocytes, but was also found in post-meiotic germ cells. **(C, D)** In the *Stra8*-Cre mediated gc*Pex13*KO mice, PEX13 showed a diffuse cytoplasmic pattern in all germ cells, including MNCs. In contrast to control testes, no punctate structures were found in a pattern that is typical for peroxisomes, indicating a loss of PEX13 already in early germ cells. Bars represent 50 µm.

In control (Figure 16A- C) and heterozygous (Figure 16D- F) mouse testes, PEX14 co-localized with the GFP-PTS1 transgene and was highly expressed in all germ cells, but was also detected in peritubular myoid and Leydig cells. In post-meiotic induced peroxisomal KO mice, a similar pattern was found for PEX14 (Figure 17B, C), as shown for control testes (Figure 17A). The anti-ABCD3

antibody showed significant immunoreactivity to peroxisomes in Sertoli cells and germ cells of the basal part of the germinal epithelium and in Leydig cells of control mice (Figure 16J, L, K, M). In *Pex13*-deficient cells of *Stra8*-Cre mediated gc*Pex13*KO testes, the peroxisomal membrane proteins were not localized to punctate structures, but appeared to be cytosolically localized (Figure 16G, H, N, O). Positive and negative controls are shown in Figure 18.

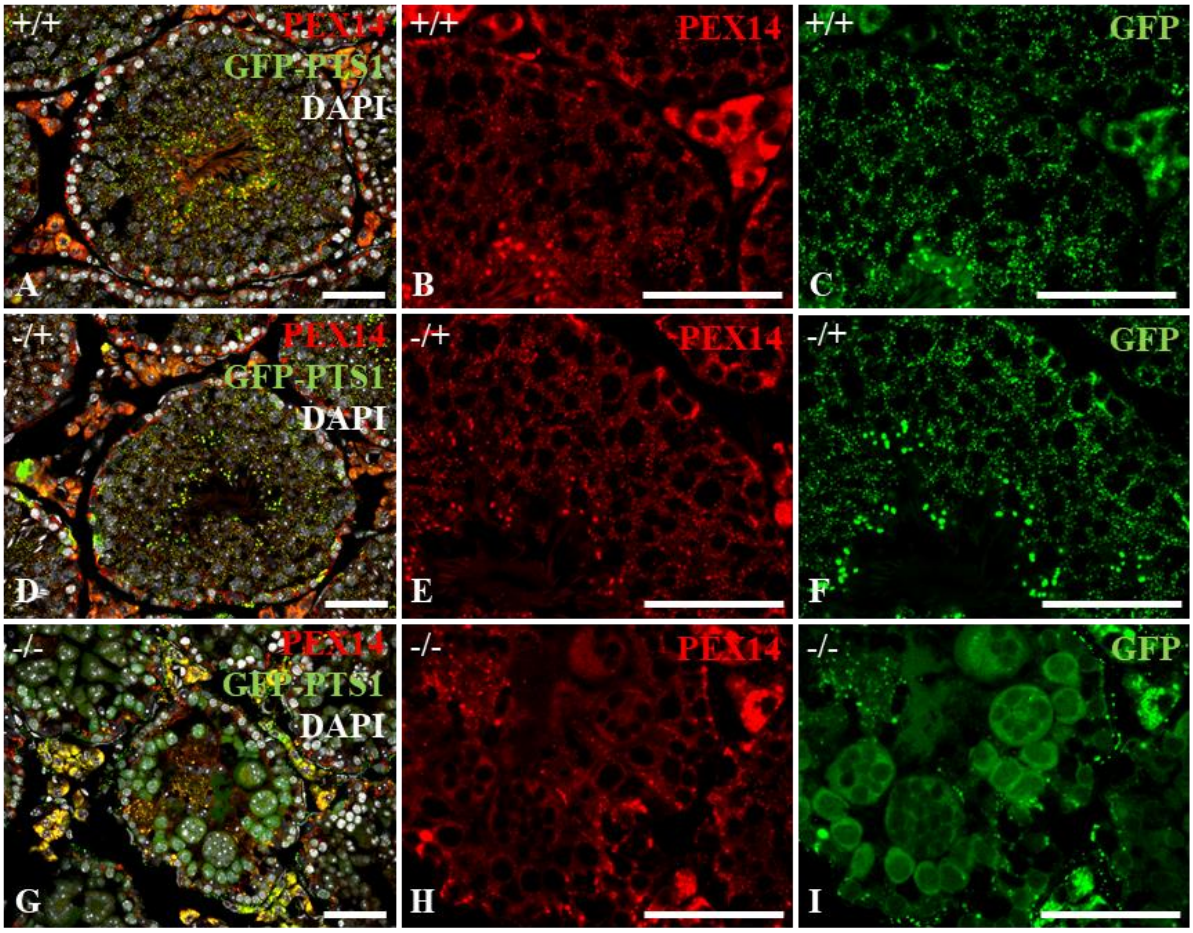

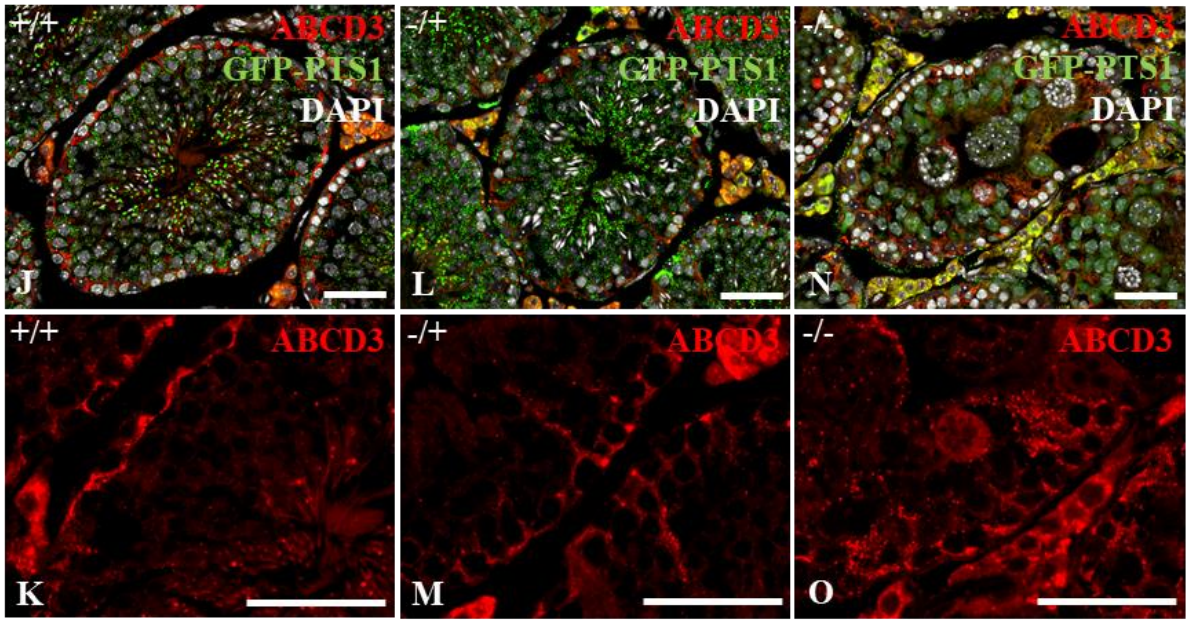

Figure 16| Immunofluorescent detection of organelle marker proteins in the seminiferous tubules of all genotypes carrying the GFP-PTS1 transgene. (A- C, J) Cryosections of GFP-PTS1 (green) transgenic control (P60), **(D- F, L)** heterozygous (P80) and **(G- I, N)** pre-meiotic induced peroxisomal KO (P80) testes were stained with **(A, B, D, E, G, H)** PEX14 (red) and **(J- N)** ABCD3 (red). **(A, B, J)** In control and **(D, E, L)** gc*Pex13*HTZ mouse testes, anti-PEX14 and anti-ABCD3 antibodies were localized in punctate structures typical for peroxisomes. ABCD3 was primarily expressed in Sertoli cells and in the basal part of the germinal epithelium. **(A, D, G)** Colocalization of anti-PEX14, **(J, L, N)** anti-ABCD3 and GFP-PTS1 in the same particles verified the peroxisomal nature of these structures (yellow). **(G- I; N, O)** In *Pex13*-deficient cells, peroxisomal membrane proteins were not localized to punctate structures. All preparations were counterstained with DAPI (grey) for labelling of nuclei. Bars represent 50 µm.

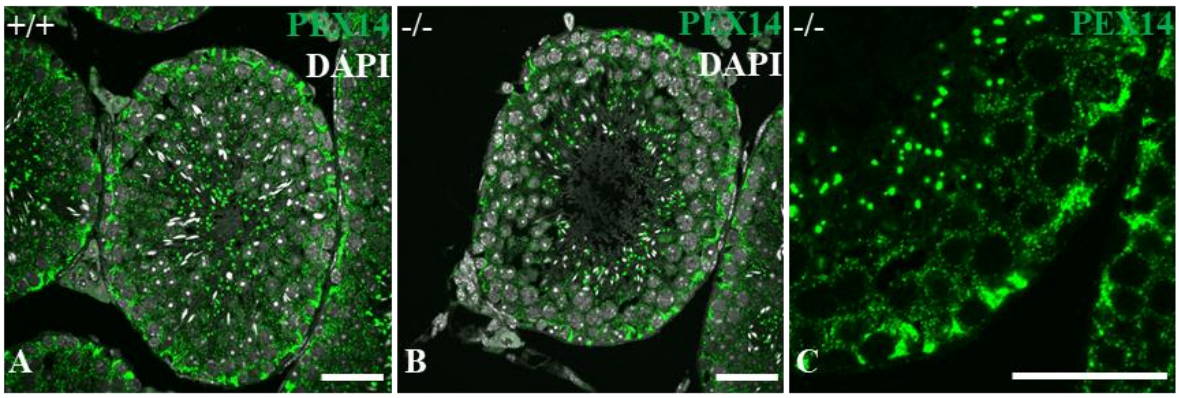

Figure 17| Immunofluorescent detection of organelle marker protein PEX14 in the seminiferous tubules of post-meiotic induced peroxisomal KO. (B, C) Localization of PEX14 showed no difference in gc*Pex13*KO testes compared to **(A)** control.

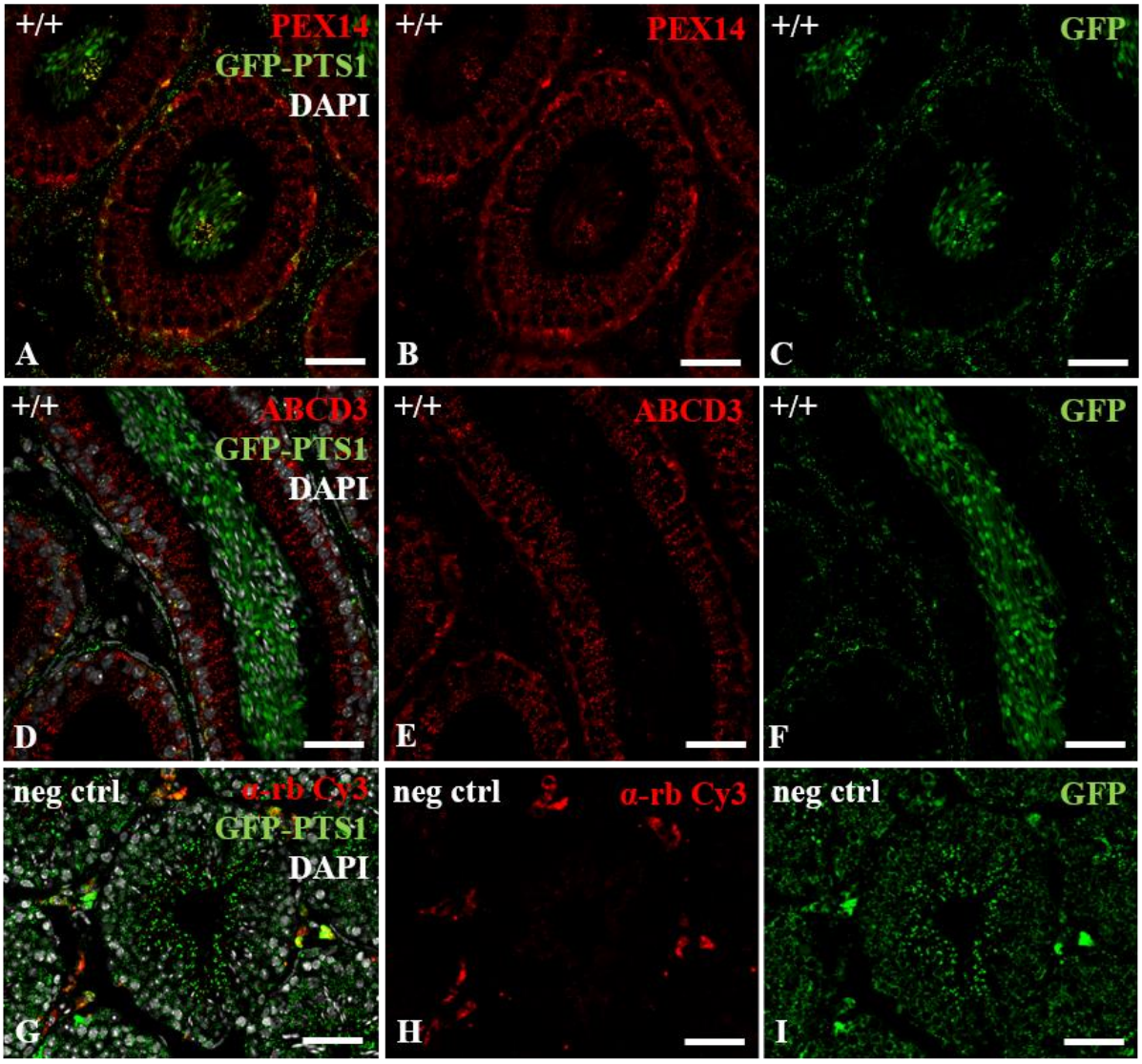

Figure 18| Positive and negative controls for immunofluorescence preparations of cryosections. (A, B) As positive controls, the epididymis of GFP-PTS1 mice were stained with anti-PEX14 and **(D, E)** anti-ABCD3 antibodies. **(G-H)** Negative controls (neg ctrl), lacking the primary antibody, show the specificity of secondary antibody reaction in mouse testes. **(A, C, D, F)** Peroxisomes are highlighted by the GFP-PTS1 signal in the epididymis and **(G, I)** testis. Bars represent 50 µm.

3.6 Peroxisomal matrix protein localization is not altered in gc*Pex13*KO mice

A double-immunofluorescent staining with vimentin (VIM), used as intermediate filament marker of Sertoli cells, and peroxisomal catalase (CAT) was performed. Vimentin labelling displayed a characteristic pattern in control (Figure 19B), heterozygous (Figure 19E) and post-meiotic induced peroxisomal KO testes (Figure 19H) with Sertoli cell intermediate filaments extending from the basal

compartment to the lumen, and lateral extensions that display the BTB. However, in the *Stra8*-Cre mediated gc*Pex13*KO mice, Sertoli cells seemed to enclose all germ cells (Figure 19K).

In control, gc*Pex13*HTZ and gc*Pex13*KO mouse testes, CAT immunoreactivity was most intense in Leydig cells, as shown in Figure 19A, C, D, F, G, I, J and L. The typical punctuate staining pattern was also found in the basal compartment of the germinal epithelium, including peritubular myoid cells and spermatogonia (Figure 19C, F, I). In the adluminal compartment, CAT showed strong immunoreactivity in the acrosome of round and elongating spermatids (Figure 19I). A faint punctuate staining could also be observed in Sertoli cells and spermatocytes (Figure 19C, F, I). In the *Prm*-Cre mediated gc*Pex13*KO mice (Figure 19G, I), the immunoreactivity for CAT was comparable to control mice. In pre-meiotic induced gc*Pex13*KO mice, CAT was also expressed in basal cells, but in a diffuse cytoplasmic pattern. It was most abundant in Leydig cells (Figure 19J, L). CAT showed immunoreactivity to the acrosome of round spermatids clustered in MNCs (data not shown).

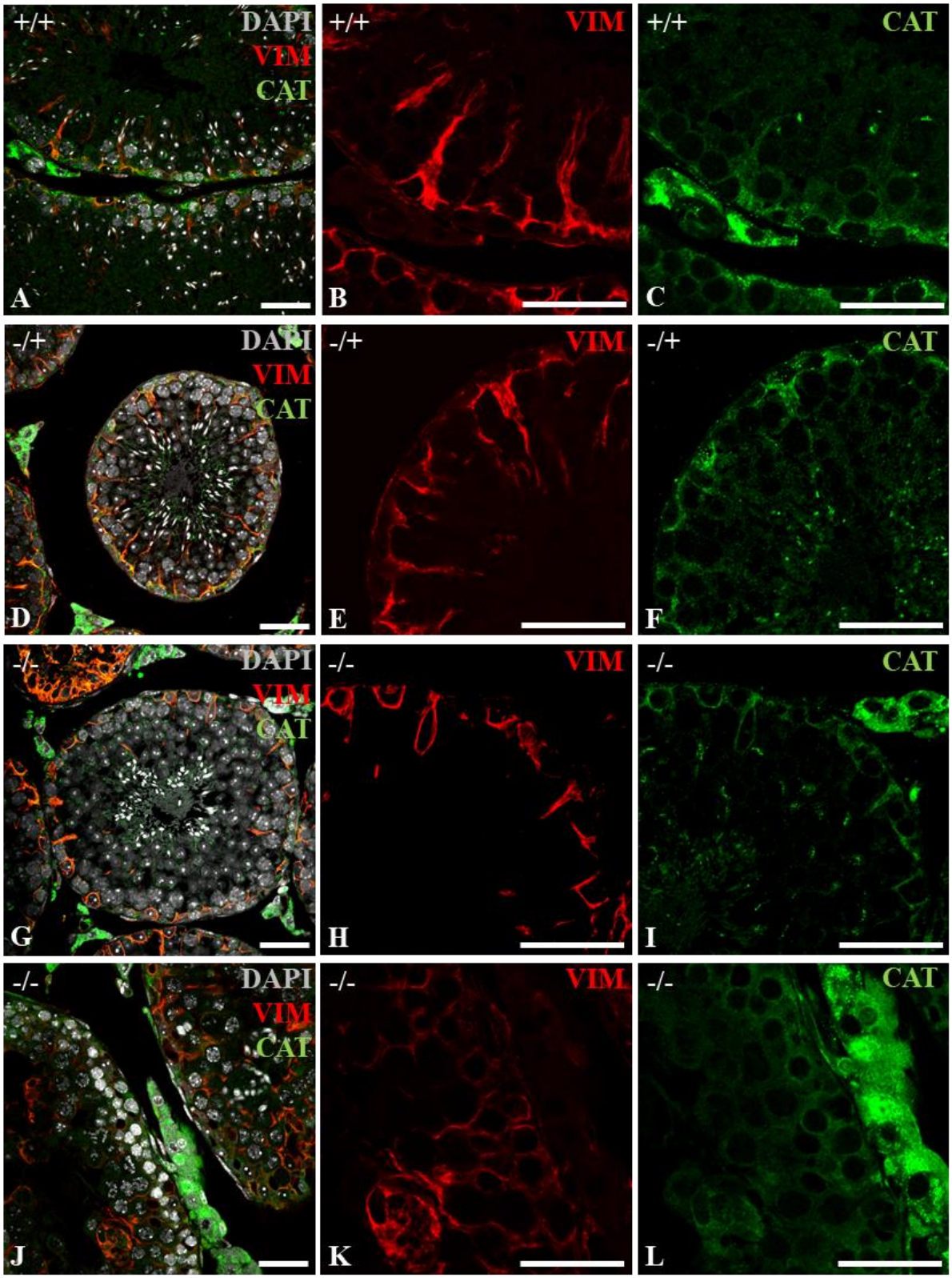

Figure 19| Immunofluorescent detection of intermediate filament marker vimentin (VIM) and peroxisomal protein catalase (CAT) in adult testes. Paraffin-embedded specimens (2 µm thickness) of mouse testis biopsies were used and double stained with catalase (CAT, red) and vimentin (VIM, red). **(A, B)** Vimentin

showed a characteristic Sertoli cell intermediate filament specific staining pattern in control, **(D, E)** heterozygous and **(G, H)** post-meiotic induced KO cells. Intermediate filaments extended from the basal compartment to the lumen, with lateral extensions, displaying the BTB. **(J, K)** In *Stra8*-Cre mediated gc*Pex13*KO, vimentin immunostaining showed an irregular pattern. **(A, C, D, F, G, I, J, L)** Catalase showed a punctuate staining pattern and was highly abundant in interstitial Leydig cells in all genotypes. **(A, C)** Germ cells as well as Sertoli cells were positive for catalase counterstain in control, **(D, F)** heterozygous and **(G, I)** post-meiotic induced gc*Pex13*KO testes. **(G, I)** Catalase was also immunoreactive in the acrosome, as shown in the seminiferous tubules of *Prm*-Cre mediated gc*Pex13*KO mice. **(J, L)** In *Stra8*-Cre mediated peroxisomal KO seminiferous tubules, CAT was localized in the cytosol. Nuclei were counterstained with DAPI (grey). Bars represent 50 µm.

The immunoreactivity for peroxisomal thiolase showed strong signals in interstitial Leydig cells of all genotypes (Figure 21A- F). For peroxisomes typical pattern was found in the peritubular myoid cells and in all germ cells of the germinal epithelium of control (Figure 21A, B), but also *Prm*-Cre mediated gc*Pex13*KO mice (Figure 21E, F). In round and elongating spermatids, immunoreactivity was at lower intensity compared to suprabasal germ cells (Figure 21A, B, E, F). The antibody showed high reactivity to residual bodies (Figure 21E, F). The characteristic staining pattern of thiolase was abolished in pre-meiotic induced gc*Pex13*KO testes (Figure 21C, D). Thiolase was present in a punctuate pattern in cells of suprabasal compartment. In *Pex13*-deficient germ cells, the distribution was clearly cytosolic.

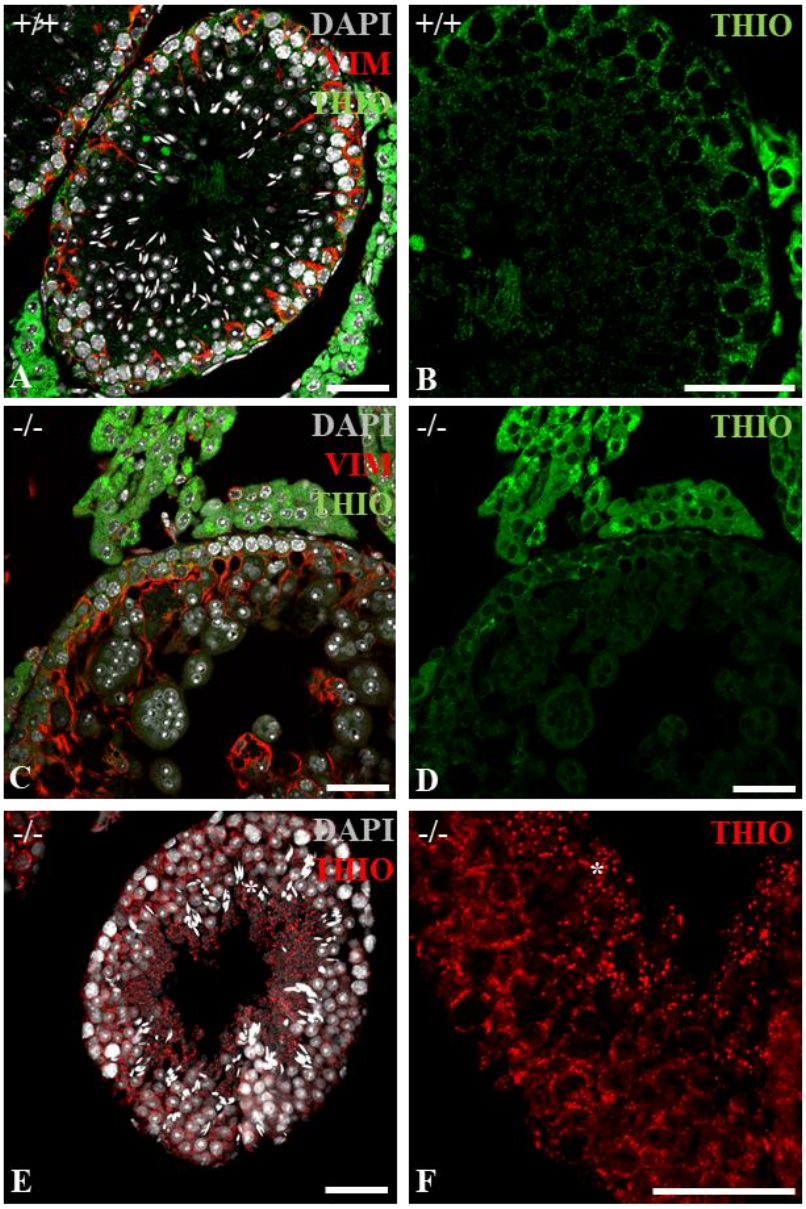

Figure 20| Presence of peroxisomal thiolase in adult mouse seminiferous tubules. (A- D) For control and *Stra8*-Cre mediated gc*Pex13*KO mice, a double immunofluorescent staining with thiolase (THIO, green) and intermediate filament marker vimentin (VIM, red) was performed. **(A- E)** In all specimens, thiolase was highly abundant in interstitial Leydig cells. **(A, B)** In control and **(E, F)** *Prm*-Cre mediated gc*Pex13*KO testes, for peroxisomes typical punctuate staining pattern was found in the suprabasal and basal layers of all germ cells in the germinal epithelium. **(C, D)** In germ cells of *Stra8*-Cre mediated gc*Pex13*KO, the protein was cytosolically localized. (**E, F)** The antibody showed high cross-reactivity to residual bodies, as shown in post-meiotic induced peroxisomal KO testes (∗). **(A- D)** In control and *Stra8*-Cre mediated peroxisomal KO testes, thiolase was tagged with Alexa488, due to double immunofluorescent staining with vimentin. **(E, F)** In the *Prm*-Cre mediated gc*Pex13*KO testes, thiolase is displayed in red (Cy3). **(A, C, E)** Nuclei were counterstained with DAPI (grey). Bars represent 50 µm.

As an internal control for organelle distribution, the immunoreactivity and localization of mitochondrial proteins was tested using antibodies against the complex III of the respiratory chain (OxPhosIII) and the mitochondrial import receptor unit (TOM70). In comparison to peroxisomal enzymes, neither mitochondrial complex III (Figure 20D, E) nor TOM70 (Figure 20F) were markedly affected in *Pex13*-deficient germ cells in *Stra8*-Cre mice. These markers showed a similar pattern in control (Figure A- C) and *Prm*-Cre mediated gc*Pex13*KO testes (Figure 20G, H). Mitochondria were mainly present in spermatocytes, but were also found in round spermatids of control and in MNCs of *Stra8*-Cre mediated gc*Pex13*KO mice.

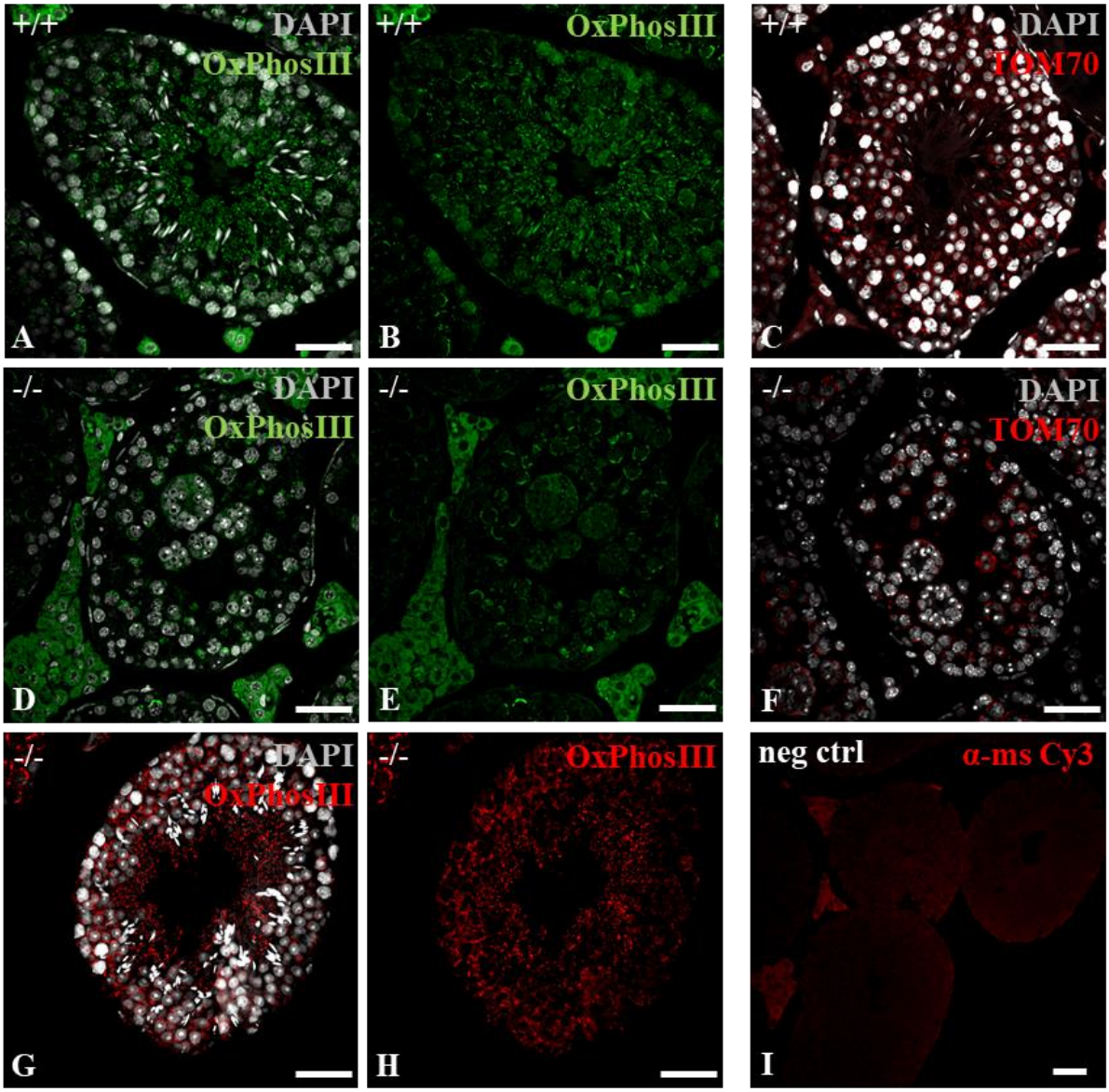

Figure 21| Fluorescence detection of mitochondrial proteins OxPhosIII and TOM70 in adult mouse testis of all genotypes. (A- C) Paraffin embedded adult specimens of control, **(D- F)** pre- and **(G, H)** post meiotic induced peroxisomal KO mice were used. **(A- H)** In all specimens, mitochondrial proteins were expressed in all

germ cells and Sertoli cells, as well as in the **(D- F)** *Stra8*-Cre mediated gc*Pex13*KO cells. **(A, B)** In control and **(D, E)** *Stra8*-Cre gc*Pex13*KO mice, OxPhosIII was labelled with Alexa488 (green). **(C)** In control and **(F)** *Stra8*-Cre gc*Pex13*KO mice, TOM70 was labelled with Cy3 (red). **(G, H)** In *Prm*-Cre mediated gc*Pex13*KO, OxPhosIII was highlighted in red. **(A- H)** Nuclei were counterstained with DAPI (grey). Bars represent 50 µm. **(I)** The negative control (neg ctrl; α-mouse), lacking the primary antibody, shows the specificity of secondary antibody reaction in mouse testes. Bar represents 20 µm.

3.7 The pre-meiotic induced gc*Pex13KO* leads to a severe disturbance in germ cell differentiation

The stages of the seminiferous cycle were defined in *Stra8*-Cre and *Prm*-Cre mediated gc*Pex13*KO testes. Compared to control mice, no differences were identified in germ cell development at all 12 stages in post-meiotic induced peroxisomal KO testes (data not shown).

In *Stra8*-Cre mediated gc*Pex13*KO testes, the classification was made upon meiotic cell divisions of spermatocytes and developmental stages of spermatids, in this case MNCs.

In stage I tubules of both control (Figure 22A) and gc*Pex13*KO mice (Figure 22B), round spermatids had a large central nucleolus, but lacked an acrosomal system. Moreover, spermatocytes were found at the very basal layer in the germinal epithelium, but no spermatogonia were present. Stage II-IV tubules were classified according to proacrosomal granules forming a large, fluid-filled acrosomal vesicle that surrounds the acrosomal granule (Figure 22C, D), indicated as a condensed structure. In some tubules, the acrosomic granule already formed an indentation of the round spermatid nucleus (data not shown). Moreover, intermediate spermatogonia with an ovoid nucleus were detected (Figure 22C, D). Stage V was judged upon the presence of B-type spermatogonia and acrosomal vesicles over the nucleus of spermatids in control (Figure 22E) and gc*Pex13*KO mice (Figure 22F). For the stages VI and VII, the identification of an appropriate tubule in pre-meiotic induced peroxisomal KO was not possible, because staging mainly refers to the migration of elongating spermatids towards the lumen and the cytoplasmic distribution along head and tail of spermatids in control (Figure 22G, H), which are absent in the *Stra8*-Cre mediated gc*Pex13*KO mice. Stage VIII in control tubules was classified according to the release of elongated spermatids through spermiation (Figure 22I). In both control and gc*Pex13*KO mice, a flattened acrosome, forming a cap-like structure (Figure 22I, J), could be identified. In gc*Pex13*KO mice, some of the spermatids, arranged as MNCs, already started apoptotic nuclear condensation (Figure 22J). An additional feature for a tubule of stage VIII was the presence of enlarged preleptotene cell nuclei in spermatocytes (Figure 22I, J). The tubules of the gc*Pex13*KO mice with slightly stained chromatin of pachytene spermatocytes was assigned to be at stage IX (Figure 22L). In control, only one generation of spermatids was located with an elongated apico-caudal axis. The presence of cytoplasmic lobes that will fuse into very large residual bodies is very characteristic for this stage (Figure 22K). Steps IX to XII in control testes were classified according to chromatin

condensation in round spermatids during their transformation into elongating spermatids (Figure 22K, M, O, Q). Stage X tubules of the *Stra8*-Cre mediated gc*Pex13*KO mice were characterized according to their pachytene spermatocytes as well as spermatocyte transition between leptotene and zygotene (Figure 22N). In stage XI tubules of control and gc*Pex13*KO testes, nuclei of diplotene spermatocytes were extended as they enter diakinesis of meiosis I (Figure 22O, P). Moreover, morphology of diplotene and zygotene spermatocytes resembled that in control germinal epithelium of stage XI. Stage XII tubules could be identified according to meiosis I and II cells, representing secondary spermatocytes (Figure 22 Q, R).

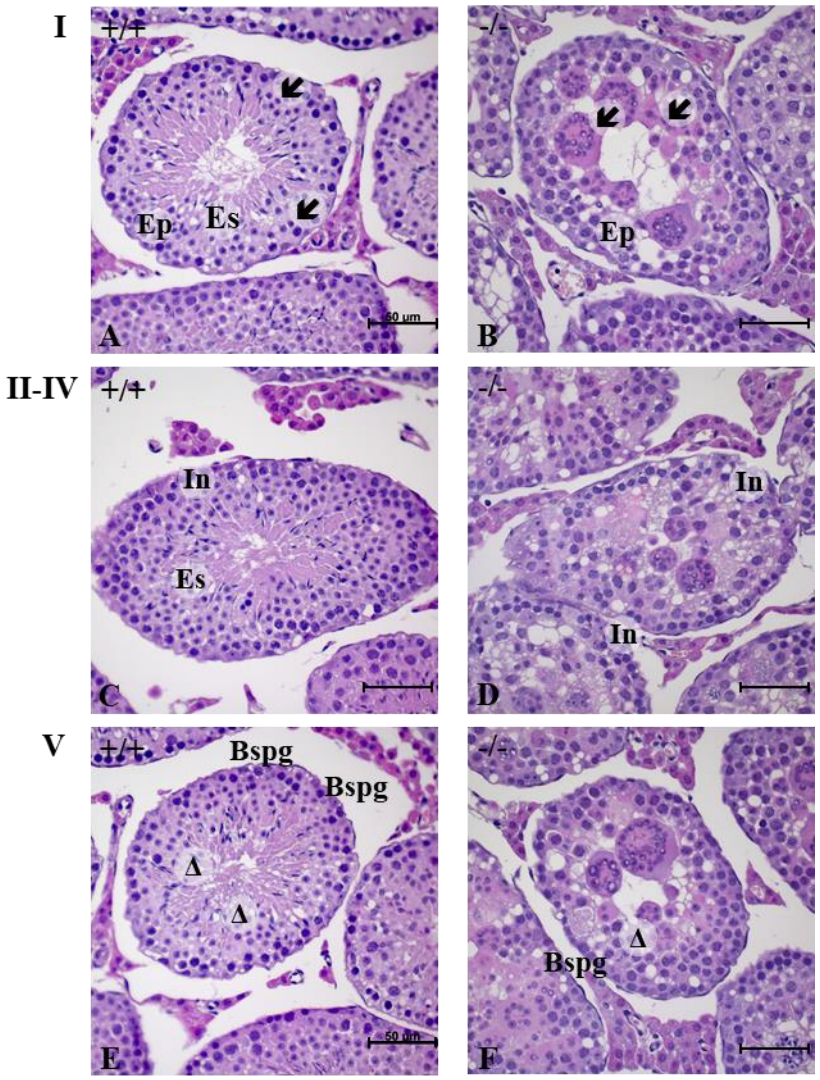

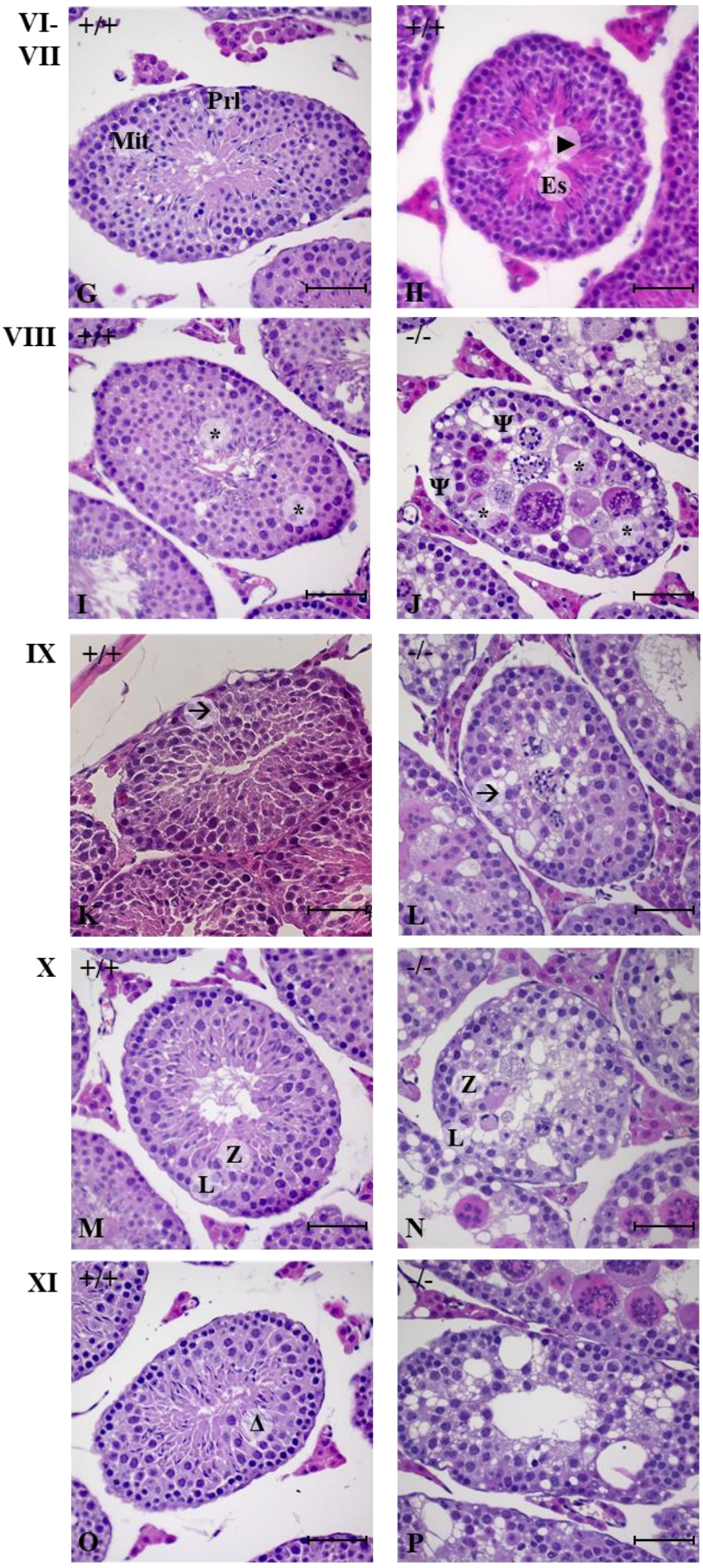
VI-VII
+/+
Prl
Mit
G
+/+
Es
H
VIII
+/+
*
*
I
-/-
Ψ
Ψ
*
*
*
J
IX
+/+
→
K
-/-
→
L
X
+/+
Z
L
M
-/-
Z
L
N
XI
+/+
Δ
O
-/-
P

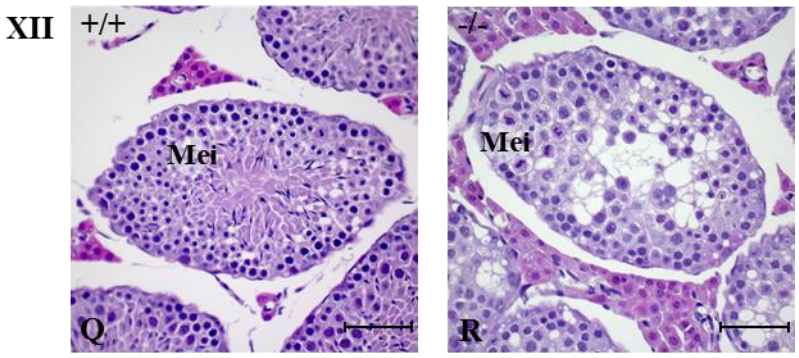

Figure 22| Staging of pre-meiotic induced gc*Pex13*KO seminiferous tubules. (A) As seen in control, stage I tubules of **(B)** gc*Pex13*KO testes showed characteristically round spermatids with a large central nucleolus (↙) and early pachytene spermatocytes (Ep) at the very basal layer in the germinal epithelium, but no spermatogonia. In contrast to gc*Pex13*KO mice, elongated spermatids (Es) were also found in **(A)** control testes. **(C, D)** In control tubules, stages II-IV were classified according to proacrosomal granules in round spermatids (Rs) and the presence of elongated spermatids. Intermediate spermatogonia (In) are characterized by an ovoid nucleus. **(E, F)** B-type spermatogonia (Bspg) and acrosomal vesicles, located at the top of the nucleus of round spermatids (Δ), are characteristic for stage V tubules. **(G)** Stage VI and **(H)** VII tubules of control testes were identified according to elongated spermatids migrating towards the lumen. Stage VI also showed mitotic events (Mit) in the basal compartment, forming (**G)** preleptotene spermatocytes (Prl). **(H)** At stage VII, elongated spermatids are at the luminal edge. Their cytoplasm was distributed along head and tail of spermatids (‣). Since gc*Pex13*KO testes were lacking elongated spermatids, no cross-sections of gc*Pex13*KO can be shown. **(I, J)** In stage VIII tubules, the acrosome is flattened, forming a cap-like structure (∗). In control tubules, elongated spermatids are released, known as spermiation. **(J)** In gc*Pex13*KO testes, some spermatids started apoptotic nuclear condensation. **(I, J)** The nuclei of pachytene spermatocytes were enlarged (Ψ). **(K, L)** Stage IX showed characteristic pachytene spermatocytes whose chromatin was slightly stained (→). **(K)** In control mice, spermatids showed an elongated apico-caudal axis. At this stage, cytoplasmic lobes fuse into very large residual bodies. **(L)** In gc*Pex13*KO testes, spermatid nuclei were clearly condensed, indicating apoptosis. **(M, N)** Stage X tubules were characterized according to the presence of pachytene spermatocytes as well as spermatocyte transition between leptotene (L) and zygotene (Z). **(M)** In control, the spermatid head formed a distinct protrusion. **(N)** In gc*Pex13*KO animals, only apoptotic spermatids were found. **(P)** *Stra8*-Cre mediated gc*Pex13*KO tubules were lacking spermatids. Prior to meiosis I, nuclei of diplotene spermatocytes are extended (stage XI). Morphology of diplotene and zygotene spermatocytes in gc*Pex13*KO resembled that of the **(O)** germinal epithelium of control mice. The spermatid nucleus of control testes is thinner and stained more intense (Δ). **(Q, R)** Stage XII tubules could be identified according to meiotic events *(*Mei). In control testes, spermatids showed an intense nuclear staining. Bars represent 50 µm.

3.7.1 Semithin sections of adult testes and epididymis confirm the spermatogenic arrest in *Stra8*-Cre mediated gc*Pex13*KO testes

Semithin sections of adult mouse testes and epididymis of all genotypes were morphologically analysed. In control (Figure 23A) and gc*Pex13*HTZ (Figure 23B) animals, regular spermatogenesis with elongated spermatids was observed. Compared to control and gc*Pex13*HTZ mice, the diameter of the seminiferous tubules of pre-meiotic induced gc*Pex13*KO testes was decreased (Figure 23C), as

already shown in a previous section (3.3), because of vacuolated germinal epithelium as well as apoptotic cells (Figure 23F).

At stage X, the germinal epithelium in *Stra8*-Cre mediated gc*Pex13*KO testes was characterized by secondary spermatocytes as well as MNCs, displaying a spermatogenic arrest at the spermatid stage, thus lacking spermatozoa. Some MNCs contained up to 32 spermatid nuclei (Figure 23C, D; XI). They were frequently present in all seminiferous tubules with a *Stra8*-Cre mediated gc*Pex13*KO (Figure 23D). Meiotically dividing spermatocytes were still detectable (Figure 23G). Round spermatids of MNCs initiated acrosome formation (Figure 23H). The interstitial space was enlarged, with an increased number of Leydig cells. Interestingly, in both interstitial cells as well as in the germinal epithelium, a remarkable accumulation of lipid droplets was found (Figure 23E). Moreover, giant phagosomes dominated in the cytoplasm of Sertoli cells (Figure 23I).

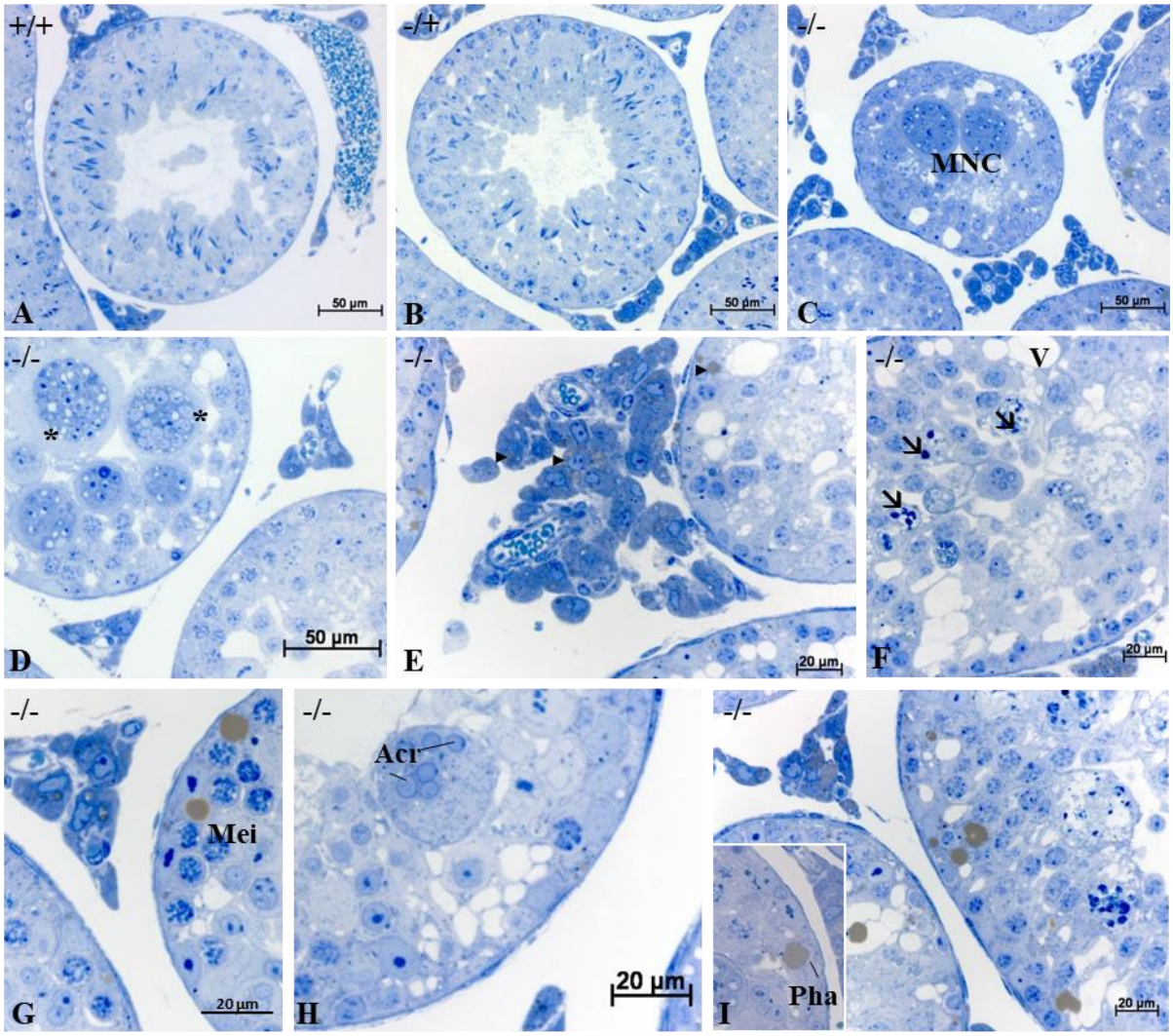

Figure 23| Semithin sections of adult mouse testes confirm spermatogenic arrest in *Stra8*-Cre mediated peroxisomal KO mice. (A) At stage X, regular complete spermatogenesis with elongated spermatids was

observed in control and **(B)** gc*Pex*13HTZ animals. **(C)** The germinal epithelium of pre-meiotic induced gc*Pex13*KO testes was characterized by a spermatogenic arrest, accompanied by the formation of MNCs. **(D)** MNCs contained up to 32 spermatid nuclei sharing the same cytoplasm (marked by asteriks (*)). **(E)** Both in the interstitium as well as in the germinal epithelium, large inclusions of lipid droplets were found (marked by arrowheads (‣)). **(F)** Shrinkage of the seminiferous tubules was caused by vacuolated germinal epithelium (*V*) and apoptotic cells (marked by small arrows (↘)). **(G, H)** However, meiosis (Mei) was not affected and round spermatids were still able to initiate acrosome formation (Acr). **(I)** Large phagosomes (Pha) were found at the basal part of the germinal epithelium.

In pre-meiotic induced gc*Pex13*KO animals, the number of Leydig cells increased with age. In juvenile (P20, P30) testes, the volume of Leydig cells was similar in all genotypes, including control (Figure 24A, B), *Stra8*-Cre (Figure 24E, F) and *Prm*-Cre mediated (Figure 24I, J) gc*Pex13*KO seminiferous tubules. In mature adult (P80) *Stra8*-Cre mediated gc*Pex13*KO testes (Figure 24G, H), the volume of Leydig cells seemed to be slightly increased compared to control (Figure 24C, D) and *Prm*-Cre mediated gc*Pex13*KO mice (Figure 24K, L). In adult mice (P360) with a *Pex13* deficiency in early germ cells, the volume of interstitial cells has clearly increased (Figure 24O, P) compared to control mice (Figure 24M, N).

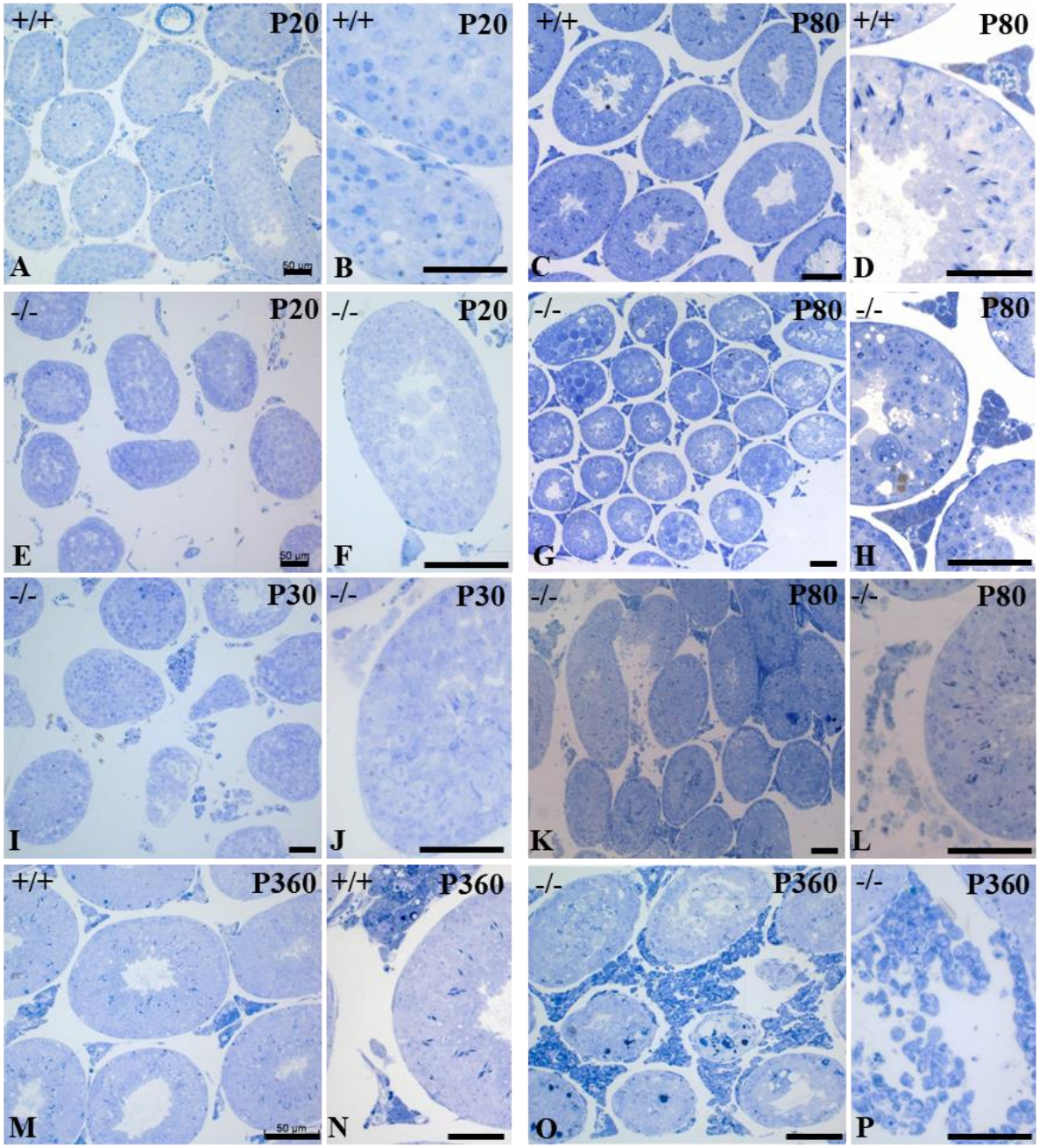

Figure 24| Comparison of interstitial cells between mice of different age groups. (A, B) Compared to control group (P20), **(E, F)** juvenile mouse testes of *Stra8*-Cre mediated gc*Pex13*KO (P20) and **(I, J)** post-meiotic induced gc*Pex13*KO (P30) mice showed a normal distribution of interstitial cells. **(G, H)** In mature adult mouse testis, the number of interstitial cells was slightly increased in *Stra8*-Cre mediated gc*Pex13*KO (P80) testes compared to **(C, D)** control testes. **(K, L)** Post-meiotic mediated gc*Pex13*KO testes showed a similar volume of interstitial cells as shown for **(C, D)** control testes. **(O, P)** In older mice (P360), the seminiferous tubules of *Stra8*-Cre mediated gc*Pex13*KO mice were shrivelled compared to **(M, N)** control. **(O, P)** Moreover, the number of interstitial cells was increased. Bars represent 50 µm.

The epithelium along the epidydimal duct did not differ between control (Figure 25A, B, E, F, I) and *Stra8*-Cre mediated gc*Pex13*KO (Figure 25C, D, G, H, J) epididymes. The initial segment was characterized according to a tall cuboidal epithelium, covered by microvilli (Figure 25A- D). In control mice, released sperm matured in the caput of the epididymis (Figure 25A- D). In the *Stra8*-Cre mediated gc*Pex13*KO, no spermatozoa were found in the lumen. The epithelium consists of endocytic columnar cells with a basal nucleus and stereocilia (Figure 25C, D). The corpus region could be identified according to columnar cells with prominent stereocilia (Figure 25E- H). Whereas spermatozoa were found in all segments of control mice, spermatozoa were absent in the epididymis of *Stra8*-Cre mediated gc*Pex13*KO (Figure 25A, B, E, F, J), confirming the spermatogenic arrest induced by the *Pex13* KO in pre-meiotic cells.

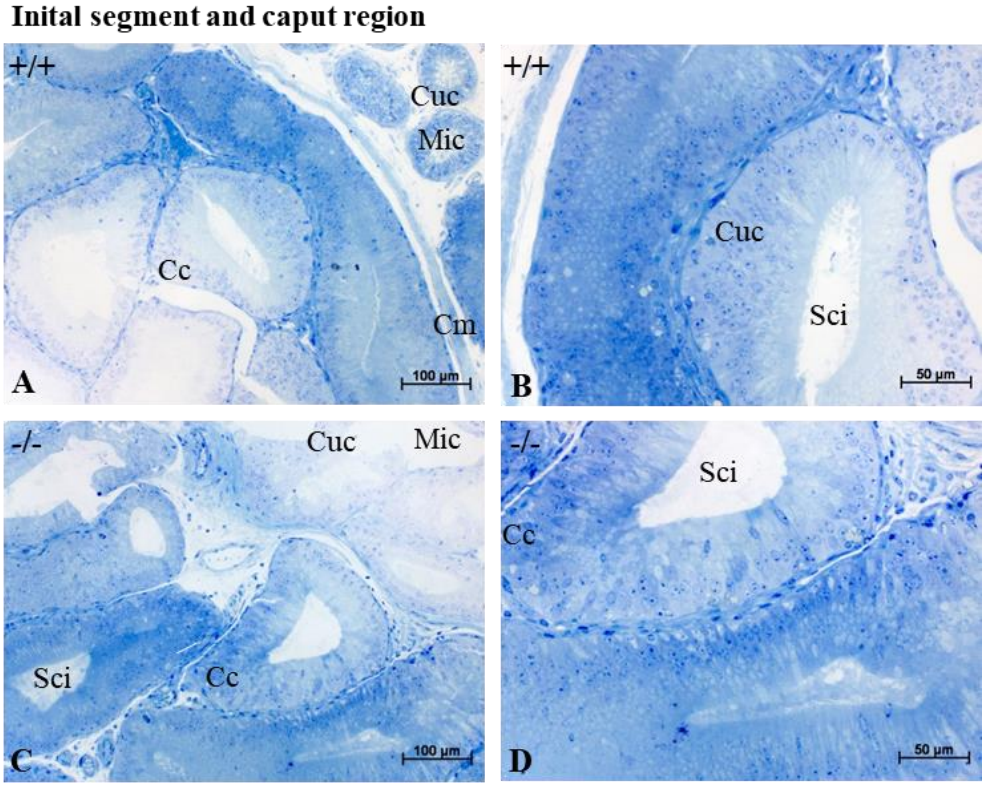

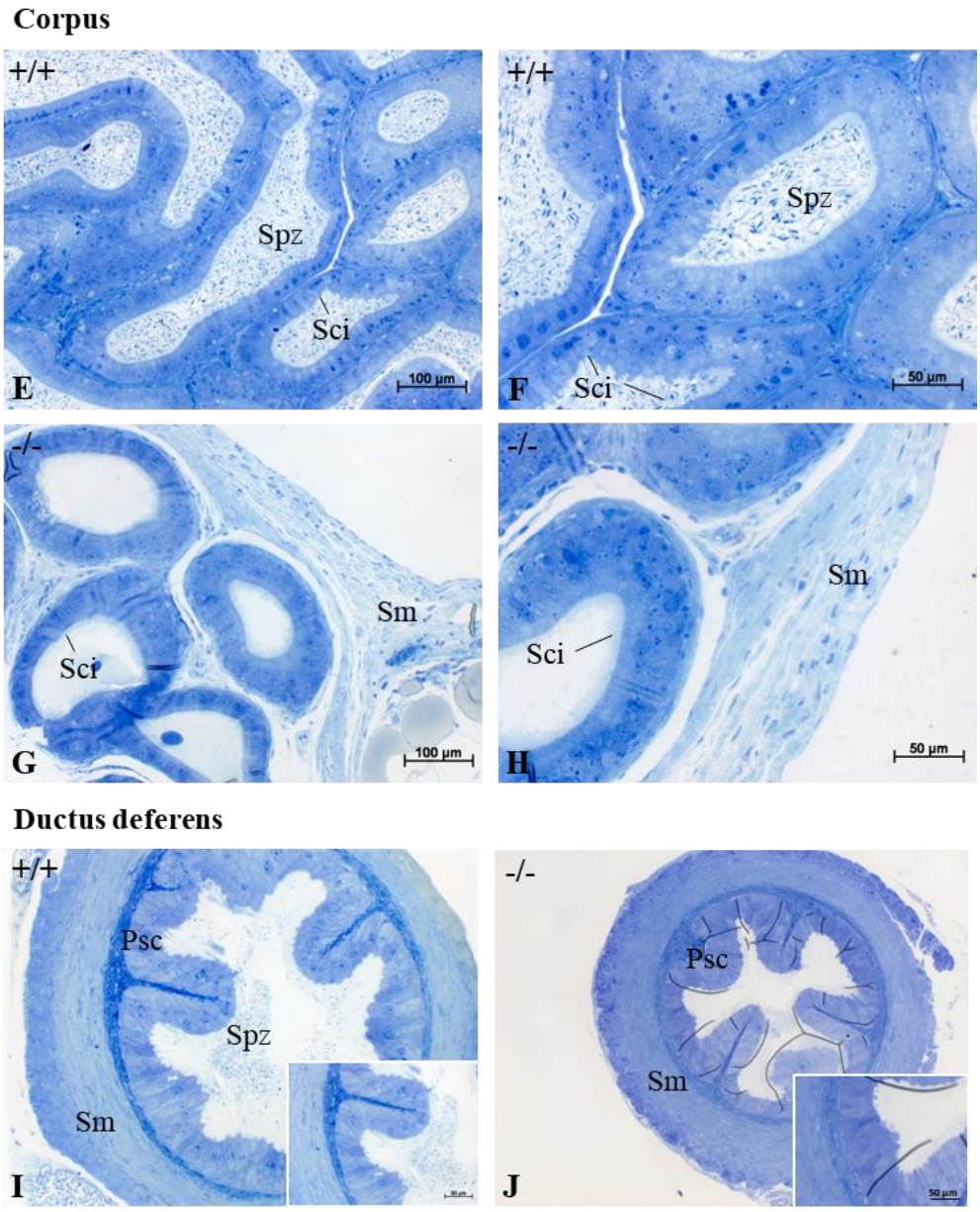

Figure 25| Semithin sections of all segments of the epididymis of gc*Pex13*WT and gc*Pex13*KO mice. The initial segment and the caput region of the epididymis are shown for **(A, B)** gc*Pex13*WT and **(C, D)** gc*Pex13*KO testes. **(A- D)** The epithelium of the initial segment consists of cuboidal cells, covered by microvilli on the luminal side. The epithelium of the caput region consists of endocytic columnar cells with a basal nucleus and small stereocilia. **(E- H)** The epithelium of the corpus contains columnar cells. The apical part of the cells is lined with stereocilia. **(I, J)** The vas deferens is characterized by a pseudostratified columnar epithelium, surrounded by a thick layer of smooth muscles and fibroblasts. In contrast to gc*Pex13*WT epididymis, in none of the segments of **(C, D, G, H, J)** gc*Pex13*KO animals, spermatozoa were found. Specimens were stained with toluidine blue. Cc- Columnar cells, Cuc- Cuboidal cells, Mic- Microvilli, Sci- Stereocilia, Sm- Smooth muscle, Spz- Spermatozoon, Psc- Pseudostratified columnar epithelium.

3.7.2 Electron microscopy reveals a severe disturbance in acrosome formation of round spermatids in pre-meiotic induced gc*Pex13*KO mice

Pathological alterations, induced by the *Stra8*-Cre mediated gc*Pex13*KO, were analysed at the ultrastructural level with focus on germ cell differentiation rather than the presence of peroxisomes. As already been shown in the histological analyses of *Stra8*-Cre mediated gc*Pex13*KO testes, round spermatids were arranged as MNCs, containing up to 32 nuclei (Figure 26A). Strikingly, all MNCs contained huge amounts of cytoplasm (Figure 26A, B, F, I). Intercellular bridges did not seem to be affected, as MNCs were still in close contact to neighbouring MNCs (Figure 26F, G). Many pleomorphic mitochondria were present in MNCs (Figure 26A, E, G, I). All spermatids started to form an acrosomic system (Figure 26B- E). In some cases, one or more spermatid nuclei even shared an acrosome (Figure 26E). In the cap phase (Figure 26C), the acrosome was enlarged through addition of glycoprotein-rich contents (not visible). Acrosome formation was finalized in the so-called acrosome phase, displayed by condensed chromatin (Figure 26D). With initiation of the transition into elongated spermatids at stage IX, nuclei of MNCs became more condensed (Figure 26H, I) as an early sign of beginning apoptosis.

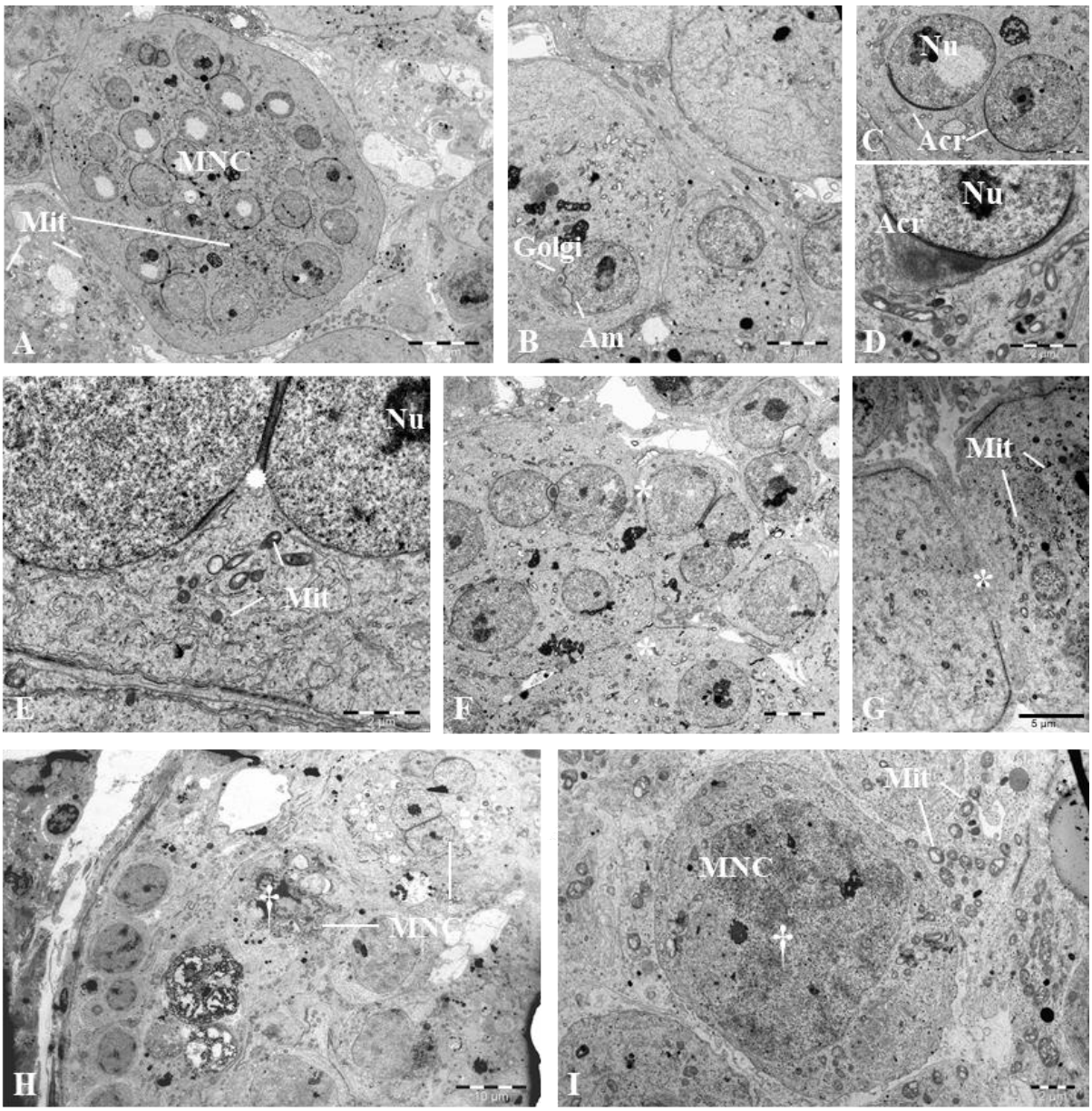

Figure 26| Electron microscopic analysis of multinucleated giant cells (MNCs) from adult pre-meiotic induced gc*Pex13*KO seminiferous tubules. (A) Round spermatids were arranged as MNCs. They contained up to 32 nuclei. **(B- E)** Round spermatids initiated acrosome (Acr) formation. **(B)** The first micrograph of acrosome formation displays the Golgi phase. **(C)** In the second phase, a cap-like structure has formed, as soon as the vesicles begin to flatten. **(D)** During the acrosome phase, the sperm chromatin has condensed. **(E)** Some acrosomes were shared by two or even more spermatid nuclei (✹). **(F, G)** MNCs were in close contact with neighbouring multinucleated giant cells, linked over intercellular bridges (*). **(H)** Some of the MNCs were lacking nuclei and only contained cytoplasm. **(I)** At stage IX, spermatid nuclei were condensed, as indication for apoptosis (†). Acr- Acrosome; Am- Acrosomal matrix; Golgi- Golgi apparatus; Mit- Mitochondria; Nu- Nucleus.

In a next step, interstitial Leydig cells as well as the germinal epithelium of mature and senior mice with a pre-meiotic induced gc*Pex13*KO were compared to testes of adult control mice, at ultrastructural level.

Whereas control mice showed normal spermatogenesis with round and elongating spermatids (Figure 27C), a spermatogenesis arrest could be stated at the spermatid stage of *Stra8*-Cre mediated peroxisomal KO animals (Figure 27A, B). Meiosis of early and late spermatocytes was not affected (Figure 27A, B). The defect in germ cell development resulted in disorganized seminiferous tubules, resulting in vacuolization of the germinal epithelium (Figure 27A, B).

As an additional effect of impaired spermatogenesis, induced by abolished peroxisomes in pre-meiotic germ cells, massive lipid droplets were accumulated in the basal part of Sertoli cell cytoplasm (Figure 27A, B). In control mice, lipid droplets were also identified in the apical part of Sertoli cells, indicating stage IX, as excess cytoplasm will be released by spermatids and phagocytosed by Sertoli cells (Figure 27C). Phagosomes were therefore found not only basal, but also apical within the cytoplasm of Sertoli cells in control mice (Figure 27F). Interestingly, the Leydig cells of mature (Figure 27G) and especially in senior *Stra8*-Cre mediated gc*Pex13*KO (Figure 27H) animals showed an increased number of lipid droplets compared to control mice (Figure 27I).

In the testes of all genotypes, areas with a higher electron density were easily identified as lysosomes, whereas mitochondria showed characteristic cisternae (Figure 27A- F). Many pleiomorphic mitochondria could be identified in the germinal compartment of 80-day old gc*Pex13*KO animals (Figure 27A, B). In 360-day old gc*Pex13*KO mice, mitochondria seemed to be enlarged and longer and exhibited dense tubular cristae (Figure 27E).

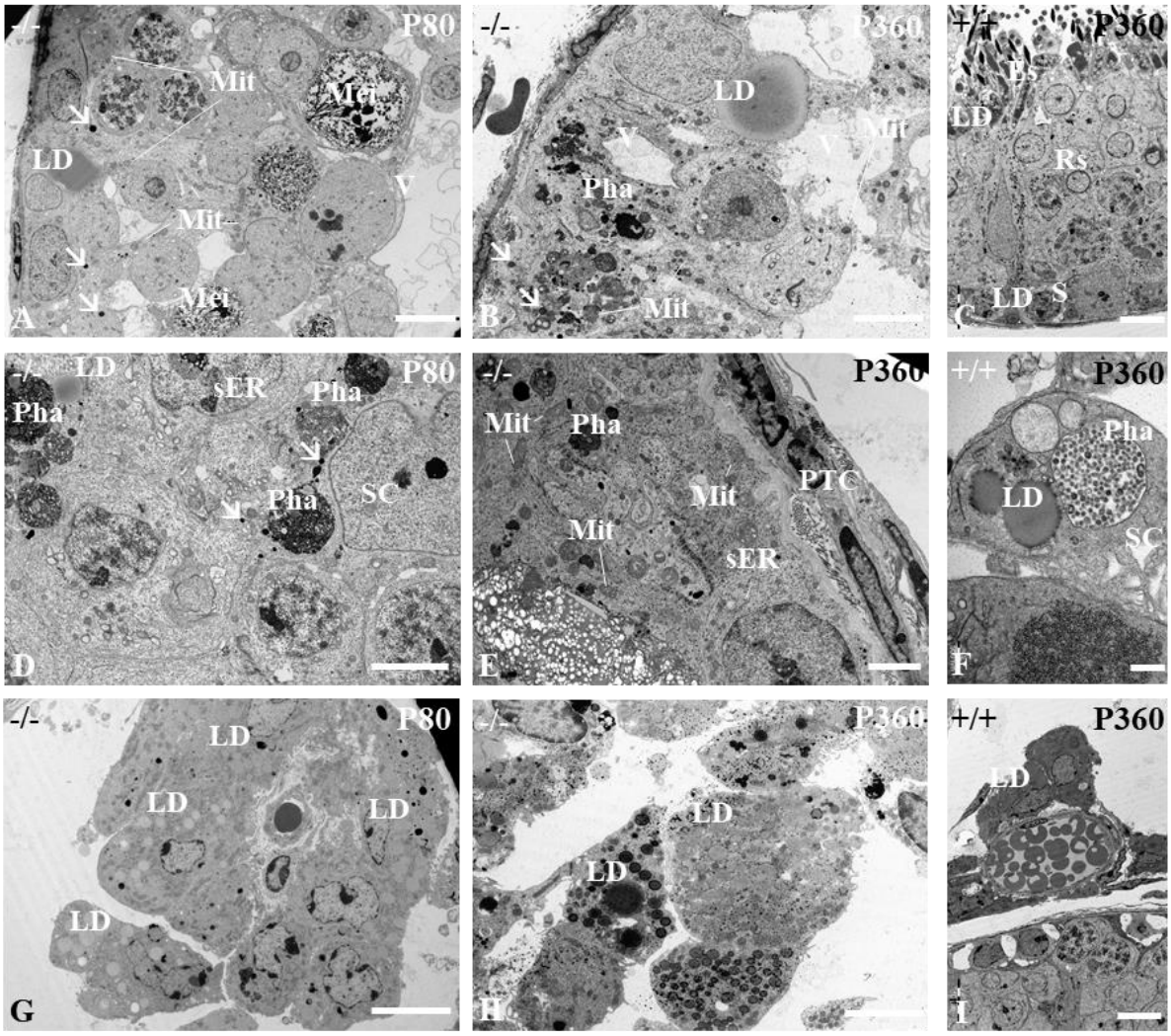

Figure 27| Ultrastructural analysis of the cellular composition in the interstitium and the germinal epithelium of mature (P80) and old (P360) *Stra8*-Cre mediated peroxisomal gc*Pex13*KO compared to control animals. (A) The germinal epithelium of *Stra8*-Cre mediated gc*Pex13*KO (P80) seminiferous tubules showed meiotically (Mei) dividing spermatocytes. A spermatogenesis arrest could be observed at the spermatid stage. **(B)** In old mice (P360), the vacuolization (V) of the germinal epithelium has proceeded. **(C)** Low magnification of the seminiferous tubule of control mic depicts normal spermatogenesis, with round (Rs) and elongated spermatids (Es). Small lipid droplets (LD) were mainly found basal of Sertoli cells (SC), but also adluminal. **(A, B)** Lipid droplets of *Stra8*-Cre mediated gc*Pex13*KO testes (P80, P360) were enlarged. **(D-F)** In Sertoli cells, many mitochondria (Mit) and lysosomes (highlighted by an arrow (↘)) were observed. **(E)** Sertoli cells of the pre-meiotic induced gc*Pex13*KO animals (P360) contained large phagosomes (Pha). Mitochondria in Sertoli cells were larger and longer in *Stra8*-Cre mediated peroxisomal KO testes compared to control group. **(I)** Compared to control animals (P360), Leydig cells of **(G)** mature and **(H)** older pre-meiotic induced peroxisomal gc*Pex13*KO animals showed a clear accumulation of lipid droplets. Es- Elongated spermatids; LD- Lipid droplets; Mei- Meiosis; Mit- Mitochondria; PTC- Peritubular myoid cells; Pha- Phagosome; Rs- Round spermatids; sER- smooth Endoplasmic reticulum; S- Spermatocytes; V- Vacuole. **(A- C, I)** Bars represent 10 µm. **(D, E)** Bars represent 5 µm. **(F)** Bar represents 500 nm. **(G, H)** Bars represent 20 µm.

Juvenile mice (P20) were analysed at ultrastructural level to compare age-dependent alterations in the germ cell development in pre-pubertal with mature mice. Testes from juvenile control mice showed regular spermatogenesis with meiotically dividing spermatocytes (Figure 28A) and single round spermatid nuclei (Figure 28C). Meiosis of early and late spermatocytes was also detected in the germinal epithelium of *Stra8*-Cre mediated gc*Pex13*KO testes (Figure 28D, E). Moreover, spermatocytes were linked to neighbouring spermatocytes via cytoplasmic bridges (Figure 28G). In relatively few seminiferous tubules of control mice small lipid droplets were present (Figure 28B). In gc*Pex13*KO animals, the number of lipid droplets was strongly increased (Figure 28F). A spermatogenic arrest at the spermatid stage was already detected in juvenile gc*Pex13*KO testes (Figure 28H). MNCs were linked to neighbouring cells via cytoplasmic bridges (Figure 28H, I). Interestingly, many mitochondria were present in germ and Sertoli cells of pre-meiotic induced gc*Pex13*KO testes (Figure 28F).

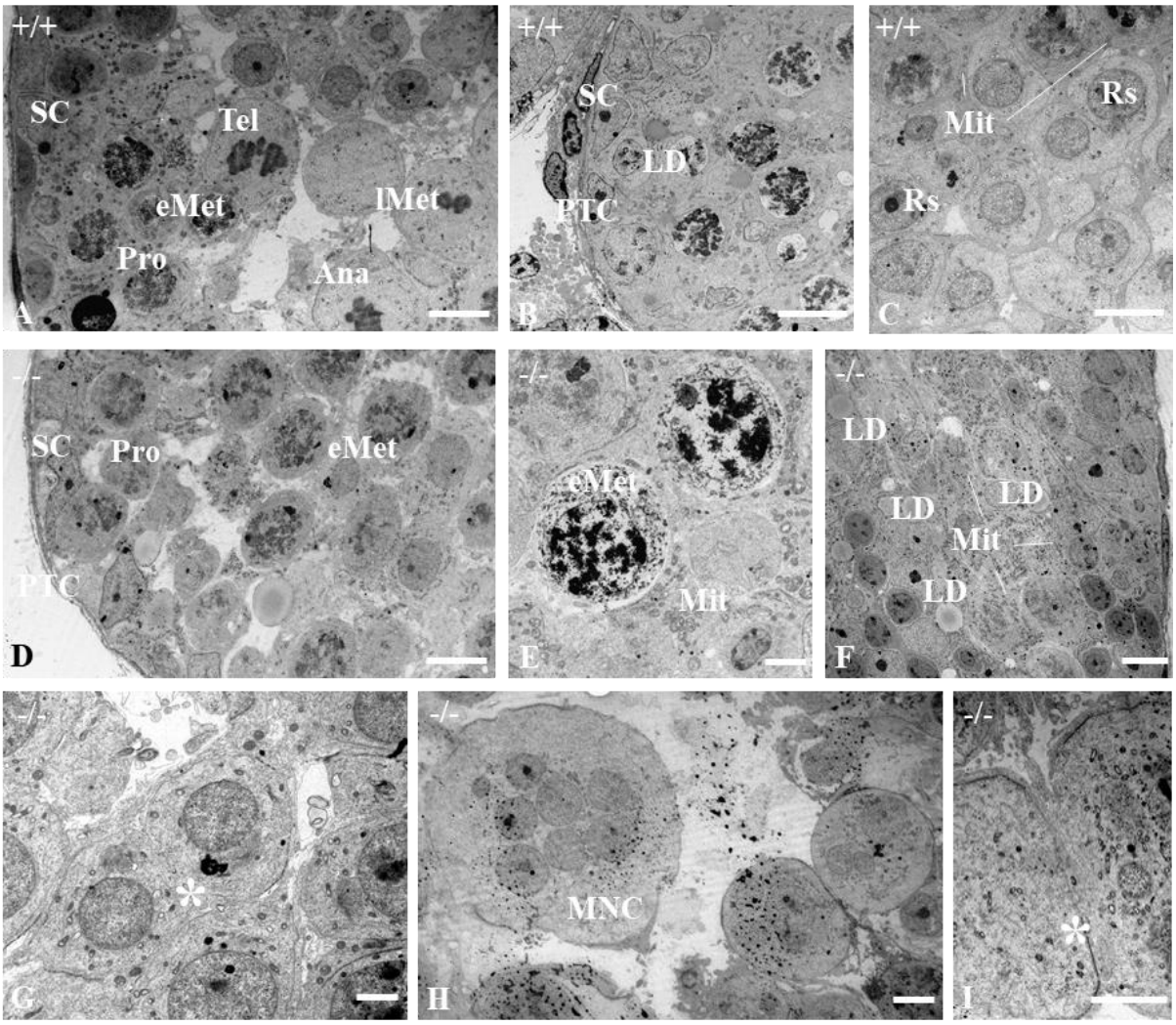

Figure 28| Ultrastructural analyses of germ cell development in juvenile (P20) *Stra8*-Cre mediated *gcPex13*KO and control animals. (A) Spermatocytes subsequently undergo meiosis in control, as well as **(D,**

E) pre-meiotic induced gc*Pex13*KO testes. **(F)** The number of lipid droplets (LD), localized to Sertoli cells, was increased in gc*Pex13*KO animals, compared to **(B)** control mice. **(G)** Spermatocytes of *Stra8*-Cre mediated gc*Pex13*KO testes were linked via cytoplasmic bridges (*). **(C)** The germinal epithelium of control mice showed normal spermatogenesis, with single round spermatid (Rs) nuclei. **(H)** The spermatogenic arrest at the spermatid stage was already indicated in juvenile gc*Pex13*KO animals that displayed MNCs, **(I)** linked to neighbouring MNCs via cytoplasmic bridges (*). **(F)** The number of mitochondria was increased in *Stra8*-Cre mediated gc*Pex13*KO animals. Ana- Anaphase; eMet- early Metaphase; lMet- late Metaphase; LD- Lipid droplets; Mit- Mitochondria; Tel- Telophase; Pro- Prophase; PTC- Peritubular myoid cells; Rs- Round spermatids; SC- Sertoli cells. **(A- D, F)** Bars represent 10 µm. **(E, G- I)** Bars represent 2 µm.

3.8 Accumulation of lipids in *Stra8*-Cre mediated gc*Pex13*KO mice

All distinct mouse genotypes were analysed for lipid distribution in and outside the seminiferous tubules. As large inclusions of lipid droplets were already identified in semithin sections, their presence was confirmed by Oil Red O (ORO) using frozen sections from control and both *Prm*-Cre and *Stra8*-Cre mediated gc*Pex13*KO mice at different ages, ranging from early mature (P30) to old (P200) mice. In testes of control (Figure 29A, C, F) and post-meiotic induced gc*Pex13*KO (Figure 29E, H) mice, lipids were mainly assigned to Leydig cells as prerequisite for steroid synthesis (Eacker *et al.* 2008). At stage VI, small deposits of lipid droplets were distributed apically in the germinal epithelium of control mice (Figure 29F). With respect to the spermatogenic cycle, lipid droplets were detectable in the basal and apical part of the germinal epithelium of *Stra8*-Cre mediated peroxisomal KO mice (Figure 29D, G). In stage IX to XI tubules, lipid droplets were mainly localized in the basal part of Sertoli cells but also near spermatogonia (data not shown). This pattern was in accordance with observations of lipid droplet distribution in post-meiotic induced peroxisomal gc*Pex13*KO testes (Figure 29E, H). Compared to control and post-meiotic gc*Pex13*KO testes, more lipid droplets were found in the basal part of the germinal epithelium of pre-meiotic induced gc*Pex13*KO testes (Figure 29G). As in control and post-meiotic induced gc*Pex13*KO mouse testes, lipid droplets were also accumulated in Leydig cells of *Stra8*-Cre mediated gc*Pex13*KO (Figure 29B).

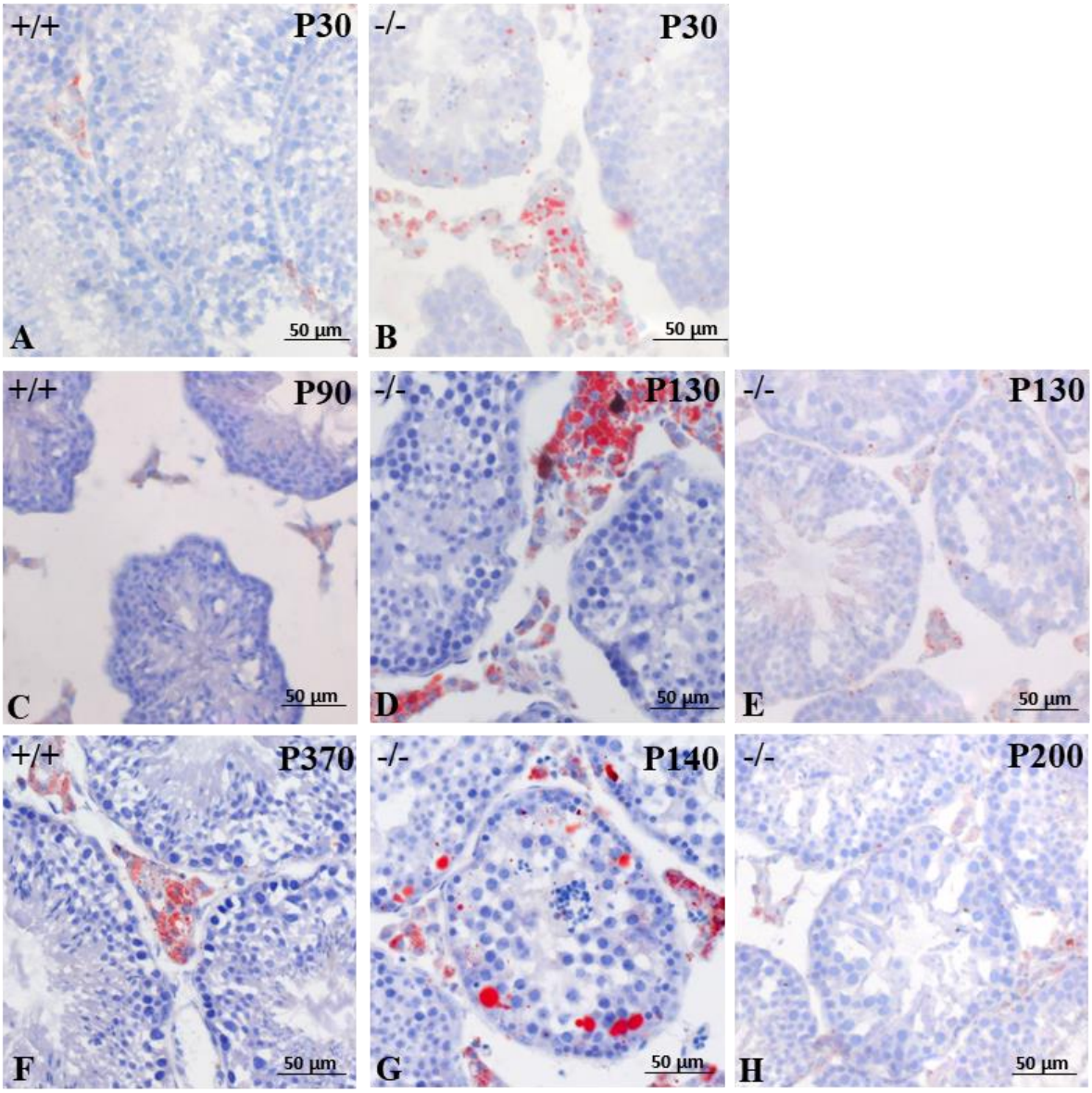

Figure 29| The presence of lipid droplets in control, *Stra8*-Cre and *Prm*-Cre mediated gc*Pex*13KO testes. **(A, B)** Testes biopsies from early mature (P30), **(C- E)** mature (P90, control; P130, gc*Pex13*KO) and **(F, G)** senior mice (P370, control; P140, pre-meiotic induced gc*Pex13*KO; P200, post-meiotic induced gc*Pex13*KO) were stained with Oil Red O for the detection of lipid droplets. With respect to the spermatogenic cycle, tiny lipid droplets accumulated in Sertoli and Leydig cells in **(A, C, F)** control and **(E, H)** post-meiotic gc*Pex13*KO testes at all ages. **(B)** In pre-meiotic gc*Pex13*KO testes, high amounts of lipid droplets were already found in the germinal epithelium and in Leydig cells of early mature mice. **(D, G)** The number of lipid droplets increased with age.

3.8.1 The peroxisomal *β*-oxidation is impaired in pre-meiotic induced gc*Pex13*KO testes

After morphological analyses revealed an accumulation of lipid droplets in the seminiferous tubules of *Stra8*-Cre mediated peroxisomal gc*Pex13*KO mice, their composition was further analysed and

compared to control and post-meiotic induced gc*Pex13*KO testes by means of gas chromatography. In pre-meiotic gc*Pex13*KO testes, phospholipids (PL) were slightly decreased (Figure 30A) and triglycerides (TGs) were increased by trend (Figure 30B). Palmitic acid (C16:0; Figure 30C) and its derivatives (Figure 30D) was higher in control (28.82 ± 1.2 % of total FAs) and in *Prm*-Cre mediated gc*Pex13*KO testes (28.43 ± 0.8 % of total FAs) compared to levels in the *Stra8*-Cre mediated gc*Pex13*KO testes with 23.11 ± 0.3 % of total FAs (Figure 30C). About 28.14 % of palmitic acid was content of PLs and 23.18 % of TGs in the *Stra8*-Cre mediated gc*Pex13*KO testes (in control: 33.13 % PL, 24.88 % TGs; in *Prm*-Cre mediated gc*Pex13*KO: 32.93 % PL; 23.33 % TGs; data not shown).

In addition, stearic acid (C18:0; Figure 30C) and its desaturated derivative oleic acid (C18:1(ω-9); Figure 30D) were significantly increased ($p = 0.0079$) in pre-meiotic peroxisomal gc*Pex13*KO testes (C18:0: 11.32 ± 1.0 %; C18:0(ω-9): 13.64 ± 1.4 %) compared to control (C18:0: 9.11 ± 0.4 %; C18:0(ω-9): 10.30 ± 1.6 %) and *Prm*-Cre mediated gc*Pex13*KO testes (C18:0: 9.53 ± 0.7 %; C18:0(ω-9): 10.90 ± 1.3 %). In total, all saturated FAs, except for palmitic acid (Figure 30C), and MUFAs (Figure 30D) were significantly increased in *Stra8*-Cre mediated gc*Pex13*KO testes, compared to control and post-meiotic induced peroxisomal KO mice. Most strikingly, concentrations of precursor ω-3 PUFAs, including eicosatetraenoic acid (C20:4(ω-3); 0.04 %; in control: 0.02 %), eicosapentaenoic acid (C20:5(ω-3); 0.38 %; in control: 0.27 %) and docosapentaenoic acid (C22:5(ω-3); 1.42 %; in control: 0.55 %) were significantly increased in *Stra8*-Cre mediated gc*Pex13*KO testes, whereas docosahexaenoic acid (C22:6(ω-3)) was significantly decreased with 4.86 ± 0.5 % of total fatty acids ($p = 0.0079$), compared to control (8.08 ± 0.8 %) and *Prm*-Cre mediated gc*Pex13*KO testes (8.05 ± 0.7 %; Figure 30E). In pre-meiotic gc*Pex13*KO, precursor ω-6 PUFAs, such as eicosatetraenoic acid (C20:4(ω-6); 13.36 ± 1.6 %) and docosatetraenoic acid (C22:4(ω-6); 2.00 ± 0.4 %) were increased. Docosapentaenoic acid (C22:5(ω-6); 6.54 ± 0.7 %), of which 7.08 % was content of PL and 3.55 % of TGs in gc*Pex13*KO testes, was significantly decreased. The ratio of C22:5(ω-6) in control group (12.57 ± 1.2 % of total fatty acids) was 13.00 % content of PL and 7.38 % of TGs (Figure 30F). The data therefore suggests an accumulation of VLCFAs in the pre-meiotic induced gc*Pex13*KO model due to a disruption of peroxisomal *β*-oxidation.

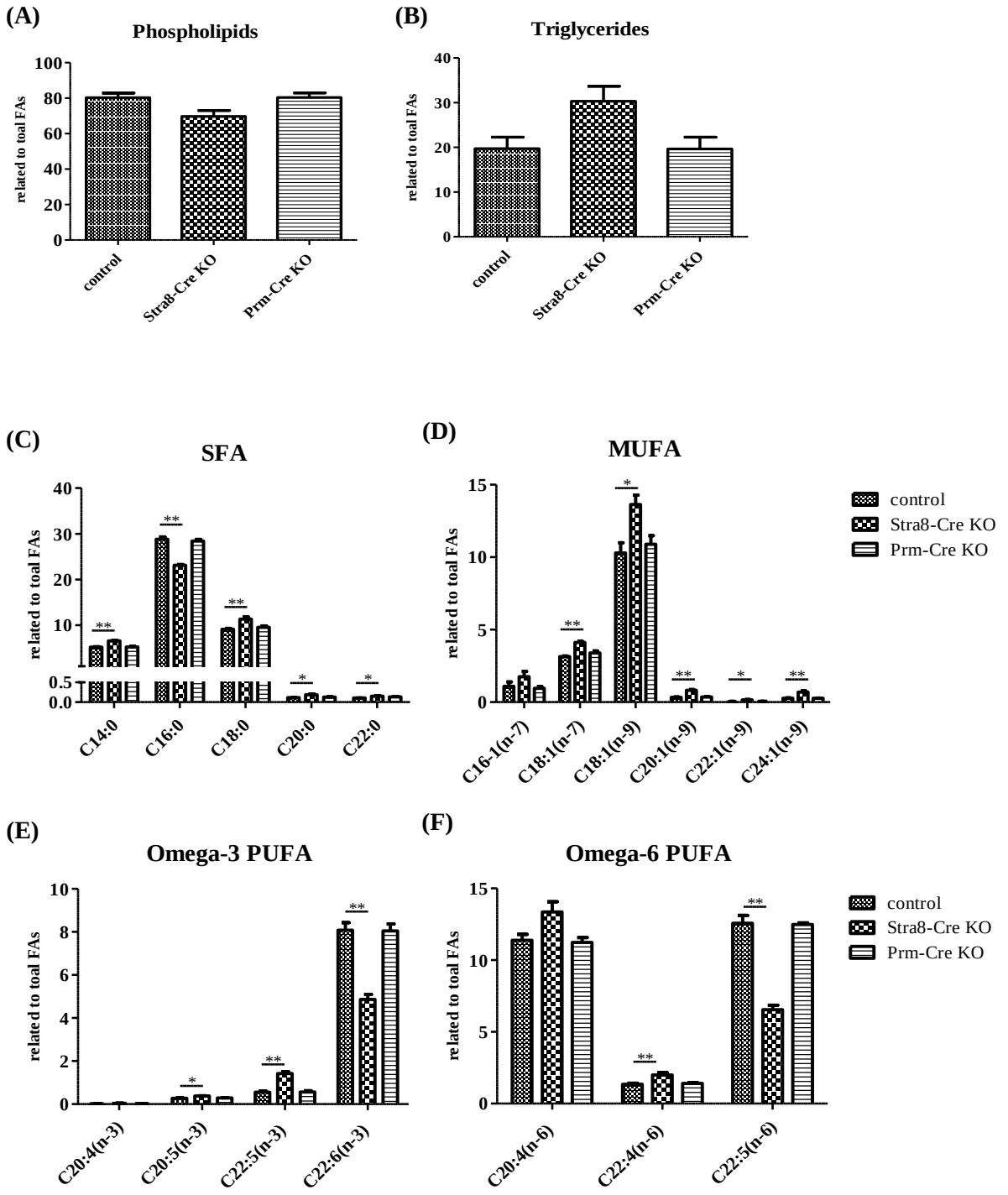

Figure 30| Levels of saturated fatty acids (SFAs), monounsaturated fatty acids (MUFAs), ω-3 polyunsaturated fatty acids (Omega-3 PUFAs) and ω-6 polyunsaturated fatty acids (Omega-6 PUFAs) in control, *Stra8*-Cre and *Prm*-Cre mediated gc*Pex13*KO testes. Fatty acids were measured by gas chromatography. **(A)** Compared to control and *Prm*-Cre induced gc*Pex13*KO testes, the ratio of lipids revealed a decrease of phospholipids and an increase by trend of **(B)** triglycerides in pre-meiotic induced gc*Pex13*KO testes (not significant). **(C)** Mainly all saturated and **(D)** monounsaturated fatty acids were slightly increased in *Stra8*-

Cre mediated gc*Pex13*KO testes, with the exception for **(C)** palmitic acid. (**E, F)** Precursors of ω-3 and ω-6 PUFAs were significantly increased (*) in *Stra8*-Cre mediated gc*Pex13*KO mice. C22:6(ω-3) (docosahexaenoic acid) and C22:5(ω-6) (docosapentaenoic acid) were significantly decreased (*) compared to control group and *Prm*-Cre mediated gc*Pex13*KO testes. The standard error of the mean (SEM) is shown. Statistical significance was determined using t-test (non-parametric Mann-Whitney *U* test). *$p \leq .05$; **$p\ 0.001 < p \leq 0.01$; *** $p \leq 0.001$.

3.8.2 mRNA levels of fatty acid enzymes involved in peroxisomal *β*-oxidation are affected in pre-meiotic induced gc*Pex13*KO mice

The results of gas chromatography analyses revealed a significant decrease in the concentration of the membrane lipid component docosahexaenoic acid (C22:6(ω-3)) that is synthesized by Δ6-Desaturase *Fads2* (Nakamura and Nara 2004; Stoffel *et al.* 2008). The expression levels of genes that encode for enzymes involved in lipid synthesis were therefore investigated by qRT-PCR in total RNA preparations.

Compared to control, gc*Pex13*HTZ and *Prm*-Cre mediated gc*Pex13*KO testes, *Fads2* expression in testes with a pre-meiotic induced peroxisomal KO was significantly increased ($p = 0.0032$). In *Prm*-Cre mediated gc*Pex13*KO mice, no changes in *Fads2* expression were found (Figure 31C). The elongation steps of VLFCAs, including PUFAs, are controlled by ELOVL2 and ELOVL5. ELOVL2 is mainly involved in the elongation of C20 into C24:4(ω-6) and C22 into C24:5(ω-3) PUFAs, whereas ELOVL5 controls the elongation of C18 to C22 substrates. *Elovl2* expression was only slightly increased by trend in the *Stra8*-Cre mediated gc*Pex13*KO testes compared to control, gc*Pex13*HTZ and *Prm*-Cre mediated gc*Pex13*KO mice (Figure 31A). Levels of eicosatetraonic acid (C20:4(ω-3)), docosapentanoic acid (C22:5(ω-3)) and adrenic acid (C22:4(ω-6)) were increased in *Stra8*-Cre mediated gc*Pex13*KO testes (3.8.1). This finding is in accordacne with the qRT-PCR data, showing significantly increased expression levels of *Elovl5* in *Stra8*-Cre mediated gc*Pex13*KO testes ($p = 0.0031$; Figure 31B). In *Prm*-Cre mediated gc*Pex13*KO mice, the levels of ELOVL2/5 were unaffected by the *Pex13* KO.

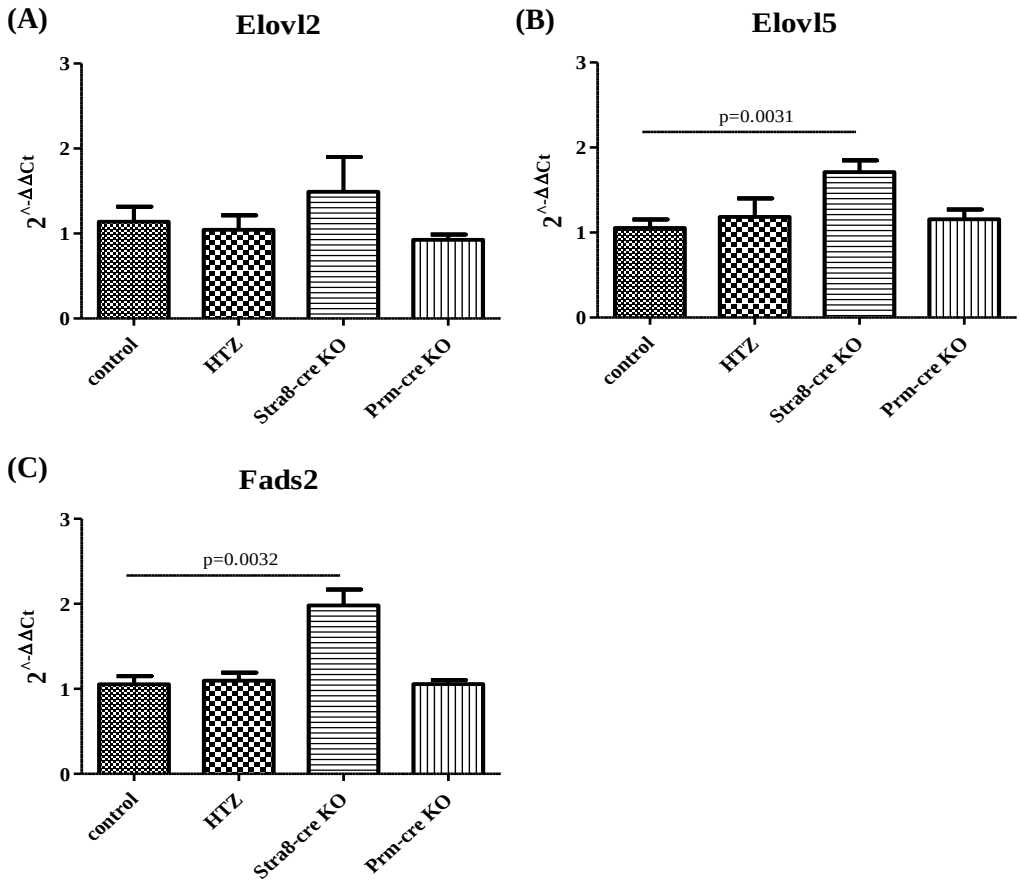

Figure 31| Quantitative analyses of elongases and desaturases involved in the fatty acid synthesis. Testicular biopsies from control, heterozygous (HTZ) as well as pre- (mediated by the *Stra8*-Cre transgene) and post- (mediated by the *Prm*-Cre transgene) meiotic induced gc*Pex13*KO testes were used. (A) Qualitative reverse transcriptase polymerase chain reaction analysis was used to assess gene expression of fatty acid elongase 2 *(Elovl2*) and **(B)** *5* (*Elovl5)* and **(C)** fatty acid desaturase 2 (*Fads2*) in testis biopsies of control group (square box bars), heterozygous (HTZ; brick bars), pre- (*Stra8*-Cre KO; horizontal line bars) and post-meiotic mediated peroxisomal KO (*Prm*-Cre gc*Pex13*KO; vertical line bars). In pre-meiotic induced gc*Pex13*KO **(A)** *Elovl2*, **(B)** *Elovl5* and **(C)** *Fads2* expression were significantly up-regulated compared to control group and to post-meiotic induced gc*Pex13*KO mice. Data represent 4 independent experiments, each assayed in duplicate, representing gene expression of 3 individuals per genotype. The standard error of the mean (SEM) is shown. Statistical significance was determined using T-test (Welch´s correction). *$p \leq .05$; **$p\ 0.001 < p \leq 0.01$; *** $p \leq 0.001$.

3.9 Measurements of serum hormones LH, FSH and testosterone

Serum hormone levels of LH, FSH and testosterone were measured by means of ELISA to investigate putative alterations in steroid biosynthesis. Serum samples from adult mice (9 to 30 weeks old), including control, Cre- negative C57Bl/6, heterozygous (HTZ), *Stra8*-Cre and *Prm*-Cre mediated gc*Pex13*KO mice were used. Apart from one outlier in pre-meiotic gc*Pex13*KO animals, the average

serum concentration of LH was in the same range (2.65 ± 1.26 µg/ml) as LH serum levels in gc*Pex13*HTZ (3.13 ± 1.59 µg/ml), control (3.11 ± 1.16 µg/ml) and WT C57Bl/6 (2.67 ± 0.67 µg/ml). LH level in serum of *Prm*-Cre mediated gc*Pex13*KO animals was not significantly reduced with 1.94 ± 0.029 µg/ml (Figure 32A). Considering FSH levels, no significant alterations were observed in pre-meiotic induced gc*Pex13*KO mice (13.19 ± 0.64 ng/ml) and *Prm*-Cre mediated gc*Pex13*KO animals (12.59 ± 0.88 ng/ml), compared to control (14.16 ± 1.93 ng/ml), heterozygous (12.69 ± 0.54 ng/ml) and WT C57Bl/6 (12.73 ± 0.59 ng/ml; Figure 32B). The serum testosterone levels of control (2.80 ± 2.57 ng/ml) and WT C57Bl/6 (2.42 ± 0.75 ng/ml) mice were comparable to the levels determined in HTZ (1.99 ± 0.4 ng/ml), *Prm*-Cre mediated peroxisomal gc*Pex13*KO (1.59 ± 0.27 ng/ml) and *Stra8*-Cre transgenic mice (1.84 ± 0.34 ng/ml; Figure 32C). Note that high standard deviations within one mouse group are due to circadian fluctuations of hormone levels.

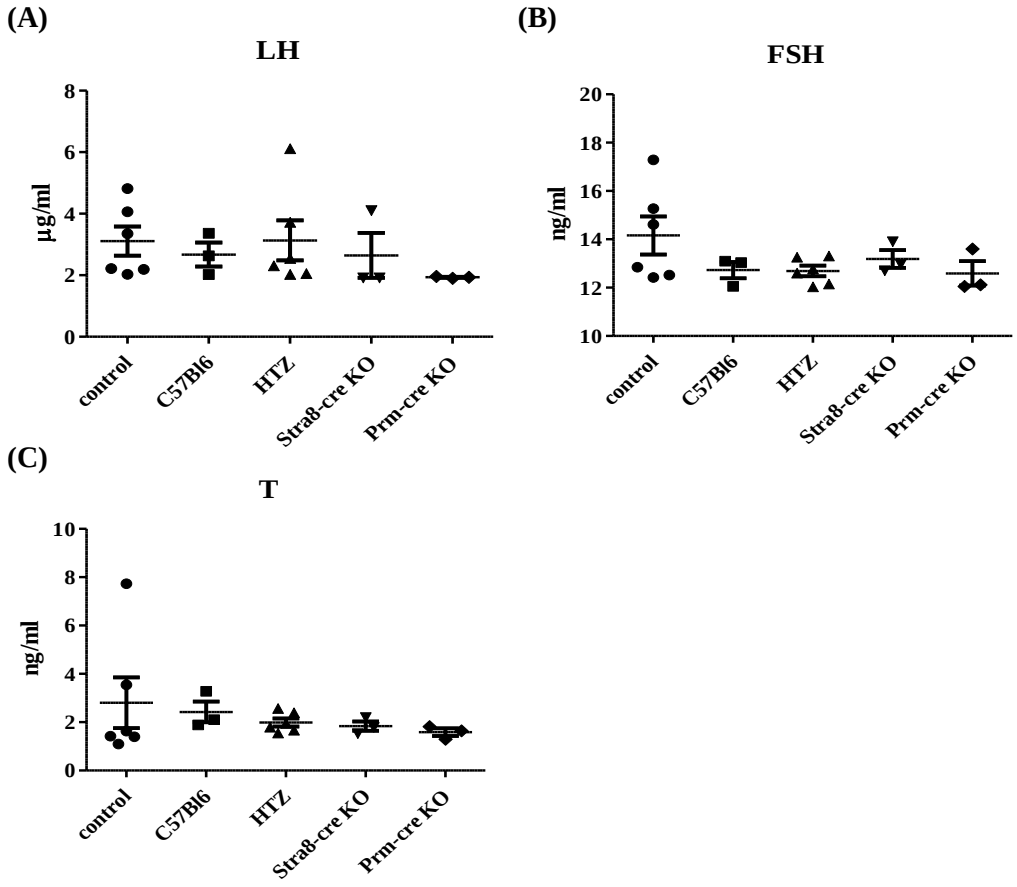

Figure 32| Comparison of hormone levels in all germ cell populations. (A) Serum levels of luteinizing hormone (LH), **(B)** follicle-stimulating hormone (FSH), and **(C)** testosterone (T) were measured in control, C57Bl6, heterozygous (HTZ), pre- (*Stra8*-Cre KO) and post- meiotic (*Prm*-Cre KO) mediated peroxisomal KO mice. None of the different levels reached statistical significance. Statistical significance was determined using One-way analysis of variance (ANOVA, non-parametric, Kruskal-Wallis test).

3.10 The integrity of the BTB is disturbed by the *Stra8*-Cre mediated gc*Pex13*KO

To evaluate pathological alterations in the germinal epithelium, a comparative analysis of tissue sections from P60 (control and *Stra8*-Cre mediated gc*Pex13*KO) or P80/P100 (gc*Pex13*KO/ *Prm*-Cre mediated gc*Pex13*KO) old mice was performed with claudin-11. Immunofluorescent staining with the anti-Claudin-11 antibody was concentrated in the suprabasal layer within the germinal epithelium of control (Figure 33A, B), heterozygous (Figure 33C, D) and *Prm*-Cre mediated peroxisomal KO mice (Figure 33G, H). In mice with a *Pex13* KO in pre-meiotic germ cells, the immunoreactivity was extended lateral and adluminal of the seminiferous tubules (Figure 33E, F), suggesting that the peroxisomal dysfunction in germ cells affects the organization of the tight junctions forming the BTB.

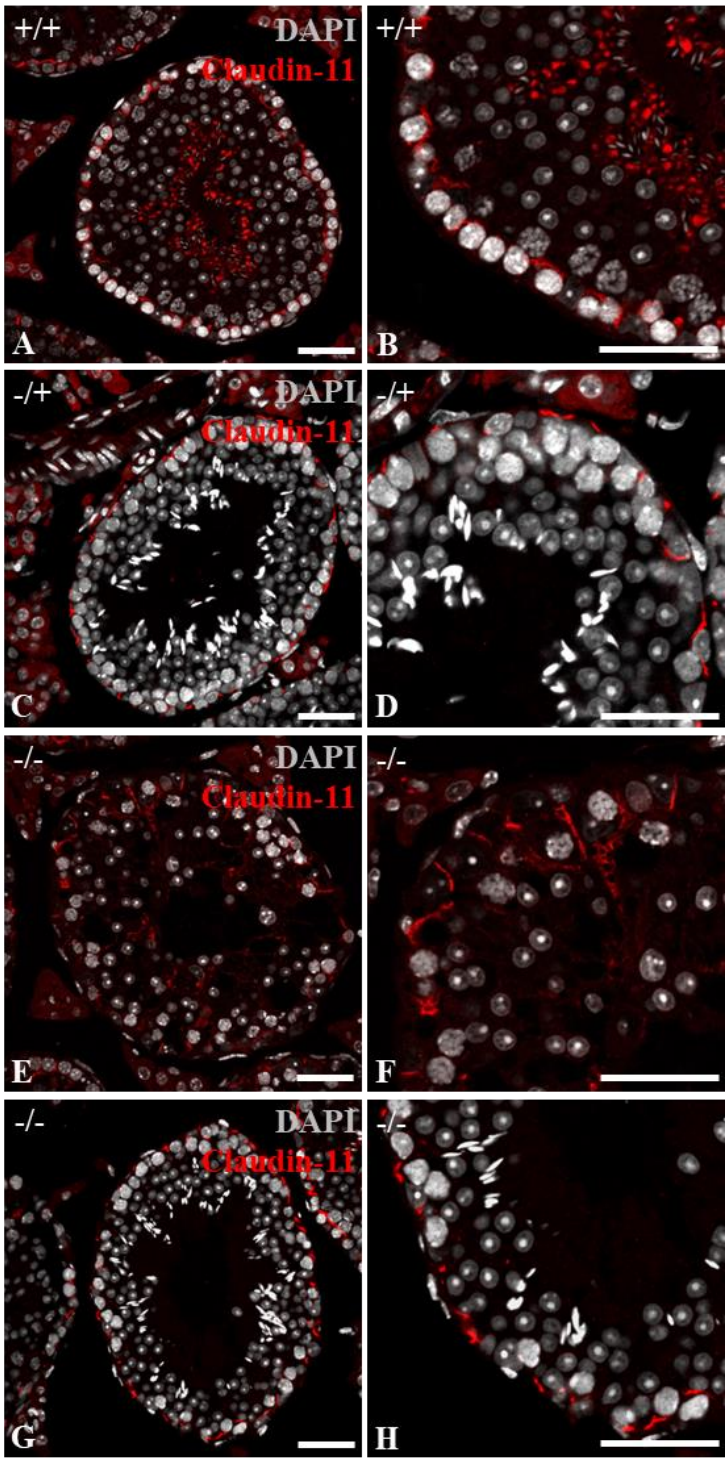

Figure 33| Localisation of blood-testis barrier (BTB) marker claudin-11 in paraffin-embedded specimens of control, gc*Pex13*HTZ and gc*Pex13*KO mice. (A, B) Immunofluorescence staining of claudin-11 in control, **(C, D)** gc*Pex13*HTZ and **(G, H)** post-meiotic induced peroxisomal gc*Pex13*KO was concentrated in the suprabasal layer within the germinal epithelium, indicating the presence of tight junctions. **(E, F)** In *Stra8*-Cre mediated gc*Pex13*KO mice, the immunoreactivity was extended focally up to the lumen of the seminiferous tubules, suggesting that peroxisome dysfunction in germ cells affects the organization of the tight junctions. Detailed immunolocalization of claudin-11 is shown at higher magnification in B, D, F and H for the corresponding genotype. DAPI stains for nuclear DNA are shown in shades of grey. Bars represent 50 µm.

3.10.1 mRNA expression of tight junction proteins is altered in pre-meiotic induced gc*Pex13*KO testis

Antibody labelling of the tight junction marker claudin-11 already indicated a structural alteration of the BTB in testes of *Stra8*-Cre mediated peroxisomal KO (3.10). Therefore, the expression of genes encoding for several tight junction proteins that compose the BTB, including claudin-3 (*Cldn3*), zonula occludens 1 (*Tjp1*) and occludin (*Ocln*), were quantified.

The mRNA levels for *Ocln* (Figure 34A) and *Tjp1* (Figure 34 B) were comparable in all genotypes with only slight but no significant deviations in pre-meiotic induced gc*Pex13*KO testes. However, the mRNA expression of *Cldn3* was significantly down-regulated in *Stra8*-Cre mediated gc*Pex13*KO ($p > 0.0001$) compared to control, gc*Pex13*HTZ and to *Prm*-Cre mediated gc*Pex13*KO testes (Figure 34C).

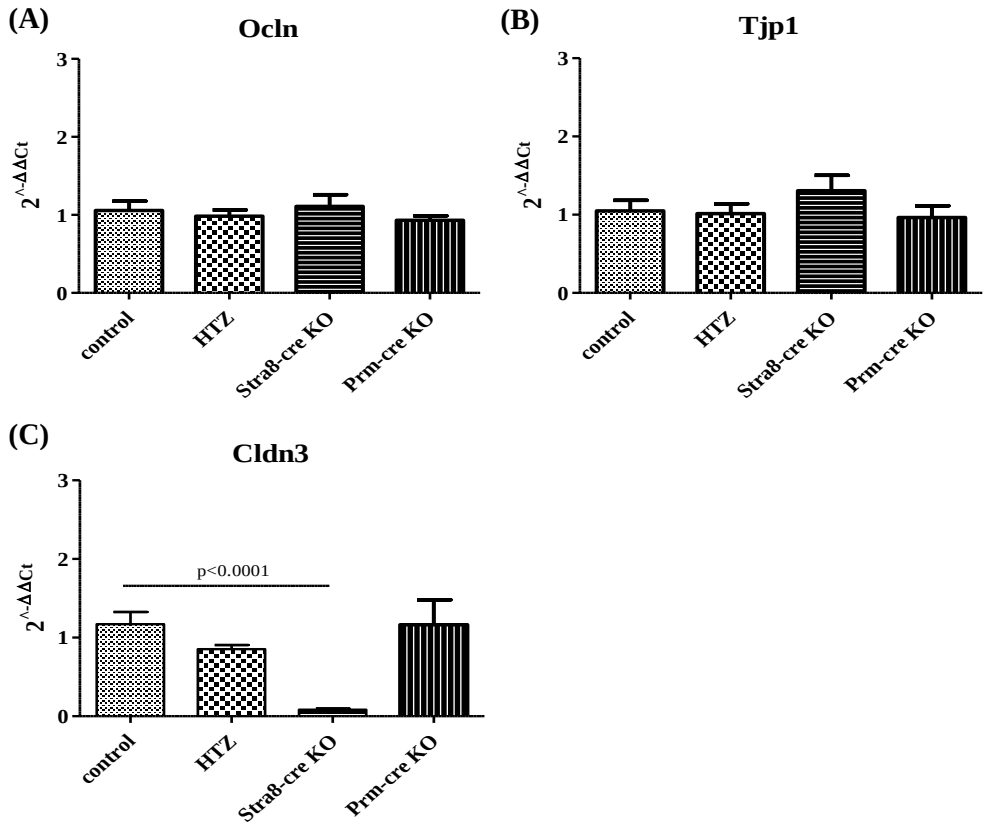

Figure 34| Characterization of the transcription level of representative genes of the blood-testis barrier in control (designated as WT), heterozygous (HTZ) as well as pre- (*Stra8*-Cre KO) and post- (*Prm*-Cre KO) meiotic induced KO testes. Qualitative reverse transcriptase polymerase chain reaction analysis was used to assess gene expression of **(A)** occludin (*Ocln*), **(B)** tight junction protein 1 (*Tjp*) and **(C)** claudin-3 (*Cldn3*) in testis biopsies of all genotypes in control group (WT square box bar), heterozygous (HTZ; brick bars), pre- (*Stra8*-Cre KO; horizontal line bars) and post-meiotic mediated gc*Pex13*KO (*Prm*-Cre KO; vertical line bars). **(C)** In pre-meiotic induced gc*Pex13*KO, *Cldn3* expression was significantly down-regulated compared to control group and to post-meiotic induced gc*Pex13*KO. Data represent 3 independent experiments, each assayed in duplicate, representing gene expression of 3 individuals per genotype; standard error of the mean (SEM).

Statistical significance was determined using T-test (Welch´s correction). *p ≤ .05; **p 0.001 < p ≤ 0.01; *** p ≤ 0.001.

3.10.2 Tracing with Evans Blue indicates a structural disturbance of the BTB in *Stra8*-Cre mediated gc*Pex13*KO testes

Staining with the Sertoli cell marker vimentin as well as quantitative analyses of tight junction proteins of the BTB already indicated alterations in *Stra8*-Cre mediated peroxisomal KO testes.
Mice of all genotypes, including control, heterozygous, pre- and post-meiotic induced gc*Pex13*KO were injected IV with Evans Blue to functionally assess the integrity of the BTB. In healthy seminiferous tubules, Evans Blue was clearly located around peritubular myoid cells and in interstitial Leydig cells (Figure 35A- D). In *Prm*-Cre mediated gc*Pex13*KO (Figure 35G) and gc*Pex13*HTZ mice (Figure 35C, D), Evans Blue localization resembled the one of control testis (Figure 35A, B), indicating a non-permeability of albumin through the BTB. In *Stra8*-Cre mediated gc*Pex13*KO mice, the distribution of injected Evans Blue was slightly different. Compared to control and heterozygous animals, Evans Blue was not only detected in interstitial cells, but also at the very basal compartment, surrounding spermatogonia (Figure 35F). However, in some seminiferous tubules, EB was partially dislocated to the adluminal part (Figure 35E, F), suggesting that BTB integrity might be functionally affected.

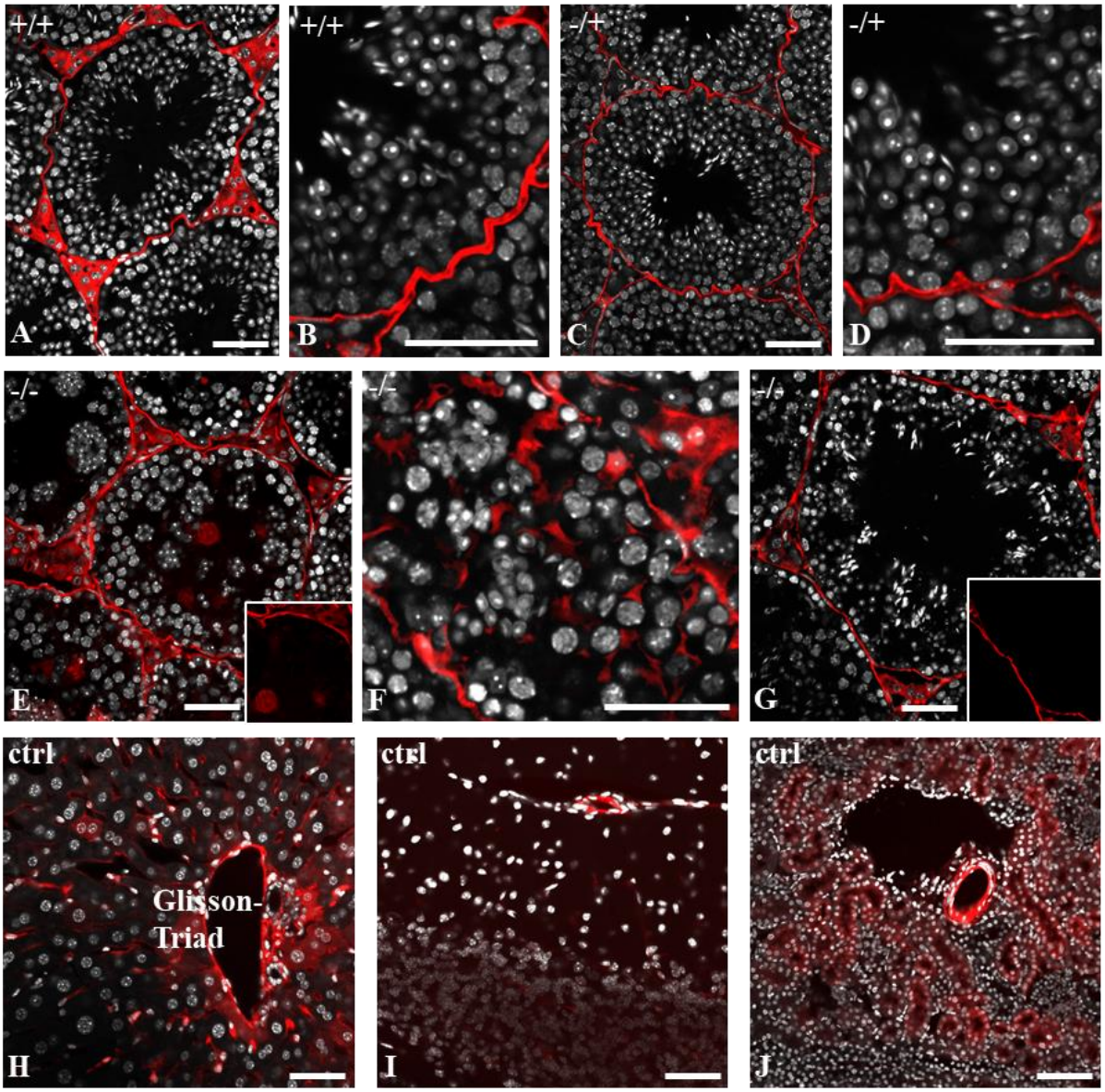

Figure 35| BTB integrity after pre- and post-meiotic induced peroxisomal KO. The integrity of the BTB was evaluated by intravenous injection of the azo-dye Evans Blue (EB). **(A, B)** In control, **(C, D)** heterozygous as well as **(E, F)** pre- and **(G)** post-meiotic induced gc*Pex13*KO testes, Evans Blue was clearly located in the suprabasal epithelium and the interstitium. **(F)** In some seminiferous tubules of pre-meiotic induced gc*Pex13*KO, EB seemed to be dispersed adluminal, indicating a putative disturbance of the endothelial BTB. **(H)** Liver, **(I)** brain and **(J)** kidney were used as positive controls. Evans Blue is indicated in red. Nuclei DAPI stains are shown in grey. Bars represent 50 µm.

3.11 Morphological analysis of immune cells in the *Stra8*-Cre mediated gc*Pex13*KO testes

An immunostaining against CD45 was performed in seminiferous tubules of all genotypes to test for an inflammatory reaction within the seminiferous tubules, as preceding event or as consequence of

putative disrupted BTB. CD45 positive cells were mainly found in Leydig cells (Figure 36A- C) and in blood vessels (Figure 36D), but also in a few peritubular myoid cells (Figure 36E). No differences in CD45 positive leukocyte localization were seen between pre-meiotic induced (Figure 35B), *Prm*-Cre mediated gc*Pex13*KO (Figure 36C) and control (Figure 36A) testis.

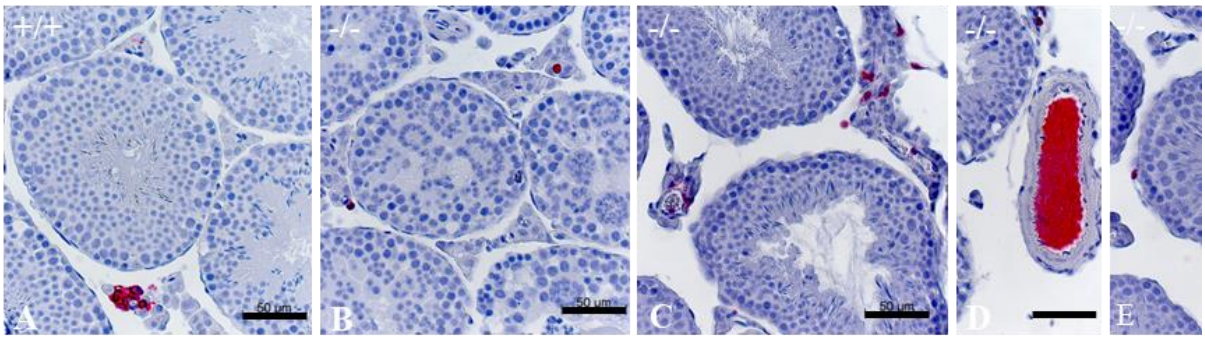

Figure 36| Histological detection of leukocytes in control and pre- and post-meiotic induced peroxisomal KO testes. Leukocytes were mainly located in Leydig cells, as shown for **(A)** control, **(B)** *Stra*-Cre mediated KO and **(C)** *Prm*-Cre mediated gc*Pex13*KO testes, **(D)** but also found in blood vessels of all genotypes (in this case, a representative of *Prm*-Cre mediated gc*Pex13*KO testes is shown) and **(E)** peritubular myoid cells. Nuclei are counterstained with haematoxylin. Bars represent 50 µm.

3.12 MNCs of pre-meiotic induced peroxisomal gc*Pex13*KO mice enter apoptosis

The observation of shrinking tubules in aging pre-meiotic induced peroxisomal KO mice, and the finding of condensed round spermatid nuclei, led to the hypothesis that MNCs might enter apoptosis. To verify this, a TUNEL assay was performed to detect DNA fragmentation as a result from activated apoptotic signalling cascades and caspase cleavage. Specimens of adult (P90) control and pre-meiotic induced gc*Pex13*KO testes were tested. In control tubules, cell death was mainly identified in meiotically dividing germ cells (Figure 37A, B). In *Stra8*-Cre mediated gc*Pex13*KO testes, a similar pattern of apoptotic cells in the germinal epithelium was observed. In addition, a high number of TUNEL positive MNCs was detected (Figure 37C, D).

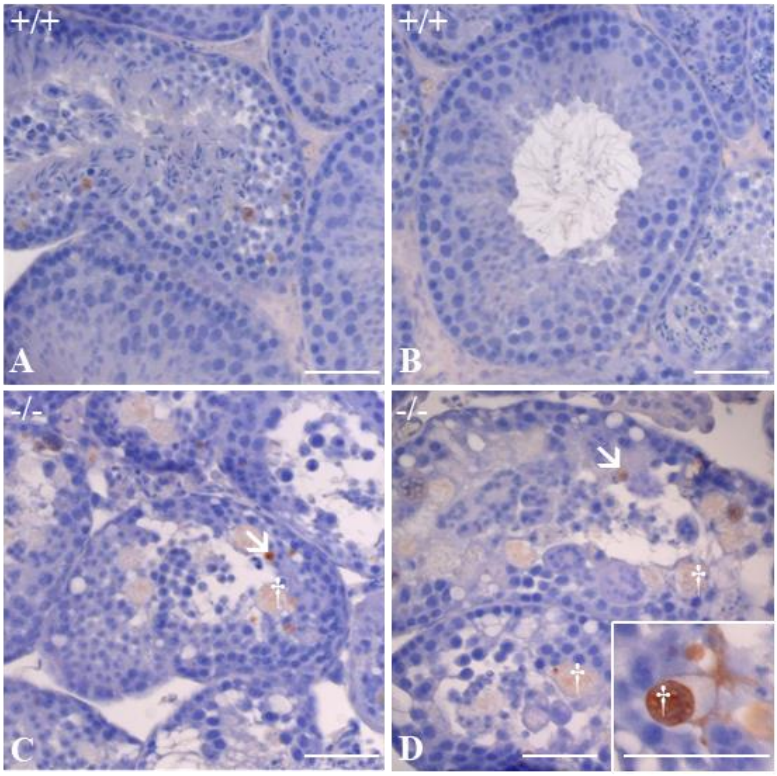

Figure 37| Representative examples of apoptotic cells in control and pre-meiotic induced gc*Pex13*KO testes (P90). *In situ* staining of DNA strand breaks was detected by TUNEL assay. **(A, B)** In control testes, cell development was characterized by regular apoptosis, as shown by TUNEL- positive spermatocytes. **(C, D)** MNCs in gc*Pex13*KO were TUNEL positive (†), with respect to their developmental stage. Only a few meiotic germ cells were also apoptotic (⇲). Bars represent 50 µm.

The dynamic expression of programmed cell death related proteins was investigated by immunofluorescent staining using anti-BAX and anti-Cleaved-Caspase-3 antibodies. Regarding the spermatogenic state, the distribution of apoptotic markers in germ cells of control (Figure 38A, B) and post-meiotic induced peroxisomal KO testes (Figure 38E, F) was similar in the way that some spermatogonia and spermatocytes were positive for Caspase-3 (Figure 38A, E) and BAX (Figure 38B, F). As already implicated by TUNEL assay, MNC of *Stra8*-Cre mediated gc*Pex13*KO mice were Caspase-3 (Figure 38C) and BAX (Figure 38D) positive.

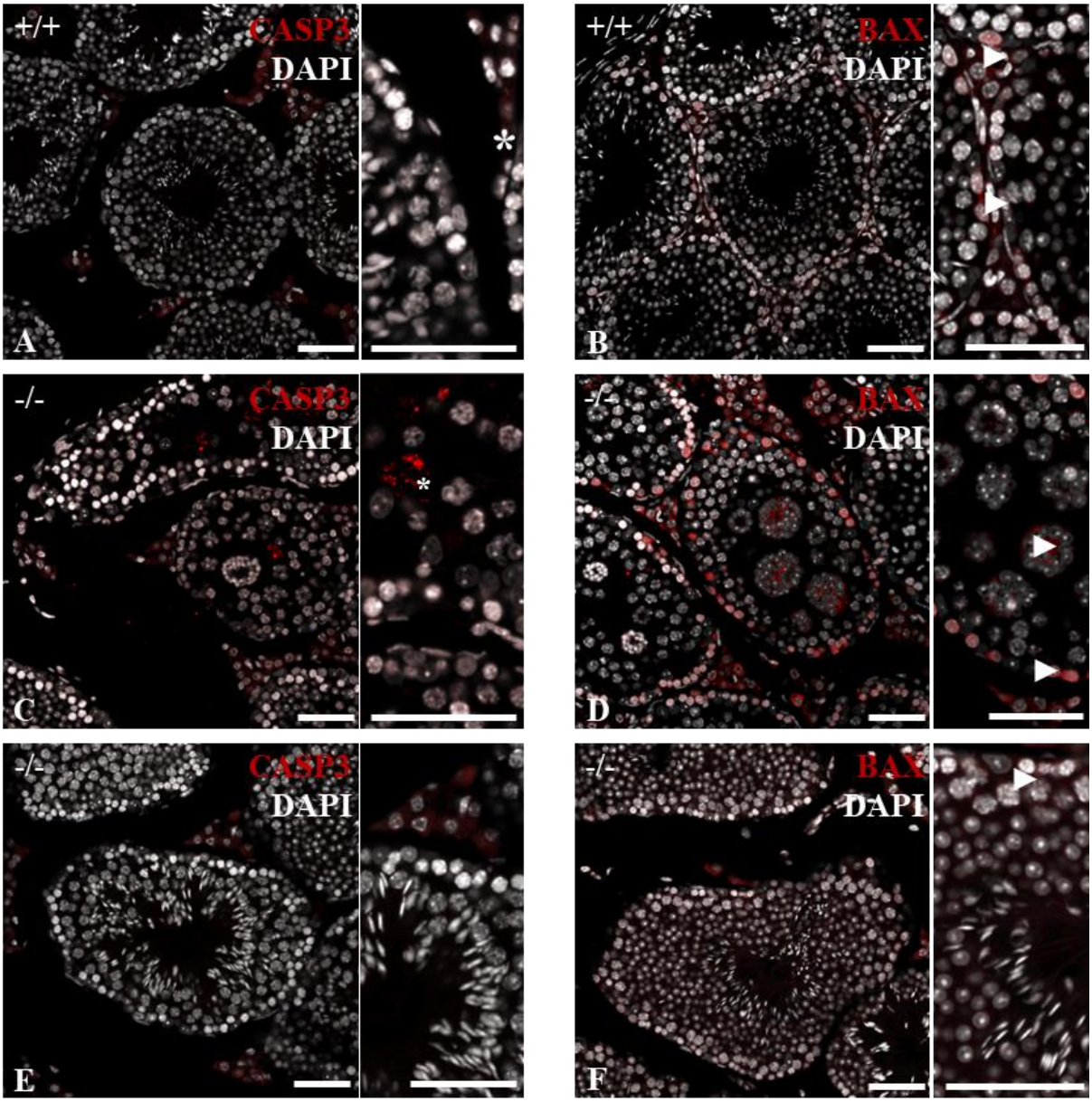

Figure 38| Immunofluorescent detection of apoptotic markers in germ cells of control and gc*Pex13*KO seminiferous tubules. **(A, B)** In control and **(E, F)** post-meiotic induced peroxisomal KO testes, some spermatogonia and spermatocytes were positive for **(A, E)** Caspase-3 and **(B, F)** BAX. **(C)** In *Stra8*-Cre mediated gc*Pex13*KO mice, proportionally more spermatogonia and spermatocytes were labelled with anti-Caspase-3 and **(D)** anti-BAX antibodies. **(C)** Depending on the differentiation state, MNCs were also positive for Caspase-3 and **(D)** BAX. A detailed representation of apoptotic cells in the corresponding germinal epithelium is shown in a higher magnification. Caspase-3 positive cells are marked by an asterisk (*). Anti-BAX labelled cells are marked by an arrowhead (►). CASP3- Caspase-3. Primary antibodies were labelled with Cy3 (red). Nuclei are stained with DAPI (shown in grey). Bars represent 50 µm.

3.13 Germ cells can be sorted according to their cell type with different techniques

Different cell sort techniques were tested to find an appropriate approach to separate germ cells, placing emphasis on purity, reproducibility, reliability, expenditure of time, costs and possibility to obtain RNA. In addition, alterations in the expression of genes involved in different peroxisomal pathways were quantified on testes biopsies from control, *Stra8*-Cre and *Prm*-Cre mediated gc*Pex13*KO mice.

3.13.1 BSA density sedimentation is a gentle cell sort technique that enables subsequent gene expression studies

A 1-3 % BSA density gradient was used to sort and enrich testicular cells according to their size. Considering 50 ml volume per fraction, 20 samples were eluted in total. Cells were further analysed according to their nuclei staining. Bigger cells were obtained in the first samples with higher concentrated BSA, whereas smaller cells were eluted in the later fractions, with a lower BSA concentration.

In cell samples #2, #5, #7 to #9, spermatocytes were enriched to 95 %, contaminated with few round and elongated spermatids (Figure 39A). Round spermatids were eluted in #14 and #15 that displayed a purity rate of about 90 % (Figure 39B). In the last samples (#19, 20), elongated spermatids were found (Figure 39C). Relative two-fold expression of the target genes *Stmn1* (marker for spermatocytes), *Cox6b2*, *Acrv1*, *Prm1* and *Tnp* (spermatid markers) were assayed in sample #8 (Figure 39B), #14 (Figure 39D) and #19 (Figure 39F). *Stmn* was up-regulated in the spermatocyte fraction (Figure 39B). The obtained round spermatid population displayed a 3-fold up-regulation in *Tnp* marker and an increase in Acrv1 expression (Figure 39D) by trend. In the sample containing elongated spermatids, *Prm1* and *Tnp* were markedly elevated (Figure 39F).

After having adjusted appropriate settings for the sorting of germ cells taken from control mice, the approach was transferred onto the separation of testicular cells of pre-meiotic induced peroxisomal KO mice. However, the enrichment of MNCs was impossible.

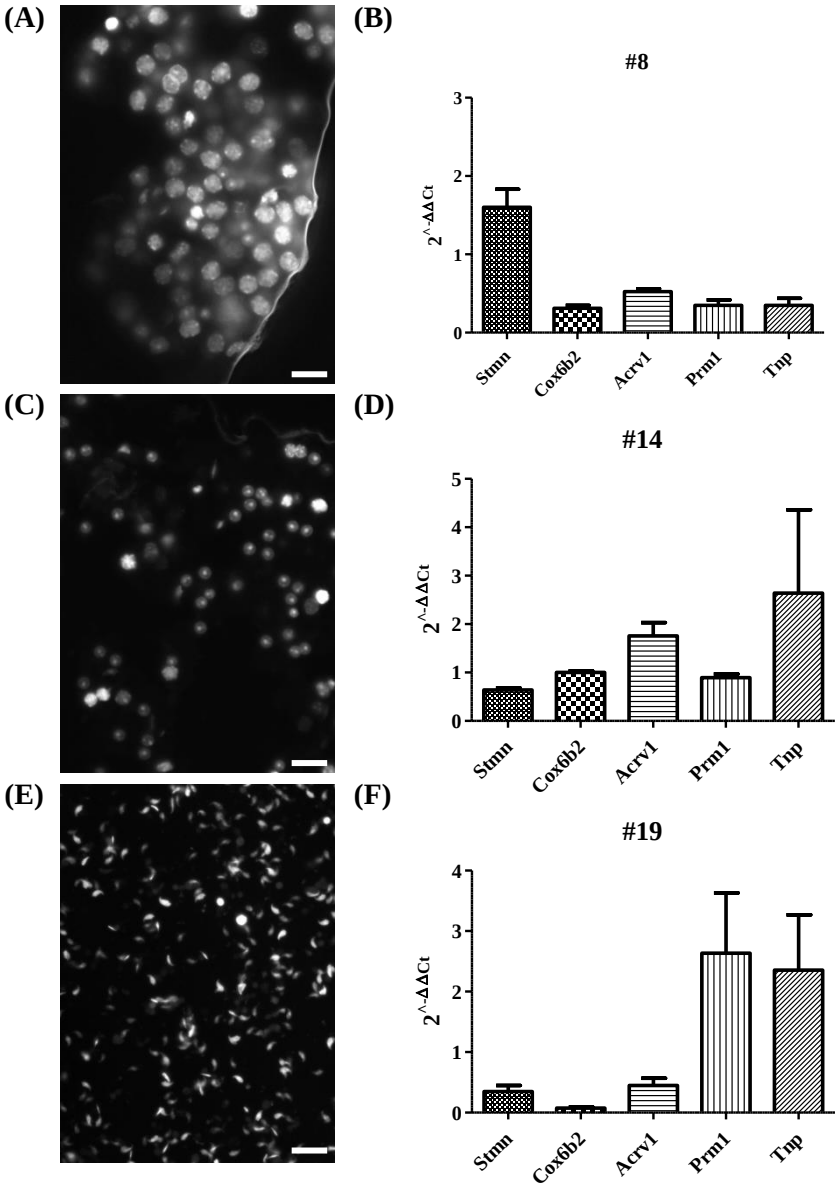

Figure 39| Morphological and quantitative mRNA expression analysis of sorted germ cell fractions by means of BSA gradient. Germ cell fractions of sample **(A)** #8, **(C)** #14 and **(E)** #19 were analysed according to their nuclei staining by fluorescent microscopy. Qualitative reverse transcriptase polymerase chain reaction (qRT-PCR) analysis was used to assess the cell-specific gene expression of cell samples sorted by BSA gradient sedimentation. Results were normalized against the reference gene *Gapdh* and converted to relative two-fold expression of the target genes *Stmn1* (marker for spermatocytes), *Cox6b2*, *Acrv1*, *Prm1* and *Tnp* (spermatid markers) in fraction **(B)** #8, **(D)** #14 and **(F)** #19. Marker expression in overall cells was normalized. Boxes represent the Ct values for each gene obtained from all experiments. Two biological replicates are shown for each sample each assayed in duplicate. The standard error of the mean (SEM) is shown. Statistical significance was not determined as the number of sample replicates was too small. Bars represent 20 µm.

.

3.13.2 Fluorescent activated cell sorting (FACS) is suitable for further mRNA profiling of purified cells

Cell sorting by means of FACS was performed on testicular cells taken from control mice. For the discrimination of cell size, granularity and DNA content, the peak height and area of the forward scatter (FSC-H and FSC-A; Figure 40B) and side scatter (SSC-H; Figure 40A) was applied in combination with the fluorescence CFP-A scatter (Figure 40C). Cells with a low Hoechst signal and small size were excluded and considered as cell debris. Cell number of every single sorted cell event was determined by the cell sorter. The number of so-called P4 and P6 fraction (elongated spermatids) varied between 6.1 x 10^5 to 3.7 x 10^6. In the P5 (spermatocyte) fraction about 9.7 x 10^5 to 2.9 x 10^6 cells were counted. About 4.6 x 10^5 to 3.1 x 10^6 cells of the P3 population (round spermatid) were counted.

This method was not suitable for the separation of testicular cells from the *Stra8*-Cre mediated gc*Pex13*KO testes. It was impossible to detect cell populations in the scatter plot that might have resembled that of MNCs. Collected cell samples contained all different germ cell types but were not enriched with MNCs (data not shown).

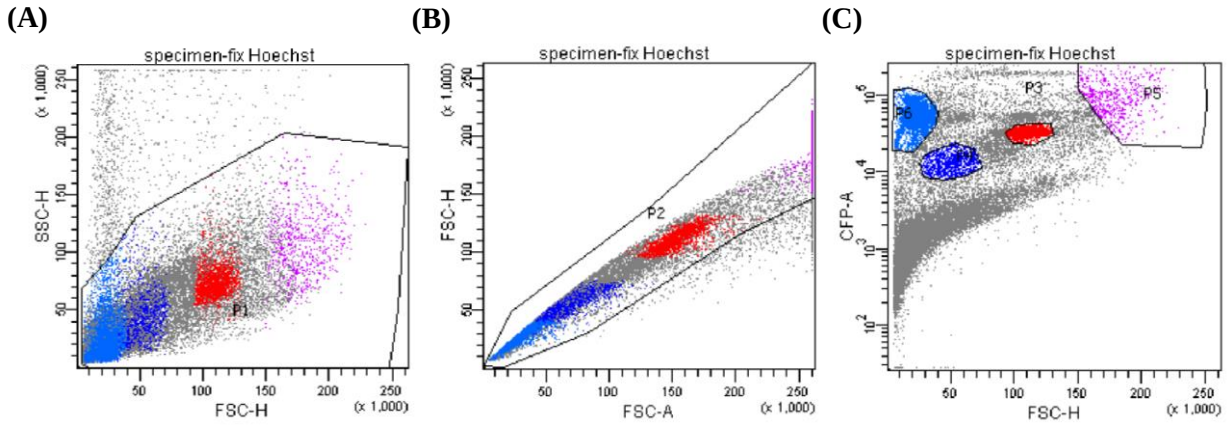

Figure 40| Fluorescent-activated cell sorting of murine testicular germ cells based on Hoechst fluorescence and light scattering parameters. (A, B) Cells were sorted according to forward scatter (FSC-H) and side scatter (SSC-H) based on cell size and internal granularity, respectively. Only the cells from the selected coloured region were subsequently sorted. **(C)** Intact, viable cells were additionally sorted according to their fluorescence intensity by CFP-A. The various cell populations are highlighted in colours and indicated as follows: P4 and P6 (blue): elongated spermatids at different developmental stages; P3 (red): round spermatids; P5 (purple): spermatocytes.

The cell populations were classified into primary and secondary spermatocytes (P5; Figure 41B), round spermatids (P3; Figure 41C) and elongated spermatids at two developmental stages (P4; P6;

Figure 41D). In the P4/P6 sample, elongated spermatids were represented at 98-99 %. The principal contaminants were round spermatids. The purity of the round spermatid fraction was in the range of 78-92 %. This fraction was slightly contaminated with elongated spermatids and spermatocytes. Spermatocytes were enriched to 95 %, being contaminated with round spermatids and a few elongated spermatids.

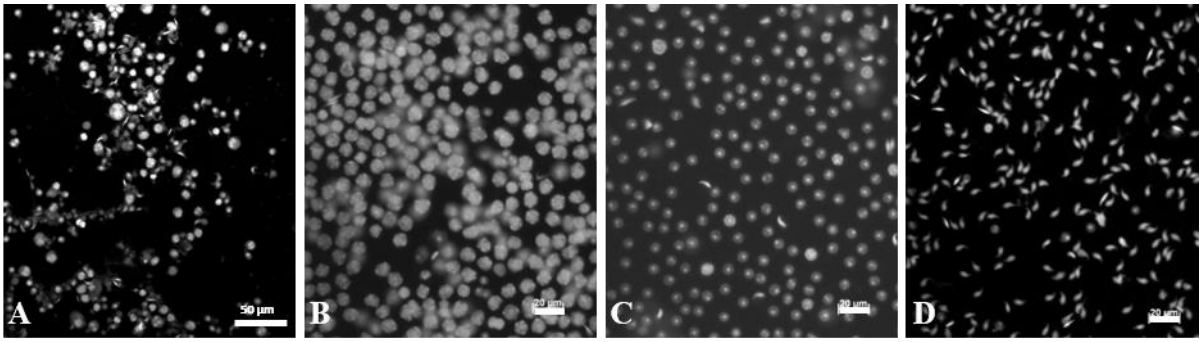

Figure 41| Isolated germ cells before and after sorting. (A) The initial overall cell fraction and **(B- D)** sorted cells were analysed according to their morphology and nuclei staining. **(A)** Photomicrograph of fixed and Hoechst stained testicular germ cells before sorting. **(B)** Isolated mouse spermatocytes. **(C)** Isolated mouse round spermatids with few contaminants of elongated spermatids and spermatocytes. **(D)** Elongated spermatids obtained by cell sort.

3.13.3 Analysis of cell integrity of sorted cells

To evaluate whether the enzymatic digestion procedure or the cell sorting might influence cell integrity, every single testicular cell sample was analysed by electron microscopy.

The membrane of cells from the initial cell fraction, taken prior to cell sort, showed irregularities in their integrity (Figure 42A, B). The morphology and cell membrane did not differ to cells that were sorted (Figure 42C- K), indicating an isolation defect. Zygotene (Figure 42C), diplotene (Figure 42D) and metaphase spermatocytes from the P5 fraction (Figure 42E) were characterized according to the condensed chromosomes and the synaptonemal complex. The cell population yielding round spermatids (P3) could be clearly identified according to acrosome formation (Figure 42F- H). The P4 and P6 fractions contained spermatids with characteristic elongated nuclei (Figure 42I- K).

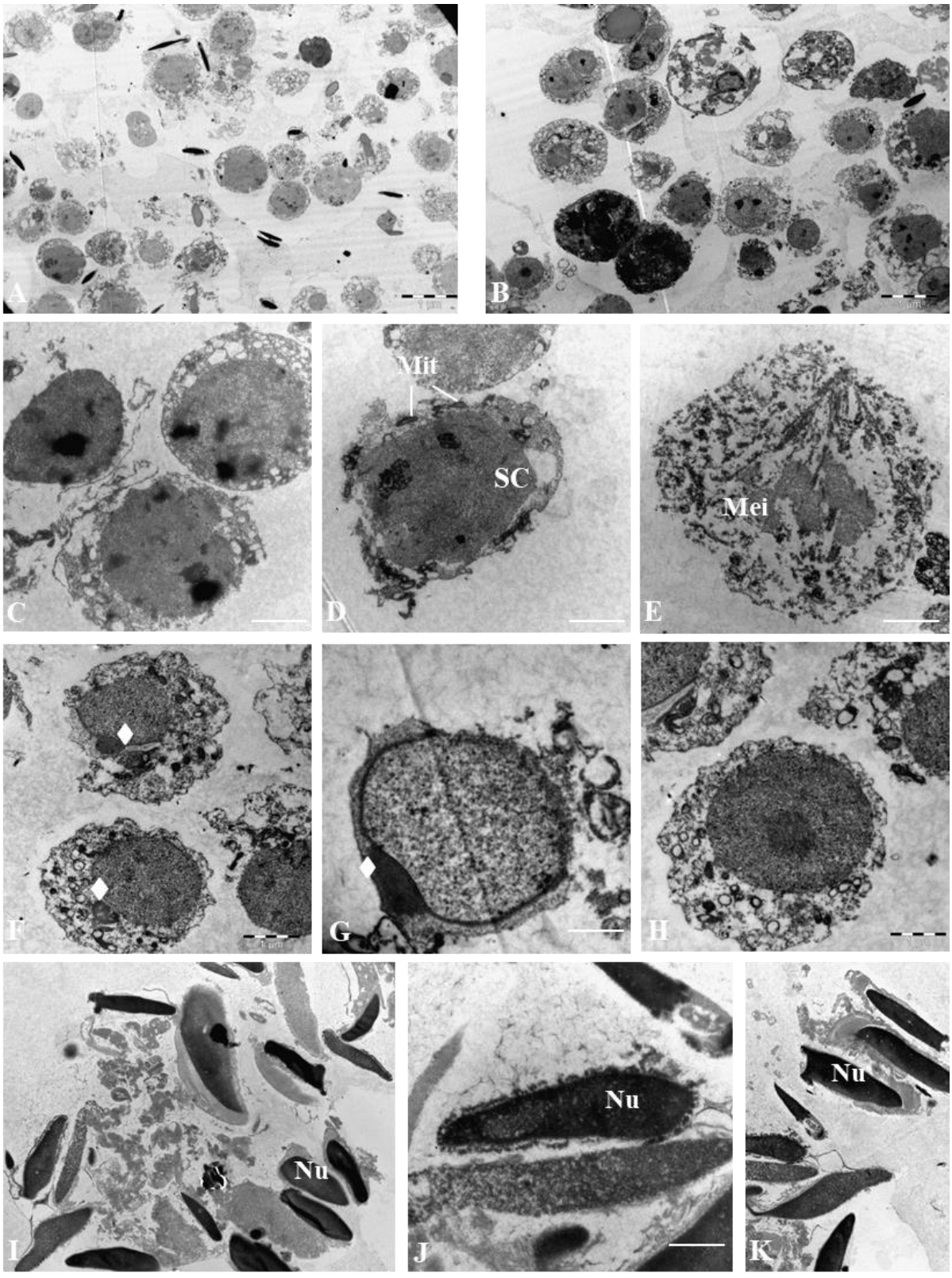

Figure 42| Ultrastructural analysis of germ cells separated by FACS. (A, B) In the initial overall cell fraction, all testicular cells are present that were mechanically and enzymatically separated prior to use for electron microscopic analysis. **(C- E)** Cells were sorted according to their size, resulting in a spermatocyte population, **(F- H)** a sample containing round spermatids and a **(I- K)** fraction with elongated spermatids. The

spermatocyte sample contained cells at different developmental stages, e.g. **(C)** zygotene, **(D)** diplotene and **(E)** metaphase spermatocytes. **(F, G)** Round spermatids were characterized according to their acrosomal cap (♦). **(I-K)** Elongated spermatids showed a characteristically large nucleus (Nu). Mit- Mitochondria; Mei- Meiosis; SC- Synaptonemal complex.

3.13.4 QRT-PCR analysis of FACS purified germ cells of C57Bl/6 mice

Prior to gene expression analyses, RNA integrity (RIN) was assessed. A RIN of 8.50 was measured for the RNA isolated from spermatocytes. In round spermatids, the averaged RIN was 6.70 of all four biological replicates. RNA extracted from elongated spermatids had a RIN of 5.30. The RNA from the overall cell fraction had a RIN of 5.70

A significantly enhanced *TacStd* expression was found in spermatocytes, compared with the expression level in the initial overall testicular cell suspension (Figure 43A). *AR* was slightly up-regulated by trend in round spermatids (Figure 43B). Spermatocyte marker expression of *Sycp3* ($p = 0.0012$; Figure 43C) and *Stmn1* ($p = 0.0106$; Figure 43D) were 5-fold up-regulated in the spermatocyte fraction compared to the overall cell fraction and significantly down-regulated in spermatids. The spermatid marker *Acrv1* (Figure 43E) was 6-fold up-regulated in the fraction containing round spermatids ($p = 0.0136$), whereas *Crem* was 2.5-fold enriched in the round spermatid sample ($p = 0.0112$; Figure 43F). *Tnp* and *Prm1* are typical markers of elongated spermatids. These markers were significantly increased in the cell sample that was morphologically determined as elongated spermatid fraction (Figure 43G, H).

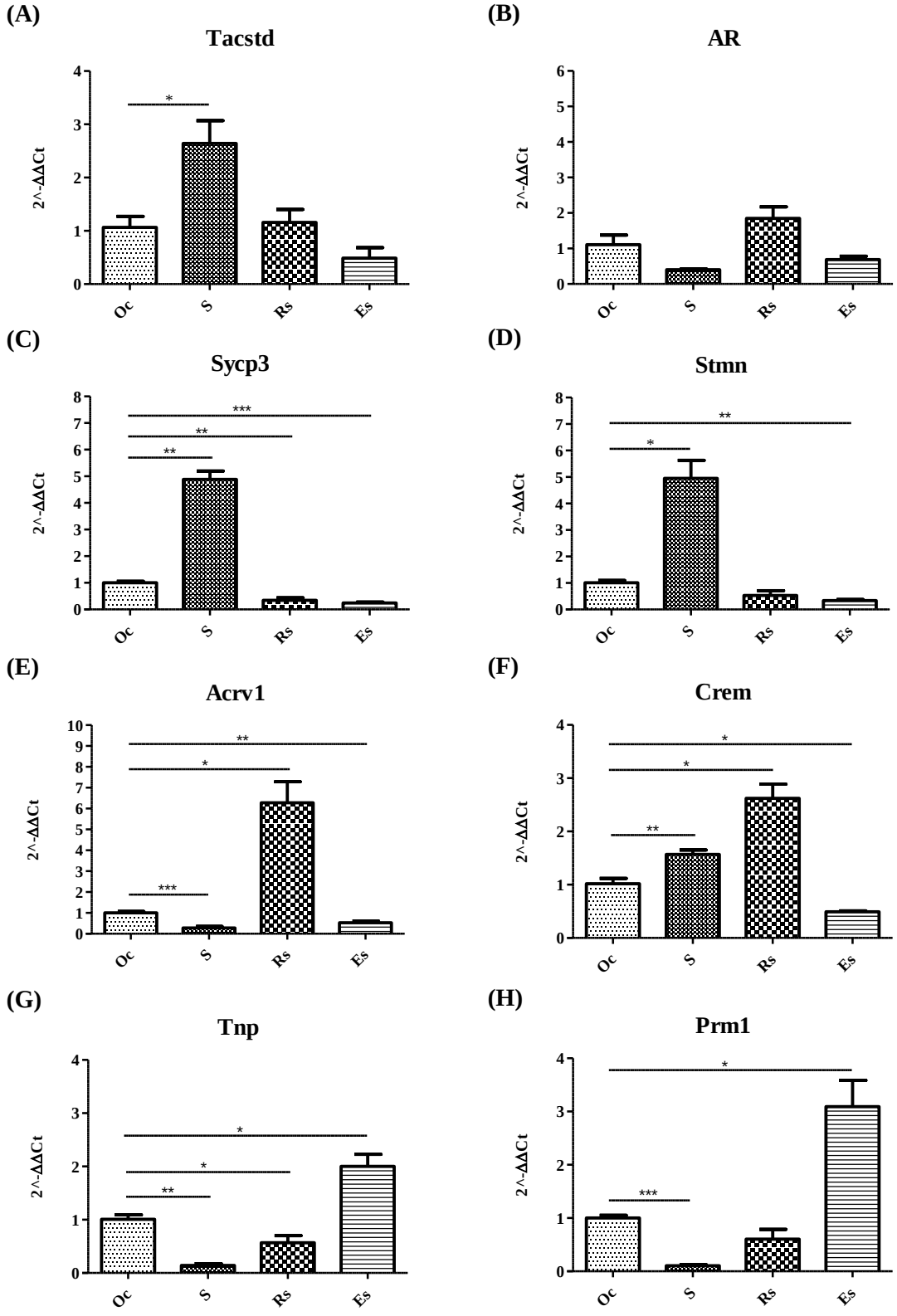

Figure 43| Quantitation of germ cell specific markers in all sorted germ cell fractions. Relative mRNA expression levels for **(A)** *Tacstd*, **(B)** *AR*, **(C)** *Sycp3*, **(D)** *Stmn1*, **(E)** *Acrv1*, **(F)** *Crem*, **(G)** *Tnp* and **(H)** *Prm1* were quantified by qRT-PCR in spermatocytes (*S*), round spermatids (*Rs*), elongated spermatids (*Es*), and initial overall cells (*Oc*) of the seminiferous tubules, using *Gapdh* and *β-actin* as housekeeping genes. Marker expression in the initial overall cell fraction was normalized. Boxes represent the $2^{\wedge-\Delta\Delta Ct}$ values for each gene

obtained from all experiments. Four biological replicates are shown for each sample. The standard error of the mean (SEM) is shown. Statistical significance was determined using t-test (Welch´s correction). *$p \leq .05$; **p $0.001 < p \leq 0.01$; *** $p \leq 0.001$.

3.13.5 Isolation and purification of MNCs by counterflow centrifugation elutriation (CCE)

In addition to BSA and FACS techniques, CCE was applied to purify MNCs from the pre-meiotic induced peroxisomal KO testes.

Flow rate and rotor speed were first calculated according to *Stoke´s law* and then experimentally modulated to achieve highest purification. The initial rotor speed was set to 1200 rpm to neither pelletize the cells nor flushing them out of the chamber. The best results were achieved with an initial flow rate of 30 ml/min that was stepwise increased up to 47.7 ml/min, whereas the rotor speed was minimized in steps of 200 rpm, down to 0 rpm.

All cell samples were collected in PBS, in a volume of 50 ml, and further examined according to their nuclei stain and shape, by means of fluorescent and phase contrast microscopy. Smaller cells, such as spermatocytes, were eluted first (Figure 44A). MNCs were enriched in the second (Figure 44B- F) and accumulated in later fractions (Figure 44H- M). However, the contamination rate was still 50 % that would have interfered with mRNA expression analysis. Contaminants were spermatocytes with a diameter of 25 µm (Figure 44K).

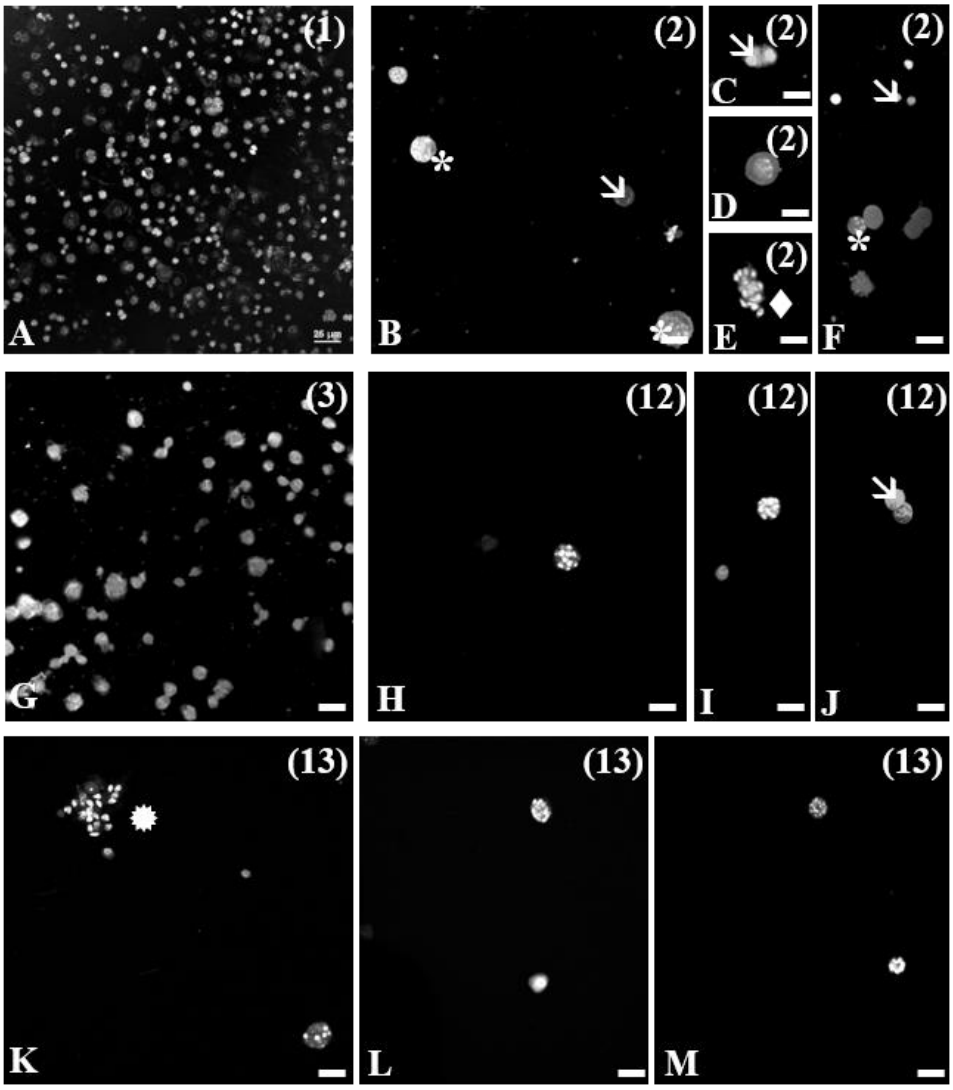

Figure 44| Morphological analysis of cells separated by counterflow centrifugation elutriation (CCE). Germ cells from the *Stra8*-Cre mediated g*cPex13*KO mice were used for cell separation by means of CCE to purify MNCs. **(A)** In the first fraction (rotor settings: 1200 rpm, flow rate: 30 ml/min), mainly small cells with a diameter ranging from 10 to 25 µm were collected. **(B)** In the following sample (1200 rpm; 31.8 ml/min), MNCs were randomly found (∗), **(C- F)** but also spermatocytes (↘) and somatic cells (♦; 2nd fraction). **(G)** In the third sample (1200 rpm; 35.3 ml/min), spermatocytes were enriched. **(H- J)** An accumulation of MNCs was detected at 400 rpm, at a flow rate of 47.7 ml/min. **(K- M)** Spermatocytes of the same size were also collected (↘). MNC were enriched after flushing the chamber with 700 ml PBS at 200 rpm and a flow rate of 47.7 ml/min (sample number 13). A heterogenous group of cells was also collected in this sample (✹). Nuclei were stained with Hoechst (shown in grey). Bars represent 25 µm.

3.13.6 Significant alterations in mRNA levels of peroxisomal genes in the *Stra8*-Cre mediated gcP*ex13*KO testes

The initial overall cell fraction taken from control, gc*Pex13*HTZ and gc*Pex13*KO testes was tested for germ cell type specific and peroxisomal gene expression. The panel included the spermatocyte specific marker *Sycp3* and the spermatid markers *Prm1* and *Acrv1*. *Sycp3* (Figure 45A), as well as *Prm1* (Figure 45B*)* and *Acrv1* (Figure 45C) were significantly down-regulated in the pre-meiotic induced peroxisomal KO. In the *Prm*-Cre mediated gc*Pex13*KO mice, *Sycp3* was slightly up-regulated (Figure 45A).

The expression of biogenesis genes, including *Pex14* (Figure 46B) and *Pex19* (Figure 46C), was decreased in the pre-meiotic induced peroxisomal KO cells. Strikingly, *Pex13* was significantly up-regulated (Figure 46A). In *Prm*-Cre mice, *Pex14* and *Pex19* were slightly increased, whereas *Pex13* was unaffected. The metabolite transporter *Abcd1* was down-regulated in *Stra8*-Cre mediated gc*Pex13*KO, and slightly increased in *Prm*-Cre mediated peroxisomal KO mice (Figure 46D). The *Stra8*-Cre mediated KO also showed a strong effect on *β*-oxidation, as *Acox1* (Figure 46E), down-stream acting *Hsd17b4* (Figure 46F) and *Gnpat* (Figure 46G) that is involved in ether lipid synthesis, were significantly down-regulated. The ROS metabolism was also affected, displaying a strong down-regulation of *Sod1* (Figure 46H) and *Cat* (Figure 46I). A slight increase by trend of *Cat* was measured in post-meiotic induced gc*Pex13*KO animals.

The gene encoding for *Dhrs4*, a member of the retinoid metabolism, was expressed at very low amounts in the *Stra8*-Cre mediated gc*Pex13*KO testes and only slightly altered in the post-meiotic induced peroxisomal KO (Figure 46J). The representative gene of the polyamine metabolism *Paox* was up-regulated in the pre-meiotic induced peroxisomal KO testes but unaffected in the *Prm*-Cre mediated gc*Pex13*KO (Figure 46K).

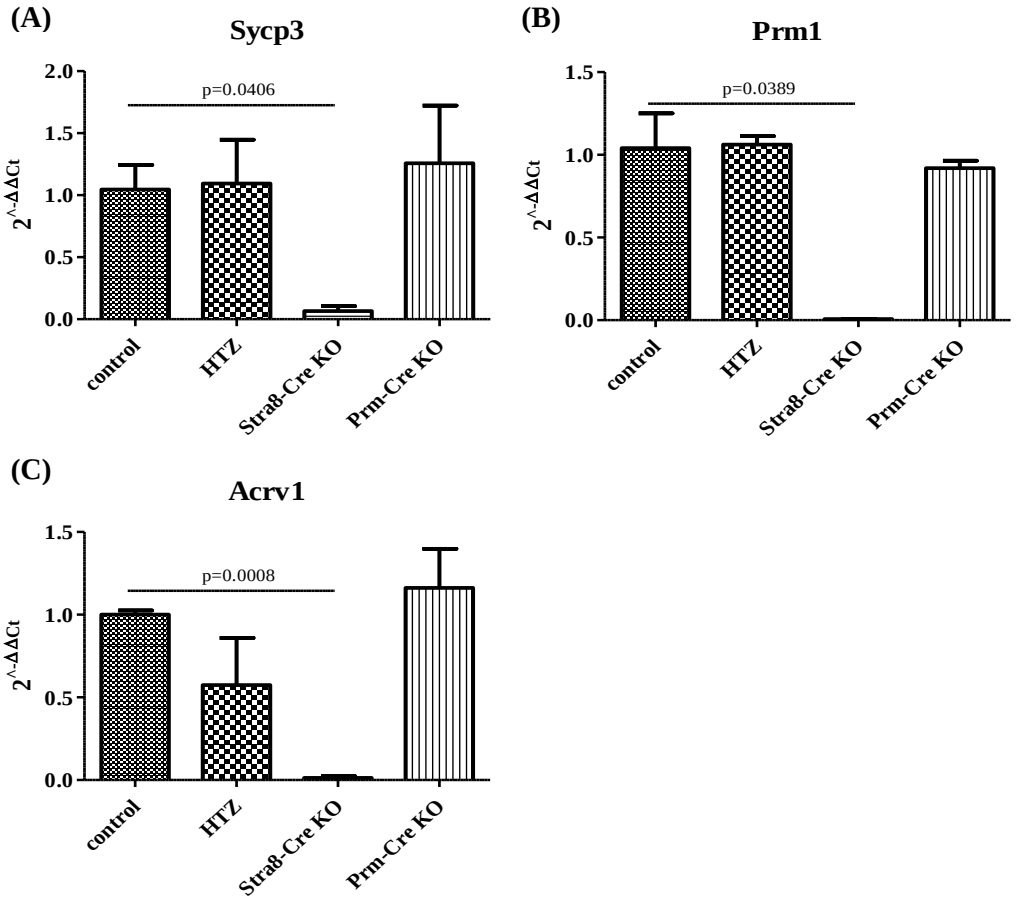

Figure 45| Cell type specific marker expression of tested overall cell fraction. (A) Representative genes for spermatocytes (*Sycp3*) and **(B, C)** spermatids (*Prm1, Acrv1*) were tested by qRT-PCR in the initial overall cell fraction of control (square box bars), heterozygous (HTZ; brick bars), pre- (*Stra8*-Cre KO; horizontal line bars) and post-meiotic mediated peroxisomal KO (*Prm*-Cre KO; vertical line bars). The standard error of the mean (SEM) was applied. Statistical significance was determined using T-test (Welch´s correction). *p ≤ .05; **p $0.001 < p \leq 0.01$; *** $p \leq 0.001$.

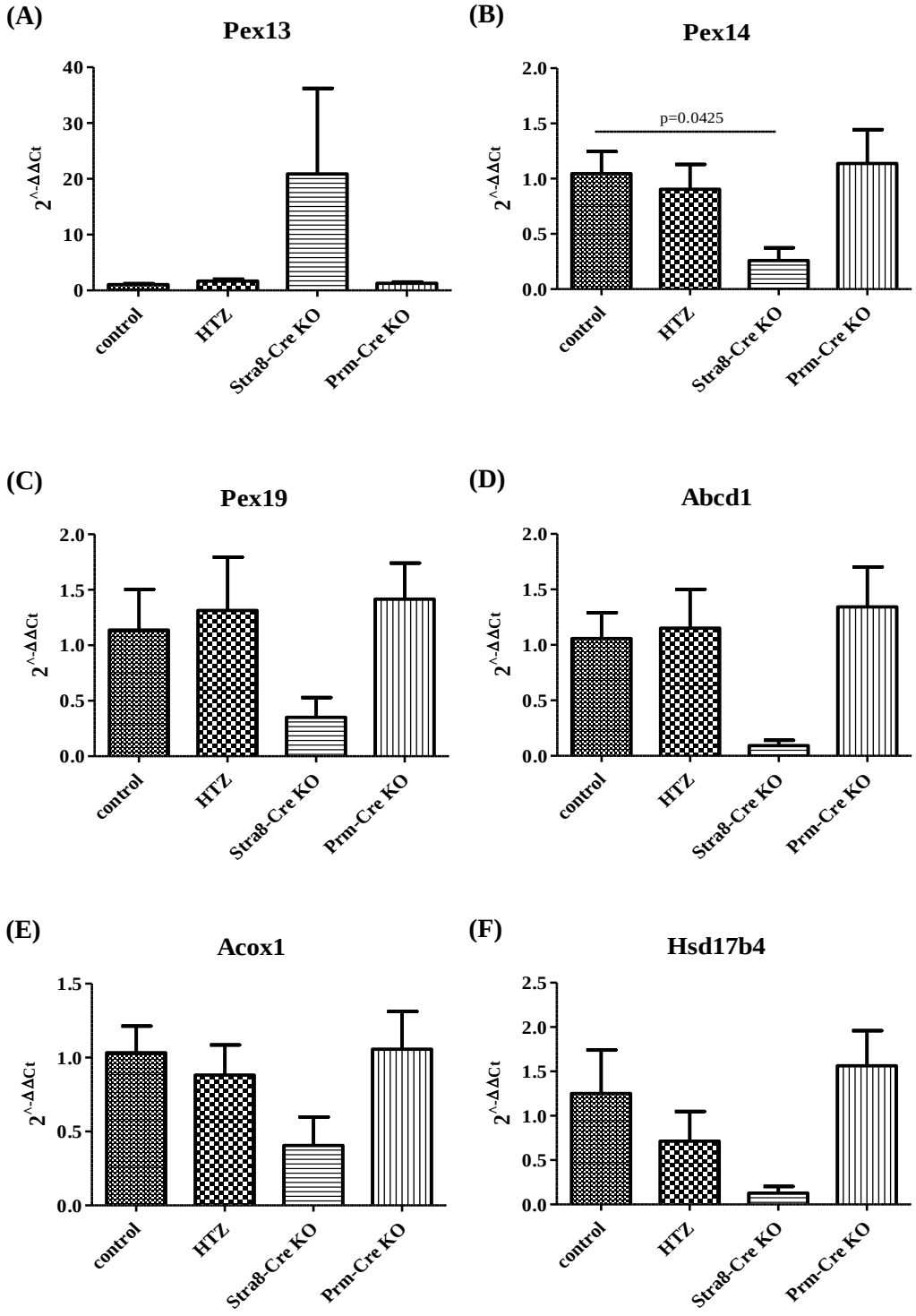
(A)
Pex13
2^-ΔΔCt
40
30
20
10
0
control
HTZ
Stra8-Cre KO
Prm-Cre KO
(B)
Pex14
p=0.0425
2^-ΔΔCt
2.0
1.5
1.0
0.5
0.0
control
HTZ
Stra8-Cre KO
Prm-Cre KO
(C)
Pex19
2^-ΔΔCt
2.0
1.5
1.0
0.5
0.0
control
HTZ
Stra8-Cre KO
Prm-Cre KO
(D)
Abcd1
2^-ΔΔCt
2.0
1.5
1.0
0.5
0.0
control
HTZ
Stra8-Cre KO
Prm-Cre KO
(E)
Acox1
2^-ΔΔCt
1.5
1.0
0.5
0.0
control
HTZ
Stra8-Cre KO
Prm-Cre KO
(F)
Hsd17b4
2^-ΔΔCt
2.5
2.0
1.5
1.0
0.5
0.0
control
HTZ
Stra8-Cre KO
Prm-Cre KO

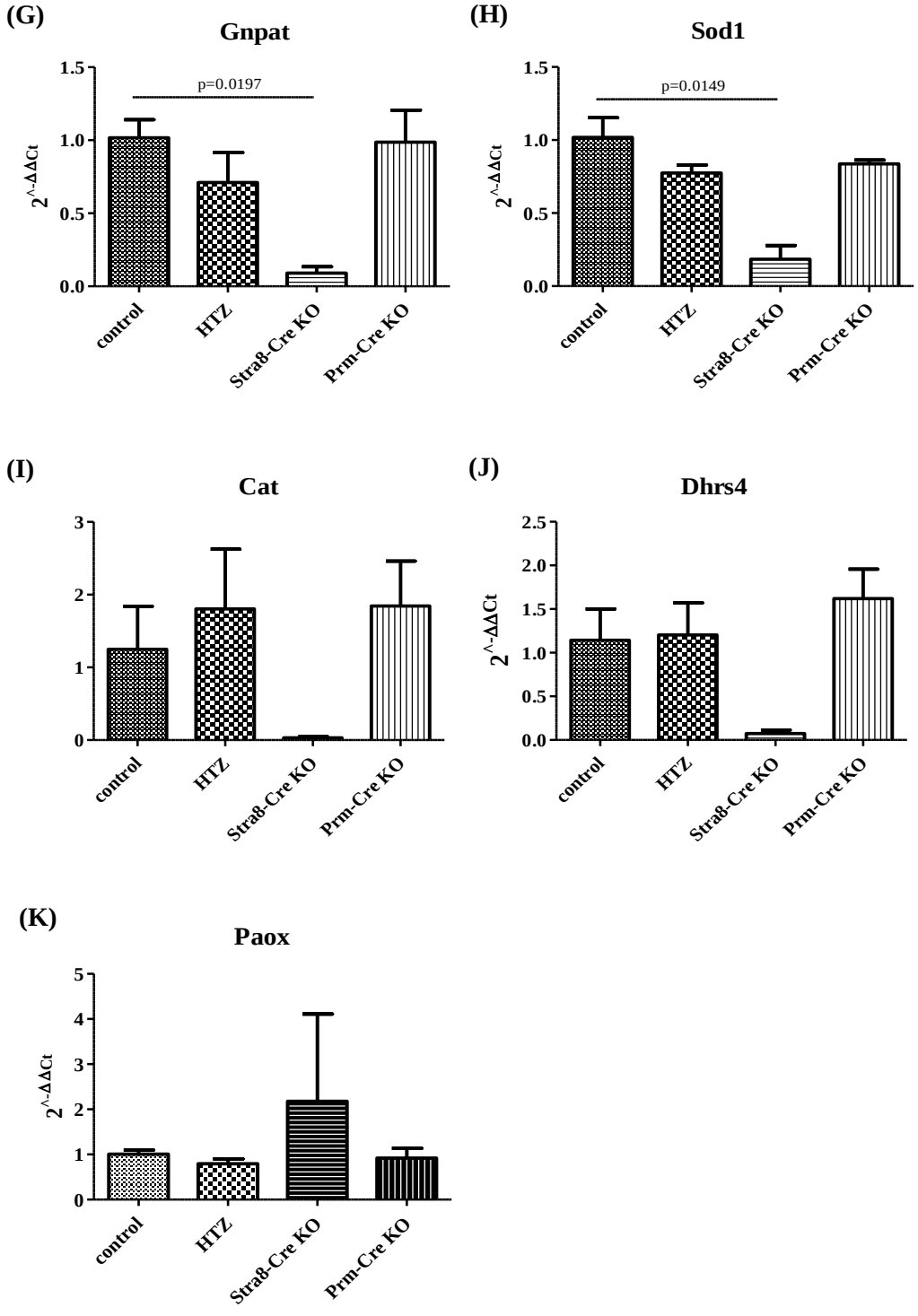

Figure 46| Peroxisomal marker expression of tested overall cell fraction. Representative genes of (A, B) the translocation machinery (*Pex13, Pex14*) and (C) peroxisomal biogenesis (*Pex19*), (D) metabolite transporter (*Abcd1*) and (E- G) *β*-oxidation (*Acox1*, *Hsd17b4*, *Gnpat*), (H, I) ROS metabolism (*Sod1*, *Cat*); (J) Retinoid metabolism (*Dhrs4*) and (K) Polyamine metabolism (*Paox*) were tested by qRT-PCR in the overall cell fraction of control (square box bars), heterozygous (HTZ; brick bars), pre- (*Stra8*-Cre KO; horizontal line bars) and post-meiotic mediated peroxisomal KO (*Prm*-Cre KO; vertical line bars); The standard error of the mean (SEM) was used. Statistical significance was determined using T-test (Welch´s correction). *$p \leq .05$; **$p\ 0.001 < p \leq 0.01$; *** $p \leq 0.001$.

4 DISCUSSION

Peroxisomes are essential cellular organelles. Defects of peroxisomes due to impaired biogenesis or protein import are linked to severe clinical disorders that can either be lethal or may have an impact on the reproductive tract, as already described by Powers *et al*. (1981). Patients with these diseases, such as X-ALD or AMN, have lesions in their testicular interstitial cells and display diminished libido, impotence and infertility.

Mouse models have been shown to be useful tools to study molecular mechanisms that are relevant for the pathogenesis of a disease in men. For the analysis of the relevance of peroxisomal function, several mouse models were established that targeted the disruption of either *Pex2* (Faust and Hatten 1997), *Pex5* (Baes et al. 1997) or *Pex11β* (Li and Gould 2002). Unfortunately, a generalized peroxisomal KO is lethal to new born pups and the only post-mortem findings being made were severe defects in the liver, including changes in the ultrastructure of the mitochondrial inner membrane (Baes and Van Veldhoven 2006). Consequently, Cre transgenic mice were established to induce a conditional gene KO (Postic *et al.* 1999; Verheijden *et al.* 2015).

For the characterization of peroxisomes exclusively in Sertoli cells, an *Amh*-Cre mediated KO mouse was generated by the group of Eveline Baumgart-Vogt to target the disruption of *Pex13*. The peroxisomal KO induced a "Sertoli cell only" syndrome with a strong increase of neutral lipids, including triglycerides and cholesteryl esters providing evidence that peroxisomes are necessary for proper spermatogenesis (Nenicu *et al.* 2007). Mutations in *Pex13* have been shown to be linked to classical Zellweger syndrome, including intra-uterine growth retardation, hypotonia, abnormal peroxisomal metabolism and neonatal lethality (Maxwell *et al.* 2003). However, the effects of a peroxisomal biogenesis defect in germ cells have not been studied yet.

For the present project, two mouse models have been established with the Cre-*loxP* technology to study a KO in *exon 2* of *Pex13* in either pre- or post-meiotic germ cells. Germ cell differentiation was extensively analysed with respect to the morphology of the germinal epithelium, cell-cell interaction between Sertoli and germ cells and the impact on peroxisomal metabolic pathways. The data provides evidence that peroxisomes are essential for germ cell development into fully functioning spermatozoa.

The first section will concentrate on the physiological significance of peroxisomes during germ cell differentiation in normal and KO mouse testes, whereas the effects of the *Stra8*-Cre mediated *Pex13* KO will be discussed first and then compared with the post-meiotic induced peroxisomal KO mice. Subsequently, the suitability of different cell sort techniques generating these results will be reviewed specifically.

4.1 The physiological significance of peroxisomes during germ cell differentiation in normal and *Stra8*-Cre mediated pre-meiotic induced gc*Pex13*KO mouse testes

4.1.1 The *Stra8*-Cre mediated KO in *Pex13* led to a generalized disruption of peroxisomal biogenesis and all metabolic functions

Based on histological analyses, the *Stra8*-Cre mediated *Pex13* KO induced a spermatogenic arrest at the spermatid stage. Instead of round spermatids, multinucleated giant cells (MNCs) were present, and mature spermatozoa were absent, resulting in infertile male mice.

Surprisingly, expression analyses showed an up-regulation of *Pex13* mRNA in the *Stra8*-Cre mediated gc*Pex13*KO testes with primers designed to specifically anneal in *exon 4*, which was not affected by the Cre mediated excision.

Up-regulated *Pex13* expression might be an indication for genetic or functional redundancy, as alternatively spliced variants might compensate for the deletion of *exon 2* (Tazi *et al.* 2009). Functional redundancy was already described in yeast for paralogous genes, thus genes that have diverged within one species with a new function (Kafri *et al.* 2005). Random mutations could be tolerated through functional redundant genes that will be expressed to compensate for a gene´s loss, thereby maintaining genetic robustness (Edelman and Gally 2001; Kitano 2004). However, PEX13 antibody was cytosolically localized in *Pex13*-deficient cells, indicating that the gene´s loss could not be compensated. The mRNA expressions of interacting partners of *Pex13,* including *Pex14* and *Pex19* were consequently quantified in the *Stra8*-Cre mediated peroxisomal KO testes. Whereas PEX14 is part of the translocation machinery, PEX19 acts as chaperone and as an import receptor for peroxisomal membrane proteins (Neufeld *et al.* 2009). Interestingly, their gene expressions were likewise down-regulated, suggesting that the cell was not able to compensate for truncated PEX13.

To verify this suggestion, peroxisomal marker proteins were localized by immunofluorescent staining on testicular cross-sections of *Stra8*-Cre mediated peroxisomal KO as well as control testes. Antibody labelling with PEX13 and PEX14 indicated the existence of peroxisomal remnants in the cytosol of *Pex13*-deficient male germ cells of *Stra8*-Cre mediated KO, whereby not only confirming the stability of the conditional peroxisomal KO of *exon2* in *Pex13,* but again assuring that its deletion resulted in a defect of peroxisomal biogenesis and thus failure of gene expression of functional redundant genes. It remains unclear, why *Pex13* was up-regulated. An additional but yet unknown function of an alternative splice variant of PEX13 could be considered.

The term of peroxisomal ghosts was introduced describing the presence of cytosolically diffusing peroxisomal proteins as their import is defect caused by the failure of peroxisomal biogenesis (Santos *et al.* 1988). The disturbed import of peroxisomal enzymes was also shown by cytosolically mis-targeted peroxisomal catalase in *Pex13*-deficient cells. In addition, the gene expressions of *Sod1* and

Cat together with other tested candidates involved in various peroxisomal pathways were significantly reduced in the overall testicular cell sample.

Intense anti-Catalase immunoreactivity was found in Leydig cells of *Stra8*-Cre mediated peroxisomal KO testes. This finding coincided with the increased number of Leydig cells in these knockouts, as shown in histological specimens. Leydig cells are the place for steroidogenesis that requires cholesterol as backbone of steroid hormones, such as testosterone. In response to the luteinizing hormone (LH), lipid peroxidation is caused, which produces reactive oxygen species (ROS) (Peltola *et al.* 1996). As peroxisomes are also involved in ROS degradation, increased catalase activity might indicate a compensatory effect to prevent accumulation of ROS in the seminiferous tubules to maintain a toxic-free environment and thus ensuring steroidogenesis (Tsai *et al.* 2003).

However, it still needs to be clarified whether *Stra8*-Cre mediated peroxisomal KO testes show increased steroid levels leading to increased catalase activity in Leydig cells or if accumulated lipid droplets in the interstitial cells have provoked enhanced *β*-oxidation to synthesize VLCFAs and thereby producing ROS.

4.1.2 The formation of MNCs are the result of the peroxisomal biogenesis defect

MNCs are consistently present in all seminiferous tubules of the pre-meiotic induced *Pex13* KO testes. The formation of MNCs has already been reported to occur during normal germ cell development in mouse (Luo *et al.* 2013), aging human testes (Holstein and Eckmann 1986) but also in pathological processes (Pitt *et al.* 1993). Their formation was shown to be associated with endocrine alterations or an age-related involutive process, following efferent duct ligation, exposure to gamma irradiation or as a consequence of administered xenobiotics (Nistal *et al.* 1986a).

A frequent occurrence of MNCs in both testicles was proposed to be linked to a specific form of degenerating germ cells as a consequence of impaired Sertoli cell maintenance of cytoplasmic bridge closure among spermatids or spermatocytes (Greaves *et al.* 2012). This failure might provoke the "fusion" of cellular contents of the conjoined cells (MacGregor *et al.* 1990; Hild *et al.* 2007; Creasy *et al.* 2012).

MNCs already occurred in juvenile *Stra8*-Cre mediated *Pex13* KO mice, thus effects due to age can be excluded. Even though hormone levels were not altered in the serum of these KO mice, the steroid concentrations in the testes must be determined to analyse putative endocrine alterations. However, it is more likely that the communication between Sertoli cells and germ cells was affected in the pre-meiotic induced *Pex13* KO mice leading to a defect in germ cell differentiation. This hypothesis will be discussed in more detail in paragraph 4.1.4.

The presence of multinucleate cells was initially described by Fawcett *et al.* (1959) after mechanical dissociation of germ cells. They claimed that the multinucleated cells have formed to maintain conjunction of cells in their original cluster after intercellular bridges were obliterated by disruption.

According to Holstein and Eckmann (1986), defects in the intercellular bridges of multinucleated spermatocytes and spermatid giant cells were also detected at ultrastructural level. In addition, they observed a confluence of membranes meaning that neighbouring germ cells were dissolved resulting in the presence of intercellular bridges in the cytoplasm of giant cells.

Intercellular or cytoplasmic bridges between germ cells result from nuclear division without complete cell division (Burgos and Fawcett 1955; Fawcett *et al.* 1959; Dym and Fawcett 1971) to assure synchronous development of germ cells by co-ordinating the cell-cycle through sharing of cytoplasmic constituents (Fawcett *et al.* 1959; Huckins and Oakberg 1978). This processes may enable haploid germ cells to remain "phenotypically diploid" after meiosis, or as elsewhere stated as "clones" (Braun *et al.* 1989; Guo and Zheng 2004), to maintain equal distribution of proteins of sex chromosome genes (Fawcett *et al.* 1959; Erickson 1973). In case of a disruption of the intercellular bridges, as shown in a Tex14 (testis-expressed gene 14) null-mutant, male spermatogenesis was disturbed leading to sterility (Greenbaum *et al.* 2007). Tex14 double mutants had no differences in their serum testosterone level compared to control mice and they displayed smaller testes, a markedly reduced number of spermatocytes but no spermatids and a significant vacuolization (Greenbaum *et al.* 2006) that is in accordance with the phenotype of the *Stra8*-Cre mediated *Pex13* KO testes.

Considering these observations, intercellular bridges could be regarded as intracellular bridges between single spermatid nuclei in the MNCs sharing a common cytoplasm. One putative mechanism could rely on the cells´ attempt to compensate for deficient peroxisomes or peroxisomal remnants because cytoplasmic bridges do not only facilitate the transport of mRNA but also organelles between haploid spermatids in a microtubule-dependent manner (Braun *et al.* 1989; Ventela *et al.* 2003).

A similar phenotype as observed in the *Stra8*-Cre mediated gc*Pex13*KO testes was described for a *Crem* KO mouse. CREM (cAMP-responsive element modulator) is involved in regulating gene expression in haploid spermatids. Its KO resulted in a lack of late spermatids and a dramatic increase of apoptotic germ cells (Nantel *et al.* 1996). Apoptosis as consequence for degenerating germ cells will be discussed in more detail in paragraph 4.1.3.

Another hypothesis is that MNCs might be formed as an effect of disturbed peroxisomal lipid metabolism. Gene expression analysis revealed an increase of the fatty acid desaturase *Fads2* in the pre-meiotic induced *Pex13* KO. *Fads* encodes for the enzyme Δ6-desaturase that catalyses the first reaction from precursor essential PUFAs linoleic (C18:2(ω-6)) and α-linolenic acid (C18:3(ω-3)) as well as the last step of docosahexaenoic acid (DHA) synthesis (Nakamura and Nara 2004). In a *fads* null mutant, spermatogenesis ceased at the stage of round spermatids. As a consequence, acrosome biogenesis, head elongation and tail formation failed (Roqueta-Rivera *et al.* 2011) leading to globozoospermia (Holstein *et al.* 1973). The authors therefore suggest that DHA may be required for acrosome formation (Roqueta-Rivera *et al.* 2011). Although ω-6-docosahexaenoic acid (C22:6(ω-6)) was significantly decreased in the *Stra8*-Cre mediated gc*Pex13*KO mice, MNCs still represented acrosomes that intended to detach prior to apoptosis. However, head elongation and tail formation

failed, leading to azoospermia. Therefore, the formation of MNCs due to a defect in peroxisomal *β*-oxidation will be discussed more extensively in section 4.1.5.

4.1.3 Increased germ cell apoptosis in the *Stra8*-Cre KO model might be the result of oxidative stress in the cell

Germ cell apoptosis is a regulated process to maintain genetic stability (Norbury and Hickson 2001; Shaha *et al.* 2010). In germ cells of elderly men, programmed cell death occurs on a regular basis (Brinkworth *et al.* 1997). In the pre-meiotic induced *Pex13* KO mice, the tubular mass as well as testes size were significantly decreased. Compared to control testes, the number of apoptotic germ cells was increased. MNCs, some spermatogonia, primary and secondary spermatocytes were TUNEL positive and showed reactivity to the apoptosis-inducing factor BAX (Antonsson 2001) and apoptosis effector Caspase-3 (Philchenkov 2003). In addition, large phagosomes were found in the cytoplasm of Sertoli cells at the ultrastructural level, indicating high activity of autophagy. Autophagy is a sign of apoptosis as it is a process at which unnecessary or dysfunctional components are disassembled, including dead cells. Apoptosis is triggered by oxidants or stimulators of ROS generation (Clement *et al.* 1998). In the *Stra8*-Cre mediated gc*Pex13*KO mice, not only apoptotic markers positive cells were found, but also down-regulated catalase activity in the testes that might have led to the accumulation of ROS, which in turn might have provoked apoptosis. In this context, PUFAs need to be mentioned as they can act as ROS scavengers (Richard *et al.*, 2008). Gas chromatography on *Stra8*-Cre mediated gc*Pex13*KO testes revealed a significant decrease of PUFAs, which would interfere with their function as antioxidants, thus leading to oxidative stress in the cell.

Another hint for induced apoptosis in the *Stra8*-Cre mediated gc*Pex13*KO testes is given by a slightly increased gene expression of the polyamine oxidase (*Paox*) that catalyses the oxidation of N_1-acetylspermine to spermidine. Polyamines, including putrescine, spermidine and spermine (Tabor and Tabor 1984) that were initially isolated from sperm (Fischer and Bohn 1957), can act as ROS scavengers (Ha *et al.* 1998; Das and Misra 2004) and are sensitive to alterations in ROS levels, pH, osmotic pressure and temperature (Valdes-Santiago and Ruiz-Herrera 2013; Miller-Fleming *et al.* 2015). They are involved in growth processes and malignant transformation (Schipper *et al.* 2000; Igarashi and Kashiwagi 2010), as shown for a leukaemia cell line with overexpressed ornithine decarboxylase (ODC1), whose increased catalytic activity led to the accumulation of putrescine and spermidine that resulted in cell death (Poulin *et al.* 1993; Poulin *et al.* 1995; Xie *et al.* 1997).

In the testis, polyamines are present in Leydig and Sertoli cells, as well as in germ cells where they are essential for steroidogenesis (Makitie *et al.* 2009) and the completion of spermatogenesis (Pegg and Wang 2009). Interestingly, peroxisomes also participate in the polyamine oxidation pathway, reinforcing the hypothesis that the spermatogenic arrest is caused by a multitude of defective peroxisomal pathways induced by the *Stra8*-Cre mediated *Pex13* KO.

As another mechanism to control spermatogenesis, the retinoid metabolism must be mentioned which is also peroxisome-related. Vitamin A, in the form of retinol or retinoic acid, is involved in cell signalling through binding to retinoid receptors (RXR; RARα in Sertoli cells and RARγ in early germ cells; Doyle *et al.*, 2007). Vitamin A was shown to be crucial for meiotic initiation and in the formation of the cycle of the germinal epithelium and the spermatogenic wave (Hogarth *et al.*, 2010). Interestingly, *Dhrs4* (short-chain dehydrogenase/reductase superfamily member 4), that reduces all-trans-retinal and 9-cis retinal and is thus involved in the breakdown of retinoids, was strongly down-regulated in the *Stra8*-Cre mediated gc*Pex13*KO. In a study from Doyle (2007), *Rarα*-deficient mice were sterile. However, the precise mechanism is still unknown and it needs to be examined, whether retinoids act directly on germ cells, which also express RARs, or whether their actions are indirectly mediated through Sertoli cells or peritubular myoid cells.

Concluding this section, several mechanisms leading to apoptotic MNCs are possible: MNCs might occur due to a disturbed communication between Sertoli and germ cells that will eventually lead to apoptosis due to a failure of cell differentiation. This hypothesis will be discussed in the next paragraph (4.1.4). The other mechanism could be that apoptotic MNCs are a result of apoptotic spermatogenic cells in the basal compartment, inducing a defect in subsequent germ cell differentiation and thereby regulating apoptosis-inducing genes in higher differentiated germ cells, as suggested by Luo *et al*., (2013).

4.1.4 Sertoli and germ cell interaction is disturbed due to the pre-meiotic induced gc*Pex13*KO

The integrity of the blood-testis barrier (BTB) is essential to maintain an immune privileged environment for germ cells to divide into functional sperm. It is assembled by specialized junctions between Sertoli cells, including basal ectoplasmic specialized (ES) protein complexes, gap junction protein complexes and actin-based tight junction (TJ) protein complexes, such as occludin (*Ocln*), tight junction protein 1 (*Tjp1*) and claudin (Furuse *et al.* 1993; Tsukita *et al.* 2001; Chihara *et al.* 2010). Their continuous remodelling enables meiotically dividing pre-leptotene spermatocytes to traverse the barrier from the basal to the adluminal compartment and thus facilitate spermatogenesis and subsequent spermiogenesis (Hess and Renato de Franca 2008; Cheng and Mruk 2012).

As spermatogenesis was disturbed in the *Stra8*-Cre mediated gc*Pex13*KO testes, a particular focus was placed on the polarization of Sertoli cells and TJ proteins. Immunolabelling against claudin-11 already indicated a severe disturbance in the structural organization of the BTB in the *Stra8*-Cre mediated peroxisomal *Pex13* KO. Gene expression analyses on the *Stra8*-Cre mediated *Pex13* KO testes revealed a significant down-regulation of *Cldn3* and a slight up-regulation of *Tjp1* and *Ocln*, thereby supporting the hypothesis that alterations of structural components of the BTB might affect its integrity.

Functional analysis based on the Evans Blue injection of the pre-meiotic induced peroxisomal protein KO mice revealed the intactness of the BTB. Even though the cytoplasm and the extracellular matrix of some MNCs in the *Stra8*-Cre KO seemed to be positive for the tracing dye, auto fluorescence due to increased lysosomal activity in dying cells was more likely to occur rather than a specific signal (Monici 2005). Another possible explanation could be that the Sertoli cell organization was altered, as the cytoskeletal marker vimentin, used to visualize the intermediate filaments of Sertoli cells, showed an irregular pattern in the *Stra8*-Cre mediated *Pex13* KO, displaying not only lateral but also cytoskeletal projections from the basal compartment to the lumen, whereby surrounding single germ cells, including MNCs, in the adluminal compartment of the germinal epithelium.

As consequence of the *Pex13* KO in pre-meiotic germ cells, the BTB was not only organized in the basal part of the germinal epithelium but also assembled adluminal, which would explain the localization of Evans Blue among MNCs. Disturbed polarized Sertoli cell function was also observed at ultrastructural level and in histological specimens displaying accumulated lipid droplets in the adluminal cytoplasm of Sertoli cells.

An immunostaining against the pan-leukocyte marker CD45 was performed to specifically test for the permeability of the BTB for immune cells. CD45 showed highest immunoreactivity in Leydig cells of all genotypes. Macrophages, which are a specific type of leukocytes, secrete growth factors and cytokines that are important for the (re-)population of Leydig cells during maturation (Gaytan *et al.* 1994; Hedger 1997). However, CD45 positive cells were absent in seminiferous tubules, indicating that the immune relevant integrity of the BTB was not affected. Furthermore, inflammation did not seem to be involved in the pathogenesis of the *Stra8*-Cre mediated gc*Pex13*KO.

Taken together, these findings suggest that the structural components of the BTB were still able to maintain an immunological barrier. As the TJ proteins were only differently expressed but not fully absent in the *Stra8*-Cre mediated *Pex13* KO mice, a compensatory effect through increased *Ocln* and *Tjp1* expression is assumed. This hypothesis is supported by the evidence that the BTB undergoes restructuring during the spermatocyte transition at stage VIII, at which the peripheral adaptors, including α-catenin and zonula-occludens-1 (ZO-1) become “disengaged” from the TJ proteins (Yan and Cheng 2005). The authors therefore suggest a switch between an “assembled” and a “dis-assembled” state of the TJ proteins that demands a certain flexibility to enable the establishment of a new BTB without disrupting the immunological barrier (Yan *et al.* 2008).

In what extent peroxisomes are implied in the maintenance of the Sertoli cell function and Sertoli cell to germ cell communication, further studies are required to understand the mechanisms in this specific KO model. According to published data, Sertoli cells secrete fibroblast growth factor (FGF) and the epithelial growth factor-α (EGF-alpha) in response to FSH. These regulatory factors are necessary for the paracrine interaction to neighbouring germ cells (Skinner and Moses 1989; Skinner *et al.* 1989). FSH and LH are known to interact in a feedback mechanism with the anterior pituitary to stimulate the production of the androgen binding protein (ABP) in Sertoli cells that itself promotes spermatogenesis.

ABP has a high affinity to testosterone (Verhoeven and Cailleau 1988). As testosterone is a steroid whose generation requires cholesterol and thus implies peroxisomal steroidogenic function (Weinbauer and Nieschlag 1997), a collapse of their biogenesis induced by the *Pex13* KO might have interfered with testosterone production. Consequently, ABP might have missed its binding partner, thereby signalling back to lower FSH formation and thus interfering with the communication between Sertoli and germ cells. However, this hypothesis can be disproved as Leydig cell proliferation was increased in the *Stra8*-Cre mediated gc*Pex13*KO and lipid droplets were accumulated, suggesting a continuous testosterone production or at least the supply of cholesterol.

Interestingly, defects in the Sertoli cell polarity were linked to PUFA substituted membrane phospholipids that are synthesized by the desaturase FADS2. In *fads*-null mutant male mice, the tight, adherens and gap junction proteins were irregularly distributed. Thus, Sertoli cell polarity and function was disturbed in these KO mice (Stoffel *et al.* 2008).

4.1.5 Impaired *β*-oxidation leads to the accumulation of lipid droplets

Plasmalogens are a type of ether phospholipids and constitute the major part of the membrane in spermatozoa (Evans *et al.* 1980). They play a role as endogenous antioxidants, mediators of membrane structure and dynamics through formation of non-bilayer lipid phases and storages of PUFAs (Lessig and Fuchs 2009; Wallner and Schmitz 2011). PUFAs and very long-chain fatty acids (VLCFAs), such as arachidonic (C20:4(ω-6)), eicosapentanoic (C20:5(ω-3)) and docosahexaenoic (C22:6(ω-3)) acid (Stoffel *et al.* 1972; Stoffel *et al.* 2008; Roqueta-Rivera *et al.* 2010), regulate the membrane fluidity.

The formation of MNCs and the lack of spermatozoa indicated an issue of the supply of ether-linked phospholipids and cholesterol that are synthesized through peroxisomal *β*-oxidation of VLCFA (C22:0, C24:0, C26:0) and different branched-chain fatty acids, including pristanic acid and its precursor phytanic acid (Smith *et al.* 2000). Consequently, substrates of the peroxisomal *β*-oxidation were analysed with particular interest.

Ether lipid biosynthesis in peroxisomes is initiated via the activity of glyceronephosphate *O*-acyltransferase (GNPAT), also known as dihydroxyacetone phosphate acyltransferase (DHAPAT) and alkylglycerone phosphate synthase (AGPS) (Brites *et al.* 2004). In the *Stra8*-Cre mediated gc*Pex13*KO mice, *Gnpat* was strongly down-regulated, already indicating a disturbance in ether lipid synthesis. A comparable phenotype to the one of pre-meiotic induced *Pex13* KO mice was shown in a work of Rodemer *et al* (2003). The disruption of DHAPAT caused a spermatogenic arrest at the spermatid stage with the lack of spermatozoa and a Sertoli cell-only phenotype.

During the process of lipogenesis and the synthesis of PUFAs (Wang *et al.* 2005), ELOVL2 and ELOVL5 are required. ELOVL2 is mainly involved in the elongation of C20 into C24:4(ω-6) and C22 into C24:5(ω-3) PUFAs (Leonard *et al.* 2000; Guillou *et al.* 2010; Zadravec *et al.* 2011), whereas ELOVL5 preferentially elongates C18 to C22 substrates. In the *Stra8*-Cre mediated KO testes, both

elovl2 and *elovl5* were significantly increased compared to control mice, indicating an accumulation of corresponding substrates. Indeed, saturated FAs, with the exception for palmitic acid and MUFAs, were slightly increased in the *Stra8*-Cre mediated *Pex13* KO mice. Moreover, eicosapentaenoic acid (C20:5(ω-3)) was also increased, whereas ω-3 docosapentaenoic acid (C22:5(ω-3)) and ω-6-docosahexaenoic acid (C22:6(ω-6)) were significantly decreased, indicating a peroxisomal defect in *β*-oxidation. This finding was mirrored by an extensive accumulation of lipid droplets in Sertoli cells, already starting in prepubertal mice and evolving in complete testicular atrophy.

The trans-membrane protein ABCD1 transports VLCFA-CoAs into peroxisomes thereby preferring hydrophobic C24:0-CoA and C26:0-CoA (van Roermund *et al.* 2008; Morita and Imanaka 2012). As shown in the gene expression studies, *Abcd1* was clearly down-regulated in the *Stra8*-Cre mediated *Pex13* KO mice. Mutations in *Abcd1* resulted in a defective *β*-oxidation of fatty acids that led to the accumulation of saturated C24-C26 VLCFAs (Mosser *et al.* 1993; Berger *et al.* 2010; Engelen *et al.* 2012). Down-stream effects of impaired *β*-oxidation were also noted in the pre-meiotic induced *Pex13* KO, as gene expression of *Acox1* was strongly decreased. ACOX1 is the first enzyme of the fatty acid *β*-oxidation pathway and catalyses the desaturation of acyl-CoA to 2-trans-enoyl-CoAs. Its deficiency leads to infertility in male mice, marked by a depletion of Leydig cells and hypo-spermatogenesis. Male mice displayed increased blood levels of VLCFAs and a decrease in plasma levels of arachidonic (C20:4) and docosahexaenoic acid (C22:6) (Fan *et al.* 1996a; Fan *et al.* 1996b).

Immunostaining against peroxisomal thiolase, an enzyme that catalyses straight chain acyl-CoAs (including the CoA esters of dicarboxylic fatty acids and eicosanoids) via peroxisomal *β*-oxidation, showed a clear cytosolic localization in all germ cells of the *Stra8*-Cre KO model. A defect in the cholesterol synthesis due to the impaired import of peroxisomal proteins is therefore assumed.

Another member of peroxisomal *β*-oxidation is HSD17B4 that catalyses the formation of 3-ketoacyl-CoA intermediates from straight-chain and 2-methyl-branched-chain fatty acids, including pristanic acid, bile acid intermediates. It was strongly down-regulated in the *Stra8*-Cre mediated *Pex13* KO mice. HSD17B4 is known as D-bifunctional protein (DBP) or D-multifunctional protein (MFP2) whose deficiency is associated with neonatal hypotonia, seizures and impaired psychomotor development (Ferdinandusse *et al.* 2006; Ferdinandusse *et al.* 2017). Leydig cells also contain excessive amounts of HSD17B4 where it is involved in steroidogenesis by oxidizing estradiol and Δ^5-androstenediol through NAD^+ (Adamski *et al.* 1992; Labrie *et al.* 1997). As discussed in the previous section (4.1.4), steroidogenesis might be affected in the *Stra8*-Cre mediated gc*Pex13*KO testes. However, data is needed to reconsider steroid synthesis in Leydig cells and the regulation of androgens in the KO testes.

In summary, the data suggests that the disruption of *Pex13* caused a severe biogenesis defect, leading to the accumulation of VLCFAs due to an impaired fatty acid transport system at the peroxisomal membrane and a collapse of peroxisomal *β*-oxidation. The absence of cholesterol and ether lipids is probably the reason for a failure of subsequent germ cell development. It again reinforces the

hypothesis that peroxisomes are not only required as ROS scavengers but are also essential for steroidogenesis and germ cell differentiation.

4.1.6 Clinical relevance of the occurrence of MNCs in the *Stra8*-Cre mediated gc*Pex13*KO testes

Based on a study from 2012, biopsies from 80 infertile males from 25 to 45 years were examined of which 57 patients (71.25 % of the cases) were azoospermic. Whereas 35.09 % of the patients with azoospermia showed normal spermatogenesis, the remaining cases displayed a Sertoli cell only syndrome (18.75 %), a maturation arrest, testicular atrophy or granulomatous inflammation of the testis (11.25 % each; Parikh *et al.,* 2012). Azoospermia accounts for 5- 20 % of infertility cases in men and is classified into pre-testicular azoospermia, testicular failure or non-obstructive azoospermia (NOA) or obstructive azoospermia (OA) (Corea *et al.* 2005; Cocuzza *et al.* 2013; Berookhim and Schlegel 2014). These clinical case studies reflect the necessity to analyse mechanisms that lead to spermatogenesis defects. The *Pex13* KO mouse models established in the course of this thesis can help to understand germ cell differentiation and suggest important parameters that allow for regular spermatogenesis.

Testicular pathologies that comprise azoospermia and the presence of MNCs, as shown in the *Stra8*-Cre mediated gc*Pex13*KO, have already been described and analysed at ultrastructural level (Holstein and Eckmann 1986; Nistal *et al.* 1986b). MNCs were found in young men with oligozoospermia and in men over 65 years whose testes was removed because of prostate cancer (1986). However, the cause for the occurrence of MNCs has not further been analysed yet. According to Holstein *et al*., the most prominent multinucleated giant cells are composed of spermatids, which coincide with the histology of the *Stra8*-Cre mediated *Pex13* KO testes. Holstein described human MNCs as extraordinarily large cells with many cell nuclei arranged around a new cytocentrum like a wreath. Moreover, he detected organelles such as acrosomes, centrioles, mitochondria and chromatoid bodies but did not mention peroxisomes, as they cannot easily be detected by conventional transmission electron microscopy. The identification of peroxisomes at ultrastructural level was first described in 1969 (Fahimi 1969). Compared to other organelles, peroxisomes can only be detected by alkaline 3, 3′-diaminobenzidine (DAB) that oxidizes in the presence of peroxidase and hydrogen peroxide. A morphological screen was initially performed in 1972, whereby peroxisomes were detected in all eukaryotic cells (Hruban *et al.* 1972) with the exception for red blood cells. The first description of peroxisomes within the testis was made only in this century (Luers *et al.* 2006) which made it impossible to directly link peroxisomes with testicular pathologies. Published data correlates oxidative stress with male infertility, caused by an imbalance of peroxidizable substances, such as PUFAs and the free radical scavenger system (Lenzi *et al.* 1996). Even though tiny amounts of ROS are required for fully functioning spermatozoa, including fertilization, acrosome reaction, hyperactivation, motility

and capacitation (Gagnon *et al.* 1991; Aitken 1997; Kefer *et al.* 2009), excess ROS leads to immature and abnormal spermatozoa human ejaculates (Alvarez and Storey 1982; Aitken *et al.* 1992; Aitken and Baker 2002). Interestingly but not surprisingly, the authors relate ROS production to the nicotinamide adenine dinucleotide phosphate (NADPH) oxidase system found in sperm plasma membranes and phagosomes (Aitken *et al.* 1991), or to the NADPH-dependent oxidoreductase (diphorase) in mitochondria (Gavella and Lipovac 1992). They do not consider peroxisome-related effects as a putative cause for increased ROS levels in germ cells as peroxisomes are not present in sperm (Makker *et al.* 2009). Nevertheless, the importance of peroxisomes for spermatogenesis was already illustrated by a study from Leath *et al.* (1983). An essential fatty acid-deficient diet given to rats resulted in decreased concentrations of PUFA in red blood cells and serum and a degeneration of the seminiferous tubules with absent spermatozoa. Since PUFAs, mainly of the ω-3 families, are most prominent in the sperm membrane, Lenzi *et al*. (1996) suggest them as markers of sperm function and propose a scavenger therapy using e.g. glutathione peroxidase to reverse dyspermia.

4.2 The conditional KO of *Pex13* in post-meiotic germ cells mediated by *Prm*-Cre displays differences in the significance of peroxisomes during spermatogenesis

As already shown in a former study (Nenicu *et al.* 2007), the presence of peroxisomes as distinct single organelles was confirmed in all testicular germ cells as well as Sertoli cells by a GFP-PTS1 transgenic mouse strain and by immunofluorescent labelling with the peroxisomal membrane proteins PEX13 and PEX14.

Using a *Stra8*-Cre and a *Prm*-Cre transgenic mouse strain to inactivate *exon 2* of floxed *Pex13* in either pre- or post-meiotic germ cells, respectively, it was possible to analyse the impact of abolished peroxisomes and all related metabolic pathways on germ cells prior to meiosis and after cell division. Based on histological analyses, the seminiferous tubules of both KO testes differed in cell morphology and differentiation processes. Whereas the *Stra8*-Cre mediated KO induced a spermatogenic arrest with the lack of mature spermatozoa and the presence of MNCs instead of regular spermatids as extensively discussed in the former paragraphs, no effect on spermatogenesis in the *Prm*-Cre mediated gc*Pex13*KO testes was observed, as the cellular composition of the germinal epithelium resembled that of control mice. A possible explanation for these phenotypic differences is that peroxisomal proteins might have been still abundant in post-meiotic cells with a *Pex13* KO. This hypothesis is sustained by the findings of the immunofluorescent staining against PEX13 and PEX14, showing a similar abundance of these proteins in all cells of the germinal epithelium, as observed in control testes, even though the excision of *exon2* in *Pex13* was confirmed by PCR.

The immunoreactivity for catalase was most intense in Leydig and in Sertoli cells but was scarcely found in the basal compartment of the germinal epithelium. Compared to control mice, *Cat* expression was slightly increased by trend in the overall cell fraction of post-meiotic induced *Pex13* KO mice,

indicating an elevated metabolic activity to detoxify the cells from ROS (Antonenkov *et al.* 2010; Fransen *et al.* 2012).

The turnover of some peroxisomal proteins has already been analysed in plants (Young and Bartel 2016) and mammals. Data suggests a half-life of peroxisomal catalase of 1 ½ days (Poole 1969). Considering that the spermatogenic cycle in the mouse was determined to be 8.6 days in the mouse (Oakberg 1957; Chandran *et al.* 2016), a peroxisomal KO at later cell differentiation stages might not be as severe as in earlier germ cells, as proteins might be still present that maintain all peroxisomal functions. Another assumption for different effects due to the induced *Pex13* knockout in either pre-or post-meiotic germ cells is that peroxisomal metabolic function might be required at different developmental stages. Prior to the release of elongated spermatids into the lumen at stage VII in rat and mouse, which corresponds to stage II in the human, spermatids discard excess cytoplasm, which will be phagocytosed by surrounding Sertoli cells (O'Donnell *et al.* 2011). These residual bodies contain cytoplasmic organelles, including ribosomes, endoplasmic reticulum, Golgi apparatus and peroxisomes, as shown in the cross-sections of GFP-PTS1 transgenic mice. It is therefore possible that peroxisomal metabolism is not essential at later developmental stages to facilitate spermiation. Indeed, the protein composition and the activity of peroxisomal enzymes are heterogeneous (Baumgart 1997).

With the *Prm*-Cre mediated KO of *Pex13* in post-meiotic cells, a reduction of peroxisomal gene expression would have been expected. However, referring to the mRNA quantitation analyses, peroxisomal biogenesis genes, as well as genes involved in various metabolic functions were expressed to a similar amount as measured in control and heterozygous mice. It is therefore most likely that peroxisomal genes are down-regulated in higher differentiated cells, which would be in concordance with the second hypothesis that peroxisomes are relevant at different developmental stages and thus regulated at distinct levels.

4.3 The suitability of different cell sort techniques to purify germ cells

4.3.1 FACS purified germ cells of WT animals are suitable for mRNA expression profiling

For the analysis of single cells of the spermatocytic lineage, cells need to be purified and separated according to their maturation and differentiation stage. For finding an appropriate approach, emphasis was placed on purity, reproducibility, reliability, expenditure of time, costs and possibility to obtain RNA out of different cell fractions for gene expression analysis of purified cell populations.

The study of germ cells is of considerable medical interest. Germ cells are a very unique cell population to study cytokinesis (Miething 1990), cell development, epigenetic events (Surani *et al.* 1990), paracrine interaction (Dym and Fawcett 1971) and gametogenesis (Gordon and Ruddle 1981).

It is challenging to separate germ cells as they are united via intercellular bridges forming a syncytium to ensure synchronous differentiation (Burgos and Fawcett 1955; Fawcett *et al.* 1959; Dym and Fawcett 1971). They are in close contact to Sertoli cells which also hampers their neat separation. For the single cell suspension, the protocol by Getun (2011) was modified in terms of buffer conditions, enzyme composition and avoidance of DMSO to minimize cell stress.

In order to obtain a homogenous cell population, a well-established and reliable approach is FACS that was used in the present study to perform gene expression studies on testicular cells of WT animals. This technique has been shown to be successful in the separation of germ cells at different developmental stages (Bastos *et al.* 2005; Russell *et al.* 2013; Lima *et al.* 2016). The benefit of FACS is to separate cells according to their size, surface granularity at each spermatogenic stage, chromosome number or cell surface markers (Toppari *et al.* 1985; Aslam *et al.* 1998; Kanatsu-Shinohara *et al.* 2011).

It has been reported that a nozzle size of 50 µm gave excellent analytical separation for male germ cells by lowering the risk of contaminations by different cell types (Mays-Hoopes *et al.* 1995). However, in order to avoid shear stress, a nozzle size of 100 µm was used in the present study and the flow rate was set onto the lowest speed. The calculated purity of sorted cell population was still 85- 99 %. While establishing the method, fixation with paraformaldehyde has proven to be the best method to ensure stability of the nuclei dye Hoechst 33342 whereby retaining cellular and subcellular structure and preventing autolysis (Russell *et al.* 2013).

Studies have already shown the successful isolation of RNA and successive mRNA quantitation out of formalin-fixed paraffin-embedded tissue (FFPE) (von Weizsacker *et al.* 1991). The group of Russell (2013) claimed that quantitation of mRNA transcripts is equally efficient in fixed versus unfixed cells using NanoString but not qRT-PCR. To verify this, the quality and size distribution of molecules of RNA extracted from every single cell population was assessed using the Agilent 2100 bioanalyzer that

categorizes RNA samples from 1 (worst) to 10 (best), considering the 28S to 18S rRNA ratio (Schroeder *et al.* 2006). The RNA integrity number (RIN) measured in all RNA samples was in the range of 5 to 8 therefore extracted RNA from every single cell sample could subsequently be used for mRNA profiling. Gene expression of cell type specific markers was quantified to judge RNA purity and integrity of cells obtained by FACS. Significant differences in cell specific marker gene expression could be made between all different cell populations confirming the reliability of using formaldehyde-fixed cells for FACS and subsequent gene expression analysis.

4.3.2 The purification of MNCs is not possible with conventional methods

Different methods have already been described for the separation of testicular cells, including unit gravity sedimentation (Bellve *et al.* 1977), magnetic cell sorting (MACS) (van der Wee *et al.* 2001), laser capture microdissection (LCM) (Liang *et al.* 2004) and centrifugal elutriation (CEE) (Barchi *et al.* 2009; Tomlinson *et al.* 2013). However, no protocol is available describing the separation of giant cells, defined as cells with a minimum size of 30 µm which would resemble those MNCs that were detected in the *Stra8*-Cre mediated gc*Pex13*KO.

Velocity sedimentation at unit gravity in BSA gradients enables the purification of testicular cells at low costs. Moreover, no DNA or cell surface marker staining is needed, which enables subsequent cultivation of isolated cells (Romrell *et al.* 1976). By using the ECET Celsep-Systems 5440 (Eppendorf; provided by Eveline Baumgart-Vogt), the separation and enrichment of specific germ cell population, derived from WT animals, was possible. However, it was not a reliable approach to purify MNCs from *Stra8*-Cre mediated *Pex13* KO mice. An explanation could be that the molecular mass of MNCs differs considerably compared to control testicular cells because MNCs rather intended to reside on top of the gradient than sediment.

Cell separation according to CCE is based on *Stoke´s law* that describes sedimentation velocity of cells and particles in an appropriate elutriation buffer according to their diameter (size) and density, whereby two forces, the gravitational field and the fluid flow, act on the cells (Grabske *et al.* 1975; Barchi *et al.* 2009). As a consequence, flow rate and rotor speed need to be adjusted until all cells of different size and thus sedimentation velocities are in equilibrium at different radial positions in the chamber. The separation of spermatocytes by CCE is possible, as also shown by Grabske *et al.* (1975). Because the density of the MNCs is not known, the calculation for the appropriate settings for cell sort by means of CCE was not possible. Thus, the flow rate and centrifugation speed were experimentally adjusted to avoid pelletizing of the cells and losing them at the same time. MNCs were still found in all samples and could only be enriched to a purification rate of 60 % that would have interfered with mRNA expression studies. Moreover, many cytoplasmic cells lacking nuclei were found in the sample, indicating a disruption of MNCs during the procedure. With increasing flow rate, a swirl was

produced within the chamber that created a push back of cells. By lowering the flow rate, cells were flushed out of the chamber leading to a high loss rate of MNCs.

Another approach to isolate germ cells was performed by using LCM (Emmert-Buck *et al.* 1996) on paraffin- or cryo- embedded tissue. The advantage is that the contamination rate is clearly reduced, since single cells of interest can be defined. Microdissected cells can also be used for mRNA expression analyses (Cohen *et al.* 2002). However, the method was limited because cells were damaged through laser activity that affected RNA quality.

Even though MNCs have already been described morphologically, nothing is known about any cell surface marker, or even other features including cell density, cell membrane integrity and rigidity which impede their separation. In the end, no suitable approach was found to isolate, purify and enrich MNCs so that gene expression studies could not be performed on single cells. Consequently, the initial overall cell fraction had to be used for mRNA profiling.

5 CONCLUSION

Peroxisomal metabolic processes contribute to the cellular function and are thus indispensable for the maintenance of cells and thereby essential for the whole organism. From the clinical perspective, peroxisomal dysfunction has been linked to severe neurological diseases, including the Zellweger syndrome which is lethal. Apart from impaired neuronal migration, brain developments and hypomyelination, Zellweger boys were also diagnosed with cryptorchidism. Milder forms of the Zellweger spectrum disorders are the X-linked adrenoleukodystrophy (X-ALD) and adrenomyeloneuropathy (AMN) that are characterized by a defect of the peroxisomal ABC transporter leading to an accumulation of very long-chain fatty acids (VLCFAs) in cells. Patients showed an impairment of testicular functions including the reduction of the size of the seminiferous tubules or a spermatogenic arrest resulting in azoospermia. As these symptoms were not in the focus of the patients´ therapy, only little is known about the peroxisomal metabolic functions in testicular cells.

For this reason, the study was conducted to characterize the consequences of a peroxisomal biogenesis defect for spermatogenesis to subsequently specify the peroxisomal metabolic processes which are most important for proper cell function.

The effects of a *Pex13* knockout in either pre- or post-meiotic germ cells mediated by the transgenic *Stra8*-Cre or the *Prm*-Cre promoter, respectively, were analysed with focus on germ cell differentiation and maturation. The peroxisomal membrane protein PEX13 is part of the translocation machinery that is required for the import of peroxisomal matrix proteins into the organelle. Its inactivation leads to a biogenesis defect of peroxisomes with the loss of all its metabolic functions.

At first, a morphological screen was performed to compare the phenotypes of control, heterozygous and both *Stra8*-Cre and *Prm*-Cre mediated gc*Pex13*KO testes, based on HE and Oil Red O (ORO) staining, TUNEL assay, electron microscopy as well as immunofluorescence and immunohistochemistry using a variety of peroxisomal and apoptotic marker proteins. In this context, the blood-testis barrier (BTB) was also studied more extensively. Next, single lipid components were further analysed by gas chromatography and the mRNA expression of enzymes of lipid metabolism were measured by qRT-PCR. As peroxisomes are involved in steroidogenesis, hormones of the hypothalamic-pituitary-adrenal axis were tested in the serum of all genotypes.

The results of the present thesis indicate that it obviously makes a difference whether a defect in peroxisomal biogenesis occurs in germ cells that enter meiosis or in cells that have successfully passed meiotic divisions and face spermiogenesis.

The *Stra8*-Cre mediated pre-meiotic peroxisomal KO induced a spermatogenic arrest at the spermatid stage with the formation of multinucleated giant cells (MNCs). Due to the absence of *Pex13*, all metabolic functions as well as matrix protein import were abolished in the *Stra8*-Cre mediated gc*Pex13*KO. PEX13 and PEX14 antibody labelling indicated the existence of peroxisomal remnants in

Pex13-deficient male germ cells. Moreover, catalase and thiolase were mis-localized into the cytoplasm of cells with a *Pex13* KO mediated by *Stra8*-Cre. The corresponding genes expressing the peroxisomal marker proteins were down-regulated likewise, whereby not only confirming the stability of the conditional *Pex13* KO, but also demonstrating a collapse of the peroxisomal biogenesis.

In contrast to the *Stra8*-Cre mediated gc*Pex13*KO testes, no alterations were observed in the germ cell differentiation of the *Prm*-Cre mediated post-meiotic gc*Pex13*KO testes. Peroxisomal genes as well as their transcripts were equally expressed in the *Prm*-Cre mediated KO testes as observed in control mice.

The seminiferous tubules of the pre-meiotic induced gc*Pex13*KO mice showed an accumulation of lipid droplets in the cytoplasm of Sertoli cells. An increase of triglycerides (TAGs) and a decrease of phospholipids by trend were observed. Fatty acid precursors of the peroxisomal *β*-oxidation were significantly increased in the *Stra8*-Cre mediated KO testes, with the exception for palmitic acid. Products of the peroxisomal *β*-oxidation, such as docosahexaenoic acid (C22:6(ω-3)) and docosapentaenoic acid (C22:5(ω-6)) were significantly decreased, compared to control group suggesting a deficiency of the peroxisomal *β*-oxidation. Steroid measurements revealed normal testosterone, FSH and LH levels in the serum of all testes genotypes. Histological and qRT-PCR analyses of the *Stra8*-Cre mediated gc*Pex13*KO testes revealed a disturbance of the tight junction proteins of the BTB, including *Ocln, Tjp1* and *Cldn3.* However, the barrier was still intact. TUNEL preparations as well as immunofluorescent staining with appropriate markers displayed germ cell apoptosis of MNCs. The expression of *Paox,* an enzyme of the polyamine pathway regulating cell proliferation and apoptosis, was increased in the pre-meiotic induced *Pex13* KO testes that could be linked to the programmed cell death of MNCs. In addition, enhanced catalase activity might have resulted in the accumulation of ROS, whereby inducing oxidative stress in the cell. Ultrastructural analysis revealed an increased number of lysosomes and phagosomes in the cytosol of Sertoli cells, supporting the hypothesis of enhanced apoptotic events in the germinal epithelium of *Stra8*-Cre mediated peroxisomal KO mice.

Considering the percentage of unexplained infertility in man, which still affects approximately 15 % males, the present study provides important findings of the significance of peroxisomal metabolic functions during germ cell development whose loss could explain at least some of the causes for idiopathic infertility. Peroxisomes are essential organelles to sustain early steps in spermatogenesis and spermiogenesis, as they regulate lipid homeostasis, they provide cholesterol and ether lipids for cell membranes, especially spermatozoa. They also act in ROS scavenging to avoid an intoxication of the germ cells and they are able to degrade bioactive lipid mediators, such as arachidonic acid or eicosanoids that is required as protective mechanism against inflammation.

Further studies are needed to analyse putative disturbances in hormone levels in the testes due to abolished peroxisomal biogenesis. Moreover, mRNA expression profiling of peroxisomal genes in MNCs might help in the understanding of underlying mechanisms that induce their formation.

6 ZUSAMMENFASSUNG

Peroxisom-spezifische metabolische Prozesse tragen einen wesentlichen Teil zur zellulären Funktion bei und sind unabdingbar für die Aufrechterhaltung von Zellen und somit auch für den Organismus. Peroxisomale Pathologien stehen im Zusammenhang mit schweren neurologischen Krankheiten, wie dem lethal verlaufendem Zellweger Syndrom. Das Zellweger Syndrom ist gekennzeichnet durch eine gestörte Migration von Nerven, Hirnschädigungen und einer Hypomyelinisierung. Junge männliche Patienten weisen zudem einen Hodenhochstand auf. Schwächere Ausprägungen des Zellweger Spektrums sind bei Patienten zu finden, die an einer X-chromosomalen Adrenoleukodystrophie (X-ALD) oder an der adulten Form, der Adrenomyeloneuropathie (AMN), leiden. Diese Stoffwechselkrankheiten zeichnen sich durch die Anhäufung sehr langkettiger Fettsäuren (VLCFA) in der Zelle aus, als Folge eines Defekts im peroxisomalen ABC Transporter. Patienten weisen zudem Störungen ihrer testikulären Funktion auf, wie z.B. eine Reduktion der Größe der Samenkanälchen oder einem Spermatogenesearrest, der eine Azoospermie zur Folge hat. Bisher standen diese Symptome nicht im Fokus der Therapie, weshalb noch immer sehr wenig über die Bedeutung von Peroxisomen in männlichen Keimzellen bekannt ist.

Aus diesem Grund diente diese Studie dazu, die Konsequenzen eines peroxisomalen Biogenese-Defekts auf die Spermatogenese zu charakterisieren, um im Folgenden spezifizieren zu können, welche metabolischen Prozesse im Peroxisom zur vollständigen Funktion der Zelle wichtig sind.

Die Auswirkungen eines gezielten *Pex13* Knockouts, der entweder in prä- oder post-meiotischen Keimzellen durch einen transgenen *Stra8*-Cre oder einem *Prm*-Cre Promoter induziert wurde, wurden unter Berücksichtigung der Keimzelldifferenzierung und -reifung untersucht.

Das integrale peroxisomale Membranprotein PEX13 ist Bestandteil des Docking-Komplexes für Matrixproteinrezeptoren. Durch das Ausschalten des Gens wird ein Biogenese-Defekt induziert, der zum Verlust aller peroxisomalen Metabolite führt.

Zunächst wurde eine morphologische Untersuchung durchgeführt, um die Phänotypen der Kontroll- und heterozygoten Tiere mit den *Stra8*-Cre oder *Prm*-Cre Promoter induzierten *Pex13* Knockout-Mäusen zu vergleichen. Hierfür wurden speziell angefertigte Hodenschnitt-Präparate mit Hämatoxylin-Eosin und Ölrot gefärbt, sowie einem Apoptose-Nachweis Verfahren, dem TUNEL-Assay, unterzogen und mittels Elektronenmikroskopie, sowie Immunfluoreszenz- und immunhistochemischen Färbungen auf peroxisomale Marker untersucht. In diesem Zusammenhang wurde auch die Blut-Hoden Schranke näher analysiert. Mittels Gaschromatographie und quantitativer Echtzeit-PCR wurden einzelne Fettsäuren und entsprechende Enzyme der Fettsäuresynthese untersucht. Da Peroxisomen zusätzlich in der Steroidsynthese beteiligt sind, wurden die entsprechenden Konzentrationen aus beteiligten Hormonen der Hypothalamus-Hypophysen-Gonaden-Achse aus dem Serum bestimmt.

Die Ergebnisse der vorliegenden Studie verdeutlichen einen Unterschied in der Auswirkung der defekten peroxisomalen Biogenese in Keimzellen vor der Meiose und in Zellen, die die Meiose bereits durchlaufen haben und sich weiter zu Spermien ausdifferenzieren.

Der *Stra8*-Cre induzierte *Pex13* Knockout führte zu einem Spermatogenese- Arrest auf der Ebene des Spermatiden-Stadiums, mit der Ausbildung multinukleärer Riesenzellen (MNCs). Als Folge des fehlenden *Pex13* Gens wurden alle peroxisomal spezifischen metabolischen Funktionen, sowie der Import von Matrixproteinen aufgehoben. Die Antikörper Markierungen gegen PEX13 und PEX14 gaben Hinweise auf peroxisomale Überreste in *Pex13*-defizienten Keimzellen. Zusätzlich konnten die peroxisomalen Enzyme Katalase und Thiolase nur im Zytoplasma detektiert werden. Die entsprechenden Gene waren runterreguliert, was nicht nur die Stabilität des *Pex13* Knockouts bestätigt, sondern auch beweist, dass durch den Knockout die peroxisomale Biogenese zusammengebrochen ist.

Im Gegensatz zum *Stra8*-Cre induzierten *Pex13* Knockout konnten keine Veränderungen in der Keimzelldifferenzierung im *Prm*-Cre kontrollierten Knockout Hoden festgestellt werden. Die Expression peroxisomaler Gene und ihrer Transkripte war vergleichbar mit derer in den Kontroll-Tieren.

Die Samenkanälchen der *Stra8*-Cre induzierten *Pex13* Knockout Mäuse wiesen eine Anhäufung von Lipidtropfen im Zytoplasma der Sertoli Zellen auf. Während Triazylglyzeride leicht erhöht waren, war der Anteil an Phospholipiden im Hoden tendenziell geringer. Mit Ausnahme der Palmitinsäure waren Vorläufer der peroxisomalen *β*-Oxidation signifikant im *Stra8*-Cre kontrollierten *Pex13* Knockout Hoden erhöht. Im Vergleich zur Kontrollgruppe waren die Produkte der peroxisomalen *β*-Oxidation, wie der Docosahexaensäure (C22:6(ω-3)) und der Docosapentaensäure (C22:5(ω-6)) deutlich runterreguliert. Diese Daten deuten auf eine deutliche Störung in der peroxisomalen *β*-Oxidation hin. Die Steroidkonzentrationen von Testosteron, FSH und LH wiesen keine signifikanten Abweichungen zwischen den verschiedenen Genotypen auf. Histologische und quantitative Echtzeit-PCR Ergebnisse zeigten, dass die Organisation der Schlussleisten-Proteine, die die Blut-Hoden Schranke abbilden, deutlich im *Stra8*-Cre induzierten *Pex13* KO Hoden verändert war. Die Barriere war allerdings noch intakt. Der Nachweis von Apoptose-Markern zeigte, dass die multinukleären Riesenzellen in den programmierten Zelltod gehen. Die Expression von *Paox*, einem Enzym der Polyamin-Synthese, die an der Zellproliferation und am Zelltod beteiligt ist, war im *Stra8*-Cre induzierten Knockout Hoden leicht erhöht. Zusätzlich zu diesem Befund konnte eine Hochregulation des peroxisomalen Stress-Markers Catalase manifestiert werden, dessen Aktivität zur Anhäufung reaktiver oxygener Spezies (ROS) und damit zu oxidativem Stress in der Zelle führt. Auf ultrastruktureller Ebene konnten viele Lysosomen und Phagosomen im Zytosol der Sertoli Zellen detektiert werden, was ebenfalls die Hypothese hoher apoptotischer Aktivität im Keimepithel unterstützt.

Wird der hohe Anteil ungeklärter männlicher Infertilität berücksichtigt, der ca. 15 % ausmacht, liefert die vorliegende Arbeit wichtige Beobachtungen zur Bedeutung peroxisomaler Metabolite für die Keimzellentwicklung, deren Verlust mögliche Ursachen idiopathischer Infertilität erklären könnte.

Peroxisomen sind essentielle Organellen, die die frühen Entwicklungsschritte der Spermatogenese und der Spermiogenese aufrechterhalten, da sie die Lipid-Homöostase regulieren und Cholesterol und Etherlipide für Zellmembranen, insbesondere Spermien, bereitstellen. Darüber hinaus fungieren mehrfach ungesättigte Fettsäuren (PUFAs) als Radikalfänger, um die Anreicherung von Zellgiften zu vermeiden. Sie sind an der Degradation bioaktiver Lipidmediatoren, wie z.B. der Arachidonsäure oder den Eicosanoiden, beteiligt, die als protektiver Mechanismus vor Entzündungen benötigt werden.

Weitere Studien sind notwendig, um mögliche Störungen im testikulären Hormonhaushalt als Folge des *Pex13* Knockouts zu untersuchen. Zur Frage, welche Mechanismen für die Degeneration von Keimzellen verantwortlich sind, sind weitere Expressionsanalysen zur Regulation peroxisomaler Gene, speziell in multinukleären Keimzellen, erforderlich.

7 ACKNOWLEDGEMENTS

I would like to especially thank my supervisor, Prof. Dr. Georg Lüers, for introducing me to the field of peroxisomes and giving me the opportunity to work autonomously whilst supporting and inspiring me with his way of thinking- thank you for an amazing time in Scotland!

I am grateful to Prof. Dr. Thorsten Burmester for being the second assessor.

I wish to express my gratitude to Prof. Dr. Udo Schumacher for his assistance and guidance and giving me the chance to work in his lab.

My special thank belongs to my closest colleagues, to Hanna Maar, Markus Heine, Sandra Hanika and Michael Horn-Glander, for persuading me, again and again, to keep on going, and for all the fun through the years. I would like to give special thanks to Arne Düsedau and his colleague Jana Hennesen for their technical support. In this context, I want to thank Grischa Fuge und Johannes Möller from the TUHH for their help in using the CCE technique.
Moreover, I want to thank Tine Stürken, Daniel Wicklein, Tobias Lange and Ursula Valentiner, as well as to Katharina Bröker and Vera Labitzky for their good advice, inspiration and knowledge. I am also indebted to my colleagues Renate Gehrcke, Anna Kerbs, Christine Knies, Susanne Feldhaus, Jennifer Schröder-Schwarz (thanks for delicious cakes), Tjandra Cöllen, Tobias Gosau and Meike Märker for motivating me and having fun.

In particular I would like to thank my best friend Jordana Siekmann for being so optimistic and enthusiastic – you were always on my side and succeeded in cheering me up. Thank you so much for being such a wonderful friend! Also, special thanks to my oldest best friend Mirjam Mehwald, who always strengthened and believed in me. Thank you for this very special friendship.

Most of all I want to thank my lovely family -my parents and my brother with his family- who always believed in me, encouraged and supported me to make this thesis possible. I am aware that you were catching the most.
Thank you, mommy and daddy, for your lifelong support! I am so lucky to call you my parents!

8 REFERENCES

Adamski, J., Husen, B., Marks, F., and Jungblut, P.W. (1992) The membrane-bound 17beta-estradiol dehydrogenase of porcine endometrial cells: purification, characterization and subcellular localization. *J Steroid Biochem Mol Biol* **43**(8), 1089-93

Agarwal, A., Durairajanayagam, D., Halabi, J., Peng, J., and Vazquez-Levin, M. (2014) Proteomics, oxidative stress and male infertility. *Reprod Biomed Online* **29**(1), 32-58

Agne, B., Meindl, N.M., Niederhoff, K., Einwachter, H., Rehling, P., Sickmann, A., Meyer, H.E., Girzalsky, W., and Kunau, W.H. (2003) Pex8p: an intraperoxisomal organizer of the peroxisomal import machinery. *Mol Cell* **11**(3), 635-46

Ahmed, E.A., and de Rooij, D.G. (2009) Staging of mouse seminiferous tubule cross-sections. *Methods Mol Biol* **558**, 263-77

Aitken, R.J. (1997) Molecular mechanisms regulating human sperm function. *Mol Hum Reprod* **3**(3), 169-73

Aitken, R.J., and Baker, M.A. (2002) Reactive oxygen species generation by human spermatozoa: a continuing enigma. *Int J Androl* **25**(4), 191-4

Aitken, R.J., Buckingham, D.W., and West, K.M. (1992) Reactive oxygen species and human spermatozoa: analysis of the cellular mechanisms involved in luminol- and lucigenin-dependent chemiluminescence. *J Cell Physiol* **151**(3), 466-77

Aitken, R.J., Irvine, D.S., and Wu, F.C. (1991) Prospective analysis of sperm-oocyte fusion and reactive oxygen species generation as criteria for the diagnosis of infertility. *Am J Obstet Gynecol* **164**(2), 542-51

Alvarez, J.G., and Storey, B.T. (1982) Spontaneous lipid peroxidation in rabbit epididymal spermatozoa: its effect on sperm motility. *Biol Reprod* **27**(5), 1102-8

Amann, R.P. (2008) The cycle of the seminiferous epithelium in humans: a need to revisit? *J Androl* **29**(5), 469-87

Antonenkov, V.D., Grunau, S., Ohlmeier, S., and Hiltunen, J.K. (2010) Peroxisomes are oxidative organelles. *Antioxid Redox Signal* **13**(4), 525-37

Antonenkov, V.D., Sormunen, R.T., and Hiltunen, J.K. (2004) The behavior of peroxisomes in vitro: mammalian peroxisomes are osmotically sensitive particles. *Am J Physiol Cell Physiol* **287**(6), C1623-35

Antonsson, B. (2001) Bax and other pro-apoptotic Bcl-2 family "killer-proteins" and their victim the mitochondrion. *Cell Tissue Res* **306**(3), 347-61

Aponte, P.M., van Bragt, M.P., de Rooij, D.G., and van Pelt, A.M. (2005) Spermatogonial stem cells: characteristics and experimental possibilities. *APMIS* **113**(11-12), 727-42

Aslam, I., Robins, A., Dowell, K., and Fishel, S. (1998) Isolation, purification and assessment of viability of spermatogenic cells from testicular biopsies of azoospermic men. *Hum Reprod* **13**(3), 639-45

Aubourg, P., Scotto, J., Rocchiccioli, F., Feldmann-Pautrat, D., and Robain, O. (1986) Neonatal adrenoleukodystrophy. *J Neurol Neurosurg Psychiatry* **49**(1), 77-86

Aversa, A., Palleschi, S., Cruccu, G., Silvestroni, L., Isidori, A., and Fabbri, A. (1998) Rapid decline of fertility in a case of adrenoleukodystrophy. *Hum Reprod* **13**(9), 2474-9

Baes, M., Gressens, P., Baumgart, E., Carmeliet, P., Casteels, M., Fransen, M., Evrard, P., Fahimi, D., Declercq, P.E., Collen, D., van Veldhoven, P.P., and Mannaerts, G.P. (1997) A mouse model for Zellweger syndrome. *Nat Genet* **17**(1), 49-57

Baes, M., and Van Veldhoven, P.P. (2006) Generalised and conditional inactivation of Pex genes in mice. *Biochim Biophys Acta* **1763**(12), 1785-93

Baker, A., Carrier, D.J., Schaedler, T., Waterham, H.R., van Roermund, C.W., and Theodoulou, F.L. (2015) Peroxisomal ABC transporters: functions and mechanism. *Biochem Soc Trans* **43**(5), 959-65

Barchi, M., Geremia, R., Magliozzi, R., and Bianchi, E. (2009) Isolation and analyses of enriched populations of male mouse germ cells by sedimentation velocity: the centrifugal elutriation. *Methods Mol Biol* **558**, 299-321

Bartelt, A., Weigelt, C., Cherradi, M.L., Niemeier, A., Todter, K., Heeren, J., and Scheja, L. (2013) Effects of adipocyte lipoprotein lipase on de novo lipogenesis and white adipose tissue browning. *Biochim Biophys Acta* **1831**(5), 934-42

Bartlett, K., and Eaton, S. (2004) Mitochondrial beta-oxidation. *Eur J Biochem* **271**(3), 462-9

Bastos, H., Lassalle, B., Chicheportiche, A., Riou, L., Testart, J., Allemand, I., and Fouchet, P. (2005) Flow cytometric characterization of viable meiotic and postmeiotic cells by Hoechst 33342 in mouse spermatogenesis. *Cytometry A* **65**(1), 40-9

Baumgart, E. (1997) Application of in situ hybridization, cytochemical and immunocytochemical techniques for the investigation of peroxisomes. A review including novel data. Robert Feulgen Prize Lecture 1997. *Histochem Cell Biol* **108**(3), 185-210

Beckman, J.K., and Coniglio, J.G. (1979) A comparative study of the lipid composition of isolated rat Sertoli and germinal cells. *Lipids* **14**(3), 262-7

Bellve, A.R. (1993) Purification, culture, and fractionation of spermatogenic cells. *Methods Enzymol* **225**, 84-113

Bellve, A.R., Cavicchia, J.C., Millette, C.F., O'Brien, D.A., Bhatnagar, Y.M., and Dym, M. (1977) Spermatogenic cells of the prepuberal mouse. Isolation and morphological characterization. *J Cell Biol* **74**(1), 68-85

Berger, J., Pujol, A., Aubourg, P., and Forss-Petter, S. (2010) Current and future pharmacological treatment strategies in X-linked adrenoleukodystrophy. *Brain Pathol* **20**(4), 845-56

Berookhim, B.M., and Schlegel, P.N. (2014) Azoospermia due to spermatogenic failure. *Urol Clin North Am* **41**(1), 97-113

Binns, D., Januszewski, T., Chen, Y., Hill, J., Markin, V.S., Zhao, Y., Gilpin, C., Chapman, K.D., Anderson, R.G., and Goodman, J.M. (2006) An intimate collaboration between peroxisomes and lipid bodies. *J Cell Biol* **173**(5), 719-31

Blanchard, K.T., Lee, J., and Boekelheide, K. (1998) Leuprolide, a gonadotropin-releasing hormone agonist, reestablishes spermatogenesis after 2,5-hexanedione-induced irreversible testicular injury in the rat, resulting in normalized stem cell factor expression. *Endocrinology* **139**(1), 236-44

Blok, L.J., Mackenbach, P., Trapman, J., Themmen, A.P., Brinkmann, A.O., and Grootegoed, J.A. (1989) Follicle-stimulating hormone regulates androgen receptor mRNA in Sertoli cells. *Mol Cell Endocrinol* **63**(1-2), 267-71

Boitani, C., Stefanini, M., Fragale, A., and Morena, A.R. (1995) Activin stimulates Sertoli cell proliferation in a defined period of rat testis development. *Endocrinology* **136**(12), 5438-44

Bonekamp, N.A., Volkl, A., Fahimi, H.D., and Schrader, M. (2009) Reactive oxygen species and peroxisomes: struggling for balance. *Biofactors* **35**(4), 346-55

Boveris, A., Oshino, N., and Chance, B. (1972) The cellular production of hydrogen peroxide. *Biochem J* **128**(3), 617-30

Braun, R.E., Behringer, R.R., Peschon, J.J., Brinster, R.L., and Palmiter, R.D. (1989) Genetically haploid spermatids are phenotypically diploid. *Nature* **337**(6205), 373-6

Braverman, N., Zhang, R., Chen, L., Nimmo, G., Scheper, S., Tran, T., Chaudhury, R., Moser, A., and Steinberg, S. (2010) A Pex7 hypomorphic mouse model for plasmalogen deficiency affecting the lens and skeleton. *Mol Genet Metab* **99**(4), 408-16

Braverman, N.E., D'Agostino, M.D., and Maclean, G.E. (2013) Peroxisome biogenesis disorders: Biological, clinical and pathophysiological perspectives. *Dev Disabil Res Rev* **17**(3), 187-96

Breucker, H., Schafer, E., and Holstein, A.F. (1985) Morphogenesis and fate of the residual body in human spermiogenesis. *Cell Tissue Res* **240**(2), 303-9

Brinkworth, M.H., Weinbauer, G.F., Bergmann, M., and Nieschlag, E. (1997) Apoptosis as a mechanism of germ cell loss in elderly men. *Int J Androl* **20**(4), 222-8

Brites, P., Waterham, H.R., and Wanders, R.J. (2004) Functions and biosynthesis of plasmalogens in health and disease. *Biochim Biophys Acta* **1636**(2-3), 219-31

Burgos, M.H., and Fawcett, D.W. (1955) Studies on the fine structure of the mammalian testis. I. Differentiation of the spermatids in the cat (Felis domestica). *J Biophys Biochem Cytol* **1**(4), 287-300

Bustin, S.A., Benes, V., Garson, J.A., Hellemans, J., Huggett, J., Kubista, M., Mueller, R., Nolan, T., Pfaffl, M.W., Shipley, G.L., Vandesompele, J., and Wittwer, C.T. (2009) The MIQE guidelines: minimum information for publication of quantitative real-time PCR experiments. *Clin Chem* **55**(4), 611-22

Chakravarti, B., and Chakravarti, D.N. (2007) Oxidative modification of proteins: age-related changes. *Gerontology* **53**(3), 128-39

Chandran, U., Indu, S., Kumar, A.T., Devi, A.N., Khan, I., Srivastava, D., and Kumar, P.G. (2016) Expression of Cnnm1 and Its Association with Stemness, Cell Cycle, and Differentiation in Spermatogenic Cells in Mouse Testis. *Biol Reprod* **95**(1), 7

Chemes, H. (1986) The phagocytic function of Sertoli cells: a morphological, biochemical, and endocrinological study of lysosomes and acid phosphatase localization in the rat testis. *Endocrinology* **119**(4), 1673-81

Cheng, C.Y., and Mruk, D.D. (2012) The blood-testis barrier and its implications for male contraception. *Pharmacol Rev* **64**(1), 16-64

Cheng, C.Y., Wong, E.W., Lie, P.P., Li, M.W., Mruk, D.D., Yan, H.H., Mok, K.W., Mannu, J., Mathur, P.P., Lui, W.Y., Lee, W.M., Bonanomi, M., and Silvestrini, B. (2011a) Regulation of blood-testis barrier dynamics by desmosome, gap junction, hemidesmosome and polarity proteins: An unexpected turn of events. *Spermatogenesis* **1**(2), 105-115

Cheng, C.Y., Wong, E.W., Lie, P.P., Mruk, D.D., Xiao, X., Li, M.W., Lui, W.Y., and Lee, W.M. (2011b) Polarity proteins and actin regulatory proteins are unlikely partners that regulate cell adhesion in the seminiferous epithelium during spermatogenesis. *Histol Histopathol* **26**(11), 1465-74

Chihara, M., Otsuka, S., Ichii, O., Hashimoto, Y., and Kon, Y. (2010) Molecular dynamics of the blood-testis barrier components during murine spermatogenesis. *Mol Reprod Dev* **77**(7), 630-9

Cho, H.P., Nakamura, M., and Clarke, S.D. (1999) Cloning, expression, and fatty acid regulation of the human delta-5 desaturase. *J Biol Chem* **274**(52), 37335-9

Clarke, I.J., and Cummins, J.T. (1982) The temporal relationship between gonadotropin releasing hormone (GnRH) and luteinizing hormone (LH) secretion in ovariectomized ewes. *Endocrinology* **111**(5), 1737-9

Clement, M.V., Ponton, A., and Pervaiz, S. (1998) Apoptosis induced by hydrogen peroxide is mediated by decreased superoxide anion concentration and reduction of intracellular milieu. *FEBS Lett* **440**(1-2), 13-8

Clermont, Y. (1972) Kinetics of spermatogenesis in mammals: seminiferous epithelium cycle and spermatogonial renewal. *Physiol Rev* **52**(1), 198-236

Cocuzza, M., Alvarenga, C., and Pagani, R. (2013) The epidemiology and etiology of azoospermia. *Clinics (Sao Paulo)* **68 Suppl 1**, 15-26

Cohen, C.D., Grone, H.J., Grone, E.F., Nelson, P.J., Schlondorff, D., and Kretzler, M. (2002) Laser microdissection and gene expression analysis on formaldehyde-fixed archival tissue. *Kidney Int* **61**(1), 125-32

Collins, J.A., and Crosignani, P.G. (1992) Unexplained infertility: a review of diagnosis, prognosis, treatment efficacy and management. *Int J Gynaecol Obstet* **39**(4), 267-75

Collins, J.A., and Rowe, T.C. (1989) Age of the female partner is a prognostic factor in prolonged unexplained infertility: a multicenter study. *Fertil Steril* **52**(1), 15-20

Cooke, H.J., and Saunders, P.T. (2002) Mouse models of male infertility. *Nat Rev Genet* **3**(10), 790-801

Cooke, M.S., Evans, M.D., Dizdaroglu, M., and Lunec, J. (2003) Oxidative DNA damage: mechanisms, mutation, and disease. *FASEB J* **17**(10), 1195-214

Cooper, T.G., Waites, G.M., and Nieschlag, E. (1986) The epididymis and male fertility. A symposium report. *Int J Androl* **9**(2), 81-90

Corea, M., Campagnone, J., and Sigman, M. (2005) The diagnosis of azoospermia depends on the force of centrifugation. *Fertil Steril* **83**(4), 920-2

Coutton, C., Arnoult, C., and Ray, P.F. (2015a) Comprehensive investigation in patients affected by globozoospermia. *Andrology* **3**(6), 1183

Coutton, C., Escoffier, J., Martinez, G., Arnoult, C., and Ray, P.F. (2015b) Teratozoospermia: spotlight on the main genetic actors in the human. *Hum Reprod Update* **21**(4), 455-85

Creasy, D., Bube, A., de Rijk, E., Kandori, H., Kuwahara, M., Masson, R., Nolte, T., Reams, R., Regan, K., Rehm, S., Rogerson, P., and Whitney, K. (2012) Proliferative and nonproliferative lesions of the rat and mouse male reproductive system. *Toxicol Pathol* **40**(6 Suppl), 40S-121S

Das, K.C., and Misra, H.P. (2004) Hydroxyl radical scavenging and singlet oxygen quenching properties of polyamines. *Mol Cell Biochem* **262**(1-2), 127-33

Das, T., Thurmond, J.M., Bobik, E., Leonard, A.E., Parker-Barnes, J.M., Huang, Y.S., and Mukerji, P. (2000) Polyunsaturated fatty acid-specific elongation enzymes. *Biochem Soc Trans* **28**(6), 658-60

Dastig, S., Nenicu, A., Otte, D.M., Zimmer, A., Seitz, J., Baumgart-Vogt, E., and Luers, G.H. (2011) Germ cells of male mice express genes for peroxisomal metabolic pathways implicated in the regulation of spermatogenesis and the protection against oxidative stress. *Histochem Cell Biol* **136**(4), 413-25

Davies, K.J. (1987) Protein damage and degradation by oxygen radicals. I. general aspects. *J Biol Chem* **262**(20), 9895-901

Davis, J.C., Snyder, E.M., Hogarth, C.A., Small, C., and Griswold, M.D. (2013) Induction of spermatogenic synchrony by retinoic acid in neonatal mice. *Spermatogenesis* **3**(1), e23180

De Duve, C., and Baudhuin, P. (1966) Peroxisomes (microbodies and related particles). *Physiol Rev* **46**(2), 323-57

de Kretser, D.M. (1979) Endocrinology of male infertility. *Br Med Bull* **35**(2), 187-92

de Kretser, D.M., Kerr, J.B., and Paulsen, C.A. (1981) Evaluation of the ultrastructural changes in the human sertoli cell in testicular disorders and the relationship of the changes to the levels of serum FSH. *Int J Androl* **4**(2), 129-44

de Rooij, D.G. (1998) Stem cells in the testis. *Int J Exp Pathol* **79**(2), 67-80

de Rooij, D.G. (2001) Proliferation and differentiation of spermatogonial stem cells. *Reproduction* **121**(3), 347-54

de Rooij, D.G., and Russell, L.D. (2000) All you wanted to know about spermatogonia but were afraid to ask. *J Androl* **21**(6), 776-98

Distel, B., Erdmann, R., Gould, S.J., Blobel, G., Crane, D.I., Cregg, J.M., Dodt, G., Fujiki, Y., Goodman, J.M., Just, W.W., Kiel, J.A., Kunau, W.H., Lazarow, P.B., Mannaerts, G.P., Moser, H.W., Osumi, T., Rachubinski, R.A., Roscher, A., Subramani, S., Tabak, H.F., Tsukamoto, T., Valle, D., van der Klei, I., van Veldhoven, P.P., and Veenhuis, M. (1996) A unified nomenclature for peroxisome biogenesis factors. *J Cell Biol* **135**(1), 1-3

Domke, L.M., Rickelt, S., Dorflinger, Y., Kuhn, C., Winter-Simanowski, S., Zimbelmann, R., Rosin-Arbesfeld, R., Heid, H., and Franke, W.W. (2014) The cell-cell junctions of mammalian testes: I. The

adhering junctions of the seminiferous epithelium represent special differentiation structures. *Cell Tissue Res* **357**(3), 645-65

Dubey, P., Raymond, G.V., Moser, A.B., Kharkar, S., Bezman, L., and Moser, H.W. (2005) Adrenal insufficiency in asymptomatic adrenoleukodystrophy patients identified by very long-chain fatty acid screening. *J Pediatr* **146**(4), 528-32

Dubois, J., Sebag, G., Argyropoulou, M., and Brunelle, F. (1991) MR findings in infantile Refsum disease: case report of two family members. *AJNR Am J Neuroradiol* **12**(6), 1159-60

Dym, M., and Fawcett, D.W. (1970) The blood-testis barrier in the rat and the physiological compartmentation of the seminiferous epithelium. *Biol Reprod* **3**(3), 308-26

Dym, M., and Fawcett, D.W. (1971) Further observations on the numbers of spermatogonia, spermatocytes, and spermatids connected by intercellular bridges in the mammalian testis. *Biol Reprod* **4**(2), 195-215

Eacker, S.M., Agrawal, N., Qian, K., Dichek, H.L., Gong, E.Y., Lee, K., and Braun, R.E. (2008) Hormonal regulation of testicular steroid and cholesterol homeostasis. *Mol Endocrinol* **22**(3), 623-35

Eddy, E.M. (1998) Regulation of gene expression during spermatogenesis. *Semin Cell Dev Biol* **9**(4), 451-7

Edelman, G.M., and Gally, J.A. (2001) Degeneracy and complexity in biological systems. *Proc Natl Acad Sci U S A* **98**(24), 13763-8

Elgersma, Y., Kwast, L., Klein, A., Voorn-Brouwer, T., van den Berg, M., Metzig, B., America, T., Tabak, H.F., and Distel, B. (1996) The SH3 domain of the Saccharomyces cerevisiae peroxisomal membrane protein Pex13p functions as a docking site for Pex5p, a mobile receptor for the import PTS1-containing proteins. *J Cell Biol* **135**(1), 97-109

Ellis, R.E., Yuan, J.Y., and Horvitz, H.R. (1991) Mechanisms and functions of cell death. *Annu Rev Cell Biol* **7**, 663-98

Emmert-Buck, M.R., Bonner, R.F., Smith, P.D., Chuaqui, R.F., Zhuang, Z., Goldstein, S.R., Weiss, R.A., and Liotta, L.A. (1996) Laser capture microdissection. *Science* **274**(5289), 998-1001

Engelen, M., Kemp, S., de Visser, M., van Geel, B.M., Wanders, R.J., Aubourg, P., and Poll-The, B.T. (2012) X-linked adrenoleukodystrophy (X-ALD): clinical presentation and guidelines for diagnosis, follow-up and management. *Orphanet J Rare Dis* **7**, 51

Erdmann, R., and Blobel, G. (1996) Identification of Pex13p a peroxisomal membrane receptor for the PTS1 recognition factor. *J Cell Biol* **135**(1), 111-21

Erdmann, R., and Schliebs, W. (2005) Peroxisomal matrix protein import: the transient pore model. *Nat Rev Mol Cell Biol* **6**(9), 738-42

Erickson, R.P. (1973) Haploid gene expresion versus meiotic drive: the relevance of intercellular bridges during spermatogenesis. *Nat New Biol* **243**(128), 210-2

Evans, R.W., Weaver, D.E., and Clegg, E.D. (1980) Diacyl, alkenyl, and alkyl ether phospholipids in ejaculated, in utero-, and in vitro-incubated porcine spermatozoa. *J Lipid Res* **21**(2), 223-8

Fahimi, H.D. (1969) Cytochemical localization of peroxidatic activity of catalase in rat hepatic microbodies (peroxisomes). *J Cell Biol* **43**(2), 275-88

Fahimi, H.D., Reinicke, A., Sujatta, M., Yokota, S., Ozel, M., Hartig, F., and Stegmeier, K. (1982) The short- and long-term effects of bezafibrate in the rat. *Ann N Y Acad Sci* **386**, 111-35

Fan, C.Y., Pan, J., Chu, R., Lee, D., Kluckman, K.D., Usuda, N., Singh, I., Yeldandi, A.V., Rao, M.S., Maeda, N., and Reddy, J.K. (1996a) Hepatocellular and hepatic peroxisomal alterations in mice with a disrupted peroxisomal fatty acyl-coenzyme A oxidase gene. *J Biol Chem* **271**(40), 24698-710

Fan, C.Y., Pan, J., Chu, R., Lee, D., Kluckman, K.D., Usuda, N., Singh, I., Yeldandi, A.V., Rao, M.S., Maeda, N., and Reddy, J.K. (1996b) Targeted disruption of the peroxisomal fatty acyl-CoA oxidase gene: generation of a mouse model of pseudoneonatal adrenoleukodystrophy. *Ann N Y Acad Sci* **804**, 530-41

Faust, P.L., and Hatten, M.E. (1997) Targeted deletion of the PEX2 peroxisome assembly gene in mice provides a model for Zellweger syndrome, a human neuronal migration disorder. *J Cell Biol* **139**(5), 1293-305

Fawcett, D.W. (1961) Intercellular bridges. *Exp Cell Res* **Suppl 8**, 174-87

Fawcett, D.W., Ito, S., and Slautterback, D. (1959) The occurrence of intercellular bridges in groups of cells exhibiting synchronous differentiation. *J Biophys Biochem Cytol* **5**(3), 453-60

Feigenbaum, V., Lombard-Platet, G., Guidoux, S., Sarde, C.O., Mandel, J.L., and Aubourg, P. (1996) Mutational and protein analysis of patients and heterozygous women with X-linked adrenoleukodystrophy. *Am J Hum Genet* **58**(6), 1135-44

Ferdinandusse, S., Denis, S., Mooyer, P.A., Dekker, C., Duran, M., Soorani-Lunsing, R.J., Boltshauser, E., Macaya, A., Gartner, J., Majoie, C.B., Barth, P.G., Wanders, R.J., and Poll-The, B.T. (2006) Clinical and biochemical spectrum of D-bifunctional protein deficiency. *Ann Neurol* **59**(1), 92-104

Ferdinandusse, S., Falkenberg, K.D., Koster, J., Mooyer, P.A., Jones, R., van Roermund, C.W.T., Pizzino, A., Schrader, M., Wanders, R.J.A., Vanderver, A., and Waterham, H.R. (2017) ACBD5 deficiency causes a defect in peroxisomal very long-chain fatty acid metabolism. *J Med Genet* **54**(5), 330-337

Ferdinandusse, S., Mulders, J., L, I.J., Denis, S., Dacremont, G., Waterham, H.R., and Wanders, R.J. (1999) Molecular cloning and expression of human carnitine octanoyltransferase: evidence for its role in the peroxisomal beta-oxidation of branched-chain fatty acids. *Biochem Biophys Res Commun* **263**(1), 213-8

Fijak, M., and Meinhardt, A. (2006) The testis in immune privilege. *Immunol Rev* **213**, 66-81

Finkel, T. (1998) Oxygen radicals and signaling. *Curr Opin Cell Biol* **10**(2), 248-53

Fischer, F.G., and Bohn, H. (1957) [Determination of spermin, spermidine, and other biogenic amines after separation by paper electrophoresis, and their quantity in animal organs]. *Hoppe Seylers Z Physiol Chem* **308**(2-4), 108-15

Franke, W.W., Grund, C., and Schmid, E. (1979) Intermediate-sized filaments present in Sertoli cells are of the vimentin type. *Eur J Cell Biol* **19**(3), 269-75

Fransen, M., Nordgren, M., Wang, B., and Apanasets, O. (2012) Role of peroxisomes in ROS/RNS-metabolism: implications for human disease. *Biochim Biophys Acta* **1822**(9), 1363-73

Freeman, B.A., and Crapo, J.D. (1982) Biology of disease: free radicals and tissue injury. *Lab Invest* **47**(5), 412-26

Fujiki, Y., Okumoto, K., Mukai, S., Honsho, M., and Tamura, S. (2014) Peroxisome biogenesis in mammalian cells. *Front Physiol* **5**, 307

Furuse, M., Hirase, T., Itoh, M., Nagafuchi, A., Yonemura, S., Tsukita, S., and Tsukita, S. (1993) Occludin: a novel integral membrane protein localizing at tight junctions. *J Cell Biol* **123**(6 Pt 2), 1777-88

Gabaldon, T., Snel, B., van Zimmeren, F., Hemrika, W., Tabak, H., and Huynen, M.A. (2006) Origin and evolution of the peroxisomal proteome. *Biol Direct* **1**, 8

Gagnon, C., Iwasaki, A., De Lamirande, E., and Kovalski, N. (1991) Reactive oxygen species and human spermatozoa. *Ann N Y Acad Sci* **637**, 436-44

Gavella, M., and Lipovac, V. (1992) NADH-dependent oxidoreductase (diaphorase) activity and isozyme pattern of sperm in infertile men. *Arch Androl* **28**(2), 135-41

Gaytan, F., Bellido, C., Aguilar, E., and van Rooijen, N. (1994) Requirement for testicular macrophages in Leydig cell proliferation and differentiation during prepubertal development in rats. *J Reprod Fertil* **102**(2), 393-9

Ghisla, S. (2004) Beta-oxidation of fatty acids. A century of discovery. *Eur J Biochem* **271**(3), 459-61

Gibson, D.M. (1965) The Biosynthesis of Fatty Acids. *J Chem Educ* **42**, 236-43

Gilula, N.B., Fawcett, D.W., and Aoki, A. (1976) The Sertoli cell occluding junctions and gap junctions in mature and developing mammalian testis. *Dev Biol* **50**(1), 142-68

Girzalsky, W., Platta, H.W., and Erdmann, R. (2009) Protein transport across the peroxisomal membrane. *Biol Chem* **390**(8), 745-51

Girzalsky, W., Saffian, D., and Erdmann, R. (2010) Peroxisomal protein translocation. *Biochim Biophys Acta* **1803**(6), 724-31

Gordon, J.W., and Ruddle, F.H. (1981) Mammalian gonadal determination and gametogenesis. *Science* **211**(4488), 1265-71

Gorgas, K. (1984) Peroxisomes in sebaceous glands. V. Complex peroxisomes in the mouse preputial gland: serial sectioning and three-dimensional reconstruction studies. *Anat Embryol (Berl)* **169**(3), 261-70

Gould, S.J., Keller, G.A., and Subramani, S. (1988) Identification of peroxisomal targeting signals located at the carboxy terminus of four peroxisomal proteins. *J Cell Biol* **107**(3), 897-905

Gould, S.J., and Valle, D. (2000) Peroxisome biogenesis disorders: genetics and cell biology. *Trends Genet* **16**(8), 340-5

Grabske, R.J., Lake, S., Gledhill, B.L., and Meistrich, M.L. (1975) Centrifugal elutriation: separation of spermatogenic cells on the basis of sedimentation velocity. *J Cell Physiol* **86**(1), 177-89

Greaves, E.A., Copeland, N.A., Coverley, D., and Ainscough, J.F. (2012) Cancer-associated variant expression and interaction of CIZ1 with cyclin A1 in differentiating male germ cells. *J Cell Sci* **125**(Pt 10), 2466-77

Greenbaum, M.P., Ma, L., and Matzuk, M.M. (2007) Conversion of midbodies into germ cell intercellular bridges. *Dev Biol* **305**(2), 389-96

Greenbaum, M.P., Yan, W., Wu, M.H., Lin, Y.N., Agno, J.E., Sharma, M., Braun, R.E., Rajkovic, A., and Matzuk, M.M. (2006) TEX14 is essential for intercellular bridges and fertility in male mice. *Proc Natl Acad Sci U S A* **103**(13), 4982-7

Gregory, M.K., Cleland, L.G., and James, M.J. (2013) Molecular basis for differential elongation of omega-3 docosapentaenoic acid by the rat Elovl5 and Elovl2. *J Lipid Res* **54**(10), 2851-7

Griswold, M.D. (1995) Interactions between germ cells and Sertoli cells in the testis. *Biol Reprod* **52**(2), 211-6

Grogan, W.M., Farnham, W.F., and Szopiak, B.A. (1981) Long chain polyenoic acid levels in viably sorted, highly enriched mouse testis cells. *Lipids* **16**(6), 401-10

Guillou, H., Zadravec, D., Martin, P.G., and Jacobsson, A. (2010) The key roles of elongases and desaturases in mammalian fatty acid metabolism: Insights from transgenic mice. *Prog Lipid Res* **49**(2), 186-99

Guo, G.Q., and Zheng, G.C. (2004) Hypotheses for the functions of intercellular bridges in male germ cell development and its cellular mechanisms. *J Theor Biol* **229**(1), 139-46

Ha, H.C., Sirisoma, N.S., Kuppusamy, P., Zweier, J.L., Woster, P.M., and Casero, R.A., Jr. (1998) The natural polyamine spermine functions directly as a free radical scavenger. *Proc Natl Acad Sci U S A* **95**(19), 11140-5

Hamada, A., Agarwal, A., Sharma, R., French, D.B., Ragheb, A., and Sabanegh, E.S., Jr. (2011) Empirical treatment of low-level leukocytospermia with doxycycline in male infertility patients. *Urology* **78**(6), 1320-5

Handel, M.A., and Schimenti, J.C. (2010) Genetics of mammalian meiosis: regulation, dynamics and impact on fertility. *Nat Rev Genet* **11**(2), 124-36

Hasan, S., Platta, H.W., and Erdmann, R. (2013) Import of proteins into the peroxisomal matrix. *Front Physiol* **4**, 261

Hedger, M.P. (1997) Testicular leukocytes: what are they doing? *Rev Reprod* **2**(1), 38-47

Hellerstein, M.K. (1999) De novo lipogenesis in humans: metabolic and regulatory aspects. *Eur J Clin Nutr* **53 Suppl 1**, S53-65

Hermo, L., Pelletier, R.M., Cyr, D.G., and Smith, C.E. (2010) Surfing the wave, cycle, life history, and genes/proteins expressed by testicular germ cells. Part 5: intercellular junctions and contacts between germs cells and Sertoli cells and their regulatory interactions, testicular cholesterol, and genes/proteins associated with more than one germ cell generation. *Microsc Res Tech* **73**(4), 409-94

Hess, R.A., and Renato de Franca, L. (2008) Spermatogenesis and cycle of the seminiferous epithelium. *Adv Exp Med Biol* **636**, 1-15

Hild, S.A., Reel, J.R., Dykstra, M.J., Mann, P.C., and Marshall, G.R. (2007) Acute adverse effects of the indenopyridine CDB-4022 on the ultrastructure of sertoli cells, spermatocytes, and spermatids in rat testes: comparison to the known sertoli cell toxicant Di-n-pentylphthalate (DPP). *J Androl* **28**(4), 621-9

Hinshaw, D.B., Sklar, L.A., Bohl, B., Schraufstatter, I.U., Hyslop, P.A., Rossi, M.W., Spragg, R.G., and Cochrane, C.G. (1986) Cytoskeletal and morphologic impact of cellular oxidant injury. *Am J Pathol* **123**(3), 454-64

Holstein, A.F., and Eckmann, C. (1986) Multinucleated spermatocytes and spermatids in human seminiferous tubules. *Andrologia* **18**(1), 5-16

Holstein, A.F., Schirren, C., and Schirren, C.G. (1973) Human spermatids and spermatozoa lacking acrosomes. *J Reprod Fertil* **35**(3), 489-91

Holtzman, E., Teichberg, S., Abrahams, S.J., Citkowitz, E., Crain, S.M., Kawai, N., and Peterson, E.R. (1973) Notes on synaptic vesicles and related structures, endoplasmic reticulum, lysosomes and peroxisomes in nervous tissue and the adrenal medulla. *J Histochem Cytochem* **21**(4), 349-85

Horie, S., Suzuki, T., and Suga, T. (1989) Existence of acetyl-CoA-dependent chain elongation system in hepatic peroxisomes of rat: effects of clofibrate and di-(2-ethylhexyl)phthalate on the activity. *Arch Biochem Biophys* **274**(1), 64-73

Hruban, Z., Vigil, E.L., Slesers, A., and Hopkins, E. (1972) Microbodies: constituent organelles of animal cells. *Lab Invest* **27**(2), 184-91

Huckins, C., and Oakberg, E.F. (1978) Morphological and quantitative analysis of spermatogonia in mouse testes using whole mounted seminiferous tubules, I. The normal testes. *Anat Rec* **192**(4), 519-28

Huyghe, S., Schmalbruch, H., De Gendt, K., Verhoeven, G., Guillou, F., Van Veldhoven, P.P., and Baes, M. (2006) Peroxisomal multifunctional protein 2 is essential for lipid homeostasis in Sertoli cells and male fertility in mice. *Endocrinology* **147**(5), 2228-36

Igarashi, K., and Kashiwagi, K. (2010) Modulation of cellular function by polyamines. *Int J Biochem Cell Biol* **42**(1), 39-51

Imanaka, T., Takano, T., Osumi, T., and Hashimoto, T. (1996) Sorting of the 70-kDa peroxisomal membrane protein into rat liver peroxisomes in vitro. *Ann N Y Acad Sci* **804**, 663-5

Iommiello, V.M., Albani, E., Di Rosa, A., Marras, A., Menduni, F., Morreale, G., Levi, S.L., Pisano, B., and Levi-Setti, P.E. (2015) Ejaculate oxidative stress is related with sperm DNA fragmentation and round cells. *Int J Endocrinol* **2015**, 321901

Islinger, M., Grille, S., Fahimi, H.D., and Schrader, M. (2012) The peroxisome: an update on mysteries. *Histochem Cell Biol* **137**(5), 547-74

Jakobsson, A., Westerberg, R., and Jacobsson, A. (2006) Fatty acid elongases in mammals: their regulation and roles in metabolism. *Prog Lipid Res* **45**(3), 237-49

Jamsai, D., and O'Bryan, M.K. (2011) Mouse models in male fertility research. *Asian J Androl* **13**(1), 139-51

Jan, S.Z., Hamer, G., Repping, S., de Rooij, D.G., van Pelt, A.M., and Vormer, T.L. (2012) Molecular control of rodent spermatogenesis. *Biochim Biophys Acta* **1822**(12), 1838-50

Jean, P., Hartung, M., Mirre, C., and Stahl, A. (1983) Association of centromeric heterochromatin with the nucleolus in mouse Sertoli cells. *Anat Rec* **205**(4), 375-80

Jiang, X.H., Bukhari, I., Zheng, W., Yin, S., Wang, Z., Cooke, H.J., and Shi, Q.H. (2014) Blood-testis barrier and spermatogenesis: lessons from genetically-modified mice. *Asian J Androl* **16**(4), 572-80

Johnson, L. (1994) A new approach to study the architectural arrangement of spermatogenic stages revealed little evidence of a partial wave along the length of human seminiferous tubules. *J Androl* **15**(5), 435-41

Jutte, N.H., Eikvar, L., Levy, F.O., and Hansson, V. (1985) Metabolism of palmitate in cultured rat Sertoli cells. *J Reprod Fertil* **73**(2), 497-503

Kafri, R., Bar-Even, A., and Pilpel, Y. (2005) Transcription control reprogramming in genetic backup circuits. *Nat Genet* **37**(3), 295-9

Kanatsu-Shinohara, M., Takashima, S., Ishii, K., and Shinohara, T. (2011) Dynamic changes in EPCAM expression during spermatogonial stem cell differentiation in the mouse testis. *PLoS One* **6**(8), e23663

Kefer, J.C., Agarwal, A., and Sabanegh, E. (2009) Role of antioxidants in the treatment of male infertility. *Int J Urol* **16**(5), 449-57

Kemp, S., Pujol, A., Waterham, H.R., van Geel, B.M., Boehm, C.D., Raymond, G.V., Cutting, G.R., Wanders, R.J., and Moser, H.W. (2001) ABCD1 mutations and the X-linked adrenoleukodystrophy mutation database: role in diagnosis and clinical correlations. *Hum Mutat* **18**(6), 499-515

Kemp, S., and Wanders, R.J. (2007) X-linked adrenoleukodystrophy: very long-chain fatty acid metabolism, ABC half-transporters and the complicated route to treatment. *Mol Genet Metab* **90**(3), 268-76

Kerr, J.B., and de Kretser, D.M. (1974) Proceedings: The role of the Sertoli cell in phagocytosis of the residual bodies of spermatids. *J Reprod Fertil* **36**(2), 439-40

Kerr, J.B., and De Kretser, D.M. (1975) Cyclic variations in Sertoli cell lipid content throughout the spermatogenic cycle in the rat. *J Reprod Fertil* **43**(1), 1-8

Kitano, H. (2004) Biological robustness. *Nat Rev Genet* **5**(11), 826-37

Kumar, N., and Singh, A.K. (2015) Trends of male factor infertility, an important cause of infertility: A review of literature. *J Hum Reprod Sci* **8**(4), 191-6

Labrie, F., Luu-The, V., Lin, S.X., Labrie, C., Simard, J., Breton, R., and Belanger, A. (1997) The key role of 17 beta-hydroxysteroid dehydrogenases in sex steroid biology. *Steroids* **62**(1), 148-58

Lazarow, P.B., and Fujiki, Y. (1985) Biogenesis of peroxisomes. *Annu Rev Cell Biol* **1**, 489-530

Leblond, C.P., and Clermont, Y. (1952) Definition of the stages of the cycle of the seminiferous epithelium in the rat. *Ann N Y Acad Sci* **55**(4), 548-73

Lejeune, H., Habert, R., and Saez, J.M. (1998) Origin, proliferation and differentiation of Leydig cells. *J Mol Endocrinol* **20**(1), 1-25

Lenzi, A., Picardo, M., Gandini, L., and Dondero, F. (1996) Lipids of the sperm plasma membrane: from polyunsaturated fatty acids considered as markers of sperm function to possible scavenger therapy. *Hum Reprod Update* **2**(3), 246-56

Leonard, A.E., Bobik, E.G., Dorado, J., Kroeger, P.E., Chuang, L.T., Thurmond, J.M., Parker-Barnes, J.M., Das, T., Huang, Y.S., and Mukerji, P. (2000) Cloning of a human cDNA encoding a novel enzyme involved in the elongation of long-chain polyunsaturated fatty acids. *Biochem J* **350 Pt 3**, 765-70

Lepage, G., Levy, E., Ronco, N., Smith, L., Galeano, N., and Roy, C.C. (1989) Direct transesterification of plasma fatty acids for the diagnosis of essential fatty acid deficiency in cystic fibrosis. *J Lipid Res* **30**(10), 1483-90

Lessig, J., and Fuchs, B. (2009) Plasmalogens in biological systems: their role in oxidative processes in biological membranes, their contribution to pathological processes and aging and plasmalogen analysis. *Curr Med Chem* **16**(16), 2021-41

Li, X., and Gould, S.J. (2002) PEX11 promotes peroxisome division independently of peroxisome metabolism. *J Cell Biol* **156**(4), 643-51

Liang, G., Zhang, X.D., Wang, L.J., Sha, Y.S., Zhang, J.C., Miao, S.Y., Zong, S.D., Wang, L.F., and Koide, S.S. (2004) Identification of differentially expressed genes of primary spermatocyte against round spermatid isolated from human testis using the laser capture microdissection technique. *Cell Res* **14**(6), 507-12

Lie, P.P., Cheng, C.Y., and Mruk, D.D. (2013) Signalling pathways regulating the blood-testis barrier. *Int J Biochem Cell Biol* **45**(3), 621-5

Lima, A.C., Jung, M., Rusch, J., Usmani, A., Lopes, A., and Conrad, D.F. (2016) Multispecies Purification of Testicular Germ Cells. *Biol Reprod* **95**(4), 85

Lindahl, P.E. (1948) Principle of a counter-streaming centrifuge for the separation of particles of different sizes. *Nature* **161**(4095), 648

Lizana, L., Bauer, B., and Orwar, O. (2008) Controlling the rates of biochemical reactions and signaling networks by shape and volume changes. *Proc Natl Acad Sci U S A* **105**(11), 4099-104

Luers, G.H., Thiele, S., Schad, A., Volkl, A., Yokota, S., and Seitz, J. (2006) Peroxisomes are present in murine spermatogonia and disappear during the course of spermatogenesis. *Histochem Cell Biol* **125**(6), 693-703

Lui, W.Y., and Cheng, C.Y. (2007) Regulation of cell junction dynamics by cytokines in the testis: a molecular and biochemical perspective. *Cytokine Growth Factor Rev* **18**(3-4), 299-311

Luo, L., Li, Y., Yang, Y., He, Y., Wang, Y., Xu, Z., and Zhang, Y. (2013) Multinucleated cells are involved in normal development and apoptosis in mouse testes. *Mol Med Rep* **8**(3), 865-70

Ma, C., Agrawal, G., and Subramani, S. (2011) Peroxisome assembly: matrix and membrane protein biogenesis. *J Cell Biol* **193**(1), 7-16

MacGregor, G.R., Russell, L.D., Van Beek, M.E., Hanten, G.R., Kovac, M.J., Kozak, C.A., Meistrich, M.L., and Overbeek, P.A. (1990) Symplastic spermatids (sys): a recessive insertional mutation in mice causing a defect in spermatogenesis. *Proc Natl Acad Sci U S A* **87**(13), 5016-20

Makitie, L.T., Kanerva, K., Sankila, A., and Andersson, L.C. (2009) High expression of antizyme inhibitor 2, an activator of ornithine decarboxylase in steroidogenic cells of human gonads. *Histochem Cell Biol* **132**(6), 633-8

Makker, K., Agarwal, A., and Sharma, R. (2009) Oxidative stress & male infertility. *Indian J Med Res* **129**(4), 357-67

Matsumoto, A.M., and Bremner, W.J. (1989) Endocrine Control of Human Spermatogenesis. *Journal of Steroid Biochemistry and Molecular Biology* **33**(4B), 789-790

Maxwell, M., Bjorkman, J., Nguyen, T., Sharp, P., Finnie, J., Paterson, C., Tonks, I., Paton, B.C., Kay, G.F., and Crane, D.I. (2003) Pex13 inactivation in the mouse disrupts peroxisome biogenesis and leads to a Zellweger syndrome phenotype. *Mol Cell Biol* **23**(16), 5947-57

Mays-Hoopes, L.L., Bolen, J., Riggs, A.D., and Singer-Sam, J. (1995) Preparation of spermatogonia, spermatocytes, and round spermatids for analysis of gene expression using fluorescence-activated cell sorting. *Biol Reprod* **53**(5), 1003-11

Miething, A. (1990) Intercellular bridges between germ cells in the immature golden hamster testis: evidence for clonal and non-clonal mode of proliferation. *Cell Tissue Res* **262**(3), 559-67

Miller-Fleming, L., Olin-Sandoval, V., Campbell, K., and Ralser, M. (2015) Remaining Mysteries of Molecular Biology: The Role of Polyamines in the Cell. *J Mol Biol* **427**(21), 3389-406

Moghissi, K.S., and Wallach, E.E. (1983) Unexplained infertility. *Fertil Steril* **39**(1), 5-21

Monici, M. (2005) Cell and tissue autofluorescence research and diagnostic applications. *Biotechnol Annu Rev* **11**, 227-56

Monosov, E.Z., Wenzel, T.J., Luers, G.H., Heyman, J.A., and Subramani, S. (1996) Labeling of peroxisomes with green fluorescent protein in living P. pastoris cells. *J Histochem Cytochem* **44**(6), 581-9

Morales, C., Clermont, Y., and Hermo, L. (1985) Nature and function of endocytosis in Sertoli cells of the rat. *Am J Anat* **173**(3), 203-17

Morales, C., Clermont, Y., and Nadler, N.J. (1986) Cyclic endocytic activity and kinetics of lysosomes in Sertoli cells of the rat: a morphometric analysis. *Biol Reprod* **34**(1), 207-18

Morita, K., Sasaki, H., Fujimoto, K., Furuse, M., and Tsukita, S. (1999) Claudin-11/OSP-based tight junctions of myelin sheaths in brain and Sertoli cells in testis. *J Cell Biol* **145**(3), 579-88

Morita, M., and Imanaka, T. (2012) Peroxisomal ABC transporters: structure, function and role in disease. *Biochim Biophys Acta* **1822**(9), 1387-96

Moser, H.W., Mahmood, A., and Raymond, G.V. (2007) X-linked adrenoleukodystrophy. *Nat Clin Pract Neurol* **3**(3), 140-51

Mosser, J., Douar, A.M., Sarde, C.O., Kioschis, P., Feil, R., Moser, H., Poustka, A.M., Mandel, J.L., and Aubourg, P. (1993) Putative X-linked adrenoleukodystrophy gene shares unexpected homology with ABC transporters. *Nature* **361**(6414), 726-30

Mruk, D.D., and Cheng, C.Y. (2004) Sertoli-Sertoli and Sertoli-germ cell interactions and their significance in germ cell movement in the seminiferous epithelium during spermatogenesis. *Endocr Rev* **25**(5), 747-806

Muciaccia, B., Boitani, C., Berloco, B.P., Nudo, F., Spadetta, G., Stefanini, M., de Rooij, D.G., and Vicini, E. (2013) Novel stage classification of human spermatogenesis based on acrosome development. *Biol Reprod* **89**(3), 60

Naidu, S., and Moser, H. (1991) Infantile Refsum disease. *AJNR Am J Neuroradiol* **12**(6), 1161-3

Nair, D.M., Purdue, P.E., and Lazarow, P.B. (2004) Pex7p translocates in and out of peroxisomes in Saccharomyces cerevisiae. *J Cell Biol* **167**(4), 599-604

Nakamura, M.T., and Nara, T.Y. (2004) Structure, function, and dietary regulation of delta6, delta5, and delta9 desaturases. *Annu Rev Nutr* **24**, 345-76

Nantel, F., Monaco, L., Foulkes, N.S., Masquilier, D., LeMeur, M., Henriksen, K., Dierich, A., Parvinen, M., and Sassone-Corsi, P. (1996) Spermiogenesis deficiency and germ-cell apoptosis in CREM-mutant mice. *Nature* **380**(6570), 159-62

Nenicu, A., Luers, G.H., Kovacs, W., David, M., Zimmer, A., Bergmann, M., and Baumgart-Vogt, E. (2007) Peroxisomes in human and mouse testis: differential expression of peroxisomal proteins in germ cells and distinct somatic cell types of the testis. *Biol Reprod* **77**(6), 1060-72

Neufeld, C., Filipp, F.V., Simon, B., Neuhaus, A., Schuller, N., David, C., Kooshapur, H., Madl, T., Erdmann, R., Schliebs, W., Wilmanns, M., and Sattler, M. (2009) Structural basis for competitive interactions of Pex14 with the import receptors Pex5 and Pex19. *EMBO J* **28**(6), 745-54

Niemi, M., and Kormano, M. (1965) Cyclical Changes in and Significance of Lipids and Acid Phosphatase Activity in the Seminiferous Tubules of the Rat Testis. *Anat Rec* **151**, 159-70

Nishimune, Y., Aizawa, S., and Komatsu, T. (1978) Testicular germ cell differentiation in vivo. *Fertil Steril* **29**(1), 95-102

Nistal, M., Codesal, J., and Paniagua, R. (1986a) Multinucleate spermatids in aging human testes. *Arch Androl* **16**(2), 125-9

Nistal, M., Santamaria, L., Paniagua, R., Regadera, J., and Codesal, J. (1986b) Multinucleate Leydig cells in normal human testes. *Andrologia* **18**(3), 268-72

Norbury, C.J., and Hickson, I.D. (2001) Cellular responses to DNA damage. *Annu Rev Pharmacol Toxicol* **41**, 367-401

O'Donnell, L., Nicholls, P.K., O'Bryan, M.K., McLachlan, R.I., and Stanton, P.G. (2011) Spermiation: The process of sperm release. *Spermatogenesis* **1**(1), 14-35

Oakberg, E.F. (1957) Duration of spermatogenesis in the mouse. *Nature* **180**(4595), 1137-8

Opalinski, L., Kiel, J.A., Williams, C., Veenhuis, M., and van der Klei, I.J. (2011) Membrane curvature during peroxisome fission requires Pex11. *EMBO J* **30**(1), 5-16

Orth, J.M., Gunsalus, G.L., and Lamperti, A.A. (1988) Evidence from Sertoli cell-depleted rats indicates that spermatid number in adults depends on numbers of Sertoli cells produced during perinatal development. *Endocrinology* **122**(3), 787-94

Oulad-Abdelghani, M., Bouillet, P., Decimo, D., Gansmuller, A., Heyberger, S., Dolle, P., Bronner, S., Lutz, Y., and Chambon, P. (1996) Characterization of a premeiotic germ cell-specific cytoplasmic protein encoded by Stra8, a novel retinoic acid-responsive gene. *J Cell Biol* **135**(2), 469-77

Paniagua, R., Rodriguez, M.C., Nistal, M., Fraile, B., and Amat, P. (1987) Changes in the lipid inclusion/Sertoli cell cytoplasm area ratio during the cycle of the human seminiferous epithelium. *J Reprod Fertil* **80**(1), 335-41

Parvinen, M. (1982) Regulation of the seminiferous epithelium. *Endocr Rev* **3**(4), 404-17

Pasqualotto, F.F., Sharma, R.K., Nelson, D.R., Thomas, A.J., and Agarwal, A. (2000) Relationship between oxidative stress, semen characteristics, and clinical diagnosis in men undergoing infertility investigation. *Fertil Steril* **73**(3), 459-64

Pegg, A.E., and Wang, X. (2009) Mouse models to investigate the function of spermine. *Commun Integr Biol* **2**(3), 271-4

Peltola, V., Huhtaniemi, I., Metsa-Ketela, T., and Ahotupa, M. (1996) Induction of lipid peroxidation during steroidogenesis in the rat testis. *Endocrinology* **137**(1), 105-12

Pereira, S.L., Leonard, A.E., Huang, Y.S., Chuang, L.T., and Mukerji, P. (2004) Identification of two novel microalgal enzymes involved in the conversion of the omega3-fatty acid, eicosapentaenoic acid, into docosahexaenoic acid. *Biochem J* **384**(Pt 2), 357-66

Philchenkov, A.A. (2003) Caspases as regulators of apoptosis and other cell functions. *Biochemistry (Mosc)* **68**(4), 365-76

Pitt, M.A., Knox, W.F., and Haboubi, N.Y. (1993) Multinucleated stromal giant cells of the colonic lamina propria in ulcerative colitis. *J Clin Pathol* **46**(9), 874-5

Pizzimenti, S., Toaldo, C., Pettazzoni, P., Dianzani, M.U., and Barrera, G. (2010) The "two-faced" effects of reactive oxygen species and the lipid peroxidation product 4-hydroxynonenal in the hallmarks of cancer. *Cancers (Basel)* **2**(2), 338-63

Plachot, M., Belaisch-Allart, J., Mayenga, J.M., Chouraqui, A., Tesquier, L., and Serkine, A.M. (2002) Outcome of conventional IVF and ICSI on sibling oocytes in mild male factor infertility. *Hum Reprod* **17**(2), 362-9

Platz, R.D., Grimes, S.R., Meistrich, M.L., and Hnilica, L.S. (1975) Changes in nuclear proteins of rat testis cells separated by velocity sedimentation. *J Biol Chem* **250**(15), 5791-800

Poirier, Y., Antonenkov, V.D., Glumoff, T., and Hiltunen, J.K. (2006) Peroxisomal beta-oxidation--a metabolic pathway with multiple functions. *Biochim Biophys Acta* **1763**(12), 1413-26

Poole, B. (1969) Biogenesis and turnover of rat liver peroxisomes. *Ann N Y Acad Sci* **168**(2), 229-43

Postic, C., Shiota, M., Niswender, K.D., Jetton, T.L., Chen, Y., Moates, J.M., Shelton, K.D., Lindner, J., Cherrington, A.D., and Magnuson, M.A. (1999) Dual roles for glucokinase in glucose homeostasis

as determined by liver and pancreatic beta cell-specific gene knock-outs using Cre recombinase. *J Biol Chem* **274**(1), 305-15

Poulin, R., Coward, J.K., Lakanen, J.R., and Pegg, A.E. (1993) Enhancement of the spermidine uptake system and lethal effects of spermidine overaccumulation in ornithine decarboxylase-overproducing L1210 cells under hyposmotic stress. *J Biol Chem* **268**(7), 4690-8

Poulin, R., Pelletier, G., and Pegg, A.E. (1995) Induction of apoptosis by excessive polyamine accumulation in ornithine decarboxylase-overproducing L1210 cells. *Biochem J* **311 (Pt 3)**, 723-7

Powers, J.M., and Schaumburg, H.H. (1981) The testis in adreno-leukodystrophy. *Am J Pathol* **102**(1), 90-8

Purdue, P.E., and Lazarow, P.B. (2001) Peroxisome biogenesis. *Annu Rev Cell Dev Biol* **17**, 701-52

Rayapuram, N., and Subramani, S. (2006) The importomer--a peroxisomal membrane complex involved in protein translocation into the peroxisome matrix. *Biochim Biophys Acta* **1763**(12), 1613-9

Reddy, J.K., and Hashimoto, T. (2001) Peroxisomal beta-oxidation and peroxisome proliferator-activated receptor alpha: an adaptive metabolic system. *Annu Rev Nutr* **21**, 193-230

Rejraji, H., Sion, B., Prensier, G., Carreras, M., Motta, C., Frenoux, J.M., Vericel, E., Grizard, G., Vernet, P., and Drevet, J.R. (2006) Lipid remodeling of murine epididymosomes and spermatozoa during epididymal maturation. *Biol Reprod* **74**(6), 1104-13

Rhodin, J.A.G. (1954) 'Correlation of ultrastructural organization and function in normal and experimentally chaged proximal convoluted tubule cells of the mouse kidney.' (Stockholm,) 76 p.

Risbridger, G.P., Robertson, D.M., and de Kretser, D.M. (1990a) Current perspectives of inhibin biology. *Acta Endocrinol (Copenh)* **122**(6), 673-82

Risbridger, G.P., Robertson, D.M., Drummond, A.E., Hedger, M.P., Clements, J.A., Li, H., and de Kretser, D.M. (1990b) Interactions between the seminiferous tubules and Leydig cells of the testis. *Reprod Fertil Dev* **2**(3), 219-23

Rivier, C., Vale, W., and Rivier, J. (1987) Studies of the inhibin family of hormones: a review. *Horm Res* **28**(2-4), 104-18

Romrell, L.J., Bellve, A.R., and Fawcett, D.W. (1976) Separation of mouse spermatogenic cells by sedimentation velocity. A morphological characterization. *Dev Biol* **49**(1), 119-31

Roqueta-Rivera, M., Abbott, T.L., Sivaguru, M., Hess, R.A., and Nakamura, M.T. (2011) Deficiency in the omega-3 fatty acid pathway results in failure of acrosome biogenesis in mice. *Biol Reprod* **85**(4), 721-32

Roqueta-Rivera, M., Stroud, C.K., Haschek, W.M., Akare, S.J., Segre, M., Brush, R.S., Agbaga, M.P., Anderson, R.E., Hess, R.A., and Nakamura, M.T. (2010) Docosahexaenoic acid supplementation fully restores fertility and spermatogenesis in male delta-6 desaturase-null mice. *J Lipid Res* **51**(2), 360-7

Roser, J.E. (2008) Regulation of testicular function in the stallion: An intricate network of endocrine, paracrine and autocrine systems. *Animal Reproduction Science* **107**(3-4), 179-196

Russell, J.N., Clements, J.E., and Gama, L. (2013) Quantitation of gene expression in formaldehyde-fixed and fluorescence-activated sorted cells. *PLoS One* **8**(9), e73849

Russell, L.D., Goh, J.C., Rashed, R.M., and Vogl, A.W. (1988) The consequences of actin disruption at Sertoli ectoplasmic specialization sites facing spermatids after in vivo exposure of rat testis to cytochalasin D. *Biol Reprod* **39**(1), 105-18

Russell, L.D., and Malone, J.P. (1980) A study of Sertoli-spermatid tubulobulbar complexes in selected mammals. *Tissue Cell* **12**(2), 263-85

Santiemma, V., Rosati, P., Guerzoni, C., Mariani, S., Beligotti, F., Magnanti, M., Garufi, G., Galoni, T., and Fabbrini, A. (1992) Human Sertoli cells in vitro: morphological features and androgen-binding protein secretion. *J Steroid Biochem Mol Biol* **43**(5), 423-9

Santos, M.J., Imanaka, T., Shio, H., Small, G.M., and Lazarow, P.B. (1988) Peroxisomal membrane ghosts in Zellweger syndrome--aberrant organelle assembly. *Science* **239**(4847), 1536-8

Schell-Steven, A., Stein, K., Amoros, M., Landgraf, C., Volkmer-Engert, R., Rottensteiner, H., and Erdmann, R. (2005) Identification of a novel, intraperoxisomal pex14-binding site in pex13: association of pex13 with the docking complex is essential for peroxisomal matrix protein import. *Mol Cell Biol* **25**(8), 3007-18

Schipper, R.G., Penning, L.C., and Verhofstad, A.A. (2000) Involvement of polyamines in apoptosis. Facts and controversies: effectors or protectors? *Semin Cancer Biol* **10**(1), 55-68

Schlatt, S., and Ehmcke, J. (2014) Regulation of spermatogenesis: an evolutionary biologist's perspective. *Semin Cell Dev Biol* **29**, 2-16

Schrader, M., Costello, J.L., Godinho, L.F., Azadi, A.S., and Islinger, M. (2016) Proliferation and fission of peroxisomes - An update. *Biochim Biophys Acta* **1863**(5), 971-83

Schrader, M., and Fahimi, H.D. (2006) Peroxisomes and oxidative stress. *Biochim Biophys Acta* **1763**(12), 1755-66

Schrader, M., and Fahimi, H.D. (2008) The peroxisome: still a mysterious organelle. *Histochem Cell Biol* **129**(4), 421-40

Schrader, M., Wodopia, R., and Fahimi, H.D. (1999) Induction of tubular peroxisomes by UV irradiation and reactive oxygen species in HepG2 cells. *J Histochem Cytochem* **47**(9), 1141-8

Schroeder, A., Mueller, O., Stocker, S., Salowsky, R., Leiber, M., Gassmann, M., Lightfoot, S., Menzel, W., Granzow, M., and Ragg, T. (2006) The RIN: an RNA integrity number for assigning integrity values to RNA measurements. *BMC Mol Biol* **7**, 3

Schulze, C. (1984) Sertoli cells and Leydig cells in man. *Adv Anat Embryol Cell Biol* **88**, 1-104

Schulze, W., and Rehder, U. (1984) Organization and morphogenesis of the human seminiferous epithelium. *Cell Tissue Res* **237**(3), 395-407

Scotto, J.M., Hadchouel, M., Odievre, M., Laudat, M.H., Saudubray, J.M., Dulac, O., Beucler, I., and Beaune, P. (1982) Infantile phytanic acid storage disease, a possible variant of Refsum's disease: three cases, including ultrastructural studies of the liver. *J Inherit Metab Dis* **5**(2), 83-90

Setchell, B.P. (1994) Possible physiological bases for contraceptive techniques in the male. *Hum Reprod* **9**(6), 1081-7

Shaha, C., Tripathi, R., and Mishra, D.P. (2010) Male germ cell apoptosis: regulation and biology. *Philos Trans R Soc Lond B Biol Sci* **365**(1546), 1501-15

Sharma, R., and Agarwal, A. (2011) Spermatogenesis: An Overview. *Sperm Chromatin: Biological and Clinical Applications in Male Infertility and Assisted Reproduction*, 19-44

Skinner, M.K., and Moses, H.L. (1989) Transforming growth factor beta gene expression and action in the seminiferous tubule: peritubular cell-Sertoli cell interactions. *Mol Endocrinol* **3**(4), 625-34

Skinner, M.K., Schlitz, S.M., and Anthony, C.T. (1989) Regulation of Sertoli cell differentiated function: testicular transferrin and androgen-binding protein expression. *Endocrinology* **124**(6), 3015-24

Slawecki, M.L., Dodt, G., Steinberg, S., Moser, A.B., Moser, H.W., and Gould, S.J. (1995) Identification of three distinct peroxisomal protein import defects in patients with peroxisome biogenesis disorders. *J Cell Sci* **108 (Pt 5)**, 1817-29

Smith, B.E., and Braun, R.E. (2012) Germ cell migration across Sertoli cell tight junctions. *Science* **338**(6108), 798-802

Smith, J.J., Brown, T.W., Eitzen, G.A., and Rachubinski, R.A. (2000) Regulation of peroxisome size and number by fatty acid beta -oxidation in the yeast yarrowia lipolytica. *J Biol Chem* **275**(26), 20168-78

Sprecher, H.W., Baykousheva, S.P., Luthria, D.L., and Mohammed, B.S. (1995) Differences in the regulation of biosynthesis of 20- versus 22-carbon polyunsaturated fatty acids. *Prostaglandins Leukot Essent Fatty Acids* **52**(2-3), 99-101

Stanley, W.A., and Wilmanns, M. (2006) Dynamic architecture of the peroxisomal import receptor Pex5p. *Biochim Biophys Acta* **1763**(12), 1592-8

Steinberg, S.J., Dodt, G., Raymond, G.V., Braverman, N.E., Moser, A.B., and Moser, H.W. (2006) Peroxisome biogenesis disorders. *Biochim Biophys Acta* **1763**(12), 1733-48

Steinberg, S.J., Raymond, G.V., Braverman, N.E., and Moser, A.B. (1993) Peroxisome Biogenesis Disorders, Zellweger Syndrome Spectrum. In 'GeneReviews(R).' (Eds. RA Pagon, MP Adam, HH Ardingeret al): Seattle (WA))

Steinberger, E. (1971) Hormonal control of mammalian spermatogenesis. *Physiol Rev* **51**(1), 1-22

Stoffel, W., Holz, B., Jenke, B., Binczek, E., Gunter, R.H., Kiss, C., Karakesisoglou, I., Thevis, M., Weber, A.A., Arnhold, S., and Addicks, K. (2008) Delta6-desaturase (FADS2) deficiency unveils the role of omega3- and omega6-polyunsaturated fatty acids. *EMBO J* **27**(17), 2281-92

Stoffel, W., Zierenberg, O., and Tunggal, B.D. (1972) 13 C-nuclear magnetic resonance spectroscopic studies on saturated, mono-, di- and polyunsaturated fatty acids, phospho- and sphingolipids. *Hoppe Seylers Z Physiol Chem* **353**(12), 1962-9

Subramani, S. (1996) Protein translocation into peroxisomes. *J Biol Chem* **271**(51), 32483-6

Surani, M.A., Kothary, R., Allen, N.D., Singh, P.B., Fundele, R., Ferguson-Smith, A.C., and Barton, S.C. (1990) Genome imprinting and development in the mouse. *Dev Suppl*, 89-98

Tabak, H.F., Elgersma, Y., Hettema, E., Franse, M.M., Voorn-Brouwer, T., and Distel, B. (1995) Transport of proteins and metabolites across the impermeable membrane of peroxisomes. *Cold Spring Harb Symp Quant Biol* **60**, 649-55

Tabor, C.W., and Tabor, H. (1984) Polyamines. *Annu Rev Biochem* **53**, 749-90

Tanaka, A.R., Tanabe, K., Morita, M., Kurisu, M., Kasiwayama, Y., Matsuo, M., Kioka, N., Amachi, T., Imanaka, T., and Ueda, K. (2002) ATP binding/hydrolysis by and phosphorylation of peroxisomal ATP-binding cassette proteins PMP70 (ABCD3) and adrenoleukodystrophy protein (ABCD1). *J Biol Chem* **277**(42), 40142-7

Tazi, J., Bakkour, N., and Stamm, S. (2009) Alternative splicing and disease. *Biochim Biophys Acta* **1792**(1), 14-26

Thannickal, V.J., and Fanburg, B.L. (2000) Reactive oxygen species in cell signaling. *Am J Physiol Lung Cell Mol Physiol* **279**(6), L1005-28

Thong, A., Muller, D., Feuerstacke, C., Mietens, A., Stammler, A., and Middendorff, R. (2014) Neutral endopeptidase (CD10) is abundantly expressed in the epididymis and localized to a distinct population of epithelial cells--its relevance for CNP degradation. *Mol Cell Endocrinol* **382**(1), 234-43

Titorenko, V.I., Chan, H., and Rachubinski, R.A. (2000) Fusion of small peroxisomal vesicles in vitro reconstructs an early step in the in vivo multistep peroxisome assembly pathway of Yarrowia lipolytica. *J Cell Biol* **148**(1), 29-44

Tomlinson, M.J., Tomlinson, S., Yang, X.B., and Kirkham, J. (2013) Cell separation: Terminology and practical considerations. *J Tissue Eng* **4**, 2041731412472690

Toppari, J., Eerola, E., and Parvinen, M. (1985) Flow cytometric DNA analysis of defined stages of rat seminiferous epithelial cycle during in vitro differentiation. *J Androl* **6**(6), 325-33

Tsai, S.C., Lu, C.C., Lin, C.S., and Wang, P.S. (2003) Antisteroidogenic actions of hydrogen peroxide on rat Leydig cells. *J Cell Biochem* **90**(6), 1276-86

Tsukita, S., Furuse, M., and Itoh, M. (2001) Multifunctional strands in tight junctions. *Nat Rev Mol Cell Biol* **2**(4), 285-93

Usuda, N., Reddy, M.K., Hashimoto, T., Rao, M.S., and Reddy, J.K. (1988) Tissue specificity and species differences in the distribution of urate oxidase in peroxisomes. *Lab Invest* **58**(1), 100-11

Valdes-Santiago, L., and Ruiz-Herrera, J. (2013) Stress and polyamine metabolism in fungi. *Front Chem* **1**, 42

van de Beek, M.C., Dijkstra, I.M., and Kemp, S. (2017) Method for Measurement of Peroxisomal Very Long-Chain Fatty Acid Beta-Oxidation and De Novo C26:0 Synthesis Activity in Living Cells Using Stable-Isotope Labeled Docosanoic Acid. *Methods Mol Biol* **1595**, 45-54

van der Wee, K.S., Johnson, E.W., Dirami, G., Dym, T.M., and Hofmann, M.C. (2001) Immunomagnetic isolation and long-term culture of mouse type A spermatogonia. *J Androl* **22**(4), 696-704

van Roermund, C.W., Visser, W.F., Ijlst, L., van Cruchten, A., Boek, M., Kulik, W., Waterham, H.R., and Wanders, R.J. (2008) The human peroxisomal ABC half transporter ALDP functions as a homodimer and accepts acyl-CoA esters. *FASEB J* **22**(12), 4201-8

Ventela, S., Toppari, J., and Parvinen, M. (2003) Intercellular organelle traffic through cytoplasmic bridges in early spermatids of the rat: mechanisms of haploid gene product sharing. *Mol Biol Cell* **14**(7), 2768-80

Verheijden, S., Beckers, L., Casazza, A., Butovsky, O., Mazzone, M., and Baes, M. (2015) Identification of a chronic non-neurodegenerative microglia activation state in a mouse model of peroxisomal beta-oxidation deficiency. *Glia* **63**(9), 1606-20

Verhoeven, G., and Cailleau, J. (1988) Follicle-stimulating hormone and androgens increase the concentration of the androgen receptor in Sertoli cells. *Endocrinology* **122**(4), 1541-50

Verze, P., Cai, T., and Lorenzetti, S. (2016) The role of the prostate in male fertility, health and disease. *Nat Rev Urol* **13**(7), 379-86

von Weizsacker, F., Labeit, S., Koch, H.K., Oehlert, W., Gerok, W., and Blum, H.E. (1991) A simple and rapid method for the detection of RNA in formalin-fixed, paraffin-embedded tissues by PCR amplification. *Biochem Biophys Res Commun* **174**(1), 176-80

Wallner, S., and Schmitz, G. (2011) Plasmalogens the neglected regulatory and scavenging lipid species. *Chem Phys Lipids* **164**(6), 573-89

Wanders, R.J., Schumacher, H., Heikoop, J., Schutgens, R.B., and Tager, J.M. (1992) Human dihydroxyacetonephosphate acyltransferase deficiency: a new peroxisomal disorder. *J Inherit Metab Dis* **15**(3), 389-91

Wanders, R.J., and Waterham, H.R. (2005) Peroxisomal disorders I: biochemistry and genetics of peroxisome biogenesis disorders. *Clin Genet* **67**(2), 107-33

Wanders, R.J., and Waterham, H.R. (2006a) Biochemistry of mammalian peroxisomes revisited. *Annu Rev Biochem* **75**, 295-332

Wanders, R.J., and Waterham, H.R. (2006b) Peroxisomal disorders: the single peroxisomal enzyme deficiencies. *Biochim Biophys Acta* **1763**(12), 1707-20

Wang, Y., Botolin, D., Christian, B., Busik, J., Xu, J., and Jump, D.B. (2005) Tissue-specific, nutritional, and developmental regulation of rat fatty acid elongases. *J Lipid Res* **46**(4), 706-15

Waterham, H.R., and Ebberink, M.S. (2012) Genetics and molecular basis of human peroxisome biogenesis disorders. *Biochim Biophys Acta* **1822**(9), 1430-41

Weinbauer, G.F., and Nieschlag, E. (1997) Endocrine control of germ cell proliferation in the primate testis. What do we really know? *Adv Exp Med Biol* **424**, 51-8

Xie, X., Tome, M.E., and Gerner, E.W. (1997) Loss of intracellular putrescine pool-size regulation induces apoptosis. *Exp Cell Res* **230**(2), 386-92

Yamamoto, K., and Fahimi, H.D. (1987) Three-dimensional reconstruction of a peroxisomal reticulum in regenerating rat liver: evidence of interconnections between heterogeneous segments. *J Cell Biol* **105**(2), 713-22

Yan, H.H., and Cheng, C.Y. (2005) Blood-testis barrier dynamics are regulated by an engagement/disengagement mechanism between tight and adherens junctions via peripheral adaptors. *Proc Natl Acad Sci U S A* **102**(33), 11722-7

Yan, H.H., Mruk, D.D., Lee, W.M., and Cheng, C.Y. (2008) Cross-talk between tight and anchoring junctions-lesson from the testis. *Adv Exp Med Biol* **636**, 234-54

Ye, S.J., Ying, L., Ghosh, S., de Franca, L.R., and Russell, L.D. (1993) Sertoli cell cycle: a re-examination of the structural changes during the cycle of the seminiferous epithelium of the rat. *Anat Rec* **237**(2), 187-98

Young, P.G., and Bartel, B. (2016) Pexophagy and peroxisomal protein turnover in plants. *Biochim Biophys Acta* **1863**(5), 999-1005

Zadravec, D., Tvrdik, P., Guillou, H., Haslam, R., Kobayashi, T., Napier, J.A., Capecchi, M.R., and Jacobsson, A. (2011) ELOVL2 controls the level of n-6 28:5 and 30:5 fatty acids in testis, a prerequisite for male fertility and sperm maturation in mice. *J Lipid Res* **52**(2), 245-55